EXECUTION AND EVALUATION OF EYE MOVEMENTS: FROM MUSCLES TO MEDIAL FRONTAL CORTEX

By

David C. Godlove

Dissertation

Submitted to the Faculty of the

Graduate School of Vanderbilt University

in partial fulfillment of the requirements

for the degree of

DOCTOR OF PHILOSOPHY

in

Neuroscience

December, 2013

Approved:

Professor Jeffrey D. Schall, advisor

Professor Geoffrey F. Woodman, chair of committee

Professor Okihide Hikosaka

Professor Gordon B. Logan

Professor David H. Zald

To Stephy,
who inspires me, with her quiet confidence, to live more fully.

ACKNOWLEDGMENTS

The Neuroscience program and Psychology department at Vanderbilt University foster a vibrant and highly collaborative environment. I wish to express my great admiration and affection for this community. It has been my privilege, honor, and joy to work alongside these talented scientists. For my initial training in basic neurophysiological and surgical techniques, I wish to thank A. B. Bonds, Brian Carriere, Vivien Casagrande, Jeremiah Cohen, Erik Emeric, Michael Fitzpatrick, Ilya Khaytin, Alex Maier, Roan Marion, Matt Nelson, Gopathy Purushothaman, Supriyo Ray, Andrew Rossi, David Royal, and Mark Wallace. For assistance in data collection, I wish to thank Debbie Boner, Mary Feurtado, Anna Garr, Namsoo Kim, Paul Middlebrooks, Courtney Segovis, Donna Siegel, Chrissy Suell, Noor Tantawy, George Wilson, and Michelle Young. For kindly providing histological material presented in Chapter 4, I wish to thank Troy Hackett and Iwona Stepniewska. For training and assistance with data analysis, I wish to thank Leanne Boucher, Erik Emeric, John Haitas, Kendra Kawala, Alex Maier, Namsoo Kim, and Rob Reinhart. For providing helpful comments on manuscripts, I wish to thank Patrick Bissett, Michele Cox, Kei Fukuda, Rich Heitz, David Leopold, Paul Middlebrooks, Braden Purcell, Katy Thakkar, and Bram Zandbelt. For help with animal care I wish to thank Troy Apple, Erin Crowder Hare, Mary Feurtado, Anna Garr, Courtney Segovis, Chrissy Suell, Polly Weigand, and Michele Young. For assistance in designing and fabricating equipment, I wish to thank Bruce and Roger Williams. For providing administrative support, I wish to thank Steve Edminster, Roz Johnson, Mary Michael-Woolman, Jen Overstreet, Gale Newton, Shirin Pulous, and Mary Early-Zald. I also wish to thank the leadership of the Vanderbilt Brain Institute and the Neuroscience program, Louis DeFelice, Doug McMahon, Elaine Sanders-Bush, and Mark Wallace.

I wish to extend special gratitude to the members of my dissertation committee who have fostered my growth as a scientist, Okihide Hikosaka, Gordon Logan, Geoff Woodman, and David Zald. Finally, I wish to thank Jeff Schall for giving me the remarkable opportunity to study in his laboratory and for mentoring me during the course of this work.

I wish to respectfully acknowledge the monkeys called Archimedes, Euler, Fechner, Upton, Yoyo, and Xena. May their contributions be immortalized in the deeper scientific understanding they have bestowed. These efforts were supported by the National Institutes of Health (grant numbers R01-MH55806, R01-EY019882, P30-EY08126, P30-HD015052) and by Robin and Richard Patton through the E. Bronson Ingram Chair in Neuroscience.

TABLE OF CONTENTS

Page

LIST OF TABLES

LIST OF FIGURES

CHAPTER 1

INTRODUCTION

1.1 Overview

I describe, in this dissertation, a series of studies observing behavior and neural activity of macaque monkeys to understand better the physiological processes that underlie saccade execution and evaluation. The studies are presented in two parts. To gain insight on saccade execution, I developed methods for recording and isolating the extraocular electromyogram (EMG) from implanted surface electrodes normally used to recorded the electroencephalogram (EEG). I also made detailed observations of the small eye movements called microsaccades elicited from monkeys while they attempted to prevent their eyes from moving. I have analyzed these data in light of current theories on the physiological basis of saccade execution. These studies, are presented in Chapters 2 and 3. In the second part of this work, I sought to better understand the neural processes that underlie saccade evaluation. To this end, I recorded the electrical activity of single neurons, small groups of neurons, and large ensembles of neurons from medial frontal cortex. This area is thought to serve a role in evaluating actions and their outcomes. The macaque monkey serves as an animal model to test theories of human cognition. The work detailed here strengthens this model, making explicit links between research carried out in human and non-human primates. By better understanding how monkeys evaluate the outcomes of their eye movements, I hope to provide insight on the neural mechanisms that underlie humans' ability to reflect on their own actions.

In this introductory chapter, I will provide background material to motivate and facilitate understanding of these studies. I will first discuss the different types of eye

movements, placing special emphasis on the saccades and microsaccades that provide the main behavioral measures in these studies. I will then turn to the oculomotor system, focusing attention on the structures that are of greatest interest to the present work. I will conclude the section on the oculomotor system with a discussion of the higher cognitive functions attributed to the medial, frontal cortex. This will lead naturally to a discussion of executive control with special emphasis on *performance monitoring*. I will then conclude this chapter by foreshadowing each of the studies with a brief summary.

However, before launching into the taxonomy of eye movements, it will be useful for us to consider a general principle that guides, informs, and provides a backdrop for this work. The oculomotor system constantly strives either to execute or to actively inhibit eye movements. This idea was alluded to by Carpenter (1981) when he coined the phrase "oculomotor procrastination". I will argue that this basic principle provides a key insight through which the oculomotor system can be understood[1].

1.2 The tension between going and stopping

To understand the primate oculomotor system, one must first appreciate several basic principles of primate vision. After all, these systems have evolved in parallel, and in mutual service to one another. With our forward facing eyes, humans can perceive ~180° of visual angle at any moment and ~140° binocularly (Carpenter, 1988; for comparison with other vertebrates see Walls, 1942). Based on subjective experience, it seems as though we perceive a large portion of this scene with high acuity. But the truth is quite different from this intuition. Unlike sensors in digital cameras, the photoreceptors

[1] Portions of this chapter were published as Godlove DC. Good looking... better looking! Performance monitoring and behavioral adjustments in the oculomotor system. Vanderbilt Reviews Neuroscience 1: 62-68, 2010, and as Schall JD, Godlove DC. Current advances and pressing problems in studies of stopping. Current Opinion in Neurobiology 22:1012-1021

of the retina that transduce light into neural impulses are not evenly distributed. Instead, specialized photoreceptors serving high-acuity vision called cones are packed most densely in the fovea, which subtends about 1° of the total inner circumference of the eye. When viewed at arm's length, one's thumbnail subtends around 1° of visual angle, so this image is approximately the same size as the fovea. Outside of this central area, acuity falls off exponentially. Within 1° of the area centralis visual acuity is reduced by half (Green, 1970). In fact, only 1 ten thousandth of the visual field can be processed with full visual acuity by the fovea at any given moment (Carpenter, 1988). It is obviously necessary for us to perceive a much larger portion of the scene before us with high visual acuity. Luckily, the solution to this problem is simple; **the optics must be moved**.

In addition to spatial considerations, the oculomotor system has demands placed on it by the temporal properties of the visual system. When the eyes move, light moves across the retina, introducing *retinal slip*. As the pattern of light fluctuates across the photoreceptors, the fidelity of the image is determined by the speed with which light can be transduced to neural impulses. The primate visual system is actually relatively slow at this process (reviewed by Carpenter, 1988). Luckily, the solution to this problem is also quite simple: **the optics must remain stationary**.

The oculomotor system is thus defined by a competition between two rival demands. On the one hand, images must be stabilized on the retina. On the other hand images must be sampled from different points in space. This concept of balancing fixations against gaze shifts provides a useful starting point for studying the oculomotor system. It will be a constant theme in this Dissertation, and frames many of the studies presented. As we shall see below, almost all eye movements fall into one of two categories; those that stabilize images on the retina such as the optokinetic reflex, and the vestibular reflex, and those that realign images with respect to the retina so that

different areas can be sampled such as saccadic eye movements. Saccades themselves are best understood as attempts to balance the competing demands of movement and fixation. The saccadic system minimizes the duration of retinal slip by executing extremely fast, accurate gaze shifts (reviewed by Carpenter, 1991). At virtually every level, from the brain stem to the prefrontal cortex, oculomotor areas contain neurons important for both fixation and gaze shifting. Accordingly, great progress has been made studying the oculomotor system using a task which capitalizes on the tension between movement and fixation. This *stop-signal task* was originally developed to study response inhibition in the skeletal motor system (Lappin and Eriksen, 1966; Logan and Cowan, 1984). The saccadic variant of this task (Hanes and Schall, 1995; Hanes and Carpenter, 1999) has proven extremely useful for elucidating properties of the oculomotor system, and it provides the main behavioral data for most of the studies described here. I will briefly introduce this task below. More thorough introduction with accompanying schematic figures will be presented in the chapters that follow.

In most implementations, the stop-signal task is simply a two-alternative forced choice task with an additional rule (reviewed by Verbruggen and Logan, 2008; Aron, 2011; Schall and Godlove, 2012). Subjects must react quickly and appropriately to stimuli that are mapped onto specific responses. The twist that distinguishes the stop-signal task from other two-alternative forced choice tasks is that subjects are also instructed to cancel partially prepared movements when infrequent stop signals occur. Thus, in practice, three trial outcomes are possible. On trials that don't contain stop signals (hereafter referred to as no-stop trials), subjects respond to stimuli. On trials that do contain stop signals a subject may either successfully cancel a movement (hereafter referred to as canceled trials) or erroneously respond even though they have been instructed not to do so (hereafter referred to as noncanceled trials). One final

characteristic distinguishes the stop-signal task from the closely related go/nogo task which is also used to study behavioral inhibition. In the stop-signal task, a range of short delays (usually ~50-500 ms) is introduced between the instruction to go and the instruction to stop. These stop-signal delays (SSDs) allow subjects to engage in brief periods of motor preparation before actions must be canceled. The longer the SSD, the further motor preparation proceeds, and the more difficult it is to stop in the event that a stop signal is presented. This clever feature of the stop-signal task also allows experimenters to measure the timing with which partially prepared responses can be withheld.

This stop-signal task provides crucial leverage to investigate response control, because performance can be understood as a race between 2 processes that initiate (GO process) or cancel (STOP process) movement (Logan and Cowan, 1984). Using this race model, the duration of the covert STOP process, known as the stop-signal reaction time (SSRT) can be derived from the proportion of successful stop trials and the distribution of reaction times (RTs) on trials without stop signals (Logan and Cowan, 1984; Colonius, 1990; Logan, 1994; Band et al., 2003; Matzke et al., 2012). SSRT measures the time needed for subjects to cancel movements, thus providing a temporal estimate of a process that cannot be observed directly. This paradigm is very general, applying to simple and choice response tasks accomplished with any effector system, including the oculomotor system (Hanes and Schall, 1995; Hanes and Carpenter, 1999; Kornylo et al., 2003). We shall now turn our attention back to the oculomotor system. I will refer to the stop-signal task throughout this discussion as I introduce relevant discoveries and concepts.

1.3 A taxonomy of eye movements

1.3.1 The gaze holding eye movements

Movements that stabilize the eyes during rapid head shifts using vestibular information from the semicircular canals and otoliths are called vestibulo-ocular reflexes. These reflexes have extremely short latencies but also decay rapidly as acceleration ceases and the sensory organs of the vestibular system habituate to constant velocities. The vestibulo-ocular reflex is complimented by the opto-kinetic reflex which stabilizes gaze during slower head shifts using feedback derived from visual cues. Opto-kinetic reflexes have longer latencies, allowing them to take over after the rapid decay of the vestibulo-ocular reflex. Using these two reflex types, animals can adjust gaze quickly in response to movements of the head and then to continuously update eye position in response to ongoing movement. Together, the vestibulo-ocular and opto-kinetic reflexes are the most phylogenetically ancient eye movements (reviewed by Goldberg et al., 1991) and can be observed even in zebra fish (Brockerhoff et al., 1995). Ongoing movements of an animal's head in relation to its surroundings do not cause the eyes to become frozen in their most eccentric positions. Instead, this situation leads to a stereotyped, sawtoothed pattern of eye movements called nystagmus. Nystagmus is characterized by a slow phase during which animals counteract head movements with eye movements to minimize retinal slip, and a quick phase during which animals reset eye position to the opposite orbital eccentricity in order to avoid freezing in a position which supplies little or no visual information (reviewed by Goldberg et al., 1991; Krauzlis, 2008). These phases of nystagmus parallel the two types of eye movements discussed in the next section, smooth pursuit and saccadic eye movements, which have evolved to allow animals to track moving objects or explore visual scenes.

1.3.2 The gaze shifting eye movements

Smooth pursuit movements use ongoing visual feedback to track targets moving at more or less constant velocities of under 30 visual degrees per second, although these movements may track faster objects if object movement follows predicable trajectories (Sparks, 2002). Traditional accounts of smooth pursuit place emphasis on pathways through the oculomotor flocculus and oculomotor vermis of the cerebellum, but recently focus has shifted to structures which are traditionally considered part of the saccadic motor system (reviewed by Lisberger et al., 1987; Krauzlis, 2004). Since these movements vary in velocity and are under control of ongoing feedback from the visual system, they are quite similar to movements during the slow phase of nystagmus. Although most authors classify smooth pursuit as gaze shifting eye movements (e.g. Carpenter, 1988; Sparks, 2002) it is worth noting that their primary purpose is to immobilize the image of a moving target on the retina. In this sense, they may be better thought of as gaze holding eye movements.

Saccadic eye movements are highly stereotyped, somewhat ballistic movements which resemble the fast phase of nystagmus (Dodge and Cline, 1901; Yarbus, 1956; Robinson, 1964; reviewed by Carpenter, 1988; Goldberg et al., 1991). An impressive volume of classic research has been carried out investigating the saccades made by human subjects while reading. These studies highlight the nuanced cognitive control of the oculomotor system. For instance, the frequency of a particular word within a sample of text is negatively correlated with the amount of time that it is fixated during reading (Just and Carpenter, 1980). And as the conceptual difficulty of a passage increases, so too does the number of *regressions* (right to left as opposed to left to right saccades while reading English) (Jacobson and Dodwell, 1979; Rayner and Pollatsek, 1989). Reading itself is a complex behavior involving high-level cognitive processes such as semantic processing. Accordingly, sacccades are used to study reading as often as

reading is used to study saccades (reviewed by Rayner, 1998). Interesting as the reading literature is, these studies tend to deal more closely with target identification than with the execution or evaluation of saccades, and they will therefore not be a focus of our discussion.

Unlike smooth pursuit movements, saccades can be prepared in response to visual stimulation or in its absence under voluntary control (reviewed by Munoz and Everling, 2004). The latency of saccadic eye movements is long compared to the other categories of eye movements at around 200 ms in humans (Westheimer, 1954; Saslow, 1967; reviewed by Becker, 1991), although "express saccades" can be generated under some conditions with latencies under 100ms (Fischer and Ramsperger, 1984). This long latency may be explained, in part, by the fact that visual acuity is much higher when saccades are NOT being made and may therefore reflect a mechanism which evolved to limit the number of saccades made (Carpenter, 1981). Thus, we see the tension between going and stopping played out behaviorally in the oculomotor system.

The velocity with which saccades are executed can be very high reaching speeds of around 800°/s. Consistent relationships between the amplitude, peak velocity, and duration of saccades have been repeatedly noted and have been termed the *main sequence* (Zuber and Stark, 1965; Bahill et al., 1975). These relationships remain constant from the very smallest saccades to saccades of around 10° in amplitude (see Chapter 3 for examples). Peak velocity saturates at ~800°/s for saccades of ~10°, and saccades of larger amplitude are not made with higher velocity. During natural viewing, saccades larger than ~15-20° are typically not elicited; larger gaze shifts usually include rotation of the head (Bahill et al., 1975; Becker, 1991). This estimate includes saccades made from one hemifield to the other, so saccades made from the *primary position* (the position of the eyes when a subject stares straight forward) during natural viewing will usually not exceed ~7.5-10°. The observation that all saccades exhibit stereotyped and

highly predictable dynamics suggests that the same neural pathways are involved in generating saccades of all sizes (Bahill et al., 1975; Martinez-Conde et al., 2009). We will return to this important point when considering fixational eye movements below. It is also worth noting that eye movements made during the quick phase of nystagmus follow the main sequence, suggesting that the same neural pathways are responsible for both types of eye movements (Carpenter, 1988).

1.3.3 The fixational eye movements

A third class of eye movements can neither be classified as gaze-holding since they do not stabilize images on the retina nor as gaze-shifting since they are not thought to realign images for high-acuity processing by the fovea (with the possible exception of microsaccades. See below.) These are the fixational eye movements. The smallest of these movements, tremor, causes the eye to oscillate slightly during fixation. These oscillations are usually of ~5 to 30 arc seconds in amplitude at frequencies ranging from 25 and 200 Hz. Tremor is thought to be a byproduct of the digital nature of the action potentials of extraocular motor neurons (Collewijn and Kowler, 2008). Each action potential causes individual sarcomeres of the extraocular muscles to contract. These tiny contractions do not completely average out as they combine to form larger muscle contractions, and they can cause the eyes to oscillate with very small amplitude. The second fixational eye movement, drift, is perhaps the most mysterious of all eye movements. Each eye constantly moves at a relatively low velocity (~4 arc min/s) in a trajectory that can best be described as a self-avoiding random walk (Collewijn and Kowler, 2008; Engbert, 2012). These movements are largely monocular, allowing each eye to move independently (Engbert and Kliegl, 2003). Currently, the mechanism and purpose of these eye movements are not well understood. Some models (e.g. Engbert, 2012) assume that these eye movements are a product of the stochastic fluctuations of

neurons in the superior colliculus (SC, discussed in more detail below). The most well-studied fixational eye movements are the fascinating microsaccades. In Chapter 3, I present a detailed study of the microsaccades elicited by monkeys during the saccade countermanding task. Therefore, I will devote some time to their introduction here.

Microsaccades are small, high velocity eye movements made by subjects during fixation (Riggs et al., 1954). Definitions vary, but there is general agreement that microsaccades are <1° in amplitude (Martinez-Conde et al., 2009; but see Collewijn and Kowler, 2008). On average, their amplitude is actually quite a bit smaller, being around 12 arc minutes. For comparison, this is roughly equal to the size of an image made on the retina by light reflecting from a thumbtack viewed at a distance of 10 feet. However, although they are typically quite small, the term "microsaccade" is actually a misnomer. These eye movements are not defined primarily by their size, but by the intention of the subject that elicits them. Subjects are able to inspect features and track moving objects by making saccades with very small amplitude. In fact, subjects are able to make saccades to track object movements as little as 10 arc seconds in amplitude (Carpenter, 1988). The saccades made during these experiments should probably still be considered normal saccades since it is the subjects intention to shift gaze when making them. Microsaccades are generally understood to be involuntary saccades made while subjects are attempting to fixate. However, while individual microsaccades are made involuntarily and without subject awareness, it is incorrect to suppose that microsaccades are completely outside of voluntary control. It is possible for subjects to suppress microsaccades when performing tasks that demand high acuity such as threading needles or sighting rifles on distant targets (Winterson and Collewun, 1976).

The purpose of microsaccades has been controversial since they first became the focus of serious study in the 1950's (reviewed by Rolfs et al., 2008). As pointed out above, the primate visual system is unable to process high temporal frequencies.

However, the system also breaks down at extremely low spatial frequencies. If images remain stationary on the retinal for extended periods of time, the photoreceptors habituate to the constant light input and cease to transduce light into neural impulses. This causes a subject to experience *Troxler fading* in which the image disappears from subjective view (Troxler, 1804; Clarke, 1961). One of the first proposals related to microsaccades is that they are necessary to prevent Troxler fading (Barlow, 1952; Ditchburn and Ginsborg, 1952; Ditchburn et al., 1959; Martinez-Conde et al., 2006). This view has intrinsic, teleological appeal and has persisted for decades in the face of much contradictory evidence. For instance, the ability to perform a change detection task is degraded, not enhanced, by the presence of microsaccades (Hafed et al., 2011). And tremor, drift, and small head movements provide ample image displacement to prevent this kind of fading (Cornsweet, 1956; reviewed by Collewijn and Kowler, 2008). Another theory suggests that microsaccades serve to synchronize the visual system by sending coordinated volleys of visual stimulation through the systems at regular intervals. The frequency of microsaccades varies somewhat across individuals and within different contexts, but it averages ~1 to 3 Hz (Collewijn and Kowler, 2008; Martinez-Conde et al., 2009). Microsaccades produce transient changes in activity in primary visual cortex and throughout extrastriate cortex (Bair and O'Keefe, 1998; Leopold and Logothetis, 1998; Martinez-Conde et al., 2000; Snodderly et al., 2001; Kagan et al., 2008). These waves of activity may serve to provide coordinated neural activity to aide in edge detection (Gaarder, 1966), to increase overall gain in the visual system while viewing static images (Martinez-Conde et al., 2000, 2002), or to reset and synchronize neural activity across areas (Leopold and Logothetis, 1998). At least two other hypotheses have been advanced. The first is that, aside from their diminutive size and the difficulty involved in measuring them, microsaccades are really no different from normal saccades. They simply form the small end of a continuum of saccade amplitude.

This theory suggests that microsaccades serve to foveate different portions of the scene for high-acuity inspection, or to correct deviations in gaze introduced by drift (Engbert and Kliegl, 2003; Ko et al., 2010; Engbert, 2012). A similar theory holds that microsaccades are just noise in the system, produced by stochastic fluctuations of neural activity (Steinman et al., 1973; Hafed et al., 2008; Hafed et al., 2009).

These competing theories can be organized around one central, unresolved question that has been asked repeatedly of microsaccades. Are they special? In other words, do they differ fundamentally in any way from normal saccades. The answer to this question may help to illuminate the underlying neurophysiology of microsaccades. Are they produced by the same neural mechanisms that give rise to regular saccades, or are there other neural mechanisms at work? Evidence that the same neural pathways give rise to saccades of all amplitude can be found in main sequence plots. It has been known for some time that the dynamics of microsaccades obey the same relationships as those of normal saccades (Bahill et al., 1975). Recently, an interesting link between attention and microsaccades has been reported in both humans (Hafed and Clark, 2002; Engbert and Kliegl, 2003) and monkeys (Hafed et al., 2011). When subjects deploy covert attention to a given area, as they do during a Posner cueing task (Posner, 1980), microsaccades tend to be elicited in that direction. As we shall see below, this finding is important in a theory of microsaccade production that places special emphasis on neurons in the rostral pole of the SC.

1.4 Elements of the oculomotor system

I will not exhaustively review all of the areas of the oculomotor system here, choosing instead to focus in more detail on several specific structures that are most relevant to the work presented in the following chapters. This is not meant to diminish the contribution of other areas to saccade. Several structures deserve special note.

The basal ganglia serve an important role in both saccade execution and evaluation (Hikosaka and Wurtz, 1989; reviewed by Hikosaka et al., 2000). The specific nuclei that have best been characterized in these respects are the substantial nigra pars reticulata (Hikosaka and Wurtz, 1983c, b, c) and the caudate (Hikosaka & Sakamoto 1989a; 1989b; Kawagoe et al., 1998). The cerebellum (Keller, 1989; reviewed by Voogd and Barmack, 2006) also serves an important role in saccade execution (Takagi et al., 1998) and in the process of tuning saccade amplitude to increase accuracy known as *saccade adaptation* (Optican and Robinson, 1980). Posterior parietal cortex, and in particular the lateral intraparietal area has also received a great deal of interest. Studies have famously concluded that it serves an important role in target selection (reviewed by Colby and Goldberg, 1999), and saccade evaluation (Platt and Glimcher, 1999). However, interesting as these areas are, we will not devote further discussion to them. We will begin our exploration of the oculomotor system with the effectors.

1.4.1 The extraocular muscles

Movements of each eye are controlled by 6 extraocular muscles (reviewed by Goldberg et al., 1991; Sparks, 2002; Krauzlis, 2008). Two muscles, the medial rectus and the lateral rectus, insert rostra-caudally into the nasal and temporal surfaces of the ocular globe respectively. Similarly, the superior and inferior recti insert rostra-caudally in the positions indicated by their respective nomenclature. Finally, the superior and inferior oblique muscles insert temporally in such a way that their fibers run more or less parallel to the ocular equator. For simplicity, consideration of the small translational movements produced by these muscles is usually omitted and the eye is conceptualized as a ball and socket joint with three rotational degrees of freedom. The antagonistic activation of the medial and lateral recti rotate the eye in the horizontal plane producing leftward and rightward movements. Movements produced by the remaining muscles are

more complex since their individual activation produces both vertical and torsional rotation, causing the eye to rotate around its polar axis. The relative amount of vertical and torsional eye movement produced by each of these muscles is dependant, in part, on the position of the eye when the movement is initiated. Thus, to obtain strictly vertical eye movements, combinations of the superior and inferior recti and oblique extraocular muscles must be recruited.

Innervation of the extraocular muscles is provided by 3 cranial nerves. The abducens nerve (cranial nerve VI) innervates the lateral rectus. Excitation of the muscle by cranial nerve VI therefore causes the eye to abduct, or rotate away from midline. The trochlear nerve (cranial nerve IV) innervates the superior oblique muscle which contributes to elevation and torsion of the eye such that the dorsal portion of the globe traverses nasally. The four remaining ocular muscles are innervated by the oculomotor nerve (cranial nerve III). Thus, horizontal, eye movements are initiated by antagonistic innervation from the oculomotor and abducens nerve, while vertical and torsional movements are (roughly) initiated by antagonistic innervation of the oculomotor and trochlear nerve. Oblique eye movements are produced by synergistic combinations of these innervations.

In Chapter 2, I report measurements of extraocular muscle activation during the saccade stop-signal task. To carry out these studies, I relied on EMG measured using EEG electrodes. In most EEG studies, electrical activity associated with eye movements are treated as nuisance artifacts and steps are taken to isolate and remove them (Luck, 2005; Godlove, 2010). One of these artifacts, the saccadic spike potential, is associated primarily with contractions of the lateral rectus muscle (Blinn, 1955; Thickbroom and Mastaglia, 1985). Instead of treating this component as an artifact, I treated the EEG activity as an artifact and developed methods to remove it, isolating the spike potential (see also Keren et al., 2010). As we shall see, activity of the extraocular muscles differs

somewhat from that reported for the skeletal muscles when movements are canceled, and the data verify predictions about eye movements based on the circuitry of the brain stem nuclei that generate saccades.

1.4.2 The brainstem saccade generator

Three brainstem nuclei innervate the extraocular muscles. The oculomotor nucleus is located most rostrally at the level of the SC, the trochlear nucleus is located more caudally at the level of the inferior colliculus, and the abducens nucleus is located most caudally in the pons inferior to the fourth ventricle (Goldberg et al., 1991). Several other brainstem nuclei house neurons important for the production of saccades. These include the rostral interstitial nucleus of the medial longitudinal fasciculus (riMLF), the paramedian pontine reticular formation (PPRF) along with its subdivision the nucleus raphe interpositius (nRIP), the interstitial nucleus of Cajal (NIC), the nucleus prepositus hypoglossi (NPH) and its companion the medial vestibular nucleus (MVN). Together, this collection of nuclei form the brainstem saccade generator (BSG) that performs necessary calculations, initiates, and executes saccadic eye movements.

Saccade-related firing patterns of motor neurons in the oculomotor nuclei consist of a *pulse-slide-step* arrangement (Fuchs and Luschei, 1970; Robinson, 1970; Fuchs et al., 1985; Scudder et al., 2002). During fixation, motor neurons discharge at a constant rate which is dependent on the current position of the eye. Five to 8 ms before a saccade in a given motor neuron's on direction (the contractile direction of the muscle it innervates) the neuron begins to fire a vigorous burst of spikes initiating the *pulse* phase of the discharge pattern. The neuron continues to fire at an elevated level throughout the saccade, but the discharge rate falls off with exponential decay. This period of the firing pattern is referred to as the *slide*. Around 10 ms before the end of the saccade the decay in firing rate asymptotes at a new tonic level proportional to the new eye position.

This final phase of the saccadic firing pattern is called the *step*. Each component of the pulse-slide-step firing profile serves a distinct function in the gaze shift. The initial pulse portion of the discharge provides strong excitation to the extraocular muscle to overcome the viscous drag of the orbital tissue (Sparks, 2002; Porter et al., 2003). The duration of the pulse discharge is directly proportional to the duration of the saccade, the number of spikes generated during the pulse is proportional to saccade amplitude, and the peak firing rate of the pulse is proportional to the peak velocity of the saccade (Fuchs et al., 1985; Sparks, 2002). As the saccade is initiated, the inertia of the eye and its surrounding connective tissue is overcome allowing it to glide more easily, but the slide portion of the saccadic discharge ensures that the eye rotates with an accelerating and then decelerating velocity arc. Finally, the step phase of the firing pattern provides tonic innervation to the extraocular muscle, allowing the new eye position to remain fixed until the next movement is generated. This tonic firing rate is highly linearly correlated with eye position although the slope of the regression line varies from one cell to another and is related to the position at which a cell is first recruited to help maintain ocular rotation, or its *position threshold* (Fuchs et al., 1985).

Neurons innervating the extraocular muscles produce this pulse-slide-step discharge pattern by integrating activity from several upstream neurons; *burst neurons* contribute to the pulse by firing short high frequency spike trains before and during saccades. Burst neurons actually form a broad class of saccade related cells. As their names imply *short lead* burst neurons and *long lead* burst neurons fire in anticipation of saccades with different lead times. Long lead burst neurons serve several different functions, they are thought to be one of the major input pathways to the BSG, and they are less well understood than short lead burst neurons. They are reviewed in depth elsewhere (Fuchs et al., 1985), and will not be discussed in detail here. Short lead burst neurons can be further subdivided based on the type of input they provide to motor

neurons. *Excitatory* burst neurons project monosynaptically to ipsilateral motor neurons where they provide the excitation leading to the initial pulse of muscle contraction. *Inhibitory* burst neurons project monosynaptically to the contralateral motor nuclei in control of muscle antagonists, where they contribute to inhibitory postsynaptic potentials during saccades (Fuchs et al., 1985). *Tonic* neurons contribute to the step by emitting a constant, lower frequency discharge in response to eye position. *Omnidirectional pause neurons* (or simply omnipause neurons OPNs) exert tonic inhibition on contralateral short lead burst neurons (Goldberg et al., 1991). By ceasing to fire when saccades are initiated, they coordinate the activity of burst neurons and thus the action of multiple extraocular muscles to produces accurate saccades. Thus, burst neurons and OPNs instantiate the tension between going and stopping at the level of the brainstem. Together, these neurons form the basic circuitry of the BSG (Fuchs et al., 1985; Goldberg et al., 1991; Scudder et al., 2002; Krauzlis, 2008)

Excitatory and inhibitory burst neurons associated with vertical saccades lie in the riMLF while those associated with horizontal saccades lie in the PPRF (Scudder et al., 2002; Sparks, 2002; Krauzlis, 2008). Tonic neurons in the NPH and MVN provide the step function to the appropriate motor neurons for horizontal saccades, while tonic neurons in the NIC provide steps to the appropriate motor nuclei to control vertical eye movements (Sparks, 2002). OPNs inhabit the nRIP of the PPRF alongside burst cells which initiate horizontal saccades.

The BSG can be conceptualized metaphorically as a function in the mathematical or computer programming sense. It acts as a unitary and largely independent system receiving input (retinal position error commands from the midbrain and cerebral cortex), performing calculations, and issuing output (instructions for coordinated muscle contractions). Inputs from these areas synapse on long lead burst neurons as well as directly on short lead burst neurons and OPNs. In addition to ipsilateral projections to

extraocular muscles, some inhibitory burst neurons in these nuclei project via the medial longitudinal fasciculus to nuclei innervating contralateral extraocular muscles (Hikosaka et al., 1978). This decussation provides a mechanism keeping the eyes tightly yoked during conjugate movements (but see Collewijn et al., 1988; Zhou and King, 1998; Sylvestre et al., 2003). As we shall see in Chapter 2, this property constitutes an important difference between the oculomotor and the spinal motor systems. Under normal circumstances, agonist and antogonist muscles of the oculomotor system are not coactivated precluding this as a viable method for canceling saccades. This circuitry also accounts for the somewhat ballistic nature of saccades (reviewed by Carpenter, 1988; Becker, 1989). The BSG calculates saccade trajectories while the OPNs ensure that gaze remains fixed. Then, all at once, OPNs release their inhibition and allow saccades to be executed in discreet quanta as all or nothing events (Carpenter, 1988).

1.4.3 The superior colliculus

The SC is a laminar midbrain structure lying in an excellent position to integrate sensory input with motor commands (reviewed by Sparks and Hartwich-Young, 1989; Guitton, 1991; Gandhi and Katnani, 2011). The superficial layers of the SC are primary related to visual processing (reviewed by Robinson and McClurkin, 1989). They receive extraretinal projections as well as projections from the ventral lateral geniculate nucleus, striate and extrastriate visual cortices, pre-motor cortex, the parabigeminal nucleus, and the pretectum. Efferents from the superficial layers include projections to pre-motor cortex, the parabigeminal nucleus, the pretectum, the lateral posterior pulvinar, and both the dorsal and ventral lateral geniculate nucleus. The deep layers of the SC exhibit more diverse anatomical conductivity. They receive afferents from many areas involved in visual, auditory, and somatosensory processing as well as areas associated with saccadic eye movements such as the frontal eye fields (FEF see below), and

supplementary eye fields (SEF see below). Efferents from the deep layers project to several thalamic nuclei including the medial dorsal nucleus (MD). This pathway plays a central role in conveying *corollary discharge* signals from SC to cortical structures, allowing fast accurate updating of changing eye positions (Sommer and Wurtz, 2002). The deep layers of SC also project to a wide array of nuclei in the pons, medulla, and mesencephelon including the BSG nuclei discussed above (Benevento and Fallon, 1975; Harting et al., 1980; Huerta et al., 1986; Huerta and Kaas, 1990; Moschovakis et al., 1996). For our purposes, it is important to note that SC projects to OPNs in the nRIP of the PPRF, and that these projections emanate most densely from rostral SC (Gandhi and Keller, 1997; Büttner-Ennever et al., 1999). Rostral SC has been found to project monosynaptically to OPNs while cells in caudal SC project disynaptically to OPNs (Shinoda et al., 2011). The majority of the descending efferents from the deep SC layers project to their targets either contralaterally via the predorsal bundle or tectospinal tract, or ipsilaterally via the tectopontine-bulbar tract. Although there has been some controversy, there is currently general agreement that the deep and superficial layers of the SC share reciprocal projections with each other as well (Sparks and Hartwich-Young, 1989; King, 2004). These connections likely help to mediate the sensorimotor transformation from target to saccade.

Lesion studies have demonstrated that the SC plays an important role in normal saccade production, although this role can be difficult to observe. Initial lesion studies just before and around the turn of the 20th century suggested little or no involvement of the SC in saccadic eye movements (reviewed by Ferrier and Turner, 1901; Sparks and Hartwich-Young, 1989). Neither lesions of SC nor lesions of striate cortex permanently impair monkeys on simple saccade detection tasks, but combined lesions of SC and striate cortex produce profound and irreversible deficits (Mohler and Wurtz, 1977). Similarly, either FEF or SC can be lesioned without significant impairment on a simple

task in which monkeys find, grasp, and feed themselves small pieces of apple. However, simultaneous lesions produced in both of these areas destroy the monkeys' ability to foveate the apple pieces as it reaches for them (Schiller et al., 1979, 1980). This is not to say that the monkey is blinded or that spatial attention has been severely compromised, because lesioned animals still reach for apple slices manually, albeit without making saccades to them.

Neurophysiological recording studies confirm the importance of SC in making saccades. The deep layers of the SC contain cells which respond to auditory, somatosensory, and visual stimuli, as well as multisensory cells which integrate stimuli from multiple modalities (Stein and Meredith, 1993; King, 2004; Stein and Stanford, 2008). In addition, the deep collicular layers contain cells which fire before and during eye movements. Saccade related SC cells respond either with low frequency prelude activity, or high frequency bursts which are more tightly coupled to saccade production, while fixation neurons in the rostral SC fire at a high tonic rate and pause when saccades are made (Munoz and Guitton, 1991; Munoz and Wurtz, 1993a; Munoz and Wurtz, 1993b; Munoz and Wurtz, 1995). Thus, the tension between gaze holding and gaze shifting is apparent in the biological responses of midbrain neurons. (Although there is some controversy concerning the actual role of the rostral SC. See below.) Saccade related neurons may also demonstrate sensory evoked responses and these responses may, in turn, be high frequency bursts tightly coupled with stimulus onset or low frequency firing patterns following the presentation. Sparks & Harwich-Young (1989) review 3 main categories of movement related cell in the SC. One category, *visual motor cells*, contains neurons which show both stimulus and saccade related activity. Another category of neuron, *visually triggered movement cells*, may appear as visual motor cells initially. However, these neurons show saccade related activity that is dependent on visual stimuli; they will not fire action potentials when saccades are

produced in the absence of a visual target. Finally, *saccade related burst neuron* is a term used to describe any cell which reliably demonstrates presaccadic activity in the clear absence of a sensory response. These cells may have long low frequency prelude activity before a saccade, or may show temporally discrete high frequency bursts 18-20 ms before saccade onset.

Saccade related burst neurons form a retinal position error map in deep SC layers. Wurtz and Goldberg (1972) first demonstrated that neurons in the deep layers of SC cells show reliable patterns of discharge before saccade initiation. Robinson (1972; see also Adamük, 1872) stimulated in the deep layers and recording eye movements. He reported that suprathreshold stimulation elicited saccades of an amplitude and velocity which was uniquely determined by the electrode location, and that this motor map showed a “delightful” correspondence with the visuotopic map reported in the superficial layers. Larger amplitude saccades are represented more caudal and saccades with upward trajectory are represented more medial. The medial/lateral dimension shows a smooth, linear transition of saccade angle, while the rostral caudal amplitude map is logarithmic: a larger portion of the map represents small amplitude saccades (Ottes et al., 1986). The saccade vectors elicited by microstimulation are not affected by eye position, and multiple “staircase” saccades are elicited with longer pulses. These observations show that the motor map in SC represents a *retinal position error* frame of reference. Robinson (1972) also noted that simultaneous stimulation of multiple sites elicited saccades which were weighted vector averages of the saccade vectors elicited with individual stimulation. These findings laid the groundwork for vector summation (Georgopoulos et al., 1986) and vector averaging (Lee et al., 1988; Walton et al., 2005) accounts of saccadic generation in the SC. Although the details of these two hypotheses differ (Gandhi and Katnani, 2011), the basic premise remains the same. Individual burst neurons in SC display broad saccade vector tuning curves. A *mound* of

neural activity (usually pictured as a two dimensional Gaussian) occurs in the deep SC leading up to a saccade. Roughly 28% of the total saccade related burst neurons are active in one SC before and during a contralateral saccade (Munoz and Wurtz, 1995). By aggregating the preferred vectors of these widely tuned neurons, precise direction and amplitude signals are conveyed to the BSG.

In considering the effects of SC microstimulation, it is important to note that elicited orienting responses are not limited to the eyes themselves (reviewed by Gandhi and Katnani, 2011). SC stimulation also elicits contractions of the neck muscles leading to orienting of the head in unrestrained animals (Cowie and Robinson, 1994; Corneil et al., 2002), and even movements of the lower body in several species (Hess et al., 1946; Schaefer, 1970; Syka and Radil-Weiss, 1971; Dean et al., 1986; Tehovnik and Yeomans, 1986). In animals with motor systems that make this possible, SC stimulation can elicit orienting of different sensory organs such as pinna movement in monkey, cats, and rodents (McHaffie and Stein, 1982; Cowie and Robinson, 1994), whisker orienting in rodents (McHaffie and Stein, 1982; Hemelt and Keller, 2008), and even vocalization signals used for echolocation in bats (Valentine et al., 2002). Finally, SC stimulation elicits escape responses in freely moving rodents (Dean et al., 1986). Similar findings have been obtained in primates using the $GABA_A$ antagonist bicuculline methiodide (DesJardin et al., 2013). These findings suggest there is still much to learn about this fascinating midbrain structure.

Reversible, chemical inactivation experiments have been particularly useful in elucidating the role of SC in generating saccades. Hikosaka and Wurtz (1985) first used small collicular injections of muscimol and bicuculline to modify saccades of specific trajectories. Reversible inactivation studies later showed that activity in SC is not strictly motor related, but that SC neurons participate in a target selection process. Reversible inactivation of a small portion of caudal SC does not lead to motor deficits *per se* but

produces selection errors during visual search when targets fall within the response field of the inactivated neurons (McPeek and Keller, 2004). Inactivation has also been critical in the study of rostral SC function. The classic view since Robinson's (1972) microstimulation experiments held that neurons in SC formed a continuous map of saccade amplitude down to the smallest saccades in the rostral pole. In a later series of studies, Munoz and Wurtz (1993a;1993b) challenged this view by showing that rostral SC contains neurons that are involved in gaze holding rather than gaze shifting. After recording from the rostral pole and describing neurons that fired briskly during fixation, they inactivated the rostral SC. They demonstrated that monkeys make more saccades and are impaired in fixation after inactivation of neurons in this region. However, these results have since become controversial. Krauzlis and colleagues have hypothesized that the classic view of Robinson is correct, and that neurons in the rostral pole of SC represents microsaccades. Supporting this view, these authors recorded neurons in the rostral pole that fire in advance of microsaccades (Hafed et al., 2009). It should be noted that Munoz and Wurtz (1993a) also observed many neurons in rostral SC that fired in advance of saccades, but they reported another smaller population that did not fire in advance of any recorded saccades. They may have overlooked these responses because their techniques were inadequate to detect microsaccades. However, it is also possible that Krauzlis and colleagues excluded neurons that did not show saccade related activity (i.e. fixation neurons) since their inclusion criteria for that study required that neurons show prelude activity before saccades (Hafed et al., 2009). Nevertheless, another discrepancy exists. Krauzlis and colleagues have also performed inactivation studies in rostral SC and have not reported any deficits in fixation behavior (Hafed et al., 2008; Hafed et al., 2009; Hafed and Krauzlis, 2012). In fact, they propose that fixation was more stabile after inactivation since the number of microsaccades they recorded

was decreased (Hafed et al., 2009; Hafed and Krauzlis, 2012). What are we to make of these conflicting reports?

Based in part on the observation that inactivation in rostral SC induces stabile eye position offsets while monkeys track an inferred target with smooth pursuit movements, Krauzis and colleagues have proposed the following model of rostral SC function (Hafed et al., 2008; Hafed et al., 2009; Hafed and Krauzlis, 2012; see also Engbert, 2012). Consistent with the classic view, neurons are thought to form a continuous map of saccade amplitude down to the smallest microsaccades in the rostral SC. Fixation is achieved when neural activity is balanced across the collicular map. Whenever the center of mass of neural activity deviates by some (yet to be determined) threshold, a microsaccade is produced. As noted above, microsaccades are often made in the direction of peripheral attention. The microsaccade hypothesis of rostral SC explains this interesting phenomenon by suggesting that peripheral attention causes subthreshold activation at the corresponding location in rostral SC (Kustov and Robinson, 1995; Bergeron et al., 2003), and this causes the collicular activity map to become unbalanced. As we shall see in Chapter 3, this model makes specific predictions about the pattern of microsaccades that should be observed when large overt saccades are canceled in the stop-signal task. Interestingly these predictions are not borne out in the data, suggesting a method of fixation other than balanced neural activity in SC.

We will now turn our attention to the cortical control of saccadic eye movements with special emphasis on areas anterior of the central sulcus. In macaque monkeys, eye movements are elicited by low-current, electrical stimulation of at least three areas of frontal and medial frontal cortex; the FEF (Bruce et al., 1985), SEF (Schlag and Schlag-Rey, 1987) and the rostral cingulate motor area of the anterior cingulate cortex (ACC) (Mitz and Wise, 1987). The first of these areas to be discovered was FEF.

1.4.4 Frontal eye field

In monkeys, FEF is located in dorso-lateral prefrontal cortex in the rostral bank and the fundus of the arcuate sulcus (Bruce and Goldberg, 1985; Bruce et al., 1985). The location of the human homologue shows some variability between subjects which is more pronounced in the medial/lateral dimension, but is usually located either in or near the precentral sulcus or in the fundus of the caudal superior frontal sulcus (Paus, 1996; Curtis, 2006; Neggers et al., 2007). FEF is densely connected with subcortical and cortical visual and oculomotor areas. FEF projects to the SC, with especially dense projections to the deep layers. FEF and SC also demonstrate similar subcortical projection patterns. FEF projects to the pretectum and many nuclei of the BSG, including the nRIP of the PPRF that contains OPNs (Schnyder et al., 1985; Huerta et al., 1986; Stanton et al., 1988; Segraves, 1992). FEF also shares a reciprocal projection with MD, allowing it to receive corollary discharge signals from SC (Huerta et al., 1986). Cortically, FEF demonstrates extensive billateral connections with adjacent areas of frontal cortex including the supplementary motor areas, pre-supplementary motor area, SEF, and periprincipal prefrontal cortex (Huerta et al., 1987). In addition, FEF shows bilateral projections with many areas of extrastriate cortex such as visual area 4 (V4), the superior temporal sulcus, and the lateral intraparietal area (LIP). Interestingly, these projections show topographical specificity such that ventral stream areas and areas representing foveal locations tend to connect with ventrolateral FEF, while dorsal stream areas, areas representing peripheral space, and areas showing auditory and multimodal responses tend to connect with dorsomedial FEF (Schall et al., 1995; Stanton et al., 1995; Bullier et al., 1996). Since neurons in the inferior, ventrolateral limb of the arcuate sulcus tend to encode saccades of smaller amplitude, while neurons in the superior dorsomedial limb of the arcuate tend to encode saccades of larger amplitude (Robinson

and Fuchs, 1969; Bruce and Goldberg, 1985; Bruce et al., 1985; Stanton et al., 1989; Schall et al., 1993), these projection patterns suggest a topographical and functional segregation of saccades for object identification and exploration vs. target localization and orienting in FEF.

Electrical microstimulation studies have long shown that areas in and around the arcuate sulcus are associated with saccades. In classic experiments Ferrier (1875) mapped the cerebral cortex of anesthetized monkeys. In all 10 of the monkeys tested, Ferrier noted that microstimulation of a large area in prefrontal cortex produced contralateral saccades and head movements, opening of the eyelids and lifting of the brow, and pupil dilation of both eyes. Other classic work replicated and extended these findings (Mott and Schaefer, 1890; Levinsohn, 1909). As microstimulation techniques were refined and frontal cortex was mapped with greater precision, the area that we now call FEF grew progressively smaller (reviewed by Schlag and Schlag-Rey, 1987). We now know that the original area studied by Ferrier using relatively large epicortical stimulating electrodes probably included not only FEF, but also SEF (see below).

Several attributes of microstimulation in FEF are very similar to microstimulation in SC. For instance, stimulation of a particular location in FEF produces fixed vector saccades and prolonged stimulation elicits “staircased” saccadic eye movements (Robinson and Fuchs, 1969). This suggests that FEF also encodes saccades in retinal position error coordinates. As in SC, stimulation of FEF produces generalized orienting responses including contractions of the neck muscles (Tu and Keating, 2000; Elsley et al., 2007; Knight and Fuchs, 2007). Also similar to SC, FEF contains a map of saccade amplitude, although this representation is much more course that it is in SC (Robinson and Fuchs, 1969; Bruce and Goldberg, 1985; Bruce et al., 1985; Stanton et al., 1989; Schall et al., 1993).

Lesion studies further elucidate the role of FEF in eliciting saccades. As stated above, selective lesions of both SC and FEF are needed to produce profound deficits in orienting responses and saccadic eye movements (Schiller et al., 1979). These findings suggest similarity and redundancy between FEF and SC, positioning them as principle players in a distributed network for saccade production. In addition to projection patterns and effects of lesion studies, FEF and SC share many similarities in neural responses and in proposed functional roles.

Seminal studies of response properties of single neurons in FEF identify several different cell types (Bruce and Goldberg, 1985; Schall, 1991b). These are commonly categorized as *visual* cells, *movement* cells, and *visual/movement* (or *vis-mov*) cells. Differences between these neuron types can be observed using a delayed- or memory-guided saccade task (Hikosaka and Wurtz, 1983a). Visual cells respond to stimuli within their receptive fields regardless of whether or not saccades are made toward these locations. Movement cells increase activity before and during saccades made into their response fields regardless of whether these saccades are made under visual guidance. Vis-mov cells respond both to visual stimuli and before and during saccades made in the directions of these stimuli. These are an interesting class of neuron, and recent functional (Ray et al., 2009) and biophysical (Cohen et al., 2009) evidence suggests that they may be fundamentally different than the other cell types listed above. Visual cells have been recorded from both supra- and infra-granular layers (Thompson et al., 1996). Pyramidal neurons that project to subcortical structures are found in infragranular layers, and particularly in layer V (Segraves and Goldberg, 1987; Segraves, 1992; Sommer and Wurtz, 2002),while cells that project to extrastriate cortex tend to originate in superficial layers (Pouget et al., 2005). As a side note, it is worth mentioning that that only about 54% of neurons in FEF show visual or movement related responses, and some types of neural responses have received little attention. For instance, although it is rarely noted,

some FEF neurons respond to auditory stimuli (Schall, 1991b). These considerations leave open the possibility that there are other important functions carried out by FEF that have not yet been identified and studied.

Neurons that are best described as fixation cells have also been identified in FEF (Hanes et al., 1998; Izawa et al., 2009). As in SC, these neurons fire at a high tonic rate, pause before and during eye movements, and increase activity when planned saccades are canceled. Thus, the tension between stopping and going is instantiated physiologically at the cortical level as well. Fixation cells are more rarely reported in the literature than visual and movement cells, and, anecdotally, they are more difficult to locate and record. At least one group reports that fixation cells are primarily concentrated near the center of FEF in the middle saccade amplitude range (Izawa et al., 2009). Although it has been proposed that fixation cells in SC actually encode microsaccades, no such proposal has been made concerning fixation cells in FEF.

FEF's primary role in the oculomotor system appears to be one of target selection. In addition to encoding the location of visual stimuli and upcoming eye movements, neurons in FEF encode the location of spatial attention. Neurons in FEF select behaviorally relevant targets from distracters(Schall and Hanes, 1993; Schall, 1995). Activity related to spatial attention can be dissociated from simple motor preparation in FEF (Sato et al., 2001; Juan et al., 2004; Schall, 2004; Schafer and Moore, 2011). From a computational standpoint, decision making has long been modeled as a process that integrates information over time accumulating activity toward a threshold (e.g. Nosofsky and Palmeri, 1997; Ratcliff and Rouder, 1998; Usher and McClelland, 2001; Bogacz et al., 2006). Recent work shows that visual neurons in FEF sample perceptual information and movement neurons integrate this activity toward a threshold (Hanes and Schall, 1996; Purcell et al., 2010; Purcell et al., 2012b; Schall et al., 2012). Thus, FEF instantiates a decision making process concerning which

upcoming stimuli to foveate. Target selection is the subject of a vast, active field of research. But it falls outside of the purview of this dissertation, which is concerned with saccade execution and evaluation and will therefore not be reviewed in detail.

1.4.5 Movement cells, fixation cells and Logan's race model

Now that we have discussed some basic elements of the oculomotor system, we may revisit the saccade-response variant of the stop-signal task (Hanes and Schall, 1995; Hanes and Carpenter, 1999). By training macaque monkeys to perform the saccade countermanding task, and recording responses of single neurons in SEF and SC, clear mechanistic explanations of saccade execution and inhibition in the oculomotor system have been obtained (Hanes et al., 1998; Paré and Hanes, 2003; Brown et al., 2008; Schall and Godlove, 2012; see also Kornylo et al., 2003). Two criteria must be met for neurons to participate in executing eye movements. First, neurons must discharge differently when movements are initiated or withheld; if neurons still discharge when movements are canceled, their activity was not affected by the stop process. Second, the differential modulation on canceled trials must occur before SSRT; otherwise, the neural modulation happens after the movement has already been canceled. Movement cells and fixation cells in FEF and SC satisfy these two criteria. After the target appears, movement-related activity begins to grow toward a threshold that triggers response initiation (Hanes and Schall, 1996). If the activity reaches threshold, a response is produced regardless of whether a stop-signal was presented. However, responses are canceled when the movement-related activity is inhibited so that it does not reach the threshold activation level. The source of this inhibition is a signal such as that conveyed by fixation neurons in FEF and SC. Crucially, the pronounced modulation of fixation- and movement-related activity precedes SSRT.

It is tempting to hypothesize that movement and fixation neurons are a literal, biological instantiation Logan's race model. But the central assumption that finish times of the GO and STOP processes must be independent complicates this interpretation (Logan and Cowan, 1984). If circuits that instantiate the race model consist of interacting neurons, how can they produce behavior that can be described mathematically by a model consisting of independent processes? This paradox has been resolved through another model consisting of a network of interacting GO and STOP units with randomly accumulating activation (Boucher et al., 2007a; see also Wong-Lin et al., 2010). This model fits performance data and replicates neural data if and only if the STOP unit inhibits the GO unit in a delayed and potent fashion. Thus, a neurally plausible mechanism of interaction is the only way that the model naturally fits behavior. This interactive race model has since been extended to a network of biophysically realistic spiking neurons (Lo et al., 2009). Thus, the race model has afforded precise description at multiple levels, both neural and behavioral, during the stop-signal task. This rare coordination between psychophysics, formal mathematical modeling, and neurophysiology establishes a clear linking proposition between the GO and STOP processes of the race model and gaze-shifting and gaze-holding neurons in the ocular motor circuit.

These gains were made possible by studying the physiological basis of response inhibition in the oculomotor system. It is obviously of great interest to know whether these findings generalize to the skeletal motor system since most stop-signal experiments test manual responses. To investigate the generality of stopping mechanisms across effectors, Boucher et al., (2007b) tested whether human subjects could stop eye and hand movements independently. SSRTs were longer for hand movements than for eye movements, and advanced knowledge of which effector to stop did not confer any stopping advantage. This study shows that there must be some

independence between the processes which stop eye and hand movements (see also Logan and Irwin, 2000). Additional evidence for differences between effectors comes from studies examining the fine dynamics of movements on stop trials. In a series of classic studies, De Jong and colleagues (1990, 1995) attempted to determine the stages of preparation during which responses can be canceled. They found that stop-signals sometimes result in partial responses (defined as subthreshold squeezes of a dynamometer) or partial EMG in the absence of an overt detectable response. These results indicate that manual responses can be canceled at any stage of preparation up to and including the initiation of the response itself. Several other groups have also reported partial muscle activation when overt manual responses are canceled (McGarry and Franks, 1997; McGarry et al., 2000; van Boxtel et al., 2001; Scangos and Stuphorn, 2010) and one group has reported reduced response force on noncanceled trials (Ko and Miller, 2011). Similarly, when combined eye and head gaze shifts are canceled, neck muscles are often active (Corneil and Elsley, 2005; Goonetilleke et al., 2010). At least one group has reported that average saccade amplitude is similarly decreased on errant noncanceled trials, suggesting that some saccades may be canceled at the latest stages of execution and truncated in midflight (Colonius et al., 2001; Ozyurt et al., 2003; Akerfelt et al., 2006). However, these results differ from the original saccade stop-signal report of Hanes and Schall (1995) in which no amplitude differences were found between no-stop and noncanceled trials. There is reason to believe that saccades are fundamentally different from manual responses and cannot be canceled at such a late stage of execution. Saccades are thought to be programmed in advance and triggered as ballistic units (Carpenter, 1988; Becker, 1989). And, owing to the circuitry of the brainstem saccade generator covered above, it should be nearly impossible to cancel saccades by coactivating agonist and antagonist muscles (Hikosaka et al., 1978; Scudder et al., 2002; Sparks, 2002). I will revisit these questions in Chapter 2 where I

present EMG measurements of the extraocular muscles during the saccade countermanding task. For now, we turn our attention back to the elements of the oculomotor system.

1.4.6 Supplementary eye field

In monkeys, SEF is located on the dorsal surface of medial frontal cortex in a slight depression known as the dorsal-medial convexity. It is a small patch of cortex (~9 mm^2) situated at roughly the same position anterior or slightly rostral to the most anterior aspect of the superior limb of the arcuate sulcus 4 or 5 mm lateral of midline. The human homologue of SEF probably lies within the medial wall in the upper part of the paracentral sulcus (Grosbras et al., 1999; Neggers et al., 2012). Like FEF, the projection patterns of SEF position it as an important structure in the oculomotor circuit. Subcortically, SEF is connected to several visual nuclei of the thalamus including MD. It also projects to subcortical oculomotor structures, including the deep layers of SC and several nuclei of the BSG including the riMLF and the nRIP of the PPRF (Shook et al., 1988; Huerta and Kaas, 1990; Shook et al., 1990). Cortically, SEF is reciprocally connected with the surrounding areas of frontal and medial cortex, including FEF, ACC, and the supplementary (SMA) and pre-supplementary (pre-SMA) motor areas (Huerta and Kaas, 1990; Bates and Goldman-Rakic, 1993; Schall et al., 1993; Stanton et al., 1993; Luppino et al., 2003) Stanton et al., 1993; Luppino et al., 2003). It receives visual input from many areas of extrastriate cortex, both in the ventral stream along the ventral extent of the superior temporal sulcus, and in the dorsal stream including area LIP, area 6a, area 7a, and the medial superior temporal area (Barbas and Pandya, 1987; Huerta and Kaas, 1990; Shipp et al., 1998). Notably, the cytoarchitecture of SEF differs from that of most other cortical areas. SEF, like many areas of motor cortex, is agranular, meaning that it lacks a granular layer IV. This is particularly interesting, because it

means that the microciruitry of SEF may differ from that of other cortical areas. The canonical microcircuit that is used as a model for every area of cortex depends critically on granular layer IV which is thought to receive ascending thalamic and cortical input (reviewed below). Afferents from extrastriate cortex tend to terminate in layers III and V of SEF, while afferents from FEF terminate in all layers (Barbas and Pandya, 1987; Huerta and Kaas, 1990; Schall et al., 1993; Stanton et al., 1993; Maioli et al., 1998; Shipp et al., 1998). How may microcircuitry in SEF differ from the canonical cortical microcircuit? I examine this issue in detail using laminar recordings from SEF in Chapters 4 and 6, and we will return to this issue below after introducing SEF in more detail.

As with FEF, SEF was first identified and characterized using electrical microstimulation (Schlag and Schlag-Rey, 1987; Schall, 1991a). However, unlike saccades elicited with FEF and SC stimulation, the trajectories of saccades elicited during SEF stimulation often depend critically on eye position. At most locations within SEF, stimulation elicits convergent saccades, in head, body, or external space centered coordinates (Schlag and Schlag-Rey, 1987; Schall, 1991a; Tehovnik and Lee, 1993; Tehovnik et al., 1998; Martinez-Trujillo et al., 2004; but see Russo and Bruce, 1993,1996). Also unlike FEF stimulation, prolonged stimulation in SEF does not lead to repetitive saccades resembling the fast phase of nystagmus. Instead, the eyes tend to converge on a single point and then to remain fixed for as long as stimulation continues (Schall, 1991a; Tehovnik and Lee, 1993; Tehovnik et al., 1994). The behavioral state of the subject also plays an important role in determining whether or not saccades will be elicited with SEF stimulation of a given threshold (Mann et al., 1988; Russo and Bruce, 1993; Fujii et al., 1995). While one can often locate sites in FEF and SC where stimulation will cause subjects to break fixation and make fixed vector saccades, it is difficult to locate sites in SEF that will cause subjects to break active fixation and

stimulation is often delivered in the absence of a visible fixation point (e.g. Tehovnik et al., 1999; Martinez-Trujillo et al., 2004). Intriguingly, stimulation delivered below the threshold for evoking saccades has been shown to elicit context-specific improvements in task performance which may take the form of either increases or decreases in saccade reaction times (Stuphorn and Schall, 2006). These findings provide valuable clues as to the role of SEF in saccade execution and evaluation.

Like FEF and SC, SEF contains neurons that are responsive to visual stimuli, and neurons that increase activity before and during saccades (Schlag and Schlag-Rey, 1987; Bon and Lucchetti, 1991; Schall, 1991a; Bon and Lucchetti, 1992; Hanes et al., 1995; Russo and Bruce, 2000). Some have also suggested that SEF contains fixation neurons, (Schlag et al., 1992; Lee and Tehovnik, 1995), but these neurons differ from those that fire tonically between saccades in FEF and SC; they are probably more closely related to anticipation of reward when monkeys are given incentive to fixate. There does exist a class of neuron in SEF that increase firing during the stop-signal task when saccades are actively canceled. But tests with the stop-signal paradigm have produced unambiguous results; unlike FEF and SC, the majority of neurons in SEF modulate too late during the stop-signal task to play a direct role in executing or withholding saccades (Stuphorn et al., 2000; Stuphorn et al., 2010). At least one report may contradict this finding. Isoda and Hikosaka (2007) recorded from an area of pre-SMA that showed saccade related activity and may therefore have included neurons from SEF. One of the tasks that monkeys performed in this study was a go/nogo task. This task resembles a stop-signal task with SSD = 0, but lacks a well-defined behavioral measure comparable to SSRT. These researchers identified some neurons in pre-SAM with increased activity on successful no-go trials that look very similar to those identified by Stuphorn and colleagues (2000; 2010) which increase activity on canceled trials. However, whereas activity in SEF modulated too late to contribute to response inhibition

in the stop-signal task, the modulation of neurons in pre-SMA (and perhaps SEF) did occur within the transition between error and correct response times during the go/nogo paradigm (Isoda and Hikosaka, 2007). Isoda and Hikosaka took this as evidence that the neurons they recorded modulated early enough to affect behavior on the current trial. Notwithstanding the high degree of experimental expertise evident in this study, it is not clear if the transition between error and correct RT distributions in the go/nogo task should be taken as a reflection of the time needed to cancel action. Further research is needed to resolve this potential ambiguity, but for now, SEF appears to modulate too late to be directly involved in saccade execution.

If SEF does not play a direct part in saccade execution, what is its role in the oculomotor system? Many different theories have been advanced. Upon verifying SEF as an eye field independent of FEF, Schlag and Schlag-Rey (1987) initially hypothesized that these areas may be important for *fixed-vector* and *goal-directed* or *self-initated* saccades respectively. These hypotheses were based in part on the observation that SEF neurons were active when monkeys made saccades in total darkness. However, in order to encourage monkeys to make saccades in darkness, these researchers periodically illuminated targets at random intervals and locations. Monkeys were then rewarded for quickly foveating these targets. Hence, monkeys were not eliciting spontaneous saccades in these studies, but were actively searching for targets in anticipation of reward. Later work showed that SEF neurons are poorly activated when animals generate truly spontaneous saccades in darkness (Schall, 1991a). I will revisit these hypotheses and provide new data in Chapter 4. Further evidence that SEF may be important for generating voluntary saccades (as opposed to the involuntary saccades often described as *ocular grasp reflexes*) comes from studies using the antisaccade task. In this task, subjects are instructed to make saccades to locations diametrically opposite of visible targets (reviewed by Munoz and Everling, 2004). Several studies

suggest that SEF neurons fire at a higher rate for antisaccades than for prosaccades (made to visible targets), and that this activity scales with the probability of successfully completing an antisaccade (Schlag-Rey et al., 1997; Amador et al., 2004). But it is difficult to evaluate whether these neural responses are specific to the antisaccade *per se* since generating an antisaccade is a complex behavior made up of several components including the suppression of a prosaccade to the visible target. An obvious suggestion is that SEF may contribute to target selection by representing salience, but recent work shows that this is not the case (Purcell et al., 2012a). The converging saccade trajectories elicited by microstimulation of SEF lead naturally to the idea that this area is important for transforming object-centered, space-centered, or head-centered reference frames into eye-centered coordinate systems (Schall et al., 1993; Olson and Gettner, 1999; Martinez-Trujillo et al., 2004; Moorman and Olson, 2007). In analogy to the complex patterns of movements elicited by long trains of microstimulation in SMA and pre-SMA, some have proposed that SEF encodes and tracks the ordinal position of learned sequences of eye movements (Isoda and Tanji, 2002; Lu et al., 2002; Isoda and Tanji, 2003; Berdyyeva and Olson, 2009). A related hypothesis is that SEF encodes the passage of time in a more general sense (Ohmae et al., 2008). Or it may be the argued that SEF is involved in maintaining the current task set (Tremblay et al., 2002; Kim et al., 2005; Yang et al., 2010; Heinen et al., 2011) or in updating stimulus reward mappings(Chen and Wise, 1995a, b, 1996). How can we distinguish between these alternatives? Is it possible that SEF is carrying out all of these functions? Are there common traits between these studies that lead to common activation of SEF during all of these tasks?

Instead of playing a direct role in saccade execution, neurons in SEF may be involved in some aspect of saccade evaluation. Indeed, in almost all of the studies mentioned above, highly trained monkeys performed tasks that required ongoing

behavioral evaluation in order to obtain appetitive rewards. Perhaps the common thread of performance monitoring unites these seemingly disparate findings. Interestingly, SEF exhibits pre- and post-saccadic activity related to evaluating the outcome of a saccade. For instance, neurons and local field potentials (LFPs) in SEF show elevated activity when subjects commit errors (Stuphorn et al., 2000; Emeric et al., 2010; Purcell et al., 2012a). SEF also shows activity in anticipation of, during, and after the delivery of reward when saccades are performed successfully or in the absence of reward when errant saccades are committed (Amador et al., 2000; Stuphorn et al., 2000; Roesch and Olson, 2003; Seo and Lee, 2009; So and Stuphorn, 2010). As mentioned above, some neurons in SEF respond preferentially when planned saccades are canceled, but they modulate too late to play a direct role in countermanding the movements. These neurons are thought to encode the degree of *response conflict* present on canceled trials (see below). Consistent with this hypothesis, their activity and the amplitude of LFPs in SEF is positively correlated with the probability of committing an error on these trials (Olson and Gettner, 2002; Emeric et al., 2010; So and Stuphorn, 2010; but see Nakamura et al., 2005). Error detection, reward prediction, and conflict monitoring are all proposed mechanisms for performance monitoring (reviewed below). Thus, the observation of these signals in SEF lead to the hypothesis that this area participates in performance monitoring of saccadic eye movements (reviewed by Schall et al., 2002; Schall and Boucher, 2007; Schall and Godlove, 2012). Careful reading of the original description of the SEF reveals mention of reinforcement related cells, and cells which discharged rhythmically when the animal licked juice reward from a spout (Schlag and Schlag-Rey, 1987). Moreover, many of the wide ranging findings from SEF detailed above can be explained in terms of performance monitoring.

Monitoring one's performance is only useful insomuch as one is able to modulate subsequent behavior. Does SEF also play a direct role in influencing oculomotor

behavior (reviewed by Stuphorn and Emeric, 2012)? To date, findings have been mixed. As mentioned above, sub-threshold microstimulation of SEF has been shown to decrease RTs when subjects make simple visually guided saccades but to increase RTs and overall accuracy in the context of the stop-signal tasks (Stuphorn and Schall, 2006). In agreement with this finding, individual neurons in SEF show both positive and negative correlations with post-error RT and accuracy within a variety of trial epochs in the stop-signal task (Stuphorn et al., 2010). However, LFPs fail to show an analogous amplitude differences that correlates with post-error adjustments (Emeric et al., 2010). Another study failed to find any differences in neural responses when executive control was exerted after errors to overcome prepotent responses engendered through priming (Purcell et al., 2012a). Thus, it is unclear whether SEF directly contributes to performance adjustments, or whether it simply monitors performance. It has been hypothesized that error-related activity in SEF may contribute to the *error-related negativity* (ERN), an event-related potential that reflects performance monitoring and is often recorded in human (see below). Much progress could be gained by establishing a clear link between activity in SEF and the ERN. On the one hand, the study of SEF could be greatly facilitated by the wealth of data that has been collected concerning the human ERN. On the other hand, investigation of the ERN could be facilitated greatly with the establishment of a clear animal model and the wealth of data that has been accumulated in SEF. In Chapters 5 and chapters 6, I report studies to establish just such a link by demonstrating a monkey homologue of the ERN, and showing that local current flow in SEF measured using the *current source density* (CSD) is predictive of ERN amplitude. Below, I will introduce ACC which has also been implicated in evaluating saccadic eye movements and follow with a more general discussion of performance monitoring framed by the ERN. But first, let us briefly turn our attention back to microcircuiry and the agranular structure of SEF.

It has long been thought that the cortex is made up of repeating elementary units. Today, this idea is encapselated by the phrase *canonical cortical microcircuit* meaning that a single recognizable pattern of interlaminar and interareal projection patterns can be found wherever one looks in cerebral cortex. This view has its roots in anatomical studies of cortical columns, so we will begin by briefly reviewing this literature.

In classic experiments using Golgi stain to visualize neurons in rat barrel fields, Lorente de Nó (1949) found connections between neurons arranged as vertical chains, leading him to conclude that information transmission between neurons occurs primarily within vertical columns. Although later work (e.g. Szentagothai, 1978) established the existence of widespread horizontal connections, the columnar view of cortical processing quickly became established. It soon drew physiological support from Mountcastle's classic recordings in somatosensory cortex (1957; Powell and Mountcastle, 1959) and Hubel and Wiesel's work in V1 (1962, 1965). Ultimately, these experiments culminated in the theory that columns are the fundamental unit of cortical processing (Hubel and Wiesel, 1972; Szentagothai, 1978), and that a ubiquitous canonical cortical microcircuit is repeated across all neocortical areas (Gilbert, 1983). This view, that neocortex is functionally homogeneous, became popular partially in reaction against the cytoarchitectonic studies of the day that sought to parse cortex into ever finer anatomical detail (Creutzfeldt, 1977; Szentagothai, 1978; Rockel et al., 1980). Nevertheless, this framework of columnar processing within canonical cortical microcircuits remains the standard simplifying assumption used to reduce and discern the vast complexities of the cerebral cortex (Mountcastle, 1997; Silberberg et al., 2002; Thomson et al., 2002; Douglas and Martin, 2004; Bastos et al., 2012), and it underlies some of most financially ambitious and computationally intensive neuroscientific research endeavors ever attempted (reviewed by Markram, 2006; de Garis et al., 2012).

However, the columnar view of cerebral cortex has been increasingly challenged in recent years, since anatomy shows great variation across neocortex both within and across species (Elston, 2000; Collins et al., 2010), since the concept of a cortical column is loosely defined and is used by various authors to describe very different anatomical and physiological phenomena (Jones, 2000; Rockland and Ichinohe, 2004; Rockland, 2009; De Felipe et al., 2012), and since columns themselves may be epiphenomenal having little or no functional significance (for review see Horton and Adams, 2005). It is ironic that the first evidence for a cortical column was derived by Lorente de Nó from rat barrel field (which he incorrectly guessed to be auditory cortex). This irony stems from the fact that barrels themselves are probably not credible examples of columns. The area surrounding a whisker on a rat's nose happens to be round. According, the cortical representation of this somatosensory region that is revealed using stains for cytochrome oxidase also happens to be round. But referring to a barrel as a column is similar to referring to a digit representation in macaque somatosensory cortex as a column. Barrels are much larger and functionally quite different from the types of columns identified neurophysiologically in early sensory cortex of monkeys. According to Hubel and Weisel

> *"Whether [barrels] should be considered columns seems a matter of taste and semantics."*
>
> *-Hubel and Wiesel 1974*

This confusion becomes a major cause for concern when we consider its implications for the Blue Brain project (Markram, 2006). The core assumptions underlying this billion dollar project to simulate a mammalian brain are that 1) the rat barrel field is a cortical column, 2) it is identical in all important functional aspect to the columns found in humans and other mammals, 3) columns and cortical microcircuits are interchangeable, and 4) by simulating hundreds of thousands or millions of barrel fields interacting with

one another one will therefore be able to simulate a rat, monkey, or human brain. On the other hand, some researchers have taken the view canonical cortical microcircuits are best described functionally, may have no clear anatomical correlate, and that these circuits transcend and exist independently of columns (da Costa and Martin, 2010). I will adopt this view for the remainder of our this dissertation.

Virtually all of our current ideas about canonical cortical microcircuits are derived from neurophysiological recordings in early sensory cortex like primary visual and primary somatosensory cortex. Granular layer IV, which is prominent in early sensory cortex plays an important role in this model as the key terminal for ascending projections. But, as mentioned above, SEF does not have a granular layer IV, and virtually nothing is known about the microcircuitry of this, or any other area of neocortex outside of early sensory areas. CSD is a powerful tool for gaining insight about cortical microcircuitry, and it also has not been recorded in any area of frontal or prefrontal cortex. Therefore, before carrying out the CSD recordings and analysis described in Chapter 6 to provide a clear link between SEF and the ERN, I carried out a preliminary set of CSD experiments detailed in Chapter 4 using CSD to characterize the intrisic microcircuitry of SEF under the same conditions that have been used to characterize microcircuitry in early visual cortex using CSD recorindgs in the past (Schroeder et al., 1998; Maier et al., 2010). This set of experiments serves 3 functions. First, it provides, foundational data about the structure and function of SEF. Second it provides the first evidence that the canonical cortical microcircuit model has validity outside of primary sensory cortex. And finally, it shows that reasonable CSD can be recorded from agranular frontal cortex, paving the way for additional CSD recordings testing functional responses in Chapter 6. But the details of these studies can wait for their appropriate chapters. For now, let us turn our attention back to the role of medial frontal cortex in evaluating eye movements.

1.4.7 Anterior cingulate cortex

In his classic studies, Broca (1861) identified ACC as the most dorsal region of what he termed the *limbic lobe*, which he presumed to be involove primarily in olfaction. Later authors identified these regions with emotional experience (Papez, 1937; reviewed by Allman et al., 2001). The word *cingulate* derives from the Latin word *cingulum* meaning "belt". This adjective is apt because the cingulate cortex traverses the medial wall wrapping around and partially encircling the dorsal aspect of the *corpos collosum*. In monkeys the anatomy of cingulate cortex is fairly similar from one animal to the next. In humans the anatomy is more variable; some subjects exhibit a second, paracingulate sulcus appearing dorsal to the cingulate proper. The presence or absence of this feature forms a continuum across subjects.

Before discussing the role that ACC plays in evaluating saccades, it is helpful to say several words concerning its anatomy. In comparison to the other areas covered thus far, our discussion of cingulate cortex is somewhat complicated by the fact that this is not one homogeneous area but instead contains many sub-regions. Both anatomically, and functionally, the cingulate cortex is also somewhat less well understood than the areas discussed above. In both the human and monkey brain, Brodmann (1909) recognized a clear distinction between anterior and posterior cingulate cortices. In the latter (area 23) Brodmann noted a clear granular layer IV, while the former (area 24) appeared agranular (see also Walker, 1940). In human tissue, Brodmann also identified dorsal divisions of both posterior (area 31) and anterior (area 32) cingulate cortex, as well as separate areas anterior to the genu of the corpos collosum (area 33) and ventral to the genu (area 25). In the monkey, Brodmann identified only 3 subdivisions; posterior (area 23) anterior (area 24), and pregenual (area 32). Matelli and colleagues (1991) further subdivided area 24 into several

cytoarchitecturally distinct subregions (see also von Economo and Parker, 1929). In the ventral to dorsal direction, they identified areas 24a, 24b, and 24c. They also described a fourth subdivision, 24d, caudal to 24c based on the presence of large pyramidal cells. Vogt (1993) proposed a separate parcellation in the rosto-caudal dimension of an anterior area 24 and a posterior area 24' based on cytoarchitectural and connectivity differences between the two areas. Vogt and colleagues later proposed similar divisions in the human brain with the addition of area 32' which forms a transitional area between frontal cortex and area 24 (Vogt et al., 1995). In later work, this group incorporated the divisions proposed by Matelli and colleagues noting in particular that area 24d can be distinguished anatomically from area 24c' and that earlier work may have conflated these areas (Vogt et al., 2005).

Because of its many sub-regions, it is difficult to elaborate possible homologies between human and monkey ACC. In Brodmann's original description (1909), he maintained that the human subgenual area 25 had no homologue in the old world monkey. This is an intuitively appealing assertion, since it is typically the rostral areas of cortex that have undergone the most evolutionary development in humans. In contrast, Vogt and colleagues (1995, 2005) suggested that there are four main ways in which human and macaque cingulate cortex differ; (1) the presence of a callosal sulcus contributing to the deep extent of cingulate cortex in humans, (2) the rostocaudal extant of the 24' areas which are larger in humans, (3) a large and folded transitional region between posterior cingulate and parietal cortex that is only present in humans, and (4) the presence of transitional region 32' between frontal cortex and areas 24/24' in humans which is lacking in monkeys. This last feature is especially important for our discussion. As we shall see below, some have suggested that this distinction is key for resolving perceived differences between human and monkey neurophysiological findings. In sum, ACC is actually a conglomeration of several different anatomical sub-

regions. Unless further distinctions are necessary, when I discuss ACC in humans I will be referring to Brodmann's areas 24, 25, 32, and 33, and when I discuss ACC in monkeys I will be referring to areas 24 and 32. It is also worth pointing out that most researchers using non-human primates to study ACC do not specify the sub-region from whence they have recorded. However, unless otherwise specified, it is safe to assume that these recordings are typically carried out in area 24 (including all subdivisions) because it is difficult to access pregenual cingulate cortex due to its close proximity with the sinuses and ocular orbits. Based on their location ventral to SEF, most of the data collected by Schall and colleagues from ACC (reviewed below) were probably recorded from areas 24a', 24b', 24c', or in the most rostral aspect of area 24d.

As with other areas involved in the execution and evaluation of saccades, microstimulation studies have been valuable for determining the function of ACC. Microstimulation of area 24d and 24c' produces many types of skeletal muscle movements (Mitz and Wise, 1987; Luppino et al., 1991) and this area sends extensive projections directly to the spinal cord (Biber et al., 1978; Dum and Strick, 1991; Dum and Strick, 1993). This area has been dubbed the rostral cingulate motor area (CMAr) to differentiate it from the two other motor representations (the dorsal and ventral cingulate motor areas) that can be found more caudal (for a compact review see Hatanaka et al., 2003). Stimulation of a specific, small region in area 24 has also been reported to produce eye movements including conjugate gaze shifts (Mitz and Wise, 1987; Mitz and Godschalk, 1989; Luppino et al., 1991). Based on the position of these stimulation sites near the fundus of the cingulate sulcus and at a rostro-caudal position near the most posterior extent of the arcuate sulcus it is likely that these eye movements were evoked from area 24c' of Vogt and colleagues (Mitz and Wise, 1987; Luppino et al., 1991) or slightly more anterior from 24c proper (Mitz and Godschalk, 1989). Projection patterns suggest that these eye movements may be elicited via a pathway through SEF. ACC

has strong reciprocal projections with SEF (Huerta and Kaas, 1990), but fewer projections with other oculomotor structures. ACC is only weakly connected to FEF (Barbas and Mesulam, 1981; Vogt and Pandya, 1987; Stanton et al., 1993). Although it certainly projects to the brainstem including several pontine nuclei, it is not clear if ACC projects specifically to the nuclei of the BSG (Schnyder et al., 1985; Keizer and Kuypers, 1989; Giolli et al., 2001), and it does not send projections to the SC (Fries, 1984)[2]. Thus, although more data must be collected, it seems that ACC is anatomically more remote from the areas involved in saccade execution than the other structures we have reviewed thus far.

A modest number of studies have been carried out testing the role of ACC in ocular motor tasks. These have almost universally implicated ACC in the evaluation of eye movements. As we shall see in the next section, these data are in agreement with the myriad studies that have implicated the ACC in action evaluation and performance monitoring more generally. Similar to SEF, single units and LFPs show error- and reward-related responses during the saccade countermanding task (Ito et al., 2003; Emeric et al., 2008). However, unlike SEF, neural signals in those areas do not encode response conflict (see also Nakamura et al., 2005). Interesting, these studies have shown that neuronal responses in the ACC tend to depend less on the animals behavior and more on trial outcome than those of the SEF. The antisaccade task has further provided evidence that neural activity in ACC is important for maintaining the current set of task rules dictating stimulus response mapping, evaluating whether or not these rules lead to desired outcomes, and recruiting executive control after errors (Johnston et al., 2007; Womelsdorf et al., 2010). Analagous to the effects observed while stimulating in SEF (Stuphorn and Schall, 2006), stimulation in ACC improves performance in the anti-

[2] Although, it is possible that this last finding was skewed by incidental damage to medial frontal cortex caused during the surgical approach to SC for tracer injections.

saccade task by reducing RT in a context-dependant manner (Phillips et al., 2010). Several other studies have been carried out using simple oculomotor tasks that varied the probability of reward, its magnitude, or the effort required to obtain it. The authors of these studies have generally concluded that ACC neurons encode and update the expected value of stimuli and/or stimulus response associations (Seo and Lee, 2007; Quilodran et al., 2008; Kennerley and Wallis, 2009b, a). However, the results of one study suggest that ACC neurons play a role in directing reward-based attention independent of stimulus value (Kaping et al., 2011). ACC has also been implicated in several aspects of performance monitoring during manual response tasks. Much of this work has been carried out using fMRI or the event-related potential technique in human subjects (discussed below). The human ACC and surrounding medial frontal cortex are thought to produce the error-related negativity that is visible on frontal medial EEG electrodes when subjects commit errors. Hemodynamic activation in ACC is often observed on error trials during fMRI experiments, and this activity is implicitly or explicitly considered synonymous with the ERN by many researchers (Botvinick et al., 2001; Kerns et al., 2004; Debener et al., 2005a; Debener et al., 2005b). One of major goals of the work presented in this dissertation has been to bridge the gap between this vast body of literature carried out using human subjects, and the work detailed above carried out using non-human primates. To this end, I investigate the functional microcircuitry of one cortical area thought to be involved in generating the ERN in Chapter 4, I demonstrate a monkey homologue of the ERN in Chapter 5, and I provide a concrete link between the microcircuitry and the ERN recorded at the surface in Chapter 6. My results show that SEF contributes to the ERN, but that other areas must also play a role in generating this ERP. Accordingly, for the rest of the introduction we will review the ERN and its proposed hemodynamic correlates in medial frontal cortex.

1.5 A wider view: Executive control beyond the oculomotor system

In the early 1990's two groups independently discovered that when humans commit errors during a speeded response task, an ERP can be reliably recorded from frontal medial electrode sites (Falkenstein et al., 1990; Falkenstein, 1991; Gehring et al., 1993). This ERP is characterized by an initial negativity, the ERN[3], peaking around 100 ms after the errant response followed by a later positivity, the Pe. Here I focus on the initial negativity (for review of the Pe, see Overbeek et al., 2005)). The ERN is observed across a wide range of tasks and in multiple response modalities (reviewed by Gehring et al., 2011). For our purposes, it is useful to note that an ERN has been consistently reported when subjects fail to cancel responses during the stop-signal task (Liotti et al., 2005; van Boxtel et al., 2005; Kramer et al., 2007; Stahl and Gibbons, 2007; Vocat et al., 2008; see also Sharp et al., 2010), and the ERN is also observed during saccadic response tasks (Nieuwenhuis et al., 2001), including the saccade stop-signal task (Endrass et al., 2005). However, the distribution and morphology of the saccadic ERN suggest that it may be generated by a slightly different, if overlapping, network in medial frontal cortex (Reinhart et al., 2012). Based in part on work carried out recording LFPs from non-human primates, Gehring suggested that ACC and SMA may produce the neural activity that gives rise to the ERN recorded at the surface (Gehring et al., 1993). Dipole source localization studies quickly lent corroborating evidence to this hypothesis (Dehaene et al., 1994). Many studies have since focused exclusively on the potential

[3] In their original reports, Falkenstein and colleagues (1990; 1991) referred to this phenomenon as the "error negativity" and abbreviated it using subscript notation (N_E), while Gehring and colleagues (1993) referred to the phenomenon as the error-related negativity (ERN). ERN now appears to be the modal terminology used throughout the literature and we adopt it herein. Pe has been generally adopted to describe the later positivity that develops after errors. Falkenstein and colleagues' original reports include neither the term "error positivitiy" nor the abbreviations P_E or Pe. However, it is easy to see how this abbreviation came into being since using ERP to denote the error-related positivity would obviously cause grief and consternation. This explains the mixture of nomenclature that currently exists in the literature.

role of ACC, although some researchers have emphasized contributions from broader areas (Dehaene et al., 1994; Kiehl et al., 2000; Menon et al., 2001; Luu et al., 2003; Agam et al., 2011). Since the ERP technique measures the combined voltage of many areas of cortex simultaneously (Luck, 2005; Woodman, 2011), and since several areas are active when errors are made as reviewed above, this historical focus on single areas may be somewhat misguided; the ERN probably measures simultaneous activity from across a broad performance monitoring network. This idea may account for the wide range of findings associated with the ERN. After all, different areas in medial frontal cortex are involved in a wide range of activities during error trials (reviewed by Ridderinkhof et al., 2004; Rushworth et al., 2004).

Around the same period of time that the ERN was initially discovered, advances in positron emission tomography (PET) and later functional magnetic resonance imaging (fMRI) technology allowed researchers to begin investigating activity associated with performance monitoring in medial frontal cortex of humans (Posner et al., 1988; Pardo et al., 1990; Carter et al., 1998; d'Esposito et al., 1998). Some researchers tend to view the functional imaging results of these and later studies as homologous and interchangeable with the ERN (e.g. Carter et al., 1998; Botvinick et al., 1999; Botvinick et al., 2001) while others tend to focus more exclusively on the ERN itself (e.g. Holroyd and Coles, 2002). Several groups have hypothesized that the ERN is actually just one ERP in a larger family of frontal medial negativities indicating *mismatch* between expected and actual events (reviewed by Folstein and Van Petten, 2008). Another frontal medial negativity can be recorded when subjects are given feedback instructing them that their previous responses were incorrect (Miltner et al., 1997; Gehring and Willoughby, 2002). This feedback-related negativity (FRN) may be elicited by the same neural generators that gives rise to the ERN (reviewed by Nieuwenhuis et al., 2004), although contradictory

evidence can also be found (Luu et al., 2003). We will explore these ideas in greater detail below as we discuss the proposed anatomical and functional bases of the ERN.

1.5.1 Neural origins of the ERN

It has been known for some time that neural activity in medial frontal cortex is correlated with performance monitoring. Gemba and colleagues (1986) recorded LFPs in ACC related to errors when monkeys made manual responses during a lever pressing task (see also Niki and Watanabe, 1979; Shima and Tanji, 1998). Based in part on these recordings, and in part on theories of the role of SMA in producing actions (Goldberg, 1985), Gehring and colleagues (1993) first suggested that these areas probably play a key role in generating the ERN. Dehaene and colleagues (1994) provided evidence to support this assertion by providing scalp distributions and modeling the probable sources of dipoles giving rise to the ERN. These researchers found a best-fitting dipole solution at midline, directed downward, and located roughly consistent with generation by ACC. Others soon replicated this result (van Veen and Carter, 2002; Herrmann, 2004; Mathewson et al., 2005). Converging evidence comes from studies combining ERPs with fMRI data. Ullsperger and von Cramon (2001) and later Mathalon and colleagues (2003) recorded ERPs and fMRI in separate sessions and located performance monitoring signals in ACC and pre-SMA. Using particularly challenging techniques both to gather and analyze data, Debener and colleagues (2005b) recorded simultaneous fMRI and EEG, used independent component analysis to isolate components across individual trials that were most closely related to the grand average ERN, convolved these components with a canonical hemodynamic function, and correlated the amplitude of this signal to the amplitude of the hemodynamic response in ACC during errors. These authors also found evidence for post-error slowing during their version of the Erikson flanker task that was correlated with the amplitude of their

single trial ERN measure. But evidence contradicting ACC and pre-SMA as the locus of the ERN can also be found. Recently, Agam and coworkers (Agam et al., 2011) recorded complimentary EEG, MEG, and fMRI and localized the origins of the ERN to posterior cingulate cortex. Contradictory evidence can also be found in the lesion literature. Although patients with damage to medial frontal cortex including ACC exhibit reduced ERN, they are still aware of committing errors (Stemmer et al., 2004). And the ERN is also reduced by lesions of lateral prefrontal cortex that spare ACC (Gehring and Knight, 2000; Ullsperger et al., 2002; Ullsperger and von Cramon, 2006; reviewed by Ullsperger, 2006). As reviewed above ACC and SEF both show error related activity in single units responses and in LFPs (Stuphorn et al., 2000; Ito et al., 2003; Emeric et al., 2008, 2010). But action potentials contribute little if any to the ERPs (Woodman, 2011). Additionally, one cannot be certain that LFPs reflect local activity that is restricted to the area surrounding an electrode: LFP activity has been documented to originate centimeters away from the location of the contact (Kajikawa and Schroeder, 2012). In comparison, SEF subtends only ~3x3 mm. Thus these studies cannot definitively localize anatomical origins of the ERN. Because of these considerations, I endeavored to determine the origins of the ERN by recording simultaneous EEG and LFPs from medial frontal cortex. I did this using a multicontact linear microelectrode array allowing me to construct CSD. These methods ensure that neural current flow measures are spatially constrained to the area bracketed by the electrode array. The results of this study are detailed in Chapter 6.

1.5.2 The ERN and behavioral adjustments

Classic psychophysics studies have identified common behavioral adjustment strategies that are evident after errors. In particular, subject tend to display increased RTs and accuracy on trials that follow errors (Rabbitt, 1966; Rabbitt and Rodgers, 1977;

Laming, 1979). One of the first reports of the ERN noted a positive correlation between the amplitude of the ERN and the RT on subsequent correct trials (Gehring et al., 1993). These authors also reported that ERN amplitude was increased in conditions that favored response accuracy over speed, that the force with which errant responses were committed decreased as the amplitude of the ERN increased, and that the probability of attempting to correct an errant response increased with the amplitude of the ERN. These findings support the hypothesis that the ERN reflects activities of a supervisory system that can recruit increased behavioral control during the execution of ongoing as well as future actions. Unfortunately however, these results have been less clear in subsequent studies. On the one hand, some researchers have replicated the first of these findings, showing that the ERN (or it's presumed hemodynamic counterpart) scales in magnitude with RT adjustments on subsequent trials (Rodriguez-Fornells et al., 2002; Kerns et al., 2004; Debener et al., 2005b; Ladouceur et al., 2007; West and Travers, 2008). On the other hand, others have not found such a link, or have found contradictory evidence (Gehring and Fencsik, 2001; Hajcak et al., 2003; Nunez Castellar et al., 2010; Reinhart et al., 2012). Part of this discrepancy may have to do with whether or not errors are perceived. At least two groups have reported that the ERN can be recorded even when patients are unaware of the errors they have made, and that awareness of these errors is necessary for post-error slowing (Nieuwenhuis et al., 2001; Klein et al., 2007; but see Woodman, 2010). Another issue may have to do with measures of performance monitoring. Post-error RT adjustments may not be the only way in which performance is modified (reviewed by Ullsperger, 2006). This is especially true in the stop-signal task, where RT slowing actually occurs after both canceled and noncanceled trials (Emeric et al., 2007; Nelson et al., 2010; Bissett and Logan, 2011, 2012). Gehring (2011) asks us to consider the whole "psychological terrain" rather than simply assuming that post-error slowing is the only strategy for optimizing behavior.

Finally, although it is rarely discussed, it is not immediately clear if the amplitude of the ERN should be taken as an indication of the strength or magnitude with which errors are detected and cognitive control should be recruited. This idea is intuitively appealing. Larger amplitude ERPs are probably produced by more extensive neural activity, and the more neurons that are recruited in a process, the stronger the activation of that process must be. But there are many reasons that this intuition may not stand up to experimental inquiry. I am not aware of any work that has sought to address this issue.

Of course, performance adjustments need not be implemented via RT adaptation alone. In the stop-signal task, subjects may also adjust SSRT. These changes may be observed by manipulating a subject's motivational state. To date, only one study has manipulated motivational state and tested for changes in SSRT (Leotti and Wager, 2010). These researchers manipulated reward contingencies to favor either speed or accurate inhibition, and found that SSRTs were lower when subjects were encouraged to value stopping. Unfortunately, SSRT estimates in this study were unreliable since only a single SSD was used. When estimating SSRT from a single SSD, it is important to use the SSD which yields 50% errors. Since the probability of making a noncanceled error was higher in the motivated speed condition, sampling error rates in both conditions at a single SSD means that SSRT was estimated from different tails of the RT distribution. Thus, the observed SSRT differences in this study probably represent well-known confounds in SSRT estimates rather than motivational factors. I shed additional light on this matter in Chapter VI by manipulating the motivational state of monkeys using an asymmetric reward paradigm. In contrast to Leotti and Wager's study, I find that SSRT does not change with motivational state.

Lesion studies have also provided mixed evidence for ERN-related performance adjustments. As we have seen above, the definitive loci giving rise to the ERN have not been precisely identified. We should note that this makes lesions studies more difficult

to evaluate in reference to the ERN. Stemmer and colleagues (Stemmers, 2000) reported that patients with damage to ACC exhibited reduced amplitude ERNs. However, post-error slowing was spared in these patients (see also Fellows and Farah, 2005). Additionally patients who have undergone cingulotomy to treat intractable epilepsy exhibit few long term deficits in performance monitoring or executive control (Cohen et al., 1999; Jung et al., 2006). In Chapter 5, I provide additional data on this subject. The ERN that I report in non-human primates was not associated with post-error slowing.

Consideration of the potential link between the ERN and performance adjustments highlights a more fundamental question. What cognitive processes or neural computations are reflected in the activity that give rise to the ERN recorded at the surface? For the remainder to the introduction we shall examine the potential cognitive functions indexed by the ERN.

1.5.3 Theories of the ERN

1.5.3.1 Error detection

The first theory of the ERN suggested simply that this component reflected the brain's process of error detection (Falkenstein, 1991; Gehring et al., 1993; reviewed by Gehring et al., 2011). According to this view, subjects have access to a representation of the correct response in a given context, and an efference copy of the actual response that was elicited. When the response and the representation are not aligned, a mismatch occurs, and an error is detected. This theory was originally proposed based on the idea that the ERN originates in ACC, and that ACC serves primarily as a neural comparator (Brooks, 1986). Evidence for this view is mixed (reviewed by Gehring, 2011). For instance, one prediction of this theory is that the ERN should be larger in amplitude when the mismatch between the intended and the actual response is greater.

Some authors report that this is indeed the case (Bernstein, 1995; Falkenstein et al., 1996) while others have gathered contrary evidence (Gehring and Fencsik, 2001). Another possible interpretation of the error detection theory is that more salient task-related cues should lead to higher magnitude ERNs. This follows because the increased cue salience should lead to stronger representations of the correct, intended response for comparison to the actual, errant response. Several researchers have confirmed this prediction (Yeung et al., 2007; Vocat et al., 2008). However, it should also be noted that these predictions are not unique to the error detection theory, but are, in fact, predicted by every major theory of the ERN (Yeung et al., 2007; Gehring et al., 2011). This points to a general shortcoming of the error-detection theory. The theory has not been stated in explicit, formal terms, making it difficult to perform rigorous hypothesis testing.

Perhaps the most forceful criticism of the error detection view is conceptual. It is unclear how or why the brain would have access to a representation of the correct response in a particular situation, but would be unable to use this information to guide action. It is a bit like stating that the brain "intended" to perform one action but performed another instead. At a deeper level, this explanation is also somewhat circular. Intending one action and committing a different action is simply the definition of an error. So, in essence, the error detection hypothesis states that the brain detects errors by detecting errors. However, these criticisms may not be as damning as they initially appear. As we shall see below, the reinforcement learning theory of the ERN is actually similar in many respects to this simple error detection hypothesis. However, instead of comparing intended responses to actual ones, this theory suggests that the ERN reflects a comparison of predicted future outcomes to an updated representation of future outcomes in light of new information arising from the subject's errant actions. Finally, from an empirical perspective, the error detection hypothesis is somewhat less attractive than other theories since it has not been elaborated in sufficient biological

detail to provide specific testable neurophysiological hypotheses. Although corollary discharge signals that provide efferent copies of motor representations have been studied (reviewed by Sommer and Wurtz, 2008), it is difficult to know what a representation of a correct response would look like or how to test for its presence or absence in terms of neural activation.

1.5.3.2 Conflict monitoring

The conflict monitoring theory of the ERN is unique in that it does not suggest that the ERN is specific to situations in which errors occur. Rather, this theory suggests that the ERN reflects a special instance of a more general neural process that monitors the degree to which competing responses are co-activated at any given time (Botvinick et al., 2001; Yeung et al., 2004). Error trials happen to coincide, on average, with trials on which there is a large degree of competition between responses, and on trials in which this competition remains at high levels during the time of response execution. Therefore, an ERP created by averaging EEG data from error trials will exhibit larger negative amplitude following the response than an ERP produced by averaging EEG from correct trials only. Unlike the other theories listed, the conflict monitoring hypothesis was not originally formulated to explain the ERN. Rather, this theory has its origins in imaging experiments that were being carried out around the time that the ERN was first reported (Carter et al., 1995, 1998, 2000; Botvinick et al., 1999). The conflict monitoring hypothesis has intuitive appeal, because it does not invoke the homunculus that many have argued is necessary in the error monitoring theory. It is also attractive from an empirical perspective, because it has been formalized as a computational model generating explicit, testable predictions. On the other hand, one may contend that the conflict monitoring theory has been heavily shaped by the methods employed in its study. The theory has been built from the "top down" to explain a particular

phenomenon observed during a few tasks (Stroop, 1935; Eriksen and Eriksen, 1974) and extrapolated to other contexts *post hoc* rather than being built from the "bottom up" to explain general phenomena and then applied to specific tasks.

Evidence for the conflict monitoring hypothesis is mixed. Influential studies have used computational modeling to show that conflict monitoring can account for and explain many key aspects of behavioral and electrophysiological data (Botvinick et al., 2001; Yeung et al., 2004). Other work has demonstrated increased activity in ACC during task switching when conflict is high (Dreher and Berman, 2002). As mentioned above, some of the findings in the error-monitoring literature can also be taken as evidence for conflict monitoring (e.g. Gehring and Fencsik, 2001). However, other reports contradict the conflict monitoring hypothesis. For instance, if we assume that response conflict can be measured based on muscle contractions in the periphery, than if follows that more forceful error responses or those that show more co-activation of competing muscle groups will be associated with increased amplitude ERNs. But when sought, this link has not been observed (Carbonnell and Falkenstein, 2006; Masaki et al., 2007). The conflict model of Cohen and colleagues predicts that increased levels of response conflict will be associated with trials on which errors are followed by fast corrections, but these trials do not produce larger amplitude ERNs (Burle et al., 2008). The same model predicts that response conflict will also occur on correct trials, though it is resolved before the response is committed. Several have suggested that the N200 reflects this conflict signal on correct trials, but this component can be experimentally dissociated from the ERN (Ridderinkhof et al., 2002; Swick and Turken, 2002). Several imaging studies have found more activation in ACC on error trials than correct trials even when both trial types contain the same degree of response conflict (Braver et al., 2001; Ullsperger and von Cramon, 2001; Garavan et al., 2003). Finally, lesion work in non-

human primates shows that bilateral damage to ACC does not impair task switching on trials with high degrees of response conflict (Rushworth et al., 2003).

The most forceful criticism of the conflict monitoring hypothesis may be that it has not been precisely defined, or rather, that the definition often differs across studies. There are several instances in which one group has documented findings inconsistent with the conflict monitoring theory only to be met with revised predictions capable of accommodating these disparate findings (e.g. Holroyd and Coles, 2002; Yeung et al., 2004; Emeric et al., 2008; Cole, 2009; Cole, 2010; Grinband et al., 2011; Yeung et al., 2011). In recent reports, some authors have begun to suggest that conflict monitoring and error detection are two distinct and dissociable processes (e.g. Cole, 2009) even though the conflict monitoring theory was originally formulated, in part, to describe how errors are detected. It is unclear why an agent would need to monitor for response conflict if errors can be detected via other means. Response conflict has begun to assume a life of its own, independent of other aspects of executive control. Emphasis has also begun to move away from *response* conflict in the pure motor sense and toward *decision* conflict in a more abstract sense (Pochon et al., 2008; Cole, 2009). This theoretical fluidity frustrates meaningful hypotheses testing.

Response conflict has often been defined as the co-activation of mutually incompatible responses (Botvinick et al., 2001; Yeung and Nieuwenhuis, 2009). This begs an operational definition for *incompatible*. In laboratory tasks, participants are often instructed to respond either with right or left hands depending on which cue is presented. In this context, these two responses may be viewed as incompatible. But in most tasks, the left and right hand work in unison. For instance, when a cyclist wishes to stop and squeezes both brake levers, the co-activation of left and right hands is compatible with the goal of braking. How does the brain keep track of context and assign the appropriate meaning to the co-activation of effectors (see Brown and Braver,

2005)? Perhaps response conflict is restricted to cases that are more naturally incompatible, such as the co-activation of agonist and antagonist muscles of the same effector. In either case, it is difficult to see how response conflict may generalize to the oculomotor system. With the exception of small vergence movements, the two eyes remain tightly yoked while moving. And recall that it is impossible to co-activate agonist and antagonist muscles of the extraocular muscle system. Still, as noted above, an ERN is clearly present during tasks which require eye movements. Perhaps the co-activation of mutually incompatible responses occurs further upstream in the oculomotor system at the level of SC or cortex before being resolved in the BSG. But the use of the stop-signal task to study executive control presents another thorny issue. Does response conflict extend to situations in which the mutual incompatibility arises between executing and canceling a response? Ironically, although these types of conflict are given little consideration in the human literature, the tension between going and stopping as expressed by movement and fixation cells in the oculomotor system may be the most well-documented and precisely defined neural description of response conflict described to date. As discussed above, movement cells and fixation cells in SC and FEF are co-activated during the stop-signal task (Paré and Guitton, 1994; Hanes et al., 1998). The degree to which these cells are co-active is dependent on the probability of making an error (Stuphorn et al., 2000). The greater the probability of error commission, the greater the co-activation of these neural populations, and hence the greater the degree of response conflict. Curiously however, this co-activation only occurs on successfully canceled trials suggesting that this type of response conflict may be a poor signal for recruiting executive control following errors. Nevertheless, the behavioral data seems to support the interpretation that this type of conflict may be utilized as an signal for increased executive control in the stop-signal task. Post-error slowing is rarely observed during the stop-signal task, but many researchers have noted slower responses after

successfully canceled trials (Emeric et al., 2007; Nelson et al., 2010)(Emeric et al., 2007; Nelson, 2010; but see Bissett and Logan, 2011) for an alternate intepretation). Thus, response conflict and subsequent increases in RT are dissociated from errors in the stop-signal task.

The response conflict that is present on successfully canceled trials in the stop-signal task is reflected in the single-unit and LFP responses of SEF, but not in those of ACC (Stuphorn et al., 2000; Ito et al., 2003; Emeric et al., 2008; Emeric et al., 2010). Since the functional imaging literature from whence the conflict monitoring hypothesis originated has focused almost exclusively on ACC, this finding has led to some controversy regarding the ability of non-human primates to monitor response conflict and the utility of this animal model of human performance monitoring and executive control (Cole, 2009, 2010; but see Schall and Emeric, 2010). As mentioned above, the area termed 32' by Vogt and colleagues (2003) forming a transitional region between frontal cortex and ACC is not observed in monkeys. Cole and colleagues (2009) suggest that this is the key region mediating conflict monitoring in humans and that its absence in monkeys render them unable to monitor conflict. Of course, this assessment ignores the fact that conflict related activity has been reported in monkey SEF (Stuphorn et al., 2000; Emeric et al., 2010). It also ignores the rather obvious fact that monkeys can learn to perform remarkably complicated tasks given that they are missing a hypothesized key aspect of executive function. Motivated in part by this controversy, I strengthen the link between human and non-human performance monitoring research by reporting an ERN recorded from monkeys in Chapter 5. I then investigate the contribution made by SEF to this ERN in Chapter 6.

1.5.3.3 Reinforcement learning

In order to understand the reinforcement learning theory of the ERN, one must first understand some basics of reinforcement learning theory itself. Reinforcement learning theory has roots in the behavioralist research of the early to mid 20th century. Based on his dissertation work studying associative processes in several species, Thorndike formulated the *law of effect* stating, in essence, that stimulus/response associations followed by favorable outcomes will be strengthened whereas those followed by negative consequences will be weakened (Thorndike, 1898, 1927 reviewed by Boring, 1950). This idea was later formalized using simple equations to represent the strength of a learned association as an exponential series in which past information about a given outcome resulting from a stimulus/response combination is integrated. The most recent information is weighted most strongly in these equations according to a variable representing the learning rate (Bush and Mosteller, 1951b, a; Rescorla and Wagner, 1972). Sutton and Barto (1998) refined this paradigm founding the current theory of reinforcement learning. Through Sutton's background in psychology and Barto's expertise in mathematics and computer science they extended these equations in search of practical, effective machine learning algorithms. Ultimately, they developed a system of equations that describes a process whereby an agent learns to predict the likelihood of future rewards given current stimuli and actions. When the resulting reward does not match the expectation, a *reward prediction error* (RPE) is encountered, and this information is used to update the value representation of the states and actions that preceded it. RPE is defined simply as the magnitude of the actual reward that is received minus the expected value of the stimulus or stimulus/action association that preceded it. Positive RPEs are experienced when unexpected rewards are encountered while negative RPEs are experienced when expected rewards are not realized. Sutton and Barto's key insight (aside from conceptualizing machines as "wanting" things) was

that an unexpected encounter with a high-value state (i.e. a state that has come to predict future reward), should also generate a RPE so that the stimulus/action association that led to that **state** can be strengthened as well. In this way, value propagates backward in time to the earliest events that predict rewards in a process called *the method of temporal differences*. These are the basic elements of the machine learning algorithm known as reinforcement learning theory.

Around the same period of time that Sutton and Barto were solidifying these ideas in what would become their most influential work (Sutton and Barto, 1998), Schultz and colleagues began a classic series of experiments recording from midbrain dopamine neurons in non-human primates (Schultz et al., 1993; Schultz et al., 1997). In a well-known series of studies, they and others demonstrated that these neurons respond to stimuli that predict upcoming reward in a manner consistent with the specific type of RPE instantiated by the method of temporal differences (reviewed by Glimcher, 2011; Schultz, 2013). Many of these neurons fire at steady tonic rates and respond with a burst of action potentials when unexpected rewards are received or with a pause in activity when anticipated rewards are not delivered.

A mistake is an unexpected event that deceases the probability of obtaining future rewards. Once an agent has sufficient experience with the contingencies associated with a particular task, mistakes should therefore elicit negative RPEs. This is the critical intuition underlying the reinforcement learning theory of the ERN first formulated by Holroyd & Coles (2002). Based loosely on earlier studies (Bunney and Aghajanian, 1976; Reader et al., 1979; Gaspar et al., 1989; Berger et al., 1991; Williams and Goldman-Rakic, 1993; Richardson and Gratton, 1998), these investigators made the following anatomical assumptions: first, a population of dopamine neurons projects to the apical dendrites of layer V pyramidal neurons in medial frontal cortex, and second, dopamine neurons exert tonic inhibition on these pyramidal cells. They then put forth

the hypothesis that the ERN reflects the negative RPE that is encountered when a subject makes a mistake. According to their theory, the negative RPE associated with an errant response is encoded as a phasic decrease in firing by midbrain dopamine neurons. This releases pyramidal neurons in medial frontal cortex (particularly ACC) from tonic inhibition, allowing widespread dendritic depolarization that sums to produce the ERN recorded from the surface. In this model, the ERN and the FRN both reflect the same process. The ERN simply reflects a RPE triggered by a subjects own actions, while the FRN reflects a RPE triggered by an external event (reviewed by Nieuwenhuis et al., 2004).

The reinforcement learning theory of the ERN has garnered interest and support, both in explaining the ERN, and in explaining hemodynamic responses in ACC. For instance, one of the main predictions of this theory is that the FRN recorded before subjects fully understand task contingencies should show larger amplitude. However, as subjects learn the task and become more adept at predicting upcoming reward based on their own actions, the FRN should grow smaller and the ERN should grow proportionally larger. These predictions have been verified in several ERP studies (Holroyd and Coles, 2002; Nieuwenhuis et al., 2002; Holroyd and Coles, 2008). Also in agreement with the hypothesis that ACC processes RPEs, both negative feedback and errors elicit similar hemodynamic responses in ACC (Holroyd et al., 2004b). Several researchers have shown that more unexpected errors or errors resulting in larger magnitude losses elicit FRNs of larger amplitude (Holroyd et al., 2003; Potts et al., 2006; Bellebaum and Daum, 2008; Goyer et al., 2008). Finally, single unit recordings in non-human primates have also identified neurons that encode RPEs in medial frontal cortex, both in ACC (Matsumoto et al., 2007; Seo and Lee, 2007) and in SEF (So and Stuphorn, 2010).

However, the reinforcement learning account of the ERN is not without shortcomings. Just as some have found that the FRN scales with the magnitude of

losses, others have found contradictory evidence (Holroyd et al., 2004a; Nieuwenhuis et al., 2004; Yeung et al., 2004; Yeung and Sanfey, 2004; Hajcak et al., 2005, 2006, 2007). Some researchers have even found evidence for a FRN on trials associated with positive RPEs resulting from unexpected favorable outcomes (Donkers et al., 2005; Donkers and van Boxtel, 2005; Oliveira et al., 2007; Alexander and Brown, 2011). One perceived positive attribute of the reinforcement learning theory of the ERN is its relative specificity in biological terms. Of the various theories relating the ERN to cognitive function, the reinforcement learning theory makes the most specific predictions concerning its underlying neural basis. Unfortunately, many of these predictions derive from scant neurophysiological evidence. For instance, there is little data to suggest that dopamine neurons tonically inhibit pyramidal cells in medial frontal cortex, or that dopamine is capable of disinhibiting these neurons quickly enough to produce the ERN (reviewed by Jocham and Ullsperger, 2009). Dopamine receptors are not ligand-gated ion channels like those activated by GABA and glutamate. Instead, they are G-coupled protein receptors that rely on slow second messenger systems to enact intracellular changes in target neurons (reviewed by Seamans and Yang, 2004). The actions of dopamine on glutamatergic neurons in medial prefrontal cortex are various, complex, and depend critically on many factors including the presence or absence of other neurotransmitters (reviewed by Tzschentke, 2001). In addition, there is also evidence that the RPE signals encoded by dopamine neurons are biased toward representing positive RPEs (reviewed by Glimcher, 2011). Another neural system, possibly involving the lateral habenula (Matsumoto and Hikosaka, 2007), and internal globus pallidus (Hong and Hikosaka, 2008) may aide in encoding negative RPEs. Finally, the central tenant of reinforcement learning theory that dopamine neurons signal RPEs has been repeatedly questioned (Pennartz, 1995; Berridge and Robinson, 1998; Redgrave et al., 1999b; for possible reconciliation see Bromberg-Martin et al., 2010) In Chapter 6, I shed

additional light on this theory by testing the hypothesis that SEF contributes to the ERN through a RPE signal when subjects make mistakes. I do this by introducing an asymmetric reward manipulatoin to the classic saccade stop-signal paradigm (Kawagoe et al., 1998) thereby inducing errors with high or low magnitudes of RPE.

1.5.3.4 Other theories

Although the theories listed above have dominated the field commanding the lion's share of attention, several other ideas concerning the ERN have also been advanced. The error-likelihood theory of ACC (Brown and Braver, 2005) is similar in many respects to the reinforcement learning account of the ERN. Both theories suggest that RPE signals conveyed by dopamine projections to the ACC produce the ERN. However, the error likelihood account differs by suggesting that ACC uses this information as a training signal to learn to predict error likelihood, whereas the original reinforcement theory of the ERN proposed by Holroyd and Coles (2002) suggests that ACC uses these signals to select an appropriate motor controller for upcoming action. In this way, the error likelihood theory is more an account of the function of ACC rather than a new explanation for the ERN. Alexander and Brown (2010, 2011) have recently updated this theory suggesting that ACC functions primarily to predict the future outcomes of current actions rather than errors in particular.

The reinforcement learning theory of the ERN has been widely influential and has sparked many studies on the potential role of dopamine. But some suggest that the ERN actually reflects the activity of other neurotransmitter systems (reviewed by Jocham & Ullsperger 2009). Surprisingly little work has actually been done to investigate these alternative neurotransmitters. Candidates include norepinephrine (Riba et al., 2005b; Riba et al., 2005a), GABA (Johannes et al., 2001; de Bruijn et al., 2004), and adenosine (Tieges et al., 2004).

Some have suggested instead that the ERN reflects the emotional reaction associated with detecting that an error has been committed (Luu et al., 2000; Luu et al., 2003). Much of the evidence for this view comes from a myriad of studies that have been published attempting to link particular traits of various clinical disorders such as obsessive compulsive disorder or depression to aspects of the ERN (reviewed by Olvet and Hajcak, 2009). From a neurophysiological standpoint, this theory is somewhat difficult to test, since it does not make specific predictions concerning neural activity. It is also worth noting that this theory is not exclusive of the others mentioned above (Luu and Pederson, 2004; Gehring et al., 2011). It is perfectly reasonable that a red flag from an error detection, conflict monitoring, or reward prediction system may lead to, or coincide with a negative affective response. Furthermore, the brain region or neural population giving rise to cognitive affect may contribute to the ERN recorded at the surface. In truth, similar logic may apply to all theories of the ERN. It may be overly simplistic to assume that the ERN reflects one single process of error detection (Logan and Crump, 2010). Different areas of medial frontal cortex have been implicated in a wide range of functions that all fall under the general heading of performance monitoring (reviewed by Ridderinkhof et al., 2004; Rushworth et al., 2004). Any, or all of these functions may be carried out simultaneously by different areas of cortex or subpopulations of neurons. This would explain why so many authors have found support for their preferred theory of the ERN. In Chapter 6, I shed additional light on the idea that the ERN may in fact reflect a mixture of activity from several different areas carrying out various performance monitoring functions using concurrent intracranial and surface recordings to link the ERN to specific aspects of performance monitoring.

1.6 The studies presented here

In the first study, detailed in Chapter 2, I investigate the pattern of extraocular muscle activation when planned saccades are quickly withheld. When manual responses are canceled during the stop-signal task, partial movement or EMG activation in the absence of overt movement is still sometimes observed (De Jong et al., 1990; McGarry and Franks, 1997; McGarry et al., 2000; van Boxtel et al., 2001; Scangos and Stuphorn, 2010). If the GO process and STOP process of Logan's race model tie, we may observe truncated motor responses. Some researchers have reported shorter amplitude saccades on noncanceled trials in the stop-signal task, suggesting a similar effect in the oculomotor system (Colonius et al., 2001; Ozyurt et al., 2003; Akerfelt et al., 2006; but see Hanes and Schall, 1995). In the spinal motor system, it is also possible that manual responses may be canceled by coactivating agonist and antagonist muscles, leading to EMG in the absence of overt responses. But based on the properties of the brain stem saccade generator detailed above, these phenomena should not be observed in the oculomotor system. Therefore, I hypothesized that I would not observe partial extraocular EMG in the absence of overt saccades when eye movements were canceled. I tested this hypothesis by recording and isolating the saccadic spike potential from anterior EEG electrodes in macaque monkeys. As I had hypothesized, there is no detectable increase in extraocular EMG when planned saccades are withheld. Thus, as anticipated by previous behavioral and anatomical studies, saccades prove to be ballistic processes and they are not canceled by coactivation of agonist and antagonist muscles. Unexpectedly however, a significant decrease in the average level of extraocular EMG is also detected when saccades are canceled. I interpret this decrease as a likely decrease in the number of microsaccades that were initiated when saccades were canceled. Thus, the process responsible for canceling large, task relevant saccades likely inhibits microsaccades as well.

In the next study, detailed in Chapter 3, I followed this hypothesis by directly measuring microsaccades while monkeys performed the stop-signal task. As reviewed above, deep layer neurons in the rostral pole of the SC have long been considered to be fixation cells. A similar population of cells is also recognized in FEF (Izawa et al., 2009). However, recently another view has been advanced, suggesting that neurons in the rostral pole of the SC actually code for microsaccades (Hafed et al., 2009). As detailed in the introduction to Chapter 3, based on the reported neural activity of neurons in SC during the stop-signal task, these two theories make different predictions concerning the overall pattern and number of microsaccades made when large task relevent saccades are canceled. In agreement with the EMG data I describe in Chapter 2 and with the hypothesis that neurons in rostral SC serve fixation, I observed decreased incidence of microsaccades. Thus the tension between movement and fixation is represented explicitly by two populations of neurons in SC and FEF.

Next, in Chapter 4, we turn our attention from the execution of eye movements and consider their evaluation. As reviewed above, the precise functions subserved by SEF are unknown, although it is thought to play an important role in the evaluation of eye movements. Various tasks have been used to correlate neural responses in this area to one cognitive process or another. These studies have yielded a wide range of observations that are difficult to evaluate as a whole. I began investigation of SEF using a different approach, choosing to characterize basic response properties and microcircuitry in this area as my starting point. Using a multi-contact electrode array to record LFP and single unit data and to derive current source density from all layers of SEF simultaneously, I characterize, for the first time, functional microcircuitry in agranular frontal cortex. The functional microcircuit in this area looks very similar to that described in early sensory cortex. I report visual and motor responses from all layers of SEF. By understanding the intracranial projection patterns of SEF as well as the

microcircuitry of this area, we can gain greater insight into its role in evaluating saccades.

In the next study, described in Chapter 5, I sought to strengthen the link between SEF and saccade evaluation, as well as provide a keystone in the bridge uniting the monkey and human performance monitoring literature. As reviewed above, it has been suggested that SEF, along with other areas of medial-frontal cortex, may contribute to the performance monitoring event related potential known as the ERN. However, although intracranial recordings have highlighted performance monitoring activity in non-human primates, it is not known if they exhibit an ERN in surface potentials homologous to those recorded in humans. By recording surface potentials, in non-human primates during the saccade stop-signal task, I report that monkeys do exhibit an ERN homologous to that recorded in humans.

Finally, to better understand the role of SEF in monitoring and evaluating the outcome of eye movements, I bring the techniques of Chapters 4 and 5 together in Chapter 6 by recording from all layers of SEF simultaneously while recording ERNs at the surface during a stop-signal task. I report error-related CSD in SEF. Using Granger causality analysis, I further show that this activity likely contributes to the ERN recorded at the surface. Finally, by using an asymmetrica reward manipulation, and recording from neurons with different response properties, I show that the contribution of SEF to the ERN is produced by a process specific to error detection, and is not mediated by reinforcement learning.

In the final chapter, we will consider these results as a whole, and discuss future directions suggested by them.

CHAPTER 2

MEASUREMENT OF THE EXTRAOCULAR SPIKE POTENTIAL DURING SACCADE COUNTERMANDING

2.1 Abstract

The stop-signal task is used to investigate motor inhibition. Several groups have reported partial electromyogram (EMG) activation when subjects successfully withhold manual responses, and have used this finding to define the nature of response inhibition properties in the spinal motor system. It is unknown whether subthreshold EMG activation from extraocular muscles can be detected in the saccadic response version of the stop-signal task. The saccadic spike potential provides a way to examine extraocular EMG activation associated with eye movements in electroencephalogram (EEG) recordings. We used several techniques to isolate extraocular EMG activation from anterior electrode locations of EEG recorded from macaque monkeys. Robust EMG activation was present when eye movements were made, but no activation was detected when saccades were deemed canceled. This work highlights a key difference between the spinal motor system and the saccade system.[4]

2.2 Introduction

Rapid inhibition of prepared motor responses has been studied extensively with the stop-signal or countermanding task (reviewed by Verbruggen and Logan, 2008). In this task, subjects make quick responses to target stimuli. On a subset of trials, a second stimulus follows the target, instructing subjects to withhold their responses.

[4] This chapter was published as Godlove DC, Garr AK, Woodman GF, Schall JD. Measurement of the extraocular spike potential during saccade countermanding. Journal of Neurophysiology 106: 104-114, 2011.

When subjects are successful in canceling their responses, behavioral measures cannot be recorded because no overt behavior occurs. However, using a modeling approach, the timing of the covert inhibitory process can be estimated (Logan and Cowan, 1984; Colonius, 1990; Logan, 1994). A saccadic response version of the stop-signal task has been used to characterize properties of the ocular motor system (Hanes and Schall, 1996; Hanes et al., 1998; Hanes and Carpenter, 1999; Logan and Irwin, 2000; Paré and Hanes, 2003; Corneil and Elsley, 2005; Walton and Gandhi, 2006; Boucher et al., 2007b; Emeric et al., 2007).

Several groups have reported subthreshold electromyogram (EMG) activation on canceled trials in the manual response version of the countermanding task (De Jong et al., 1990; McGarry and Franks, 1997; McGarry et al., 2000; van Boxtel et al., 2001; Scangos and Stuphorn, 2010). However, it is unknown if partial extraocular EMG activation is present when eye movements are deemed canceled. The possibility that extraocular muscles may contract without producing detectable eye movement seems unlikely. However, the literature is inconclusive on this point. While it is true that the inertia of the eye within the orbit is negligible, the surrounding tissue of the oculomotor plant exerts viscous and elastic forces on the eye which are significant (Porter et al., 2003). It is difficult to estimate the extent to which these forces counteract eye movement production, because research has resulted in contradictory evidence (Robinson, 1964; Sklavos et al., 2005; Anderson et al., 2009; Quaia et al., 2009). In fact, very few experiments have been reported on this matter. Furthermore, most of these studies have been conducted using anesthetized animals, but larger time constants for visco-elastic relaxation of orbital tissues have been noted in alert animals (Anderson et al., 2009).

When considering whether or not extraocular muscles are able to generate contractions that do not result in eye movements, it is also important to consider the

muscles themselves. The extraocular muscles are relatively poor actuators. During periods of fixation, only 23% of muscle innervation is ultimately transferred to the tendons to result in rotation of the eyeball (Quaia and Optican, 2003). Thus, when saccades are initiated, a force of much larger magnitude must be supplied to overcome that dissipated by the muscles themselves. This initial burst of force can be observed in the well known "pulse-slide-step" discharge pattern of oculomotor neurons (Fuchs and Luschei, 1970; Robinson, 1970). The "pulse" portion of muscle innervation is thought to be necessary in order to overcome static viscous drag exerted by the passive orbital tissue (Sparks, 2002). These considerations leave open the possibility that small extraocular muscle contractions may occur in the absence of detectable eye movements.

If partial EMG activation were observed in the primate ocular motor system when trials were deemed canceled, it would provide a powerful and versatile tool for examining motor control in saccadic tasks. This development would be particularly useful for neurophysiological research, since most work using the stop-signal paradigm with monkeys has been carried out in the ocular motor domain. On the other hand, there is reason to believe that partial muscle activation should not be readily produced by the primate ocular motor system. First, saccades are thought to be initiated in an all-or-none manner. Second, although manual responses can be canceled by coactivating agonist and antagonist muscles, it should be nearly impossible to perform this type of cancelation in the ocular motor domain. The contralateral inhibitory circuitry of the brainstem saccade generator precludes this type of muscle coactivation (Hikosaka et al., 1978; Scudder et al., 2002; Sparks, 2002).

Because of their positions in the orbit, it is difficult to record EMGs directly from the extraocular muscles. However, an EEG effect associated with eye movements, the saccadic spike potential (SP), has been consistently noted in humans and monkeys

(Blinn, 1955; Keren et al., 2010; Sander et al., 2010). Several studies provide strong evidence that the SP does not originate in cortical activity or from the corneo-retinal potential (Thickbroom and Mastaglia, 1985; Moster and Goldberg, 1990; Picton et al., 2000). Instead, this component is myogenic, derived from contraction of the lateral and medial recti (Blinn, 1955; Thickbroom and Mastaglia, 1985). The SP appears as a prominent, high-frequency component occurring just prior to or concomitant with saccade onset. It takes the form of a frontal negativity with scalp distribution ipsilateral to the direction of eye movements (Thickbroom and Mastaglia, 1985; Moster and Goldberg, 1990; Keren et al., 2010). With appropriate filtering techniques, SPs have been shown to reliably precede saccades as small as 0.2° in amplitude, and to predict saccades with amplitudes less than 0.2° above chance level (Keren et al., 2010)[5]. Research on the SP has lapsed over the last few decades, but interest was recently renewed with the observation that many findings of gamma-band activity in scalp EEG recordings that were attributed to cognitive processes may actually have been artifacts from the SP associated with microsaccades (Yuval-Greenberg et al., 2008). Consequently, methods for isolating and removing SP activation from EEG recordings have been described (Keren et al., 2010).

In the present study, we tested the hypothesis that partial activation of eye-movement responses are made in the stop-signal task, similar to findings from manual

[5] Keren et al. (2010) report data from a bin that included saccade amplitudes ranging from 0.2° to 0.5°. As correctly pointed out by an anonymous reviewer, the distribution of saccade amplitudes within this bin was not reported. Strictly speaking, it is therefore impossible to say with certainty that SPs associated with saccades of 0.2° in amplitude could be reliably detected. However, it is well known that histograms displaying amplitudes of saccades recorded during a given time interval tend to take the form of decreasing exponential distributions (e.g. Collewijn & Kowler, 2008). In other words for any given distribution, saccades of smaller amplitude tend to be made with exponentially higher frequency than saccades of larger amplitude. Therefore, it is reasonable to expect that saccades with amplitudes ~ 2° made up a large proportion of the saccades used for this analysis.

stop-signal studies. This hypothesis predicts that partial muscle activation can occur on canceled trials. We tested this prediction by recording EEG and isolating SPs during periods when eye movements were prepared but not detected. We found strong SPs when saccades were made, but found no evidence of SP activation when movements were deemed canceled.

2.3 Methods

2.3.1 Animal Care

Data were collected from one male bonnet macaque monkey (*Macaca radiata* ~8.5 kg) and one female rhesus macaque monkey (*Macaca mulatta* ~7 kg). Both animals were cared for in accordance with policies set forth by the USDA and Public Health Service Policy on Humane Care and Use of Laboratory Animals. Animal care, procedures, and experiments were also carried out with supervision and approval from the Vanderbilt Institutional Animal Use and Care Committee. Fruit juice was given as positive reinforcement for correctly completed trials. During periods of testing, *ad libitum* access to liquids was withdrawn. In consultation with attending veterinarians, each animal's weight and food intake were monitored, and fluids were supplemented as needed.

2.3.2 Surgical Procedures

All surgical procedures were carried out under aseptic conditions. Access to food was withdrawn 12 hours prior to surgery. Animals were sedated with ketamine (10-30 mg/kg) and provided with an initial dose of buprenorphine (0.005-0.010 mg/kg) to alleviate post operative discomfort. Ophthalmic ointment was applied to prevent corneal drying. Robinul (0.004-0.008 mg/kg) was administered to minimize mucosal secretions and help prevent vagal bradycardia. Animals were intubated and catheters were

inserted into saphenous veins for administration of support fluids throughout the procedure. Monkeys were anesthetized with an isoflurane/oxygen mixture (1-3% $C_3H_2ClF_5O$), shaved, positioned in stereotax, and scrubbed. EKG, rectal temperature, respiration, and blood pressure were monitored. Expiratory CO_2 was maintained at ~4%. After subcutaneous administration of lidocaine (~1-2 ml of 2% soln'), the subjects' skulls were exposed and titanium headposts were firmly attached with titanium, orthopedic screws (Synthes, West Chester, PA) to immobilize the animals' heads during testing. Solid gold surface electrodes, Teflon coated stainless steel wires, and plastic connectors were constructed and implanted following the method of Woodman et al. (2007). Surgical sutures and staples were used to close incisions in layers. In consultation with attending veterinarians, analgesics (bupronorphine 0.005-0.010 mg/kg) and prophylactic antibiotics (naxcel 2.2 mg/kg) were administered for at least 3 days following surgery.

2.3.3 Task

During testing, monkeys were seated comfortably 51 cm from a cathode ray tube monitor (48 x 48°, 80Hz) in enclosed polycarbonate and stainless steel primate chairs and head restrained using surgically implanted head posts. Stimulus presentation, task contingencies related to eye position, and delivery of liquid reinforcement were all under computer control in hard real time (TEMPO, Reflective Computing, Olympia, WA). Stimuli were presented using computer-controlled raster graphics (TEMPO Videosync 1,280 x 1,040 pixel resolution , Reflective Computing, Olympia, WA). Stimuli had a luminance of 30 cd/m^2 (fixation point) or 10 cd/m^2 (targets) on a 1 cd/m^2 background.

Behavior and electrophysiological signals were recorded during the countermanding (i.e., stop-signal) task (Figure 2.1). Additional details about the behavioral training regime and task have been described previously (Hanes and Schall,

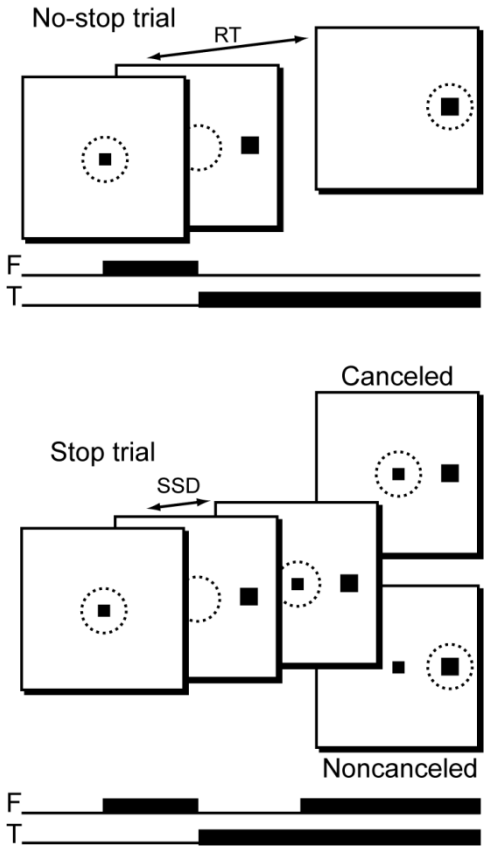

Figure 2.1. The stop-signal (or countermanding) task in a schematic representation. **No-stop trials** (top) were initiated when monkeys fixated a centrally presented fixation point. After a variable time, the fixation point was extinguished and simultaneously a peripheral target was presented at one of two possible locations. Monkeys were required to fixate targets with quick saccades for juice rewards. **Stop trials** (bottom) were initiated in the same way. After a variable time termed stop-signal delay (SSD) the fixation point was reilluminated, instructing the monkeys to withhold movement. Successful inhibition of saccades resulted in rewarded **Canceled trials**, but errant saccades resulted in unrewarded **Noncanceled trials**. Black squares indicate stimulus locations. Dotted circles represent area of fixation. F = fixation point, T = target, RT = reaction time, SSD = stop-signal delay.

1995; Hanes et al., 1998). Trials were initiated when monkeys fixated a centrally presented square which subtended 0.34° of visual angle. After a foreperiod ranging from 200 ms to 1100 ms, the central fixation point was extinguished and a target subtending 3° of visual angle simultaneously appeared at 10° to the left or right of fixation. The foreperiod was randomly sampled from a distribution described by the function;

$$p(t) = (1 - \exp(-t/\tau_g)) \cdot (\exp(-t/\tau_d))$$

where $p(t)$ describes the probability of selecting a specific foreperiod, τ_g describes the growth rate, and τ_d describes the decay rate. We chose a growth rate of 1000 ms and a decay rate of 200 ms to approximate a non-aging foreperiod. We added 200 ms to this distribution and truncated it at 1100 ms to achieve the desired range. On no-stop trials (Figure 2.1 top), no further visual stimuli were presented. Monkeys were required to make a saccade to the target within 600 ms to obtain reward. Correct trials were rewarded with several drops of juice and an audible tone. On stop trials (Figure 2.1 bottom), the fixation point was re-illuminated after a variable delay providing a “stop-signal” which instructed the monkeys to cancel their impending eye movements and maintain central fixation. In practice, two trial outcomes were then possible. If monkeys successfully withheld the eye movement and maintained fixation for a minimum of 600 ms, they obtained tone and juice reward. These trials were designated as "canceled”. If monkeys were unable to inhibit the movement, a 1500 ms timeout was added to the normal inter-trial interval of 200 ms, no rewards were given, and the trial was termed “noncanceled”. The stop-signal delay (SSD) or time between target and stop-signal presentation determines the probability with which movements can be successfully countermanded (Logan and Cowan, 1984). An initial set of SSDs from 0 to 420 ms and separated by either 40 or 60 ms was selected for each recording session. We then manipulated SSD using an adaptive staircasing algorithm which adjusted stopping

difficulty based on performance. When subjects failed to inhibit responses, the SSD was decreased by a random step of 1, 2, or 3 increasing the likelihood of success on the next stop trial. Similarly, when subjects were successful in inhibiting the eye movement, the next SSD was increased by a random step of 1, 2, or 3 decreasing the future probability of success. This procedure was used to ensure that subjects failed to inhibit action on ~50% of stop trials overall. Stop trials were 30 to 70% of all trials in a given session with a typical session consisting of several thousand trials. Reaction time data did not show any evidence that subjects slowed responses to "wait for" the stop signal (see Results). Saccade initiation and termination were detected offline using a custom algorithm implemented in the MATLAB programming environment (MathWorks, Natick, MA) which first detected instantaneous velocity elevated above 30°/s and then calculated the beginning and ending of the monotonic change in eye position.

2.3.4 Data Acquisition

Time stamps of relevant trial events were recorded at 1 kHz with analog data using a Plexon Multichannel Acquisition Processor (MAP) box (Plexon, Dallas, TX). Eye position was monitored using a video based infrared eye-tracking system (ASL, Bedford, MA) and was streamed to the Plexon MAP box parallel with trial events and EEG data using a 64 channel Plexon Breakout Board (PBOB, Plexon,Dallas, TX). We estimated the spatial resolution of our eye tracking setup by recording standard deviations while monkeys were actively fixating the central fixation point. Across all sessions, the mean standard deviations were ±0.54° and ±0.51° for monkeys F and Y respectively. The maximum standard deviations while fixating for a session were ±0.74 and ±0.67 for monkey F and Y respectively. Unfortunately, this spatial resolution was not high enough to detect microsaccades, although it was more than sufficient to detect the onsets of large task related responses. Implanted EEG surface electrodes were referenced to clip

style Ag/AgCl cup electrodes (Electro-Cap International, Eaton, OH) which were filled with conductive paste and clipped to either the left ear (monkey F) or linked to both ears (monkey Y). All data are recorded from an electrode approximating Fz of the international 10-20 system for humans in monkey F, and an electrode approximating Fpz in monkey Y. Since data are reported from a single midline electrode in both subjects, the asymmetric referencing used for monkey F did not result in any significant differences. The EEG from each electrode was amplified with a high-input impedance head stage (>1 GΩ , ~2 pF of parallel input capacitance, HST/8o50-G1-GR, Plexon Inc.) and filtered between 0.7 and 170 Hz with two cascaded, one-pole, low-cut, Butterworth filters and a four-pole, high-cut, Butterworth filter.

2.3.5 Race model behavioral analysis

A race model has been used with great success to account for both behavioral performance and neural activity in the countermanding paradigm (Logan and Cowan, 1984; Boucher et al., 2007a; Lo et al., 2009; reviewed by Verbruggen and Logan, 2008). On no-stop trials, reaction times (RTs) can be observed directly. On stop-signal trials, noncanceled RTs can be recorded, along with the probability of committing an errant noncanceled saccade at each SSD. The latter measure tends to assume the form of an increasing sigmoid curve, and has traditionally been referred to as an inhibition function. By treating the inhibition function as a cumulative probability distribution and comparing it to the distribution of RTs on no-stop trials, one is able to use the logic of the race model to estimate the median time required to cancel execution of a motor response (Logan, 1994; Band et al., 2003; see also Colonius, 1990). This stop-signal reaction time (SSRT) provides a measure of the otherwise covert stop process.

Following the methods of Hanes et al. (1998), we first fit a Weibull function with the following form to the inhibition function for each monkey averaged across sessions.

$$W(t) = \gamma - (\gamma - \delta) \cdot \exp(-(t/\alpha)^{\beta})$$

Where t = time after target onset, γ = the maximum probability value, δ = the minimum probability value, α = 64% of the maximum probability value, and β = slope. Next, we used the fitted inhibition functions and the combined no-stop RT data to estimate SSRTs for each monkey using two different methods. The first of these methods assumes that SSRT is a random variable, while the second method assumes that SSRT is constant across SSDs (Hanes et al., 1998; Band et al., 2003). Since there is no reason to suppose an advantage of either of these SSRT estimation methods, we averaged the two estimates together to obtain a final SSRT estimate separately for each monkey (Hanes et al., 1998; Paré and Hanes, 2003).

A robust finding in the stop-signal literature is that noncanceled RTs are significantly lower than no-stop RTs. This is a straightforward prediction of Logan and Cowan's (1984) horse race model, since trials with faster GO processes will tend to finish before the STOP process, thus escaping behavioral inhibition. It also suggests that noncanceled trials cannot be accurately compared to the entire distribution of no-stop trials when RT is a potential confounding variable. An accurate comparison can only be made between noncanceled trials and no-stop trials with relatively faster RTs. Specifically, noncanceled trials should only be compared to no-stop trials with RTs < SSRT + SSD. These are the trials which would have escaped behavioral inhibition and resulted in errant saccades had a stop-signal been presented. Similarly, for accurate comparisons, canceled trials must be matched to slower no-stop trials with RTs > SSRT + SSD. Thus, even though no response is generated on successfully canceled trials, RT ranges can be estimated for this trial type. The technique of matching noncanceled and canceled trials to no-stop trials with RTs from the appropriate portion of the RT distribution has been termed “latency matching” (Hanes et al., 1998). In the current study, it was especially important that we compare canceled trials to their latency

matched no-stop counterparts. This allowed us to estimate times when eye movements were likely even though they were not detected. Where appropriate, we used our derived SSRT estimates to latency match at each SSD.

2.3.6 Event-Related Potential (ERP) and Event-Related Velocity (ERV) analyses

ERPs were time-locked to saccade initiation or target onset and baseline corrected to the interval from 150 ms to 50 ms before these events. Canceled trials did not contain saccade events. Instead, a virtual saccade event was created for trials in this condition by randomly sampling from the distribution of latency matched no-stop RTs with replacement. Canceled trials were then aligned to this virtual saccade event and baseline corrected . Trials with voltage deflections greater than ±300 μV due to artifacts were excluded from further analysis. This threshold for rejection was an order of magnitude greater than the variability in the ERPs observed across monkeys (i.e., maximum root mean square for monkey F target aligned no-stop trials = 42.2 μV, canceled trials = 39.8 μV, noncanceled trials = 41.4 μV; maximum root mean square for monkey Y target aligned no-stop trials = 42.7 μV, canceled trials = 45.2 μV, noncanceled trials = 40.7). Single trial EEG signals were truncated 50 ms before the onset of the second, non-task related saccade to eliminate “smeared” saccade related artifacts. It was important to estimate the relative timing of saccades and to display this estimate graphically. Instead of using a traditional method such as displaying a histogram of saccade latencies, we collapsed across saccade velocity profiles. This method is essentially the same as creating an ERP from EEG data, except the data were radial eye velocity traces (Figure 2.2). The resulting average does not only contain information about saccade latency, but also takes into consideration saccade amplitude and duration, making it a more complete descriptor of average saccade dynamics. Since these velocity profiles have been aligned to particular events and collapsed across trials

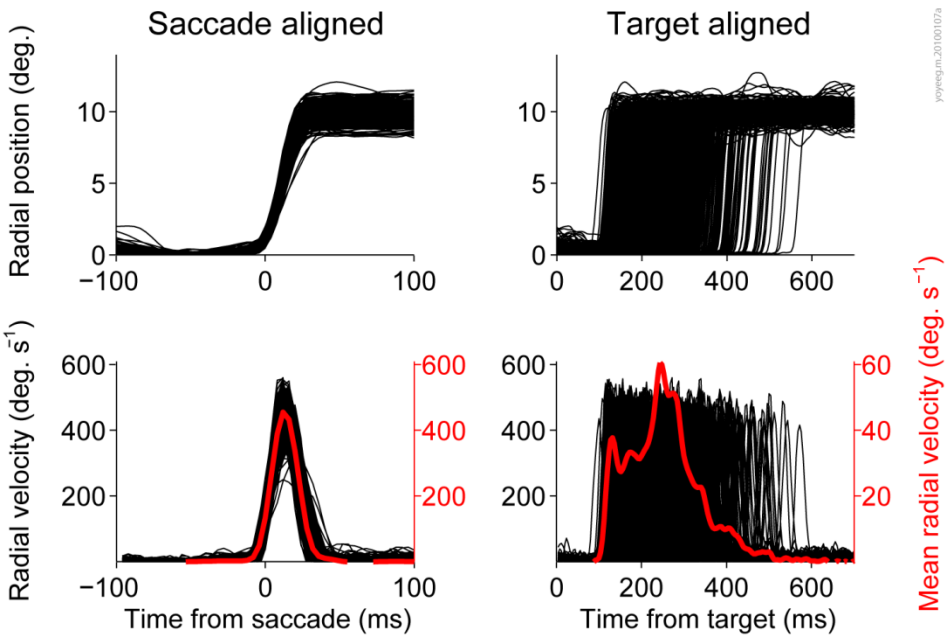

Figure 2.2. The timing of eye movements relative to task events was displayed using event related velocity (ERV) plots. This technique is similar to creating ERPs from raw EEG signal. Top left shows single trial radial positions for a sample session aligned on saccade onset. Bottom left shows instantaneous radial velocity for the same trials (**black**) along with the mean instantaneous velocity collapsed across all trials (**red**). Top right shows the same single trial radial positions in relation to target onset. Bottom right shows single trial instantaneous velocity in relation to target onset, as well as the average radial velocity collapsed across all trials. This target aligned ERV gives information about average saccade latency, velocity, and duration relative to target onset.

in the same way as ERPs, we will refer to them as "event-related velocities" (ERVs). ERVs were not baselined since an ERV value of 0 is not arbitrary as it is in an ERP. As a rule, the single trial velocity profiles which made up the ERVs were truncated at the onset of the second, non-task related saccade to avoid contamination of the task related saccade velocity trace.

Narrow digital band-pass filters (frequency ± 1 Hz) were employed to discriminate the SP from other saccade related components (see results). Each filter was created using a Hamming window of length $(2 \cdot T + .001)$s, where $T = \frac{1}{f}$. A zero phase-shift digital filter was applied to the data using the specified hamming window. Analytical power of the filtered data at each time t_i was approximated using a sliding window function of the form:

$$P(t_i) = \frac{\max(A) - \min(A)}{2}$$

where *A* is the time interval $[t_{i-\frac{T}{2}} \; t_{i+\frac{T}{2}}]$.. These methods ensured a high level of filter specificity while minimizing sacrifices in timing estimation accuracy at each band-pass frequency.

A signal to noise ratio was estimated for each applied filter to assess how well it isolated the SP from the surrounding EEG. After applying each filter to single session data and estimating analytical power, the mean value in a 41 ms time window centered on the peak of the SP was recorded. This value was termed the "signal". The mean value in a 1 s time window centered on saccade onset and excluding the signal time window was also recorded. This value was termed "noise". (Note that in this context, noise does not just refer to variability, measurement error, or unwanted line voltage fluctuations. Noise also refers to EEG fluctuations and includes those fluctuations which are task related. Task related EEG fluctuations do not average out in ERPs, and they

can obscure the SP which is our component of interest.) The filter yielding the highest signal to noise ratio was then used to isolate single trial SPs in subsequent analysis.

2.4. Results

2.4.1 Behavior

Reaction times, average probability of committing errors, and SSRT estimates collapsed across sessions are summarized in Table 2.1. Both animals exhibited noncanceled trials with probability > 50%. Since we used a staircasing algorithm to adjust SSD, this departure suggests that both animals tended to speed up, causing a reduction in SSD. This pattern of behavior has been described before in animals performing the saccade stop-signal task, and it appears to be an effective strategy for speeding up trial presentation and maximizing the rate of reward delivery (Godlove et al., 2009). In any case, our estimates of SSRT are lower than the more typical estimates of 80 to 100 ms recorded in the literature. If our estimates are artificially low due to violations of the race model, it presents a problem for latency matching, since we may have erroneously underestimated the time of probable SP activation on canceled trials. Accordingly, when results depend on latency matching, large reaction time windows have been displayed and analyzed to ensure that late SP activation was not missed in canceled trials.

2.4.2 Saccade Dynamics

Figure 2.3 plots main sequences of no-stop (blue) and noncanceled (red) saccades separately for each subject and each target. These data are summarized numerically in Table 2.2. We carried out 3 way ANOVAs to test the hypotheses that saccade amplitude and/or velocity differed between subjects, targets, or trial types. Both amplitude ($p < 0.001$, $df = 87$), and velocity ($p < 0.001$, $df = 87$) were found to differ

	no-stop RT	noncanceled RT	p(noncanceled)	SSRT
monkey F	224 ± 52	211 ± 57	0.58	59
monkey Y	243 ± 77	206 ± 75	0.53	59

Table 2.1. Summary statistics for stop-signal task performance. Reaction times (± 1 standard deviation), probability of committing errant noncanceled saccades, and SSRTs for each subject collapsed across sessions.

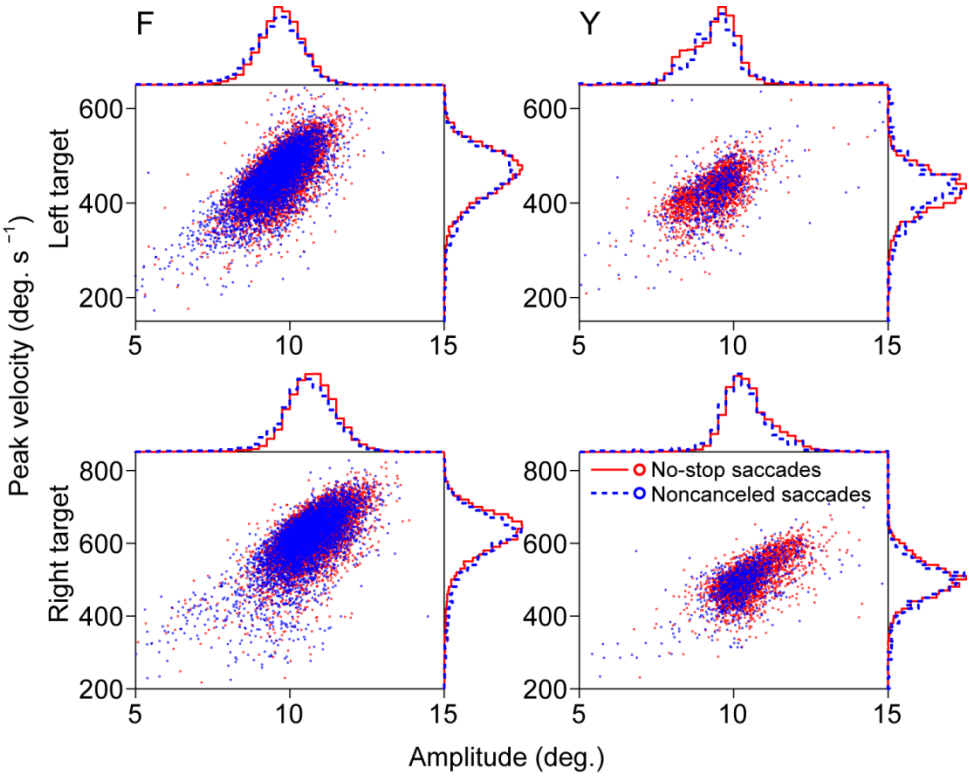

Figure 2.3. Saccade dynamics do not differ between no-stop and noncanceled trials. Scatter plots display saccade amplitude vs. peak saccade velocity (main sequences) across all sessions. Histograms display associated probability densities for each measurement. Binwidths are 10 deg/s for velocity distributions and 0.25 deg for amplitude distributions. Blue dots and broken lines represent saccades on no-stop trials. Red dots and solid lines represent saccades on noncanceled trials. Rows separate data by target. Columns separate data by subject.

	amplitude (deg.)				peak velocity (deg. s^{-1})			
	left target		right target		left target		right target	
	no-stop	noncanceled	no-stop	noncanceled	no-stop	noncanceled	no-stop	noncanceled
monkey F	9.7 ± 0.7	9.6 ± 0.9	10.7 ± 0.8	10.5 ± 1.2	473 ± 92	463 ± 97	623 ± 66	607 ± 104
monkey Y	9.3 ± 0.9	9.8 ± 2.9	10.5 ± 0.9	10.5 ± 2.2	428 ± 97	469 ± 306	502 ± 52	509 ± 247

Table 2.2 Countermanding saccade dynamics. Mean amplitude and mean peak velocities (± 1 standard deviation) across sessions separated by subject, target location, and trial type.

between targets. Monkeys tended to make slightly larger amplitude and higher velocity saccades toward the right target. This may be an artifact induced by the monocular eye tracking procedures we employed. Since we only tracked the right eye of each subject, saccades traces to the right target reflected abduction of the tracked eye while saccade traces to the left target reflected adduction of the tracked eye. On the other hand, the difference may reflect a real bias that both monkeys developed toward the right target. Peak saccade velocity was also found to differ between subjects ($p < 0.001$, $df = 87$). Monkey F made saccades with higher peak velocities than monkey Y. However, neither amplitude ($p = 0.701$, $df = 87$) nor peak velocity ($p = 0.380$, $df = 87$) differed significantly between trial types. Since main effects of around 1° proved highly significant in the target contrast, the failures to reject null hypotheses in the trial type contrasts cannot be attributed to a deficiency of statistical power. These results replicate earlier findings by Hanes and Schall (1995).

2.4.3 Saccade Aligned ERPs

Figure 2.4 plots saccade aligned ERPs and ERVs from both subjects. On trials in which saccades were detected, we observed a high amplitude, high frequency negativity occurring concomitant with or slightly before saccade initiation. This saccade-related component has been described many times in human subjects (Evdokimidis et al., 1991; Everling et al., 1997) and at least once in non-human primates (Sander et al., 2010).

For our purposes, the most important finding is the absence of the SP on canceled trials. At least two alternatives exist to explain this finding. First, we may conclude that partial muscle activation does not occur on canceled saccade trials, so no saccadic SP is evident. Second, we may conclude that aligning EEG to a virtual saccade event obtained by random sampling from existing RT distributions is too coarse a method to detect the saccadic SP on canceled trials. If partial motor activation did

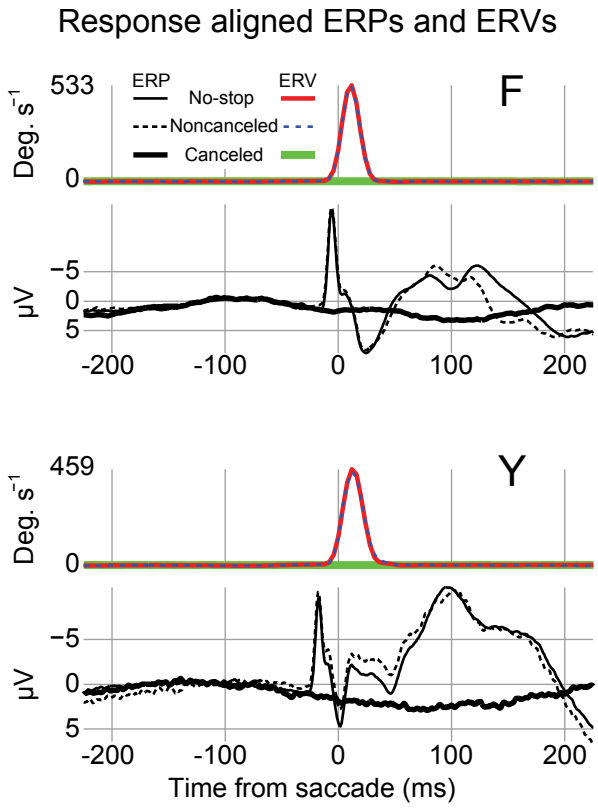

Figure 2.4. No SP is evident in canceled trials aligned on a virtual saccade event. Black traces show ERPs and colored traces show ERVs (see text). The thin solid traces show saccade aligned ERPs and ERVs on no-stop trials. The most prominent components in the ERPs are the sharp negative SPs, which occurs just prior to or concomitant with saccade onset and the several positive and negative deflections which follow. The first several components which follow saccade onset probably include a strong contribution from the corneo-retinal potential. The broken traces show ERPs and ERVs on errant noncanceled trials. Note the extreme similarity of the ERVs for no-stop and noncanceled trials. Note also the similarity between no-stop and noncanceled ERPs. This similarity is especially apparent in the time before saccade onset when the SP is visible. The thick solid traces depict ERPs and ERVs on canceled trials aligned to a virtual saccade event. No elevated velocity can be detected in the ERVs, and no SP can be detected around time 0 in the ERP. Data are collapsed across 15 sessions and recorded from a location approximating Fz for monkey F. Data are collapsed across 7 sessions and recorded from a location approximating Fpz for monkey Y. ERP data are baselined to the period from 150 ms to 50 ms before saccade onset. The number of trials in each ERP follows. Monkey F; no-stop n = 13,764, canceled n = 6,256, noncanceled n = 6,552. Monkey Y; no-stop n = 4,782, canceled n = 1,489, noncanceled n = 1,120.

occur on these trials, we do not know when. Therefore, aligning on virtual randomly sampled RT events and collapsing across the data may have smeared any partial SPs and rendered them difficult to detect. We note that even if small amplitude SPs had been generated on the canceled trials but were temporally smeared by averaging, they should be revealed by a low amplitude, broad negativity during the measurement epoch. As is evident in Figure 2.4, we did not observe a waveform on canceled trials consistent with this pattern. However, we carried out an additional time-frequency analysis to isolate SP activation from the surrounding EEG and test for the presence of extraocular EMG activation during canceled stop trials.

2.4.4 Isolated SP activation

In our data, the SP is readily visible as a stereotyped high frequency negativity (Figure 2.4). Because of its unusually high frequency and its invariance across sessions, we hypothesized that SP activation could be discriminated from the surrounding EEG on a trial-by-trial basis after application of an appropriate filter (see also Keren et al. 2010). We applied narrow digital band-pass filters in steps of 10 Hz to search for a frequency which optimally discriminated SP activation from the surrounding EEG. After filtering the data and calculating power as a function of time, we constructed response aligned ERPs for no-stop trials at each band-pass frequency for each recording session. We then calculated signal-to-noise ratios for each filtered ERP. The result of this analysis is plotted in Figure 2.5f. A band-pass filter centered on 95 Hz was found to provide the greatest discrimination between the SP and the surrounding EEG for monkey F, while a band-pass filter centered on 35 Hz was found to be optimal for monkey Y. At first glance, this difference may seem surprising. However, our technique does not simply measure the frequencies contributing power to the SP. Instead, it isolates the frequency which optimally discriminates the SP from the surrounding EEG.

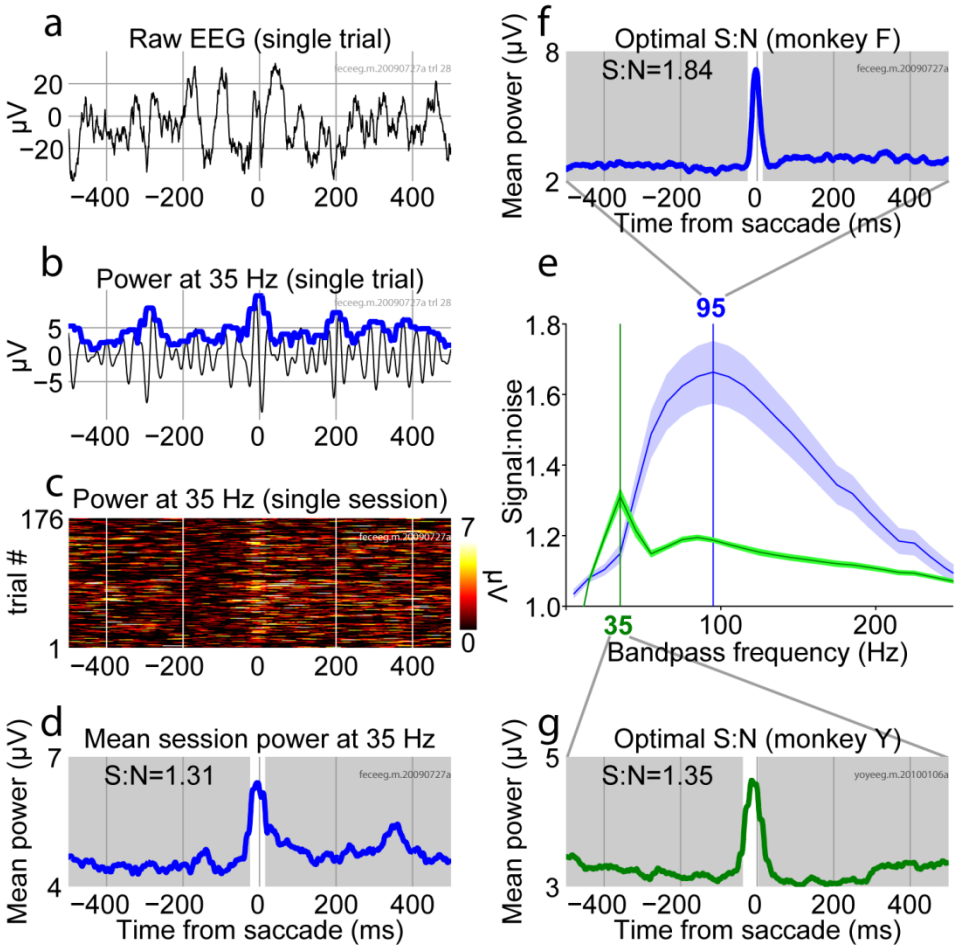

Figure 2.5. Band-pass filters were optimized to find frequencies which allowed for the highest discrimination between the SP and non SP components. **a** One second example of raw EEG centered on saccade onset. Note that in this and following panels negative is plotted down so that later power traces appear facing upward. **b** The same EEG signal processed with a 35 Hz band-pass filter. After filtering, the analytical power was estimated (see methods) and this estimate is depicted by the thick blue line. **c** Power at 35 Hz for every no-stop trial in the example session. Each horizontal line of color depicts a single trial centered on saccade onset. Warmer colors indicate more power. Note the faint band adjacent to saccade onset indicating that the 35 Hz band-pass filter was somewhat successful in isolating SP related activation. **d** This result is further demonstrated by collapsing across all trials and creating an ERP from the power traces at 35 Hz. A "signal" and "noise" time period was chosen based on SP peak time measured from unfiltered session ERPs. The time period highlighted in white was the signal time period, and the time period in gray was the noise time period for monkey F. Average power in both time periods was recorded and used to calculate signal to noise ratios (S:N). **e** S:N for each band-pass frequency was calculated for each session. These traces show the average S:N separately for monkey F (blue) and monkey Y (green) ± SEM. The highest S:N was found at a band-pass frequency of 95 Hz for monkey F (**f**) and 35 Hz for monkey Y (**g**).

therefore, this difference reflects variations in overall EEG frequency spectra between the two monkeys. Differences in EEG frequency spectra are to be expected due to several factors. For example, the skulls of monkeys F and Y were observed to be of different thicknesses during surgery (Nunez and Srinivasan, 2006).

Application of optimal discrimination band-pass filters allowed us to observe the SP separate from the surrounding EEG. By using this technique, we were able to search for SP activation in target aligned ERPs made up either of no-stop or canceled trials. This comparison is plotted for for a sample session from monkey F in Figure 2.6. The SP is visible in the unfiltered data when aligned on response onset, but is impossible to resolve, even on no-stop trials, when aligned on target onset (left column). After filtering, the SP is readily apparent in the response aligned, single trial data as a vertical band of elevated power (Figure 2.6 top right). A diffuse band of power can also be observed in the target aligned no-stop trials during the period of time when saccades are initiated (Figure 2.6 middle right). But no coherent band of elevated power can be discriminated on successfully canceled trials (Figure 2.6 bottom right).

Our band-pass filtering technique also provided us with power measurements which were amenable to statistical testing. After filtering the data, and performing latency matching to compare canceled trials with the appropriate no-stop trials, we measured average normalized power during a discrete window around mean RTs. For our window, we chose the period from the 25th percentile RT to the 75th percentile RT. Following this method ensured that we sampled power on canceled trials during the period of time when SPs were most likely to occur. Since power was baseline corrected to the interval 150 ms to 50 ms before target onset, power measurements collected at each SSD could be subjected to *t*-tests allowing us to test the null hypothesis that canceled trials do not show SP activation in the absence of overt eye movements. Results from this analysis are plotted in Figure 2.7. Each observation represents the

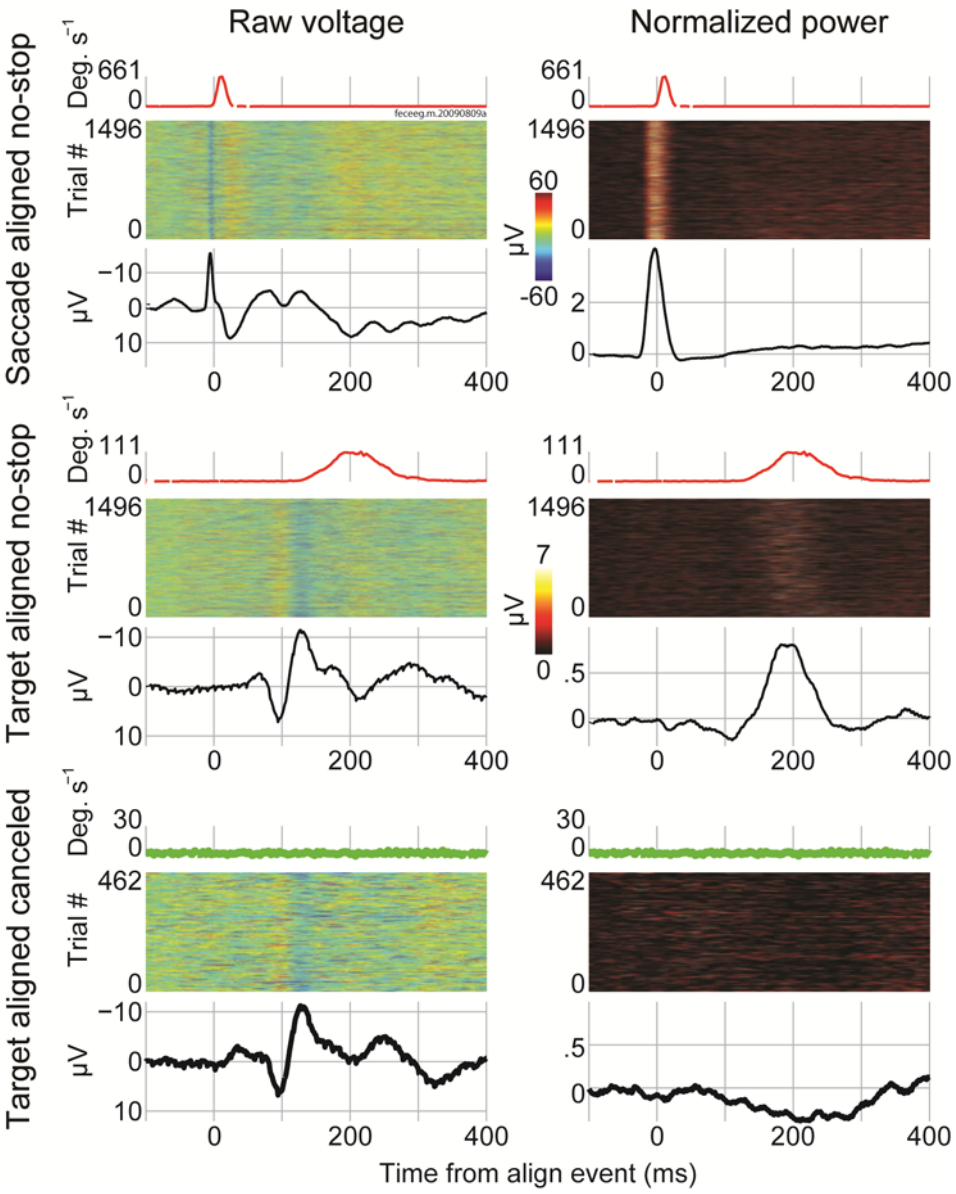

Figure 2.6. Filtering EEG makes it possible to observe the SP independent of surrounding EEG, but no SP is observed on canceled trials. Traces at top show ERVs to display saccade timing (conventions as in Figure 4). Heat maps show individual trials (conventions as in Figure 5). Black lines show ERPs collapsed across trials. Thin lines show no-stop trial ERPs, and thick lines show canceled trial ERPs. The left column displays raw voltage. At top, data are presented from no-stop trials aligned to saccade onset. The ERV appears as a narrow component beginning at saccade onset. The heat maps display negative bands of activation at saccade onset corresponding to the SP. Collapsing across the data in the ERP makes the SP readily apparent in both the raw and filtered data. At middle, data are presented from no-stop trials aligned to target onset. The ERV reflects this change. Now saccades are smeared around 200 ms centered roughly at 210 ms after target onset. Because of this smearing, it is no longer possible to discern negative activation associated with the SP in the raw heat map. This activation should be apparent centered around 200 ms after target onset. SP activation is also smeared in the raw ERP, rendering it invisible. However, in the filtered data, SP

activation is clear around 200 ms in both the heat map and ERP. At bottom, data are presented from canceled trials aligned to target onset. The ERV never approaches 30 deg. s^{-1} (criteria for saccade initiation). No SP is apparent in the raw heat map data, or in the raw ERP. But it is impossible to tell if no SP exists, because it is also unobservable in the raw no-stop data plotted above due to overlapping components and smear. The filtered data at right allows for examination of SP activation. No SP activation can be observed in the time around saccade initiation. If anything, a small depression in high frequency SP activation is all that can be observed.

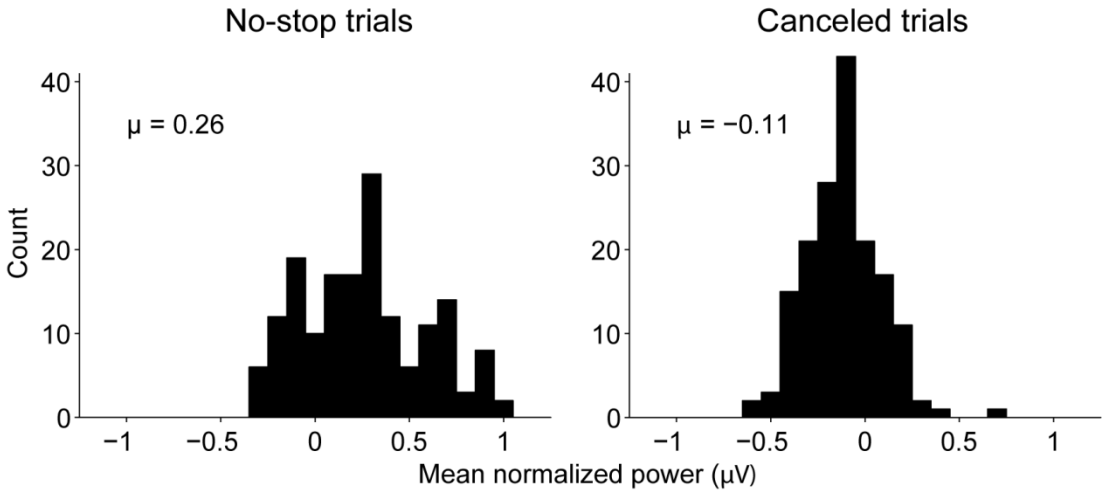

Figure 2.7. No-stop trial EEGs display significantly increased SP activation during periods when saccades are produced, but canceled trial EEGs show no increase in SP activation. After latency matching trials and filtering EEG data (see Figure 6), the average power during a discreet time window was measured on a trial by trial basis. For the time window, we chose the period between the 25th and 75th RT percentiles. Since no-stop trials were latency matched to canceled trials, this is the period of time during which SP activation was most likely to occur in both trial types. Power averages were collected from this time window at each SSD. Each SSD from each recorded session yielded a single observation for each trial type. Histograms depict the results of this analysis. The observations are gathered in 0.1 μV bins for display purposes. Grand average power is reported for each trial type above the appropriate histogram. Note that the sign of these averages is negative for canceled trials. Both distributions deviate significantly from 0 (students t-test, $p < 0.001$, $df = 167$).

average power for one SSD measured during the period of time when saccades were likely. No-stop trials (left) show an increase in power above baseline when saccades were produced (mean = 0.26 μV). This increase is statistically significant ($p < 0.001$, $df = 167$), and demonstrates that there was a reliable increase in SP activation associated with saccades. In contrast, canceled trials (right) show slightly decreased power during the period of time when saccades were likely to occur (mean = -0.11 μV). Although this effect is small, it is statistically significant ($p < 0.001$, $df = 167$) suggesting a small but reliable decrease in SP activation during periods when saccades were canceled. Thus, no partial EMG activation is present when monkeys cancel eye movements in the saccade countermanding task.

2.5 Discussion

We have provided evidence indicating that partial muscle activation does not occur in the primate ocular motor system when monkeys inhibit saccades in a countermanding task. Our conclusion is supported by the following observations. First, when canceled ERPs are aligned on a virtual saccade event to create saccade aligned ERPs, no evidence of EMG activation in the form of a SP can be observed around the time of saccade initiation. Second, when the SP activation is isolated from the surrounding EEG using band-pass filters, no-stop trials show EMG power which is significantly elevated above baseline while saccades are being made. Canceled trials, on the other hand, do not show EMG power that is elevated above baseline. Instead, trials in which saccades were deemed canceled display slightly reduced EMG activation as measured by the SP. This is strong evidence against partial motor activation in the ocular-motor system on canceled saccade trials.

The saccadic countermanding paradigm is a versatile tool which has led to many key findings over the last two decades. Human psychophysics experiments using the

saccadic stop-signal task have helped elucidate the nature of conjugate gaze shifts (Corneil and Elsley, 2005), differences between predictive and reactive stimulus tracking (Joiner et al., 2007), the relative contributions of reflexive foveal stimulation to stopping (Cabel et al., 2000), and the influence of stimuli timing and salience on saccade inhibition (Morein-Zamir and Kingstone, 2006; Stevenson et al., 2009). Physiological recordings from monkeys carrying out the stop-signal task have helped uncover cortical (Hanes et al., 1998; Brown et al., 2008; Ray et al., 2009; Scangos and Stuphorn, 2010; Stuphorn et al., 2010) and subcortical (Paré and Hanes, 2003) mechanisms of saccade generation. The task is useful for investigating performance monitoring in both human (Curtis et al., 2005; Endrass et al., 2005) and animal subjects (Stuphorn et al., 2000; Ito et al., 2003; Stuphorn and Schall, 2006; Emeric et al., 2008, 2010). In addition, the saccadic countermanding task has given rise to a strong computational modeling literature leading to breakthroughs in understanding neural saccade production and regulation (Hanes and Schall, 1996; Asrress and Carpenter, 2001; Boucher et al., 2007b; Lo et al., 2009; Wong-Lin et al., 2010). Finally, the saccadic stop-signal task has had broad clinical significance, providing insight on the action of several popular anesthetic agents (Khan et al., 1999; Nouraei et al., 2003), as well as the core dysfunctions underlying disorders such as mild traumatic brain injury (DeHaan et al., 2007), Parkinson's disease (Joti et al., 2007), and ADHD (Armstrong and Munoz, 2003; Hanisch et al., 2006). Given the wide experimental significance of the saccadic stop-signal paradigm, the observation of partial muscle activation on canceled saccade trials would have provided important theoretical leverage to the study of behavioral inhibition.

Several groups have found partial motor activation on canceled trials during the manual response version of the countermanding task. Partial motor activation on canceled trials has been taken as evidence against a ballistic phase of motor execution (De Jong et al., 1990; McGarry and Franks, 1997; McGarry et al., 2000). Partial motor

activation has also been used to study the unity or diversity of stopping under different circumstances (De Jong et al., 1990; van Boxtel et al., 2001). In addition, partial motor activation on canceled trials has been compared to full motor activation on no-stop trials, used as a proxy measure for SSRT, and compared to neural data to assess the relative contribution of supplementary motor neurons to movement initiation (Scangos and Stuphorn, 2010). Clearly, partial motor activation on canceled trials is a useful measurement for characterizing countermanding behavior. In contrast to manual response countermanding, partial extraocular muscle activation appears to be absent on canceled trials in the saccade countermanding task.

Lack of partial extraocular muscle activation on canceled trials is not surprising given our current understanding of the saccadic system. The saccadic system and the spinal motor system differ in several important ways. Unlike manual responses and smooth pursuit eye movements, saccade initiation is, in many ways, ballistic (reviewed by Sparks 2002; Scudder et al. 2002). Kornylo and colleagues (2003) found that pursuit eye movements could be canceled more quickly than saccadic eye movements, and concluded that saccade production includes a final ballistic stage which is not observed during pursuit.

One possible criticism of this work concerns the linking proposition identifying the SP with the extraocular EMG. Since its first observation and characterization as the external rectus muscle potential (Blinn, 1955) the SP has been almost uniformly appreciated as myogenic in nature (Picton et al., 2000; but see also Kurtzberg and Vaughan, 1982; Balaban and Weinstein, 1985; Riemslag et al., 1988). This conclusion is supported by the following seven observations. First, the corneo-retinal potential cannot contribute to the SP since the SP can still be recorded in total darkness (Riggs et al., 1954; Moster and Goldberg, 1990) and observed in patients with ocular prosthesis and intact extraocular musculature (Thickbroom and Mastaglia, 1985). Second, the SP

is not considered to be cortical in origin, since it has been obtained with normal topography after complete hemispherectomy (Thickbroom and Mastaglia 1985). Third, the SP is attenuated or absent in patients with lateral rectus palsy or patients in whom the intra-orbital musculature have been surgically removed (Thickbroom and Mastaglia, 1985). Fourth, the amplitude of the SP remains constant, but its scalp distribution changes predictably with saccades made in different directions (Thickbroom and Mastaglia, 1985; Moster and Goldberg, 1990; Keren et al., 2010). Fifth, both its scalp distribution (Moster and Goldberg, 1990; Lins et al., 1993a; Keren et al., 2010; Sander et al., 2010) and dipole source modeling (Thickbroom and Mastaglia, 1985; Lins et al., 1993b) suggest that the SP is maximal around the eyes. Sixth, there is a close and consistent timing correlation between the peak of the SP and saccade onset (Thickbroom and Mastaglia, 1985; Keren et al., 2010). Seventh, the amplitude of the SP shows a positive correlation with saccade amplitude (Keren et al., 2010). Thus, using the strong inference method advocated by Platt (1964), an extensive body of evidence demonstrates that the SP should be viewed as an extraocular EMG. It is a natural step then, to search for the presence of extraocular EMG activation using SPs recorded in the stop-signal task.

Another possible criticism concerns the resolution of our EMG measurement. One may argue that our proxy measure of extraocular EMG was not sensitive enough to detect small muscle activations. If so, partial muscle activation may have been present on some canceled trials which was unobservable as single trial SP. Using a wide band-pass filter, Keren et al. (2010) were able to reliably isolate single SPs from the raw EEG. They then used signal detection theory to quantify the accuracy with which single SPs predict saccades. These researchers found that they could detect greater than 80% of saccades 0.5 - 1° in amplitude with close to zero false alarms, and they could detect saccades of 0.02 - 0.2V° in amplitude above chance level. They concluded that single

SPs might serve as more reliable saccade indicators than the traditional method of detecting corneo-retinal dipole shifts in EEG recordings.

We refined the technique presented by Keren et al. (2010) by adopting a frequency optimization procedure which ensured that small SPs would be highly detectable. The average power traces which we were able to construct for no-stop trials containing 10° saccades suggest that we would have been able to detect SPs associated with very small amplitude movements (see Figures 2.5 and 2.6). Still, the fact remains that canceled trials may be associated with subthreshold EMG activation which is too small to detect with surface electrodes. In order to test this hypothesis further, recordings would be needed from microelectrodes inserted into the motor nuclei themselves.

It is noteworthy that we did not simply observe a lack of extraocular EMG on canceled saccade trials. Instead, we report a small but significant decrease in EMG activity when eye movements were withheld. Before baselining, a tonic increase in EMG was observed in the period of time around task related saccades. (Figure 2.5f and 2.5g.) We speculate that this tonic resting EMG activity was produced by microsaccades which occurred throughout our recordings (Yuval-Greenberg et al. 2008). On canceled trials, we observed a significant decrease in tonic EMG activity during periods when saccades were likely (Figure 2.6 lower right). Following this logic, we suggest that fewer microsaccades are probably made while eye movements are suppressed during canceled trials. This would be an interesting finding, useful for further characterizing the function of fixation cells during the countermanding task. Unfortunately, the spatial resolution of our current eye tracking data set does not allow us to test this hypothesis directly. Future work should measure the presence or absence of microsaccades during periods when task related saccades are canceled in the countermanding task.

In summary, we isolated EMG activation associated with eye movements from the EEGs of monkeys performing a saccade-countermanding task. We found that eye movements were reliably accompanied by EMG activation on noncanceled trials, but no subthreshold EMG activation was detectable on successfully canceled trials. This finding demonstrates the ballistic nature of saccade initiation, and highlights a basic difference between the spinal motor system and the saccadic ocular motor system.

CHAPTER 3

MICROSACCADE PRODUCTION DURING SACCADE CANCELATION IN A STOP-SIGNAL TASK

3.1 Abstract

We obtained behavioral data to evaluate two alternative hypotheses about the neural mechanisms of gaze control. While there is agreement that the caudal superior colliculus (SC) is involved in saccade production to peripheral targets, disagreement persists about the role of rostral SC. The “fixation” hypothesis states that rostral SC maintains fixation of gaze. The “microsaccade” hypothesis states that rostral SC produces microsaccades rather than fixation per se. These hypotheses have been framed as mutually exclusive and have not been tested under normal physiological conditions. Previously reported neuronal activity in monkey SC during the saccade stop-signal task leads to specific, dissociable predictions of these two hypotheses. When subjects are required to cancel partially-prepared saccades, unbalanced activity spreads across rostral and caudal SC with a predictable, temporal profile. Because of unbalanced activation in monkey SC, the microsaccade hypothesis predicts increased microsaccade production with bias toward the target location during the period when response saccades are canceled. The fixation hypothesis predicts decreased microsaccade production during this time period. With this neural data in mind, we adopted a psychophysical approach to test predictions of the fixation and microsaccade hypotheses. We measured microsaccades of monkeys performing the saccade stop-signal task. We found that microsaccade production was consistent with the fixation hypothesis but not the microsaccade hypothesis. We suggest that the fixation and

microsaccade hypotheses are not mutually exclusive because both types of neurons are present in rostral SC.[6]

3.2 Introduction

The caudal superior colliculus (SC) plays an important role in gaze-shifting (e.g., Munoz et al., 2000; Munoz and Schall, 2004; Krauzlis, 2008; Gandhi and Katnani, 2011). However, disagreement persists about the role of neurons in rostral SC. One line of work indicates that neurons in rostral SC aide in gaze-holding (Munoz and Wurtz, 1993a). Electrical stimulation in rostral SC can interrupt saccades midflight (Munoz and Wurtz, 1993a; Paré and Guitton, 1994; Munoz et al., 1996). This effect is probably mediated by connectivity with brainstem omnipause neurons (OPNs) that exert potent inhibition on saccade-related burst neurons. Anatomical studies show that rostral SC projects more heavily than caudal SC to brainstem OPNs (Gandhi and Keller, 1997; Büttner-Ennever et al., 1999). Inactivation of rostral SC with the GABA agonist muscimol has been reported to increase saccade production (Munoz and Wurtz, 1993b). Thus, SC may be composed of spatially organized gaze-shifting "movement" and gaze-holding "fixation" neurons. We will refer to this view as the "fixation hypothesis".

Another line of work indicates that rostral SC neurons contribute to small eye movements called microsaccades (Krauzlis et al., 1997; Hafed and Krauzlis, 2012). During visual fixation, balanced population activity of SC neurons averages to a vector with zero magnitude, resulting in no eye movements (Goffart et al., 2012). However, fluctuations in firing rates or subthreshold activation in caudal SC can create an imbalance in this activity that is supposed to lead to microsaccades (Hafed et al., 2008; Hafed and Krauzlis, 2012). The microsaccade hypothesis accommodates some findings

[6] This chapter has been submitted as Godlove DC, Schall JD. Microsaccade production during a stop-signal task.

that seem incompatible with the fixation hypothesis (Sugiuchi et al., 2007; Gandhi and Katnani, 2011). For example, trajectories show deviation when saccades are interrupted by stimulation of rostral SC (Gandhi and Keller, 1999b). This stimulation may excite microsaccade neurons causing deviation in the vector average guiding saccade production. Neural chronometry also indicates that rostral SC projections do not provide simple driving input to OPNs (Gandhi and Keller, 1997; Everling et al., 1998; Gandhi and Keller, 1999a) results summarized above, inactivation of rostral SC has been reported to decrease saccade production (Hafed et al., 2008; Hafed et al., 2009; Goffart et al., 2012). Thus, rostral SC neurons may encode small motor error and produce microsaccades. We will refer to this view as the "microsaccade hypothesis".

The microsaccade hypothesis may explain a possible link between microsaccades and covert attention (Hafed and Clark, 2002; Engbert and Kliegl, 2003; Hafed et al., 2011; but see Tse et al., 2004; Horowitz et al., 2007) through an imbalance in the saccade map. Vector average asymmetries are thought to be caused by subthreshold activation of caudal SC at the attended location (Hafed et al., 2009). Thus, attention-related microsaccades may stem from partially prepared saccades leading to unbalanced activation in SC (Engbert, 2012).

A saccade stop-signal task is ideally suited to test these hypotheses (Hanes and Schall, 1995; Hanes and Carpenter, 1999) (Figure 3.1). Task participants are instructed to cancel partially prepared saccades shortly after a cue to respond. These conditions mirror those thought to give rise to microsaccades. Furthermore, recordings from macaque monkeys have revealed the detailed time course of unbalanced neural activity in SC (Paré and Hanes, 2003) and FEF (Hanes et al., 1998) during this task (Figure 3.2). Specifically, activity in caudal SC is interrupted as neurons in rostral SC rapidly increase firing rates during saccade cancelation. Critically, this modulation occurs within *stop signal reaction time* (SSRT), the duration of the STOP process in Logan's race

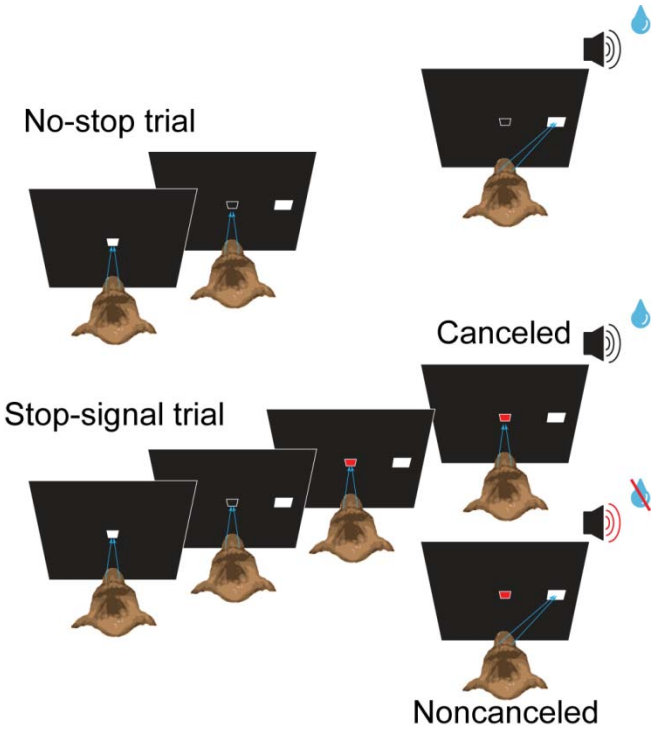

Figure 3.1. The saccadic stop-signal (countermanding) task. Top, No-stop trials were initiated when monkeys fixated a central point. After a variable time, the center of the fixation point was extinguished leaving an outline. A peripheral target was presented simultaneously at one of two possible locations. Monkeys were required to fixate targets with quick saccades for juice rewards. Bottom, Stop trials were initiated in the same way. After a variable time (SSD), the center of the fixation point was reilluminated in a different color, instructing the monkeys to withhold movement. Successful inhibition of saccades resulted in rewarded canceled trials, but errant saccades resulted in unrewarded noncanceled trials. Microsaccade data from canceled trials were analyzed.

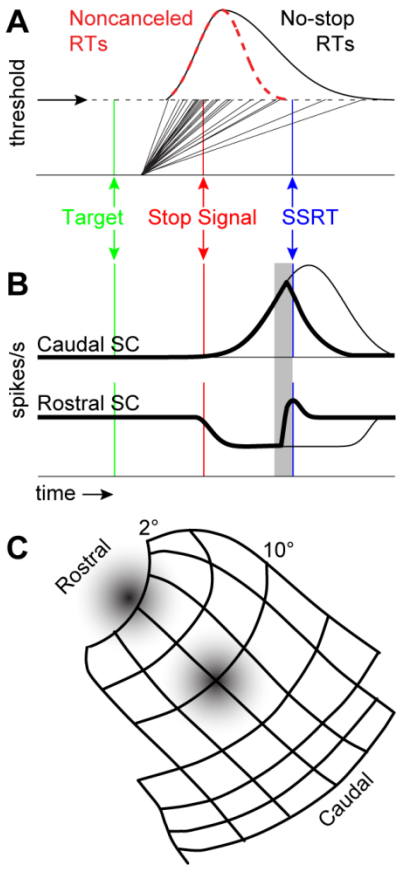

Figure 3.2. Timing and spatial distribution of unbalanced activity in superior colliculus (SC) during the stop-signal task. **A** Application of Logan's race model yields estimates of stop-signal reaction time (SSRT blue). This is the time necessary for a movement to be canceled. Given the presentation of a stop-signal on a particular trial, motor processes on trajectory to reach threshold after SSRT will not result in movement, effectively truncating the reaction time distribution. **B** Unbalanced activity in SC shows a predictable spatial and temporal evolution during the saccade stop-signal task. Thick traces represent activity on canceled trials. Thin traces depict activity on latency matched no-stop trials. Diagram is adapted from data presented by Paré and Hanes (see their Fig. 3 and Fig. 7). **C** Spatial activity in SC is stereotyped around SSRT. Neural activity is taken from gray window in B. Rostral and caudal SC show coactivation just before and concomitant with SSRT on canceled trials. This coactivation is most pronounced at longer stop-signal delays (SSDs). According to the microsaccade hypothesis, this coactivation should increase the likelihood of microsaccades concomitant with SSRT.

model (Logan and Cowan, 1984; Boucher et al., 2007a; Lo et al., 2009). Thus, movement-related neurons in caudal SC and neurons in rostral SC are concurrently active before SSRT and show maximal coactivation resulting in maximal collicular imbalance, concomitant with SSRT (Hanes et al., 1998; Paré and Hanes, 2003).

The microsaccade hypothesis predicts that unbalanced activation across the collicular map will lead to increased microsaccade production (Hafed et al., 2009; Hafed and Krauzlis, 2012). During the stop-signal task, unbalanced activity in SC is maximal concomitant with SSRT (Paré and Hanes, 2003). It follows logically that we should observe, on average, increased microsaccade activity concomitant with SSRT on canceled trials during the stop-signal task. Furthermore, microsaccades should proceed toward target locations, because unbalanced vector averages will be biased toward targets by increased activity in caudal SC (Hafed et al., 2008; Hafed et al., 2009). In contrast, the fixation hypothesis predicts that microsaccade production will decrease concomitant with SSRT; elevated activity of gaze-holding fixation neurons will inhibit task-related saccades and microsaccades alike. We previously reported that extraocular electromyogram (EMG) activity showed a small but reliable decrease during periods when saccades were successfully canceled (Godlove et al., 2011a). This finding provides preliminary support for the fixation hypothesis. In the current study, we use high-resolution eye tracking and detection techniques in macaque monkeys to test predictions of these 2 hypotheses directly.

3.3 Materials and Methods

3.3.1 Animal care

Data were collected from 3 male bonnet macaques (*Macaca radiata* 6.9 to 8.5 kg) and one female rhesus macaque (*Macaca mulatta* 6 kg). Animals were cared for in accordance with policies set forth by the USDA and Public Health Service Policy on

Humane Care and Use of Laboratory Animals and all procedures were carried out with supervision and approval from the Vanderbilt Institutional Animal Care and Use Committee. Titanium headposts were surgically implanted to facilitate head restraint during eye tracking. Surgical methods have been described in detail (Godlove et al., 2011b).

3.3.2 Stimuli and Task

Monkeys were seated in enclosed primate chairs with heads restrained using surgically implanted head posts. Depending on primate chair and recording setup, monkeys sat 43-49.5 cm from a 70 Hz CRT monitor subtending 47.8-51.8° horizontal visual angle and 34.5-37.4° vertical visual angle. Stimulus presentation, task contingencies related to eye position, and delivery of liquid reinforcement were all under computer control in hard real time (TEMPO, Reflective Computing, Olympia, WA). Stimuli were presented using computer-controlled raster graphics (TEMPO Videosync 640 x 400 pixel resolution, Reflective Computing, Olympia, WA). Stimulus sizes and eccentricities were automatically adjusted by the computer program to account for subject viewing distance and had luminance values of 10 cd/m^2 on a 0.02 cd/m^2 background or 39 cd/m^2 on a 10 cd/m^2 depending on which recording setup was used.

Data were recorded during the saccade stop-signal (i.e., countermanding) task (Figure 3.1). Additional details about the behavioral training regime and task have been described previously (Hanes and Schall, 1995; Hanes et al., 1998). Trials were initiated when monkeys fixated a centrally presented square which subtended 0.34° of visual angle. After a foreperiod ranging from 600 ms to 1100 ms, the center of the fixation point was extinguished, leaving an open square outlined 1 pixel thick, and a target subtending 3° of visual angle simultaneously appeared centered at 10° to the left or right

of fixation. The foreperiod was approximately non-aging, randomly sampled from a distribution described by the function:

$$p(t) = e^{-t/k}$$

where the probability of selecting a specific foreperiod *p(t)* is an exponential function with time constant of *k*. We set *k* equal to 250 ms and shifted the distribution to fall between 600 and 1100 ms. On no-stop trials (Figure 3.1 top), no further visual stimuli were presented. Monkeys were required to make a saccade to the target within 800 ms and hold fixation for 600 ms to obtain reward. Correct trials were rewarded with an audible tone followed 600 ms later by several drops of juice. On stop trials (Figure 3.1 bottom), the center of the fixation point was re-illuminated either red or green (constant for each monkey) after a variable delay providing a “stop-signal” which instructed the monkeys to cancel their impending eye movements and maintain central fixation. In practice, two trial outcomes were then possible. If monkeys successfully withheld the eye movement and maintained fixation for a minimum of 1600 ms, they obtained tone and juice reward. These trials were designated as "canceled”. If monkeys were unable to inhibit the movement, an audible tone signaling timeout sounded and a variable timeout was added to the normal inter-trial interval. These trials were termed “noncanceled”. During some recording sessions with monkey X, a third trial type was introduced containing an irrelevant visual stimulus. These trials will be the subject of a future report, and their presence did not change behavior in the main task. An initial set of SSDs was selected for each recording session based on the animals' previous behavior. We then manipulated SSD using an adaptive staircasing algorithm that adjusted stopping difficulty based on performance. When monkeys failed to inhibit responses, the SSD was decreased by a random step of 1, 2, or 3 increasing the likelihood of success on the next stop trial. Similarly, when monkeys successfully inhibited an eye movement, the next SSD was increased by a random step of 1, 2, or 3 decreasing the future probability

of success. This procedure was used to ensure that subjects failed to inhibit action on ~50% of stop trials overall. Stop trials comprised 30-50% of all trials in a given session with a typical session consisting of several thousand trials.

3.3.3 Data acquisition

All data were streamed to a single data acquisition system (Plexon, Dallas, TX). Time stamps of trial events were recorded at 500 Hz, while eye position was recorded at 1 kHz. Eye position data were calibrated, acquired, and streamed to the Plexon computer using the EyeLink 1000 infrared eye-tracking system (SR Research Kanata, Ontario, Canada). This system has a resolution of 0.01° (36″).

3.3.4 Saccade detection

All saccade analyses were performed in the MATLAB programming environment using custom written code. Eye channels were first convolved with a 12 ms Gaussian polynomial to remove small line voltage fluctuations. We then used a modified version of the algorithm proposed by Engbert and Kliegl (2003) to detect microsaccades. In this method, instantaneous velocity measures are obtained by calculating the first derivative across a 20 ms window separately for horizontal and vertical eye positions. This procedure yields a representation of eye positions in 2 dimensional velocity space. Values tend to cluster around zero, and outliers signal eye movements. Trial by trial noise levels are calculated and used to set detection thresholds. Since horizontal and vertical eye velocities are calculated separately, detection thresholds assume elliptical shapes in velocity space reflecting horizontal and vertical noise levels on each trial. Finally, monocular eye movement events are excluded since microsaccades are binocular. We modified this procedure in the following ways. Since our task included large response saccades, we focused on periods of fixational eye movements for

threshold estimation by removing periods when radial velocity was elevated above 30°/s. We were unable to judge binocularity with our monocular eye tracking setup, so we excluded tremor, drift, and false positives using several other common-sense criteria. First, we excluded post-saccadic drift and eye tracker ringing by removing eye movements that began less than 50 ms prior to the end of the preceding eye movement. Respecting the eye tracker limitations, we excluded eye movements with amplitude < 0.01°, and eye movements which strayed outside of our calibrated field (central 22° x 22°). Finally we excluded saccades with excessively short or long durations. Inspection of color-coded main sequence plots showed that 10 - 65 ms provided a reasonable range for acceptable saccade durations. We defined microsaccades as those with amplitude ≤ 1° (Martinez-Conde et al., 2009). We repeated our analysis using the more conservative definition of ≤ 15′ (Collewijn and Kowler, 2008). These analyses yielded qualitatively identical results.

3.3.5 Saccade analysis

We constructed sorted rasters and peri-event time histograms of microsaccade frequency using standard methods (Lemon, 1984). We convolved the peri-event time histograms with a Gaussian kernel (σ = 10 ms) to create microsaccade density functions.

We used a running Wilcoxon rank-sum test to judge times at which microsaccade frequency became significantly elevated or depressed relative to baseline levels. First we constructed microsaccade density functions for each session as described above. Baseline average microsaccade frequency was measured in the 50 ms before target onset. The frequency of microscaccade production was contrasted with this baseline at ms resolution. Probability for significance was set at < 0.01. The results were not different if 10 or 50 ms windows were tested. This approach was also used to test for

differences between microsaccade frequency in different conditions. Each session contributed a single observation to these tests, and significance was again assessed at the $p < 0.01$ level.

3.4 Results

3.4.1 Behavior

We recorded data from 4 monkeys that performed the saccade stop-signal task (Figure 3.1) summarizes behavior for each monkey. Reaction times and probability of committing errors show that monkeys were appropriately sensitive to the stop signal and did not violate the assumptions of Logan's race model. In particular, noncanceled saccade RTs were less than saccade RTs on trials with no stop signal. Stop-signal reaction times (SSRTs) are within the range of those reported previously for monkeys carrying out the same task. Figure 3.3 shows normalized inhibition functions and Weibull distribution fits for each monkey collapsed across all sessions. Z-scoring inhibition functions normalizes them in time, allowing them to be compared across recording sessions regardless of incidental reaction time differences due to normal fluctuations in arousal and motivation. Short stop-signal delays yielded near 0% errors while long stop-signal delays yielded near 100% errors. These inhibition functions rise in an ordered and predictable fashion. Error rates on stop trials were close to 50% for all monkeys demonstrating the success of the SSD tracking algorithm. Thus, the performance conformed very well to race model assumptions, and SSRT estimates are reliable. These considerations validate the use of
SSRT as an index of maximal unbalanced activation in SC based on previous work (Paré and Hanes, 2003).

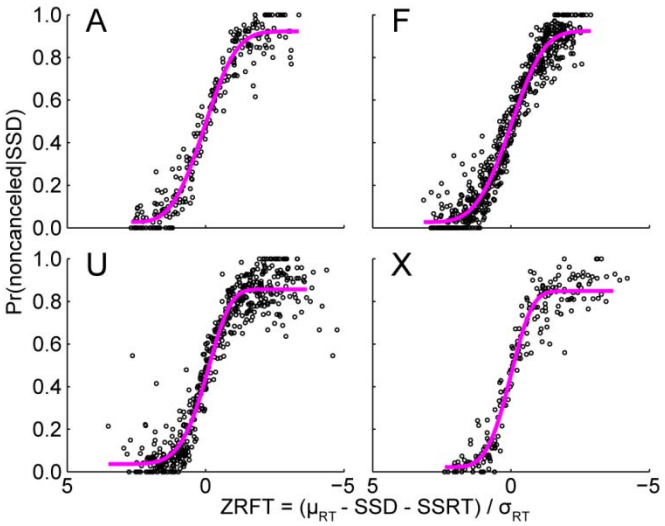

Figure 3.3. ZRFT (z-scored inhibition) functions and Weibull distribution fits for each monkey. Inhibition functions plot the probability of committing a noncanceled error at each SSD.

3.4.2 Microsaccade frequency

We used a modified version of Engbert and Kliegl's (2003) algorithm for saccade detection. The well-known relationship between saccade velocity, duration and amplitude, known as the "main sequence" (Zuber and Stark, 1965; Bahill et al., 1975) is displayed for each monkey in Figure 3.4. Our saccade detection method identified eye movements with very small amplitudes having the same main sequence relationship as those of larger magnitude. This finding replicates well-known observations and demonstrates the robustness of our saccade detection approach.

We studied the evolution of microsaccade production during canceled trials by constructing rasters marking the time of each microsaccade and deriving density functions collapsed across sessions for each monkey (Figure 3.5)[7]. Data were aligned on target presentation and on stop-signal presentation. The raster plots are useful for illustrating relationships between microsaccade frequency and task events, while the density functions show differences in microsaccade frequency relative to pre-target levels. Following changes in visual stimuli, microsaccade production shows a characteristic suppression followed by facilitation in humans (Engbert and Kliegl, 2003; Laubrock et al., 2005; Valsecchi and Turatto, 2007; summarized by Rolfs et al., 2008) and macaques (Brien et al., 2009; Cui et al., 2009; Hafed et al., 2011). Consistent with these reports, the raster plots and density functions show clear changes in microsaccade production following stimulus presentation. We used a running Wilcoxon approach to test for periods of elevated or depressed microsaccade frequency relative to baseline (see *Materials and Methods*). Gray bars beneath microsaccade density

[7] In these and following plots, please note differences in ordinate scale of microsaccade density functions. In particular, all monkeys showed similar baseline levels of microsaccade production as reported in Table 1. Monkey U showed the same patterns of microsaccade modulation as the other monkeys, but peak levels of microsaccade production were reduced for this monkey compared to the other monkeys. This is consistent with individual differences noted in humans (Collewijn and Kowler 2008).

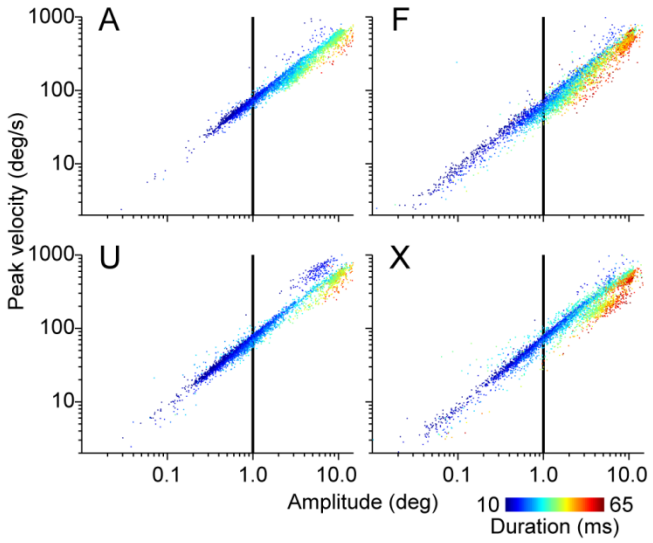

Figure 3.4. Saccade velocity plotted against saccade amplitude with duration color-coded for each monkey. Microsaccades (left of vertical black lines) are continuous with main sequence of longer saccades. Each plot displays 5000 randomly sampled saccades drawn from complete data sets.

functions show periods of depressed microsaccade frequency, while black bars show periods of elevated microsaccade frequency ($p < 0.01$). Each monkey made significantly fewer microsaccades after target presentation, show a second decrease in microsaccade production associated with stop-signal presentation. At shorter SSDs, microsaccade suppression associated with the target and the stop-signal overlap. It is less clear if the decrease associated with the stop-signal is absent for monkeys F and X, or if the two periods of microsaccade suppression have simply merged into one. Subsequent to this suppression, all monkeys showed elevated microsaccade production beginning on average ~220 ms after the stop-signal (Figure 3.5 right column black bars after stop signal and SSRT; latencies relative to stop-signal Monkey A 178 ms, F 239 ms, U 276 ms, X 182 ms). The rasters show clearly that this elevation is synchronized on the stop-signal and not the target.

The timing of microsaccade production during canceled trials permits a test of the fixation and the microsaccade hypotheses. The first prediction of the microsaccade hypothesis is that microsaccade production increases with the elevated discharge rate of rostral SC neurons concomitant with SSRT (Hafed et al., 2009; Hafed and Krauzlis, 2012). We found that during the 50 ms around SSRT, microsaccade frequency showed significant suppression in all 4 monkeys relative to baseline levels (Figure 3.5 right column gray bars in interval around SSRT). The later increase of microsaccade production occurred on average ~100 ms after SSRT (Figure 3.5 right column black bars after stop signal and SSRT; latencies relative to SSRT Monkey A 85 ms, F 119 ms, U 174 ms, X 51 ms). Even allowing for efferent delay (Hafed and Krauzlis, 2012) and 10-20 ms standard deviation in the estimate of SSRT (Table 3.1), the timing of microsaccade production is inconsistent with the microsaccade hypothesis.

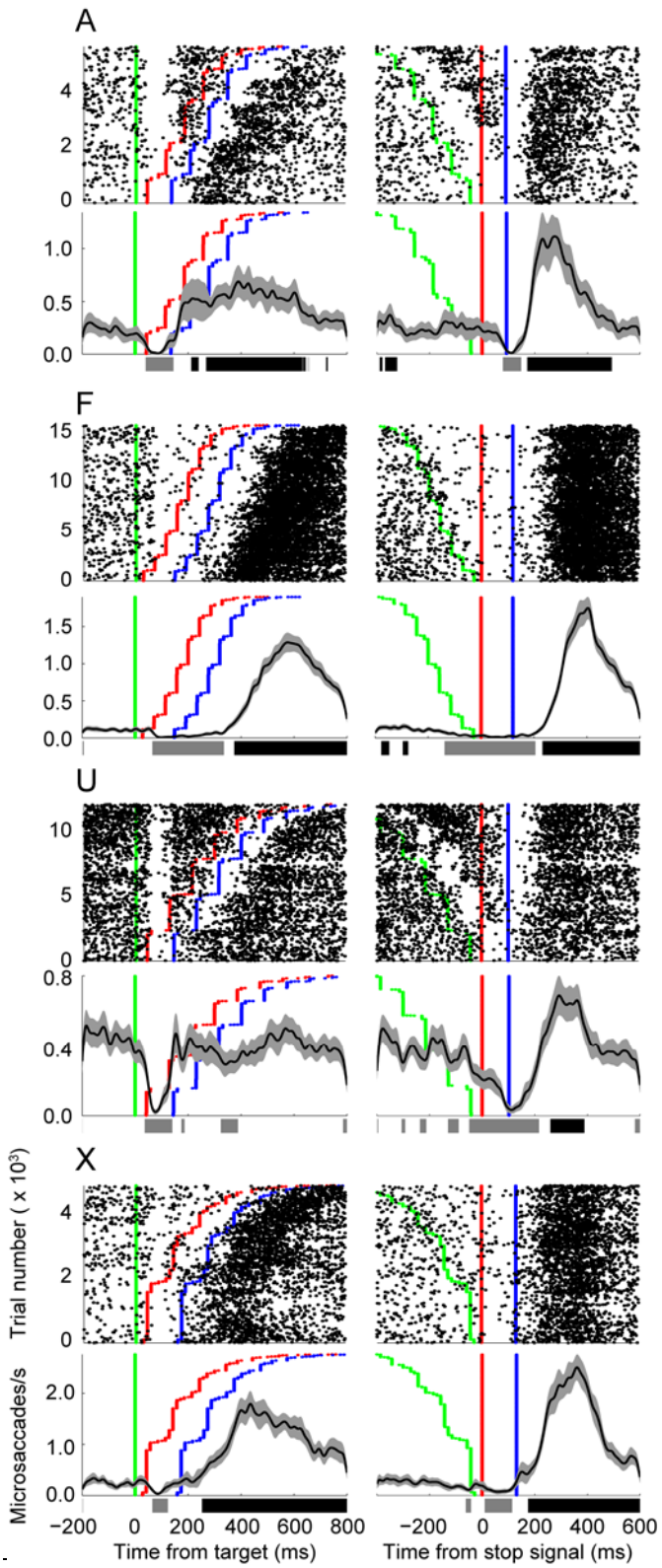

Figure 3.5. Microsaccade production plotted for each monkey in rasters (top) and density functions (bottom) aligned to presentation of target (left) and stop-signal (right). Target presentation (green), stop-signal presentation (red), and average stop signal

reaction time (SSRT) (blue) are indicated for each discrete stop signal delay. Gray outlines on density functions indicate 95% confidence intervals across recording sessions. Gray bars beneath density functions denote periods when microsaccade frequency is suppressed below baseline levels, while black bars denote periods when microsaccade frequency exceeds baseline levels ($p < 0.01$). Axes are scaled to accommodate idiosyncratic differences in microsaccade rate. Each monkey exhibited a pronounced reduction of microsaccades after the stop signal followed by an equally clear elevation well after SSRT.

	no-stop RT	noncanceled RT	p(noncanceled)	SSRT	mean fixating microsaccade rate (s^{-1})
monkey A	355 ± 44	321 ± 38	0.49	93 ± 15	0.19
monkey F	350 ± 34	315 ± 27	0.47	120 ± 10	0.11
monkey U	399 ± 80	368 ± 73	0.50	102 ± 18	0.42
monkey X	371 ± 43	353 ± 41	0.45	130 ± 20	0.23

Table 3.1. Summary statistics for stop-signal task performance. Values are means ± SD.

The direction of microsaccade production during canceled trials permits another test of the microsaccade hypotheses. The second prediction of the microsaccade hypothesis is that on canceled trials microsaccades should proceed more often toward the target because of unbalanced activation in SC (Hafed et al., 2008; Hafed et al., 2009). Figure 3.6 plots the frequency of microsaccades toward and away from the target as a function of time. We used a running Wilcoxon approach to test differences between the frequency of saccades directed toward or away from the target (see *Materials and Methods*). Black bars beneath microsaccade density functions illustrate periods of significant differences between microsaccade direction ($p < 0.01$). Around 200-300 ms after the target, all monkeys except for U made significantly more microsaccades toward the target location (Figure 3.6 left column black bars after target onset). However, the increases in microsaccades observed after SSRT (Figure 3.6 right column black bars after stop signal and SSRT) were directed away from the target more often than expected by chance (A, F, U) or showed no significant directional bias (X). Although these microsaccades tended to move the eyes away from the target location, they did not cause the eyes to exit the invisible fixation window. Also, the peak in microsaccade production was followed by reduced microsaccade production throughout the 1500 ms period until reward delivery (data not shown).

In sum, all 4 of the monkeys produced microsaccade patterns inconsistent with either the first or the second prediction of the microsaccade hypothesis.

3.4.3 Directional biases

We studied microsaccade frequency as a function of visual field. Figure 3.7 plots the results of this analysis. Each monkey showed an idiosyncratic pattern of spatial bias in microsaccade frequency that appeared unrelated to the task. These biases did not depend greatly on alignment event, so we describe them as a whole. After target and

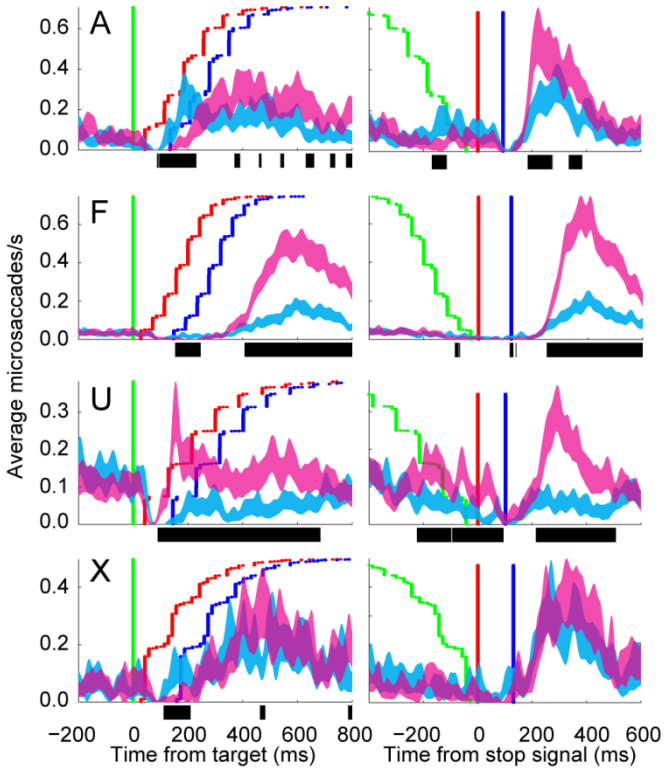

Figure 3.6. Microsaccades produced toward (cyan) or opposite (magenta) the target (± 45°) aligned to target (left) and stop-signal (right) presentation. Black bars denote periods of significant differences between density functions. Conventions as in Figure 3.5.

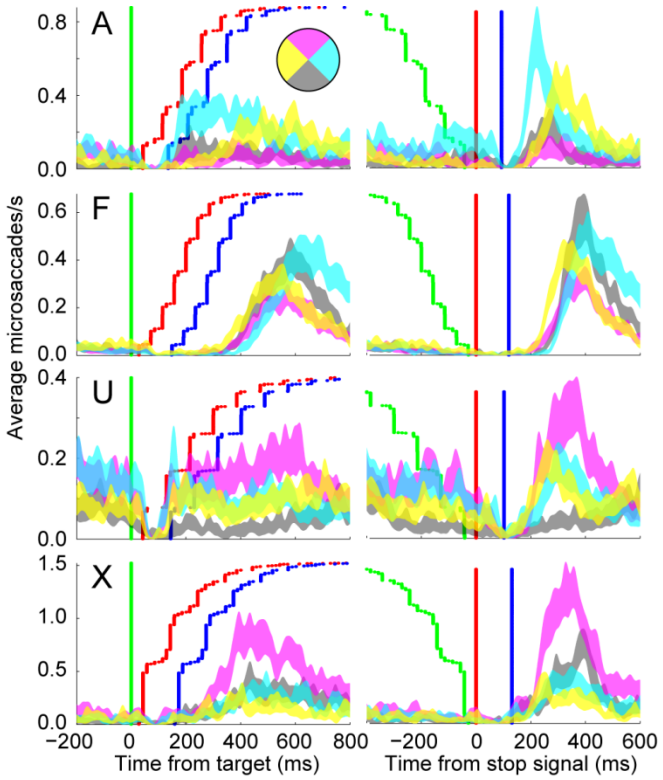

Figure 3.7. Microsaccade density functions by direction plotted individually for each monkey. Microsaccades are separated depending on whether they were directed right (cyan), up (magenta), left (yellow), or down (black). Conventions as in Figure 3.5.

stop signal presentation, Monkey A tended to make microsaccades initially to the right, followed by microsaccades to the left. Monkey F showed the opposite pattern with initial microsaccades to the left followed by ones to the right. Monkey F also showed a tendency to make microsaccades in the downward direction during the period after target and stop-signal presentation. Monkey U showed a bias for upward saccades and a smaller bias for left and right saccades. Monkey X tended to make more saccades in the upward and downward direction than in the left and right direction. Of these, monkey X favored upward more frequently.

A speaker positioned either in front and above the animal or directly on the left provided secondary reinforcement and punishment depending on trial outcome. On successfully canceled trials, secondary reinforcement was delivered 1600 ms after stop signal onset. We hypothesized that covert attention may have been directed toward the speaker after stop-signal onset in anticipation of this tone, and that this may have led to additional microsaccades in the direction of the speaker. Figure 3.8 displays the results of this analysis. As in Figure 3.6, black bars illustrate periods of significant differences between microsaccade direction ($p < 0.01$). During the period after the stop signal, Monkey A and F made microsaccades in the direction opposite the speaker, while monkey U and X tended to make microsaccades toward speaker locations. Directional biases away from the speaker location can also be observed during the pre-target and pre-stop-signal intervals in data collected from monkeys A, U, and X. These results provide no conclusive evidence that attention-related microsaccades were directed toward the location of secondary reinforcement delivery.

3.4.4 Conservatively defined microsaccades

We repeated our main analyses using a more conservative definition of microsaccades, only including high-velocity fixational eye movements ≤ 15′ amplitude

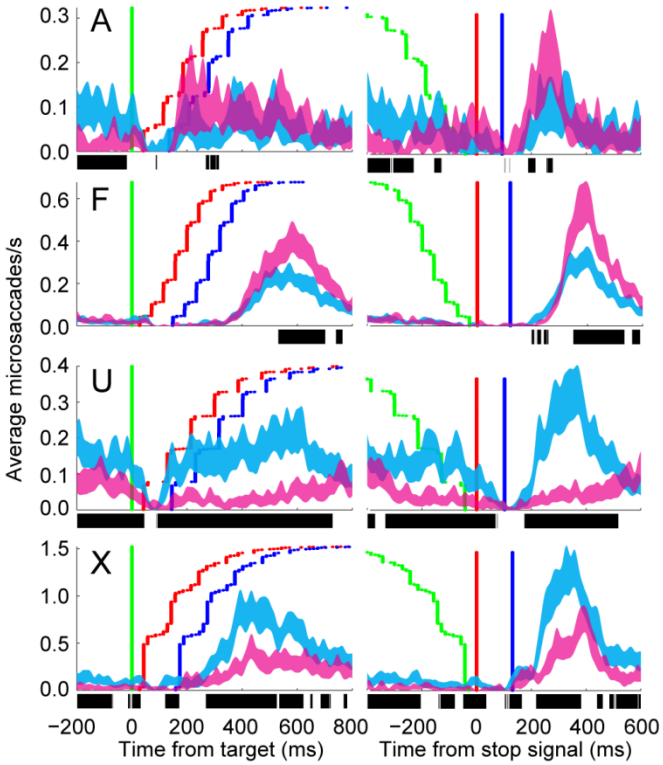

Figure 3.8. Microsaccades produced toward (cyan) or opposite (magenta) the speaker location (± 45°) aligned to target (left) and stop-signal (right) presentation. Conventions as in Figure 3.5.

(Collewijn and Kowler, 2008). The same basic results are obtained with the data subsampled in this manner (Figure 3.9). No monkeys exhibited the increase in microsaccade production concomitant with SSRT predicted by the microsaccade hypothesis. An increase in conservative microsaccade frequency occurred after SSRT in three monkeys (143 ms monkey A, 351 monkey F, 123 ms monkey X) with an increase that did not reach statistical significance for the fourth monkey. With this conservative data set, only monkey U produced significant differences in microsaccade direction (Figure 3.10); these microsaccades were more likely to be directed away from the target. In sum, neither of the predictions of the microsaccade hypothesis were obtained even when analysis was restricted to a conservative subset of fixational eye movements.

3.5 Discussion

Contrary to predictions of the microsaccade hypothesis, monkeys did not make more target directed microsaccades during periods of unbalanced activation in SC. Monkeys actually exhibited attenuation of microsaccade production around SSRT when they canceled saccades to perform the saccade stop-signal task. This was followed by a late period of elevated microsaccade production around the fixation spot but avoiding the direction of the target. Interpreted in light of previous neurophysiological findings (Paré and Hanes, 2003), these results are inconsistent with the hypothesis that rostral SC functions solely to produce microsaccades. But the data are consistent with the hypothesis that rostral SC contributes to gaze-holding. Further evidence for active gaze-holding during this task comes from our previous observation of reduced EMG when task-related saccades are canceled indicating that fixational eye movements are also gated during this time period (Godlove et al., 2011a).

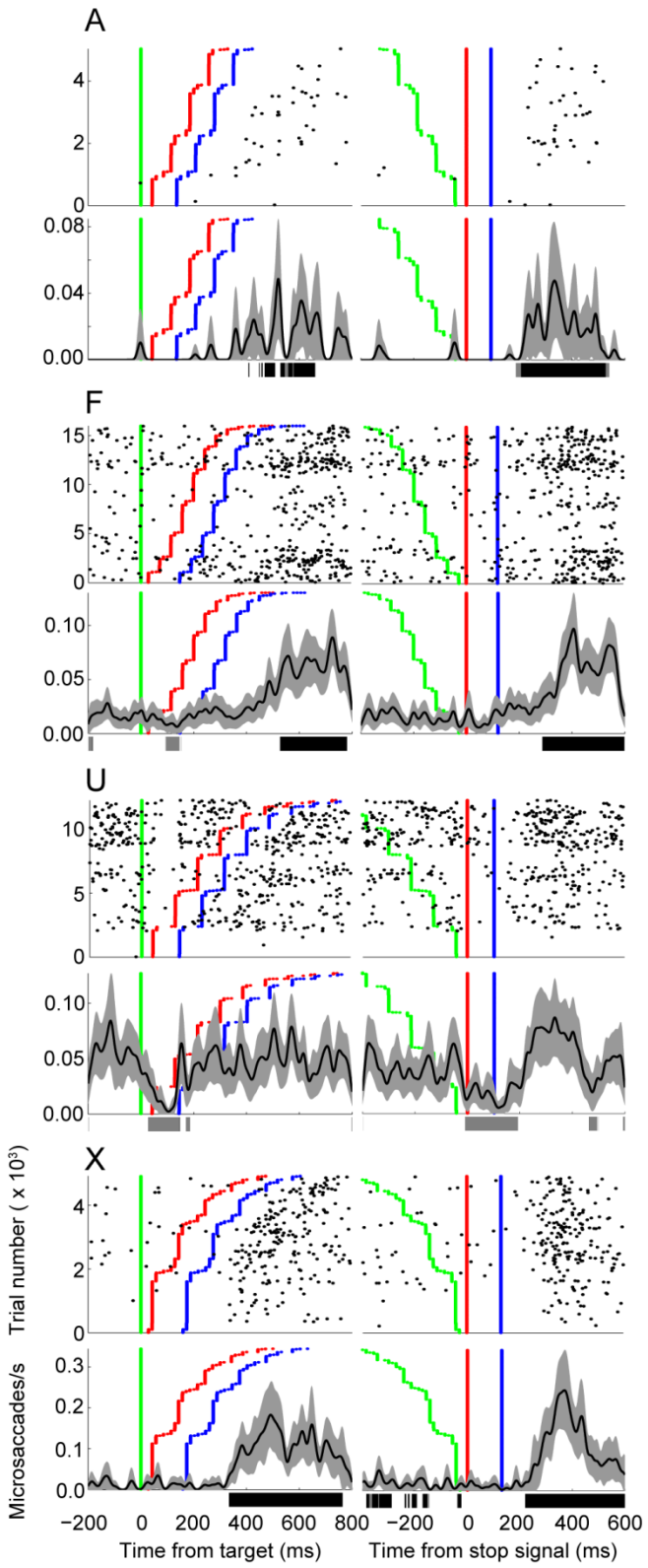

Figure 3.9. Conservatively defined microsaccade production plotted for each monkey in rasters (top) and density functions (bottom) aligned to presentation of target (left) and

stop-signal (right). Microsacades are here defined as high velocity fixational eye movements ≤ 15′ amplitude. Conventions as in Figure 3.5.

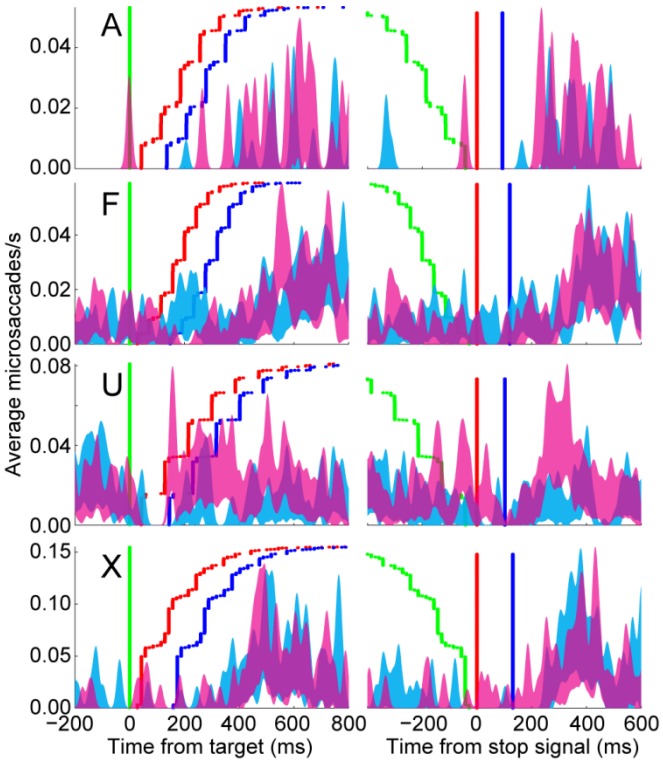

Figure 3.10. Conservatively defined microsaccades produced toward (cyan) or opposite (magenta) the target (± 45°) aligned to target (left) and stop-signal (right) presentation. Microsacades are here defined as high velocity fixational eye movements ≤ 15′ amplitude. Conventions as in Figure 3.5.

The remarkable consistency of our results across tens of thousands of trials and 4 individual monkeys should be stressed. All 4 monkeys showed significantly reduced microsaccade frequency in the interval around SSRT corresponding to increased activity in rostral SC. Similarly, all 4 monkeys showed increased microsaccade production away from the target, opposite the prediction of the microsaccade hypothesis; this observation reached statistical significance in 3 of the monkeys tested. This stereotyped, predictable behavior is even more surprising when contrasted with the idiosyncrasies observed in microsaccade directional bias. Even though all monkeys made microsaccades with different directional biases during the task, and these directions were unaffected by the location of secondary reinforcement, all monkeys made the same stereotyped responses with respect to target location during saccade cancelation. This stereotyped behavioral suggests consistency in the underlying neurophysiology as well. Indeed, neurons in SC show predictable responses across visually-guided oculomotor tasks (Gandhi and Katnani, 2011), and both SC and FEF neurons show similar responses during the stop-signal task when compared across studies (Hanes et al., 1998; Paré and Hanes, 2003). All in all, it can be reasonably concluded that neural activity in SC of the monkeys completing our task did not differ substantially from that reported previously.

It may be argued that rostral SC functions exclusively to produce microsaccades, but that microsaccade activity is gated downstream of SC during saccade cancelation under cortical control. For example, FEF is known to project to both SC and to the paramedian pontine reticular formation (PPRF) including the nucleus raphe interpositus (nRIP) that contains OPNs (Huerta et al., 1986; Stanton et al., 1988). FEF fixation neurons may be responsible for issuing a saccade cancelation command to brainstem OPNs. In this scenario, activity in rostral SC would be gated by fixation neurons in FEF through brainstem OPNs preventing microsaccades. Our present data cannot exclude

this alternative. However, we consider it unlikely, because fixation neurons in FEF and SC probably carry out similar functions. First, these cell types are very similar in their physiological responses (Bizzi, 1968; Hanes et al., 1998; Paré and Hanes, 2003; Izawa et al., 2009). Second, both FEF and SC project to PPRF with similar density (Scudder et al., 2002), and both areas project specifically to nRIP (Stanton et al., 1988; Büttner-Ennever et al., 1999). The distribution and morphology of these projections are suggestive of a fixation role for rostral SC. The majority of projections from SC to nRIP arise from the rostral pole of SC, and these tend to be thick collateral axons, whereas projections to nRIP from more caudal regions tend to show up as thin branching axons (Büttner-Ennever et al., 1999). Other cortical eye fields are less likely to gate microsaccade activity during saccade cancelation. The supplementary eye field also projects to nRIP (Huerta and Kaas, 1990; Shook et al., 1990), but the neural activity in this area does not control directly saccade initiation (Stuphorn et al., 2010). And while the lateral intrapariatal area projects to dorsal and lateral pontine nuclei, projections to PPRF are lacking (May and Andersen, 1986; Schmahmann and Pandya, 1989). In sum, functional and anatomical data are in agreement with the fixation hypothesis, showing that rostral SC is equally or better positioned to serve fixation functions than cortical oculomotor areas.

How can these results be reconciled with recent findings supporting the microsaccade hypothesis? Until now, the fixation and microsaccade hypotheses have been framed as mutually exclusive. But this need not be the case. The most graceful reconciliation seems the acknowledgement that some neurons in rostral SC are involved in producing microsaccades while other neurons are responsible for gaze-holding. It seems beyond dispute that some neurons in rostral SC contribute to generating microsaccades (Munoz and Wurtz, 1993a; Hafed et al., 2009; Hafed and Krauzlis, 2012). Consistent with the model of Hafed et al. (Hafed et al., 2009), 3 of 4 monkeys

tested exhibited increased microsaccade production toward target locations 200-300 ms after target onset. But it is equally clear that gaze-holding fixation neurons exist in rostral SC (Munoz and Wurtz, 1993a) as well as frontal eye field (Segraves and Goldberg, 1987; Hanes et al., 1998; Izawa et al., 2009) and the basal ganglia (Hikosaka and Wurtz, 1983b). Consistent with this well-known finding, we observed decreased microsaccade production coinciding with periods of increased activation of neurons in rostral SC and of fixation neurons in FEF. Some recent studies contradict this interpretation, suggesting that microsaccade cells constitute the same population of neurons originally described as fixation cells (Hafed et al., 2009; Hafed and Krauzlis, 2012). However, we note that the inclusion requirement of these studies dictated that neurons demonstrate build up activity in the interval before memory-guided saccades. This means that neurons with unequivocal gaze-holding activity were explicitly excluded from analysis.

Replicating many studies (Engbert and Kliegl, 2003; Laubrock et al., 2005; Valsecchi and Turatto, 2007; Rolfs et al., 2008; Brien et al., 2009; Cui et al., 2009; Hafed et al., 2011), we also found increased microsaccade production ~220 ms after the visual stimulus used as the stop signal. These microsaccades were elicited too late to be a product of unbalanced activity in SC associated with SSRT (Hafed and Krauzlis, 2012). Surprisingly, they also tended to be directed contralateral to the target, and ipsilateral to SC activation. The timing and direction of these microsaccades are reminiscent of the "inhibition of return" phenomenon (Posner and Cohen, 1984; Klein, 2000) that has been associated with oculomotor programming (Rafal et al., 1989) mediated at least in part by SC (Dorris et al., 1999). Future work will aim to elucidate the neural mechanisms underlying this interesting observation.

In sum, our results provide a better understanding of the neural mechanisms underlying response inhibition. They extend our original finding that partial muscle

contraction does not occur when saccades are successfully countermanded (Godlove et al., 2011a). Furthermore, they demonstrate that microsaccades do not occur when normal saccades are canceled. Together with previous work, these findings show that the prevention of saccade initiation in a stop-signal task is accomplished by explicit motor inhibition.

CHAPTER 4

FUNCTIONAL EVIDENCE FOR A CANONICAL CORTICAL MICROCIRCUIT IN AGRANULAR CORTEX

4.1 Abstract

Neuroscientists frequently rely on the assumption that a canonical microcircuit is repeated throughout neocortex. This biological blueprint, derived from primary sensory cortex, emphasizes ascending input to granular layer IV that is then transmitted to upper and lower cortical layers. Here we show that an area lacking a granular layer, the supplementary eye field (SEF), also exhibits laminar processing consistent with this canonical microcircuit. We recorded visually evoked spikes and field potentials simultaneously from all layers of SEF. Multiple predictions derived from the canonical microcircuit model were confirmed. Most notably, synaptic current flow began in the middle layers and spread sequentially to superficial and deep layers. At the neural level, firing patterns exhibited a period of enhanced spiking that was followed by suppression, the spike suppression lasted longer in superficial versus deep layers, and putative pyramidal cells and interneurons displayed similar response latencies. These findings are consistent with the hypothesis that the entire neocortex is comprised of a canonical microcircuit.

4.2 Introduction

The hypothesis of a *canonical cortical microcircuit* (CCM) was originally formulated based on data from primary visual cortex (V1) where most ascending projections from the dorsal lateral geniculate nucleus terminate in a dense granular layer

IV (Figure 4.1A) (Gilbert, 1983; Callaway, 1998; Douglas and Martin, 2004). Layer IV neurons project to layers II and III, which project to layers V and VI in turn. In addition to these interlaminar projections, local, recurrent interactions between neurons play an important role (Figure 4.1B). Ascending input targets both pyramidal cells and interneurons (Douglas and Martin, 1991). Recurrent connections amplify this input, producing an initial wave of excitation (Douglas et al., 1995), followed by a longer lasting period of suppression (Douglas and Martin, 1991). Owing to differences in $GABA_A$ and $GABA_B$ receptor distribution, superficial layers show longer lasting suppression than deep layers. These defining features of a CCM are hypothesized to be repeated throughout neocortex (Douglas and Martin, 2004). The importance of this CCM hypothesis cannot be overstated. Among other consequences, it guides influential cortical hierarchies (Felleman and Van Essen, 1991; Markov et al., 2011), it underlies the interpretation of the fMRI BOLD signal (Logothetis, 2008; Boynton, 2011), and it is the foundation for large-scale implementations of cortical function including the ambitious Blue Brain Project (Markram, 2006; Heinzle et al., 2007; Helmstaedter et al., 2007). This basic, textbook idea is crucial to our understanding of neocortex.

Physiological evidence for this CCM has been obtained from several species and sensory areas using various techniques. For instance, optogenetic studies in mice describe specific contributions of neurons in deep and superficial layers to local recurrent network dynamics (Olsen et al., 2012; Petersen and Crochet, 2013). Similarly, post-synaptic current source density (CSD) derived from recordings of local-field potentials (LFPs) across layers in visual cortex (Mitzdorf and Singer, 1979; Schroeder et al., 1998), auditory cortex (Lakatos et al., 2007), and somatosensory cortex (Lipton et al., 2010; Riera et al., 2012) exhibit the earliest current sinks in granular layer IV followed by activation in supragranular and infragranular layers.

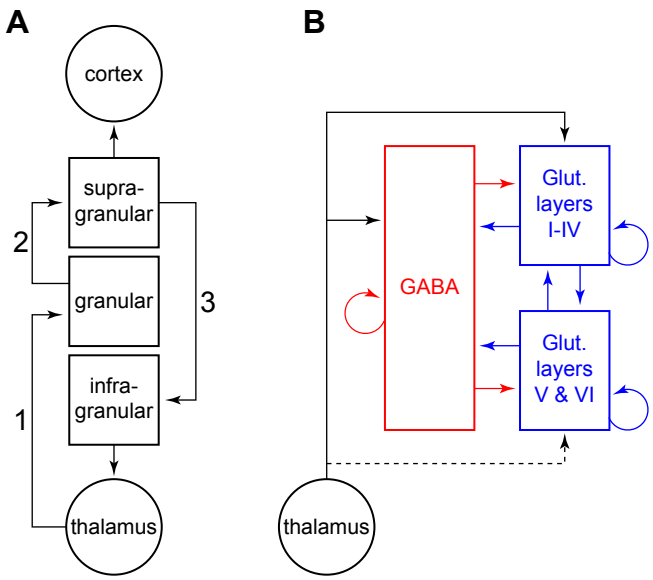

Figure 4.1. Essential characteristics of the CCM. **A**) Interareal and interlaminar excitatory projections, highlighting projections thought to determine the timing of Current Source Density (CSD) in specific laminae. Projections are numbered in order of temporal precedence for clarity. (Diagram adapted from Gilbert, 1983.) **B**) Lateral, recurrent excitatory and inhibitory projections. GABA-ergic projections exert inhibitory influence and are depicted in red. Glutamatergic projections exert excitatory influence and are depicted in blue. Pools of superficial and deep layer pyramidal neurons are modeled separately to account for differences in $GABA_A$ and $GABA_B$ receptor distributions. (Diagram adapted from Douglas and Martin, 1991.)

However, the universality of CCM across neocortex is not guaranteed because of pronounced architectural variation across cortical areas (Brodmann, 1909; Elston, 2000; Collins et al., 2010). Virtually all data supporting CCM has been obtained from sensory areas, and CSD in frontal cortex has never been reported. Thus, the pivotal idea of a functionally uniform neocortex is a convenient assumption rather than an established fact.

We investigated the universality of the CCM by recording laminar spiking activity and CSD from an area of frontal, motor cortex that lacks a granular layer. The supplementary eye field (SEF) is located in area 6 (also known as F7) (Schlag and Schlag-Rey, 1987), a classical agranular area in frontal cortex (Matelli et al., 1991). Examined with Nissl stain, neurofilament protein (SMI-32), myelin, and acetylcholinesterase (AChE), SEF differs markedly from primary visual cortex. Most notable is the absence of a granular layer IV (Figure 4.2). The structure of frontal, motor areas is so different from sensory cortex that accommodating it in the CCM framework seems very challenging. How can a pattern of microcircuitry that stresses granular layer IV as the critical input hub be a global blueprint for cortical areas lacking any granular layer (Shipp, 2005)?

The location and functional responses of SEF facilitate testing the generality of the CCM hypothesis. First, macaque SEF is located in the dorsal medial convexity, making it readily accessible for laminar electrode array recordings perpendicular to the cortical layers. Second, neurons in SEF display visual responses (Schall, 1991a; Pouget et al., 2005) making it possible to evaluate laminar CSD and spiking responses with the same procedures used in sensory areas. Neurons in SEF also exhibit modulated activity associated with eye movements (Schlag and Schlag-Rey, 1987; Schall, 1991a; Olson and Gettner, 1995; Stuphorn et al., 2010; Heinen et al., 2011) affording investigation of

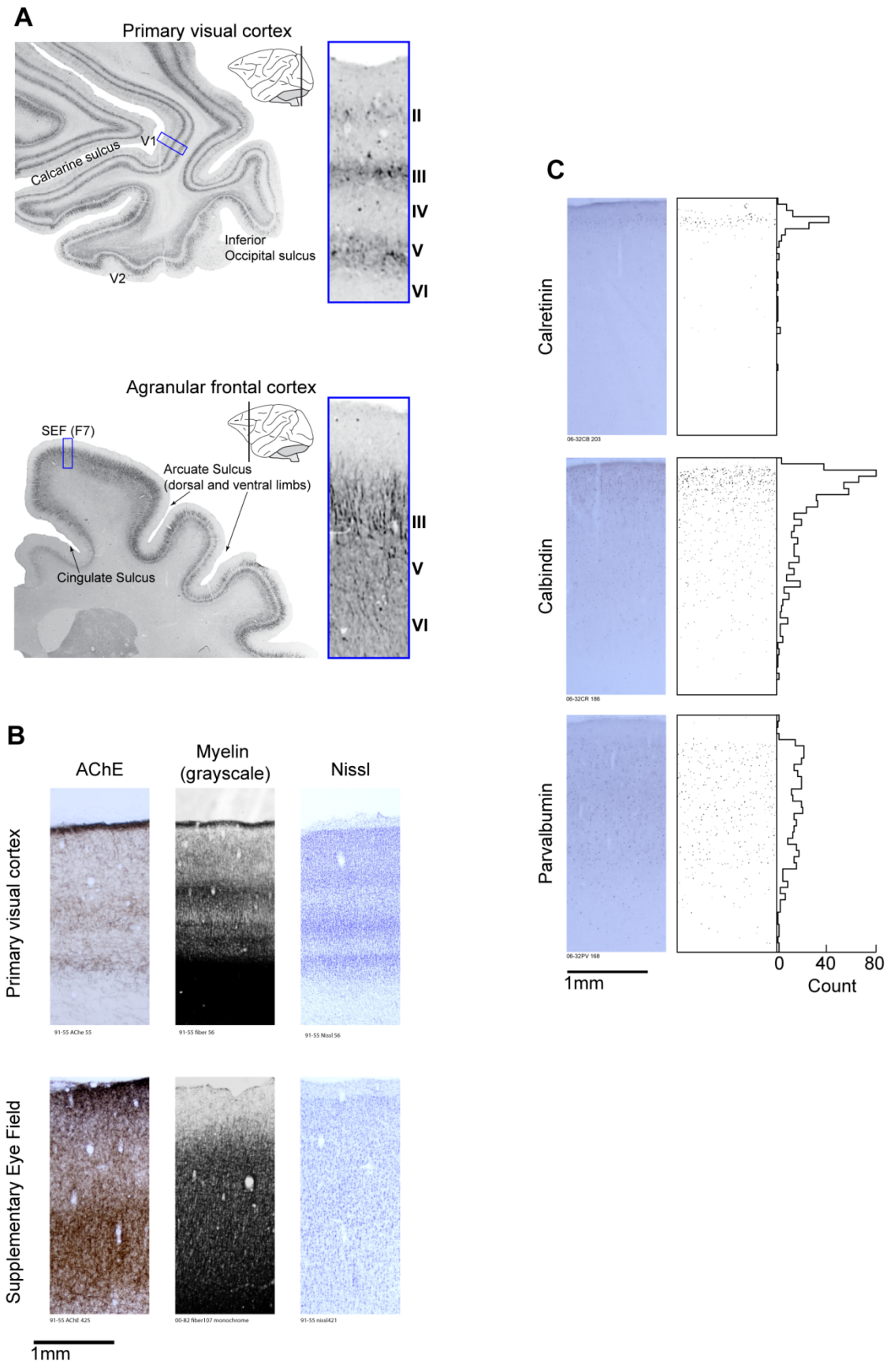
A
Primary visual cortex
Calcarine sulcus
V1
V2
Inferior
Occipital sulcus
II
III
IV
V
VI
Agranular frontal cortex
SEF (F7)
Arcuate Sulcus
(dorsal and ventral limbs)
Cingulate Sulcus
III
V
VI
B
AChE
Myelin
(grayscale)
Nissl
Primary visual cortex
Supplementary Eye Field
1mm
C
Calretinin
Calbindin
Parvalbumin
0
40
80
Count
1mm

Figure 4.2 (opposite). Cytoarchitecture of early visual areas contrasted with that of agranular frontal cortex. **A**) Data reproduced from (Paxinos et al., 2000) with permission. Sections were reacted immunohistochemically for the demonstration of neurofilament protein SMI32. Sulcal landmarks and specific areas are labeled to aid in orientation (V1 primary visual cortex, V2 visual area 2, SEF supplementary eye field). Schematic insets show approximate planes from which sections were taken. Areas outlined in blue are magnified at right. V1 can be clearly delineated by laminae and shows a distinct layer IV separating layers III and V. In contrast, SEF exhibits clusters of pyramidal cells in layer III with less dense pyramidal cells in layer V (see also Geyer et al., 2000). **B**) Comparison of laminar distribution of acetylcholinesterase (AChE), myelin fibers and Nissl substance in primary visual cortex (top) and SEF (bottom). Each pair represents tissue taken from the same monkey. The pronounced laminated structure of visual cortex contrasts with the more homogeneous appearance of SEF. The laminar pattern of AChE staining in SEF is very different from that in V1, being most dense in layer I and dense as well in layers V and VI. Likewise, the laminar pattern of myelin fiber staining in SEF is markedly different from that in V1, lacking lamination and being most dense only up to layer II. In Nissl SEF is quite distinct from V1 with no clear boundary separating the homogeneous layers II and III that contain mostly small pyramids except in the lowest part of III in which medium-size pyramids are present. Layer VI contains mainly fusiform cells and can be divided by cell density into superficial, relatively sparse and deeper, relatively dense sublayers (Matelli et al., 1991) (Histological material kindly provided by T. Hackett). **C**) Distribution of GABA-ergic interneurons in SEF. Color panels on the left show coronal sections through SEF immunohistochemically reacted for the calcium binding proteins indicated. Panels on the right plot the location of reacted neurons identified using a semi-automatic classification routine (see Supp Experimental Procedures) and display associated histograms. Calretinin and calbindin neurons are densest in layer II with diminishing deeper density, while parvalbumin neurons are more uniformly distributed across layers. (Histological material kindly provided by I. Stepniewska).

whether laminar CSD and spiking patterns are consistent across sensory and motor processes.

4.3 Results

Using linear microelectrode arrays (150 μm inter-contact spacing), we recorded visually evoked and saccade-related LFPs and spikes from SEF of 2 macaque monkeys across 17 sessions. SEF was located through intracortical electrical microstimulation to elicit eye movements (Schlag and Schlag-Rey, 1987; Huerta and Kaas, 1990) (Figure 4.3 A,B). To obtain interpretable CSD, we verified that electrode arrays entered the cortex perpendicular to the cortical surface through combined MR and CT imaging (Figure 4.3 C-J). After the electrode array had settled in the cortex (>4 hrs), we presented wide-field (40° x 36° visual angle) light flashes (34.80 cd/m^2) in blocks of 100-200 presentations, similar to stimuli used previously to characterize laminar microcircuitry in visual cortex (Schroeder et al., 1998; Maier et al., 2010). Interleaved with these blocks of visual stimulation, we recorded activity during spontaneous eye movements produced while the monkeys rested in darkness for periods of 5-10 minutes.

The laminar sequence of CSD and spike rate facilitation and suppression corresponded well to predictions of the CCM. These findings suggest that the neocortex is indeed organized according to a common blueprint.

4.3.1 Single-session visually evoked CSD

Figure 4.4 shows data collected during a representative session. To interpret these data, it was necessary to estimate the depth of the electrode array relative to gray matter (see Experimental Procedures). Several physiological measures provided information about electrode position. First, an artifact associated with the cardiac rhythm (hereafter referred to as the pulse artifact) was observed on a superficial channel. This

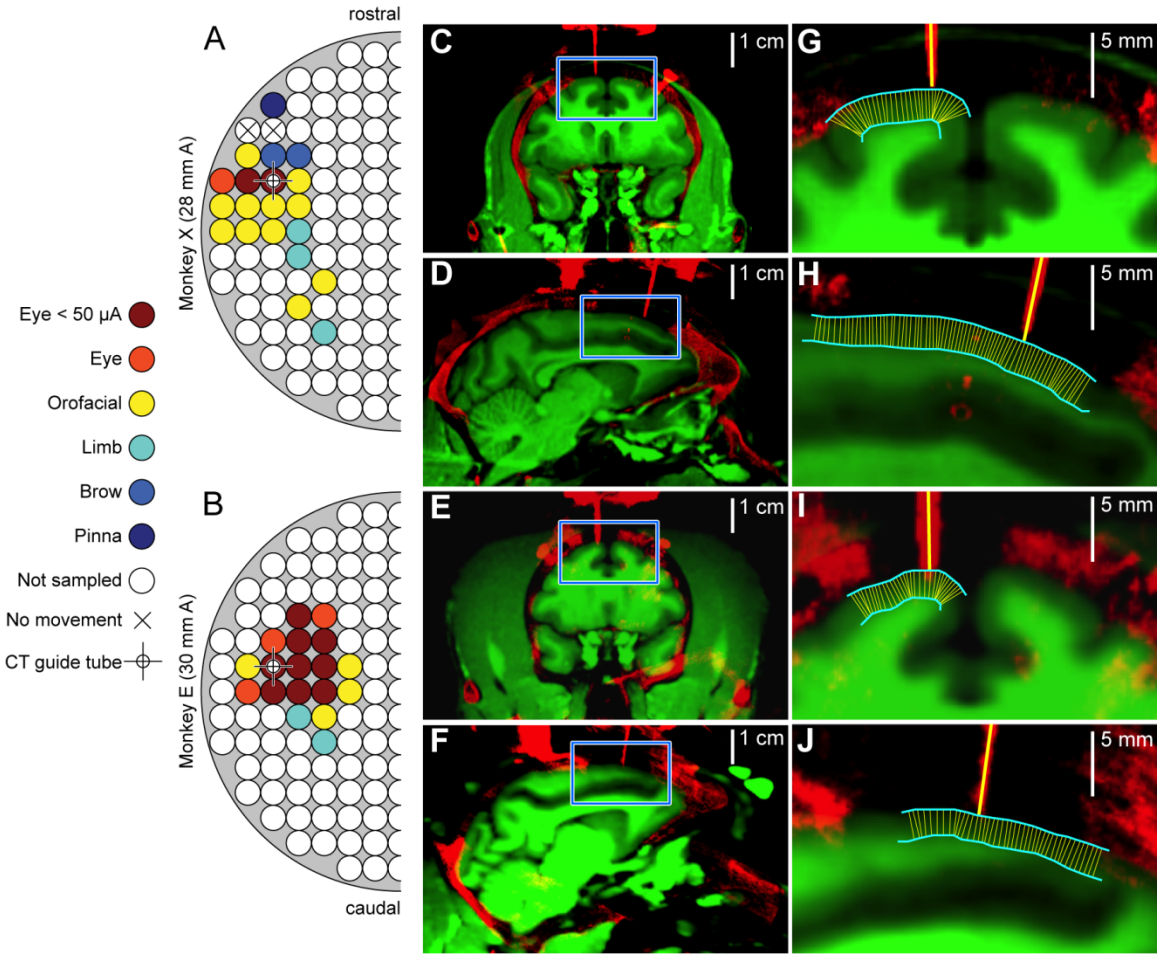

Figure 4.3. Location and penetration angle of recordings. (**A,B**) Maps derived from effects of intracortical electrical microstimulation for both monkeys. The anterior location of the center of the chamber is indicated at left. Circles depict grid hole locations spaced 1 mm apart. Legend shows the types of movement that were elicited with 50-200 µA of injected current. Crosshairs show the locations of guide tubes in CT images on right. (**C-J**) Co-registered MR (green) showing soft tissue including gray matter and white matter with CT (red) showing bone, stainless steel chamber adapters, titanium screws, titanium headposts, some dental acrylic used in the implants, and stainless steel guide tubes. (**C**) and (**D**) show coronal and sagittal planes for monkey X. (**E**) and (**F**) show coronal and sagittal planes for Monkey E. Blue squares in (**C-F**) are magnified in (**G-J**). Cyan lines in (**G-J**) show pial surface and transition from gray matter to white matter. Thin yellow lines show the result of an automated algorithm that minimized distance between the pial surface and gray matter to calculate angles perpendicular to gray matter (see Experimental Procedures). Thick yellow lines plot the trajectory of electrode arrays based on the orientation of guide tubes. Thick and thin yellow lines are virtually parallel at points of entry. This orientation validates the CSD measurement.

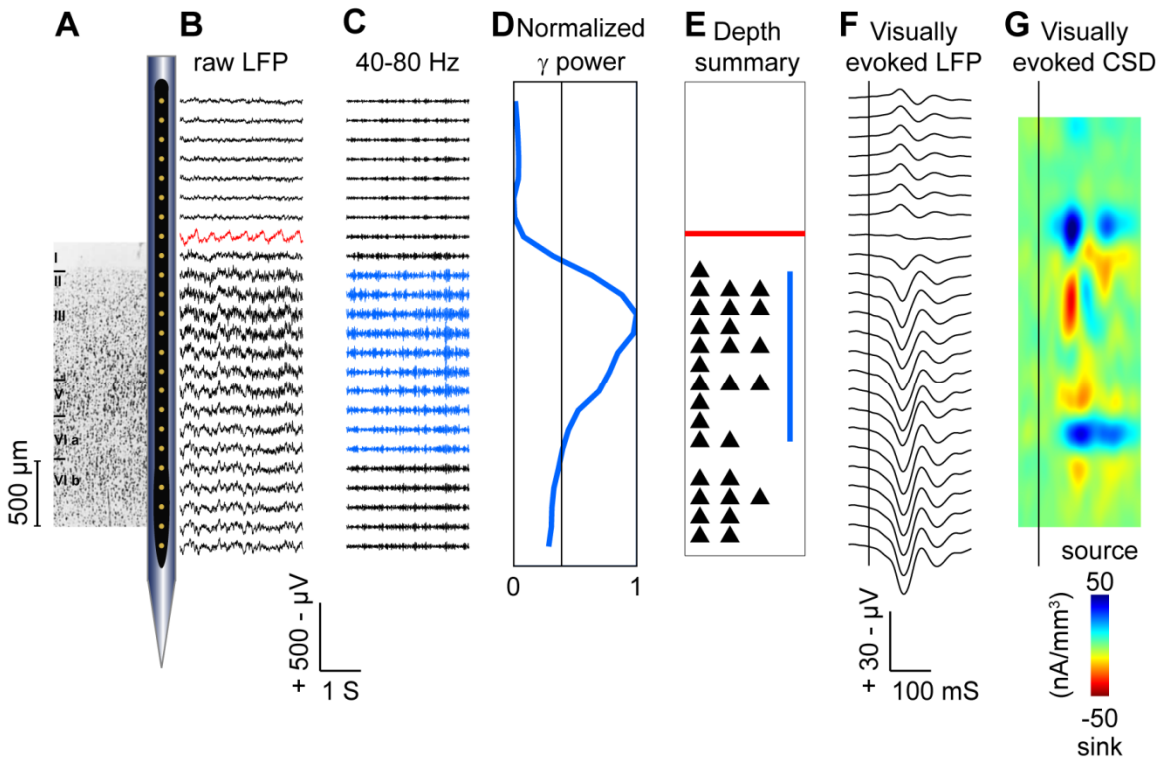

Figure 4.4. Raw and processed data from a representative session (1,316 trials). (**A**) Schematic diagram of electrode array drawn to scale and positioned on Nissl section from SEF (adapted from Matelli et al., 1991 with permission). (**B**) 3 s of raw LFP recorded from each of the contacts. The red trace (8th from top) shows pulse artifact. (**C**) LFP bandpass filtered from 40 to 80 Hz. Blue traces show γ activity elevated above the mean. (**D**) Normalized mean γ power recorded at each electrode site across entire session (blue) compared to average gamma power recorded across all contacts (vertical black line). Note the pronounced increase in γ power at the contacts in the neuropil. (**E**) Summary figure showing depth of pulse artifact (red line), elevated γ power (blue line), and the number of well-isolated single units (black triangles) recorded simultaneously. During this session, we recorded 29 well-isolated single units with 2 units on 5 channels and 3 units on another 5 channels (examples of isolation quality are illustrated in Fig S2). (**F**) 300 ms of event related LFP aligned to the flash stimulus (vertical black line). Note the reversal in voltage polarity occurring on the channel with the pulse artifact. Above this channel the signal is volume conducted EEG moving through saline in the recording chamber. Below this channel the signals is either the electrocorticogram recorded from the pial surface (perhaps in the 9th channel from top) or LFPs recorded from within gray matter. (**G**) 300 ms of CSD derived from the LFP, interpolating between contacts with 10 µm resolution. Vertical black line shows onset of flash stimulus.

signal indicated where the electrode was in contact with either the *dura mater* or the epidural saline in the recording chamber, which pulsated visibly with the monkey's heartbeat. Second, across all sessions, we observed a marked increase of power in the γ frequency range (40-80 Hz) at several electrode contacts, which diminished gradually at deeper locations. Several recent studies have shown elevated γ power in superficial and middle layers (Maier et al., 2010; Xing et al., 2012; Smith and Sommer, 2013), so this measure provides another useful marker for estimating depth. Finally, we recorded well-isolated single units simultaneously with the LFP, and co-localized their position with the markers described above (Figure 4.5C). This set of diverse physiological signals provided converging evidence to evaluate the electrode position with regard to laminar depths that were assigned through an automated alignment procedure described below.

Based on the known thickness of individual layers in SEF (Matelli et al., 1991), we estimated laminar boundaries and assigned visually evoked current sinks to specific layers. In the representative recording session, the largest sink (min -42 nA/mm^3) occurred in layer III starting ~50 ms after presentation of the stimulus. A second sink (min -25 nA/mm^3) began a few milliseconds later in layer V. A later sink (min -23 nA/mm^3) occurred more superficially in layers I/II, and additional weaker sinks (min -20 nA/mm^3) were evident in layer VI. Effectively simultaneous sinks in layers III and V are consistent with anatomical studies of the laminar termination of visual afferents in middle layers of SEF (reviewed by Shipp, 2005).

Several current sources are also apparent, including one at the level of the pulse artifact. Consistent with existing research, we interpret this source as passive current returning to the sinks below because it was recorded at the same level as the pulse artifact, and therefore, cannot have a cortical origin (Mitzdorf, 1985). In general, current sources can be caused either by passive return current or dendritic hyperpolarization

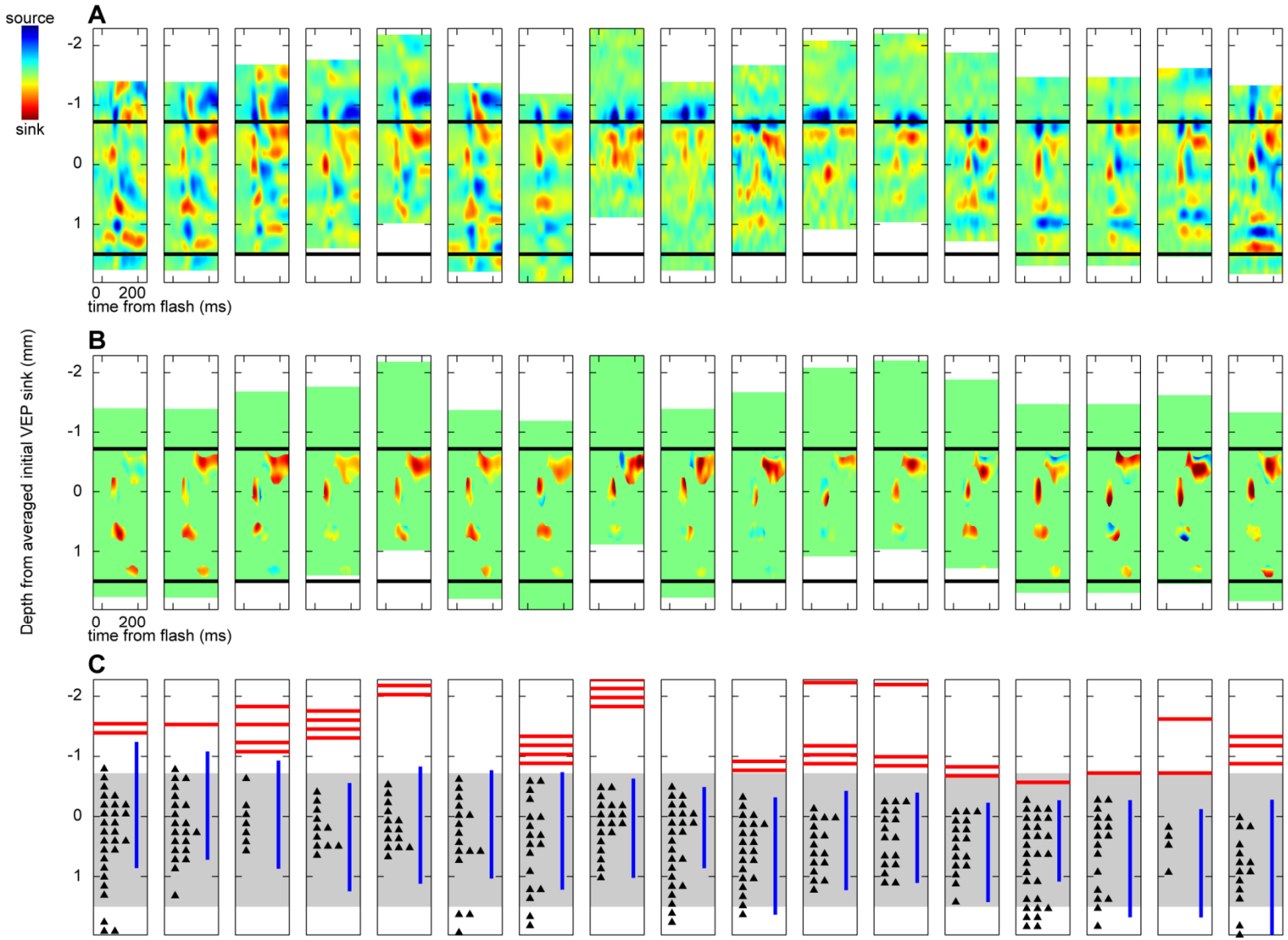
source
sink
A
-2
-1
0
1
0 200
time from flash (ms)
B
Depth from averaged initial VEP sink (mm)
-2
-1
0
1
0 200
time from flash (ms)
C
-2
-1
0
1

Figure 4.5 (opposite). Results of the automated alignment procedure for estimating recording depth across sessions. **A**) Visually evoked CSD recorded individually for each session. The first 7 sessions are taken from monkey E and the remaining 10 sessions were recorded from monkey X. Black bars indicate our estimate of the average location of gray matter based on the observed physiological signals. **B**) Visually evoked CSDs masked to show locations of the 4 grand-averaged visually evoked sinks reported in Fig. 4. Note the close correspondence in location of these sinks across recording sessions demonstrating the similarity in CSD recorded on subsequent days, and the success of our automated alignment procedure. **C**) Physiological signals apparent in the raw data on individual sessions. Pulse artifact (red lines), elevated γ activity (blue lines), and single-units (black triangles) show good correspondence with our estimate of the location of gray matter (gray shading).

making them harder to interpret than current sinks (Nicholson and Freeman, 1975; Mitzdorf, 1985). We therefore focus on current sinks for the remainder of this study.

To increase the signal-to-noise ratio, we averaged the evoked CSD patterns across recording sessions, analogous to creating grand average ERPs from EEG data, as done previously (Maier et al., 2010; Riera et al., 2012). To do this in an unbiased, data-driven manner, we developed an automated depth alignment procedure to maximize similarity between recording sessions using the entire source and sink laminar structure and timing. This mathematically optimized solution for depth alignment relies on the simple assumption that there are reliable similarities in CSD measured across recording sessions (see Experimental Procedures). Figure 4.5 shows the results of this procedure with data from every recording session. In every session, we observed a clear sink in layer III ~50 ms after the visual stimulus. In 15 of 17 sessions (88%) we also observed a second sink in layer V, and in 16 of 17 sessions (94%) we observed a third sink in layers I/II. On several recording sessions we placed our electrode array too superficial to sample from layer VI, but we observed a sink in this location in 11 of 13 sessions (85%). These consistencies validate the assumption that CSD is reliable across recording sessions and monkeys. Our automated alignment technique was blind to the physiological signals detailed above (i.e., pulse artifact, LFP γ power, and single unit locations), because it relied only on the CSD data. Nevertheless, we observed a close correspondence between its estimates of cortical depth and the other physiological signals observed in the raw data, lending further support for the accuracy of this approach (Figure 4.5C). Additional evidence for the accuracy of our automated alignment procedure comes from our findings of neural responses that differ by layer in SEF (see below). An alternate alignment procedure based on the depth of increased LFP γ power yielded the same qualitative results (Figure 4.6, see section 4.6.2),

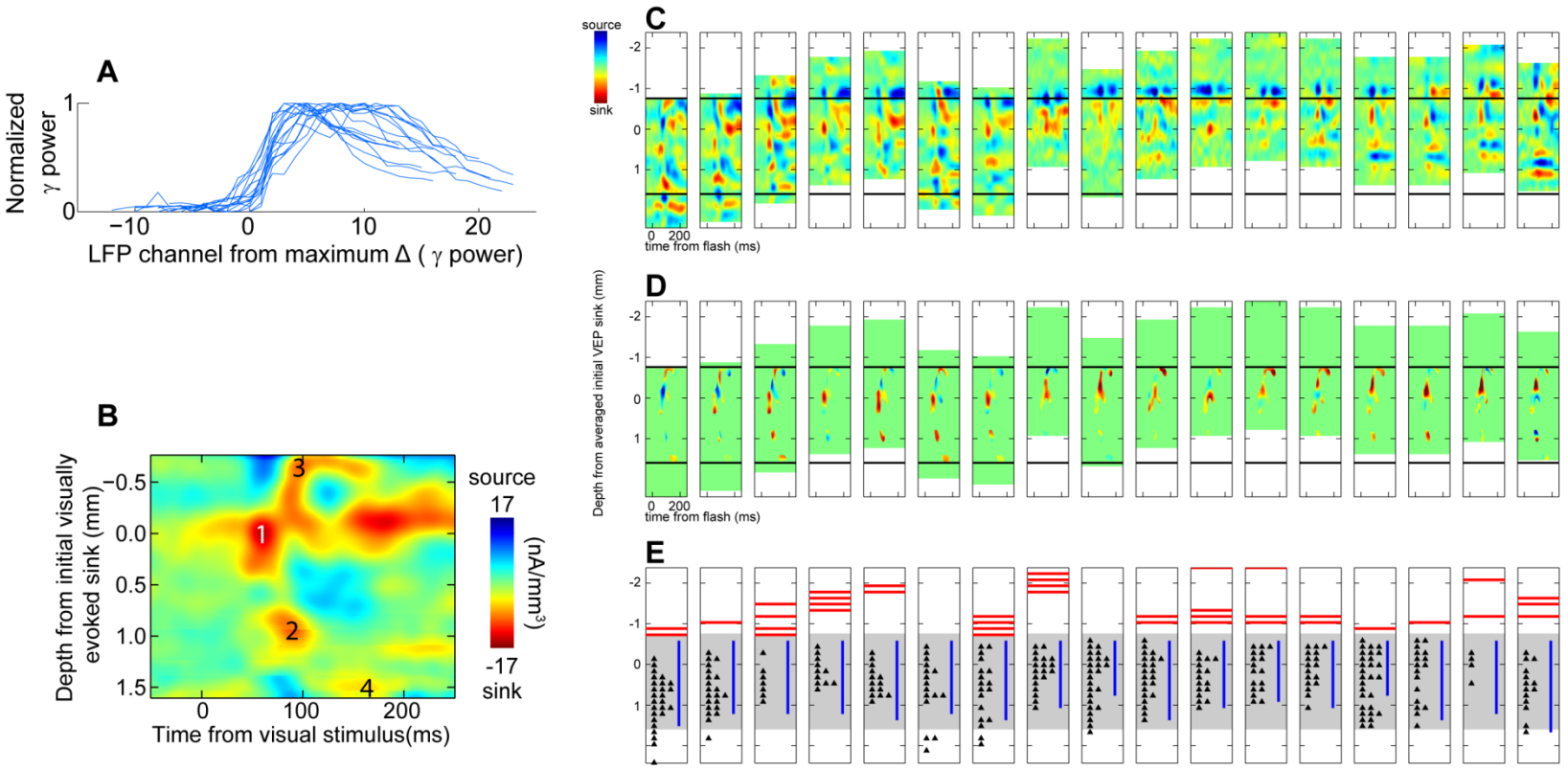

Figure 4.6. Results of aligning based on γ power **A**) Normalized mean γ power recorded at each electrode site on every individual session. A pronounced increase followed by gradual decrease in γ power was observed in each individual session. **B**) Grand average visually evoked CSD replicated using the γ -based alignment. Conventions as in Figure 4.4. Note the presence of 4 initial visually evoked current sinks consistent with the results obtained using the automated alignment technique. Note also the decrease in scale indicating a weaker effect using the γ -based alignment. **C-E**) Results of the γ -based alignment procedure showing data from each individual session. Conventions as in Figure 4.5.

although the CSD was spatially "blurred" due to variability in aligning to elevated γ power reducing the overall magnitude.

4.3.2 Visually evoked CSD

Visually evoked current sinks were observed across 2 mm of recording depth, and reached a maximum magnitude of -25 nA/mm^3 (Figure 4.7). This is only ~15% of the magnitude of visually evoked current flow reported for V1 using similar recording and analysis techniques (Maier et al., 2010).

Nevertheless, a clear laminar sequence of current sinks was apparent. Two initial sinks were observed in the grand average CSD, suggesting that visual afferents terminate in 2 distinct laminae. These findings agree with published anatomy. SEF is reported to be 1,992 μm (± 31 μm) thick in histological preparations (Matelli et al., 1991). Although it lacks a granular layer, SEF contains 2 layers of relatively dense pyramidal cells, one in deep layer III and a second forming layer V, which both receive visual input (Maioli et al., 1998; Shipp et al., 1998). The first sink (min -25 nA/mm^3) appeared in layer III 51 ms after the stimulus, becoming maximal after 72 ms. The second sink (min -22 nA/mm^3) developed in layer V at 55 ms, becoming maximal after 105 ms. Subsequent sinks occurred in layer I/II (min -14 nA/mm^3) at 147 ms (peaking at 168 ms) and in layer VI (min -10 nA/mm^3) at 172 ms (peaking at 173 ms).

To quantify these observations, we divided the time course following visual presentation into early (51-150 ms) and late (151-250 ms) epochs and conducted a between session 4x2 ANOVA using layers and epochs as factors. We observed significant differences in CSD by layer [$F(3,122) = 177.74$, $p < 0.001$], and a marginally significant decrease in CSD across layers during the late epoch [$F(1,122) = 78.40$, $p = 0.05$]. Importantly, a significant interaction between layers and time periods was also observed in the grand average CSD [$F(3,122) = 264.97$, $p < 0.001$]. Thus, even though

the magnitude of current density was lower than that observed in early sensory cortex, the pattern of middle layer synaptic current followed by current in superficial and deep layers was consistent across sessions and reflected CSD obtained in early sensory cortex (Mitzdorf and Singer, 1979; Schroeder et al., 1998; Lakatos et al., 2007; Lipton et al., 2010; Riera et al., 2012). As an additional test, we conducted across-session running Wilcoxon tests on channels binned by the inter-electrode spacing (150 μm). All 4 current sinks differed significantly from baseline (Figure 4.7C).

4.3.3 Saccade-related CSD

To determine whether this pattern of sinks is specific to visual input or occurs with other events during which SEF is modulated, we derived CSD associated with self-generated saccadic eye movements in darkness. The saccade-related CSD on individual sessions was very weak, but following alignment and averaging we observed distinct sinks (Figure 4.7B,D). Although SEF neurons tend to have contralateral movement fields (Schall, 1991a), no channels showed significant differences between ipsilateral and contralateral conditions (Wilcoxon rank sum, $p > 0.05$), so we describe the findings collapsed across all saccade directions. Saccade related CSD was of comparatively small magnitude, mainly post-saccadic, and concentrated in the upper layers, peaking in layer III (min -9 nA/mm^3) 32 ms after saccade initiation and more superficially (min -10 nA/mm^3) after 162 ms. The absence of a strong presaccadic sink in layer V is consistent with other evidence that SEF does not contribute directly to saccade production (Stuphorn et al., 2010). Thus, the pattern of current sinks elicited by visual stimulation is specific to visual input.

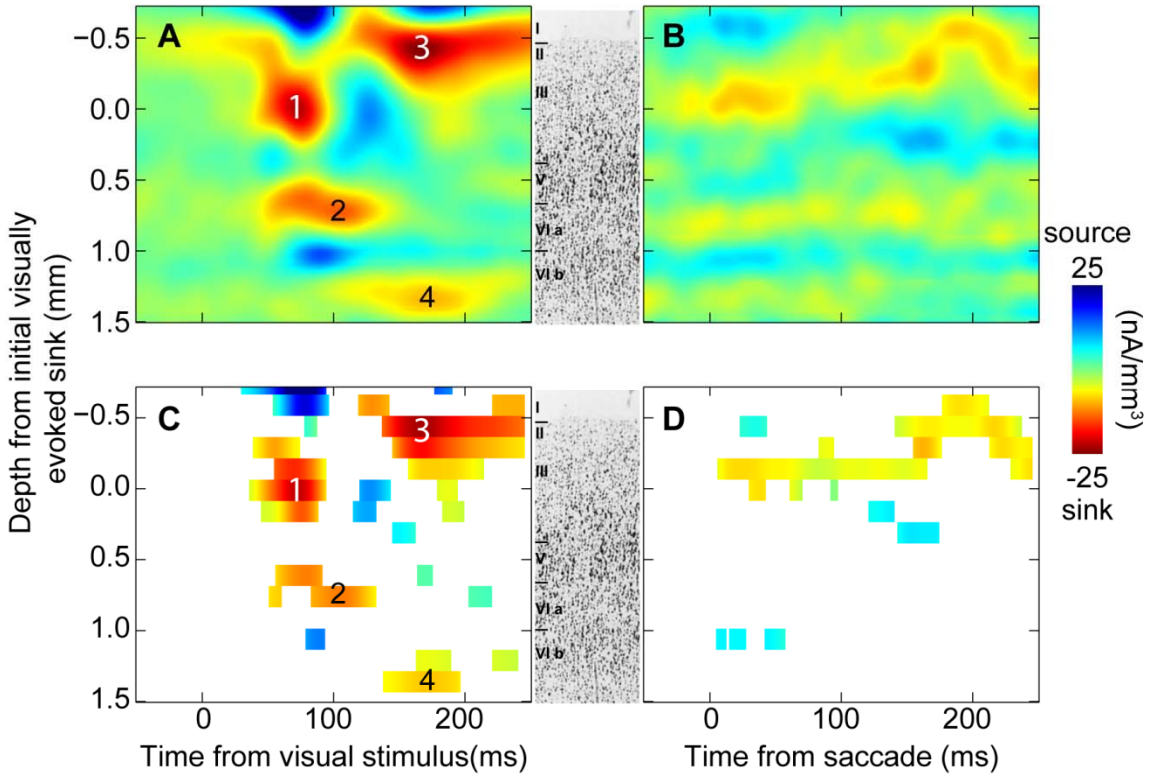

Figure 4.7. Grand average visually evoked and saccade-related CSD from SEF. Nissl section from SEF in center indicates laminar architecture(adapted from Matelli et al., 1991 with permission). (**A**) CSD recorded while monkeys passively viewed wide-field flashes of light. Four current sinks were observed and are numbered in order of appearance for clarity. (**B**) CSD recorded while monkeys made spontaneous saccades in darkness. (**C,D**). Data from **A,B** reproduced without interpolation highlighting times periods when channels deviate significantly from baseline. (Running Wilcoxon, $p < 0.05$ for > 5 consecutive ms in 10 ms window). Sixteen channel depths are shown. Due to the placement of the electrode array, deeper channels were sampled less often than superficial channels (N = 17 channels 1-12, N = 15 channel 13, N = 13 channel 14-15, N = 11 channel 16).

4.3.4 Visually evoked spiking activity

The CCM hypothesis makes detailed predictions about spiking activity (Douglas and Martin, 1991; Douglas et al., 1995). First, excitation followed by suppression is proposed to be a common feature of the CCM. Second, excitatory and inhibitory neurons receive synchronized inputs; otherwise, recurrent excitatory connections would lead to unrestricted excitation. Third, in an effect thought to be mediated by the action of $GABA_A$ and $GABA_B$ receptors, intracellular recordings in V1 show that pyramidal cells in superficial layers reach a maximum state of hyperpolarization later than those in deep layers.

To test these predictions, discharge rates were measured from 295 well-isolated single units recorded simultaneously with the LFPs (115 monkey E, 180 monkey X, see section 4.6.1, Figure 4.8, and Figure 4.9 for details). Of these units, 103 (35%) showed clear modulation following presentation of the flashed stimulus (63 monkey E, 40 monkey X). We also recorded visually evoked, thresholded multi-unit activity with clearly defined latencies from 58 electrode contacts (42 monkey E, 16 monkey X). Units with saccade-related modulation were also recorded from all layers of SEF. However, unlike visually responsive units, saccade-related responses were weak and relatively rare, also consistent with evidence that SEF does not contribute directly to saccade production (Stuphorn et al., 2010) (Table 4.1). Consequently, we focus on units with visual responses.

Visually responsive single units were recorded in all layers of SEF (Figure 4.10). As reported before (Schlag and Schlag-Rey, 1987; Schall, 1991a; Chen and Wise, 1995a) some units showed spiking enhancement (80, 50%) and others showed spiking suppression (81, 50%) following visual stimuli. We carried out a 4x2 ANOVA to determine whether the latency of these responses differed between layers (4 levels) and response types (i.e. enhancement vs. suppression). Latencies were significantly shorter

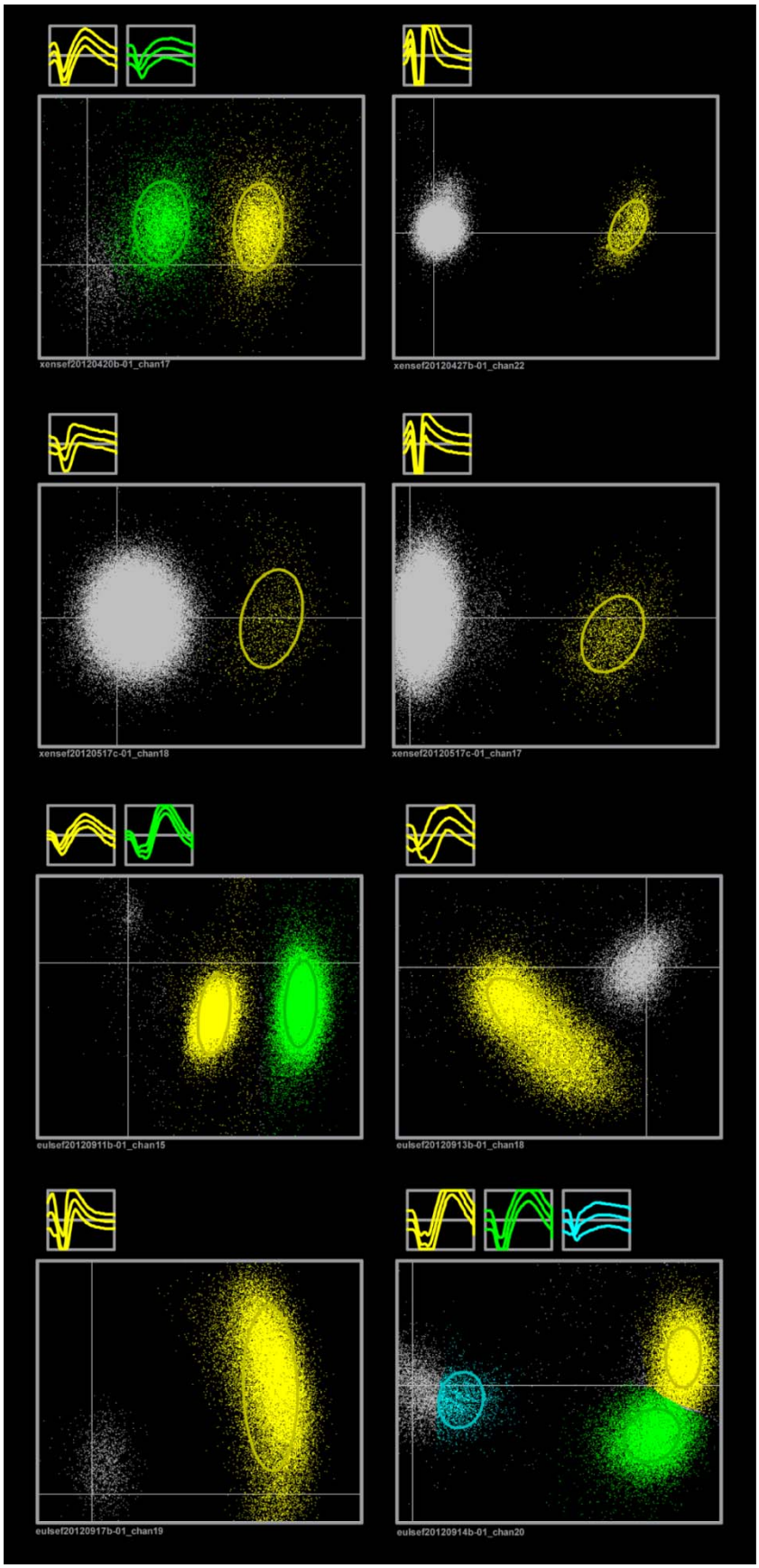
xensef20120420b-01_chan17
xensef20120427b-01_chan22
xensef20120517c-01_chan18
xensef20120517c-01_chan17
eulsef20120911b-01_chan15
eulsef20120913b-01_chan18
eulsef20120917b-01_chan19
eulsef20120914b-01_chan20

Figure 4.8 (opposite).Sample waveforms and PCA space for 8 sorted channels. Channels 1-4 are taken from recordings with monkey X and channels 5-8 are taken from recordings with monkey E.

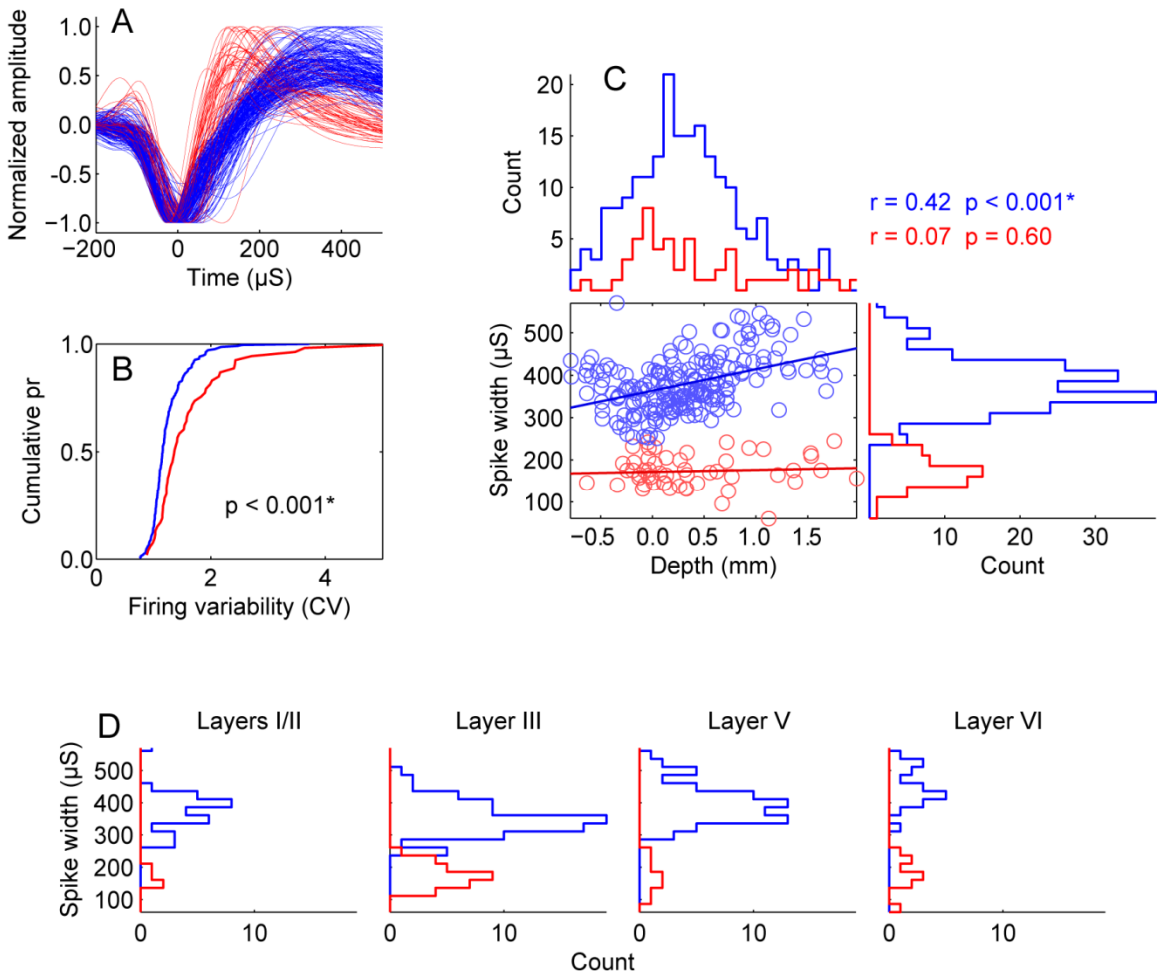

Figure 4.9. Biophysical characteristics of single units. **A**) All biphasic waveforms in population. Red and blue denote narrow and broad spikes respectively (split at 250 μS). This color code is the same in remaining panels. **B**) Cumulative probability distributions of coefficient of variation (CV) of inter-spike intervals plotted separately for broad spiking and narrow spiking units. Narrow spiking units showed more variability in spike timing. **C**) Spike width as a function of recording depth. Scatter plot shows regression of spike width by depth separated by broad and narrow spiking populations. Histograms show distributions of broad and narrow spiking units across each dimension. Broad spiking units increased in width with depth. No such trend was observed for narrow spiking units. **D**) Counts of broad spiking and narrow spiking units recorded in each layer.

	# of SU	# of MU	Enhancement latencies	Suppression latencies
Layer II	12	12	78(53)	120(45)
Layer III	41	17	84(41)	119(41)
Layer V	33	12	82(37)	99(38)
Layer VI	17	17	89(51)	120(47)

Table 4.1. Summary statistics of units with saccade-related responses recorded from each layer. SU = single units. MU = multi units. Latencies are means (SD)

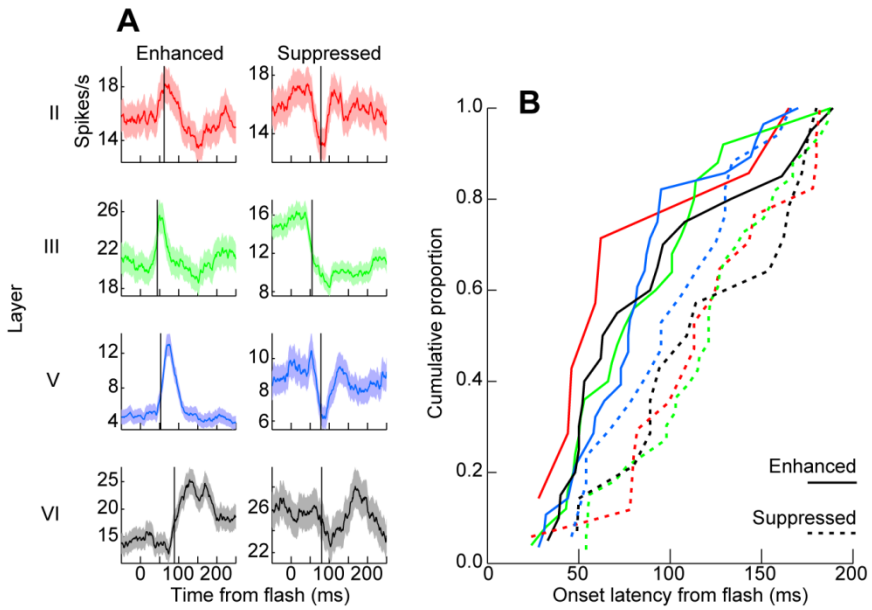

Figure 4.10. Single and multi-unit visually evoked responses to flashed stimuli. (**A**)**.** Representative units recorded from layer II (red), layer III (green), layer V (blue), and layer VI (black) demonstrating either enhanced (left) or suppressed discharge (right) rates following the stimulus. Fill area represents 95% confidence intervals measured across stimulus presentations. Vertical lines mark response latencies. (**B**)**.** Cumulative distributions of unit response latencies separated by layer and response type. Enhanced responses showed shorter latencies than suppressed responses. See also Table 4.1 and Table 4.2.

for units with enhanced than for units with suppressed responses [$F(1,153) = 17.64$, $p < 0.001$]. Thus, collectively, SEF exhibits excitation followed by suppression. The latencies of visually evoked unit responses were not significantly different across layer [$F(3,153) = 0.77$, $p = 0.51$], nor was the interaction between layers and response type [$F(3,153) = 0.48$, $p = 0.67$] (Table 4.2). Thus, the temporal and spatial pattern of excitation and suppression in SEF is consistent with the CCM model.

To test whether excitatory and inhibitory neurons receive synchronized inputs, we determined whether putative pyramidal cells and interneurons in SEF show similar latencies. We classified neurons as either putative pyramidal cells or putative interneurons based on spike width (Constantinidis et al., 2002; Mitchell et al., 2007). New evidence for this biophysical distinction was obtained (Figure 4.9 and section 4.6.4). Narrow spiking neurons exhibited greater spiking variability. Also, the spike width of the broad spiking neurons increased with depth in parallel with the increase in pyramidal cell size from upper to lower layers of SEF. Meanwhile, the spike width of the narrow spiking neurons did not vary with depth. The incidence of narrow spiking neurons corresponded to the density of parvalbumin but not of calretinin or calbindin neurons in SEF (Figure 4.2C). Of neurons so classified, 101 broad spiking units and 22 narrow spiking units showed clearly detectable onset times (means ± SD, 108 ± 44 ms broad spiking units, 98 ± 38 ms narrow spiking units). Consistent with predictions of the CCM model, these onset times did not differ significantly (Wilcoxon rank sum $W = 6403$, $p = 0.35$).

Finally, to test whether superficial and deep layers can be distinguished based on the timing of hyperpolarization, we determined whether visually-evoked spike suppression followed a longer time course in neurons recorded from upper versus lower layers in SEF. Further, because the classic CCM model replicates neural responses using a single pool of GABAergic neurons (Figure 4.1), we predicted that this effect

	# of SU	# of MU	Enhancement latencies	Suppression latencies
Layer II	4	5	-27(46)	7(43)
Layer III	12	8	27(52)	-6(41)
Layer V	7	5	22(41)	29(55)
Layer VI	4	6	-3(46)	48(45)

Table 4.2. Summary statistics of units with visual responses recorded from each layer. SU = single units. MU = multi units. Latencies are means (SD)

would be restricted to broad spiking units only. Extracellular recordings in SEF confirmed these predictions (Figure 4.11). We limited this analysis to visually related units that showed any decrease in spiking after stimulus onset relative to baseline. The time of maximum spike suppression recorded from units in layers II and III (mean ± SD, 144 ± 61 ms), was significantly later than the time of maximum spike suppression from units recorded in layers V and VI (mean ± SD, 115 ± 62 ms) (Wilcoxon rank sum $W = 6223$, $p < 0.01$). We further probed this effect by analyzing broad and narrow spiking units separately. As predicted, broad spiking neurons recorded in superficial layers showed significantly later spike suppression than broad spiking neurons recorded in deep layers (Wilcoxon rank sum $W = 1719$, $p < 0.01$), but this was not observed for narrow spiking units (Wilcoxon rank sum $W = 471$, $p = 0.13$). Adding evidence for differences in inhibition between layers, the overall probability of recording units with suppressed responses was also higher in superficial layers as reflected by a significant difference in depth by response type (Wilcoxon rank sum $W = 7353$, $p < 0.01$). Thus, the time course of inhibitory processes in SEF is consistent with the CCM model.

4.4 Discussion

Our data provide the first physiological evidence that the CCM framework can be applied to primate agranular motor cortex in the frontal lobe. The fact that a functional parallel can be drawn between anatomically distinct granular (sensory cortex) and agranular (motor cortex) provides critical support to the hypothesis that CCMs are a universal feature of neocortical architecture. (See section 4.6.5 for discussion of these results in relation to previous physiological studies.)

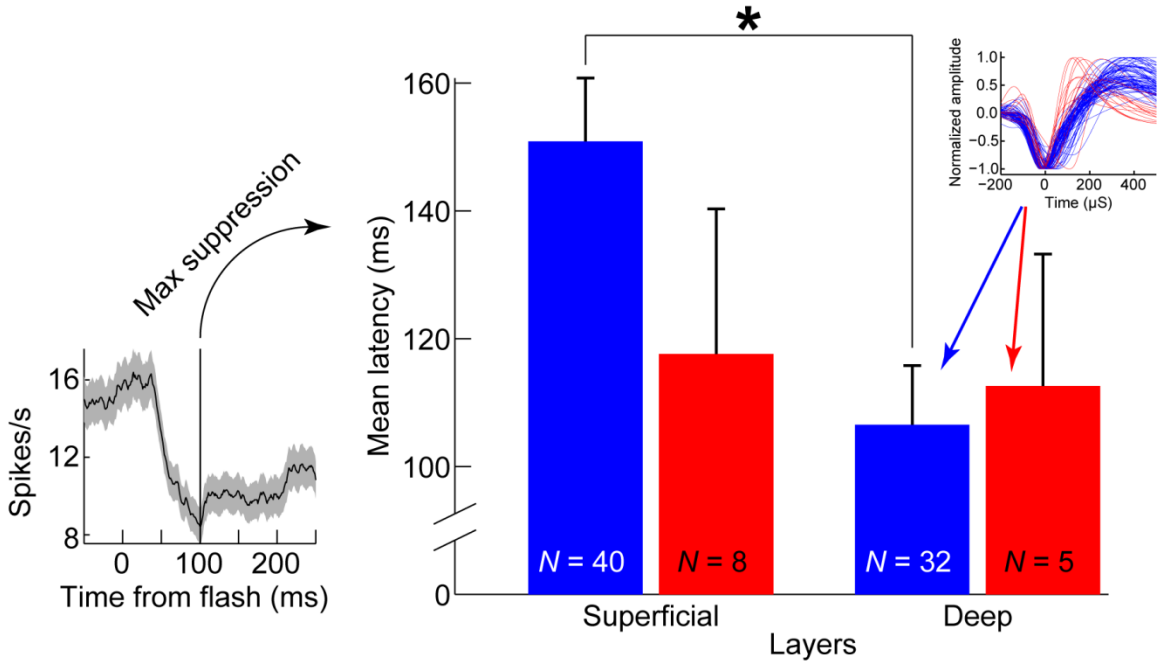

Figure 4.11. Latency to maximum spike suppression differentiated by depth and width. Superficial layers (II and III) vs. deep layers (V and VI) and broad spiking units (in blue) vs. narrow spiking units (in red). Error bars are SEM. Left, representative unit illustrating the estimate of latency to maximum spike suppression. Upper-right inset shows broad and narrow spikes for the sample. A statistically significant difference was observed in the latency to maximum spike suppression between broad units recorded in superficial layers and broad units recorded in deep layers. No other comparisons differed significantly.

4.4.1 Relation to models of CCMs

Based on data collected in V1, Gilbert and Wiesel (Gilbert, 1983) provided the first account of a laminar CCM. They described the ascending projections that underlie our current understanding of CCMs (Gilbert, 1983; Callaway, 1998; Douglas and Martin, 2004). The sequential, laminar pattern of CSD that we report mirrors this CCM derived from early visual cortex. The earliest sinks in SEF were in the middle layers and spread to more superficial and deeper layers. Douglas and Martin extended and refined the CCM model by describing the recurrent activity that amplifies (Douglas et al., 1995) ascending input and the recurrent inhibition (Douglas and Martin, 1991) that prevents uncontrolled excitation (see also Haider et al., 2006). Their model was spawned by the observation that stimulation of thalamic afferents produced brief excitation followed by longer lasting suppression in all layers. We found a similar sequence of activity in SEF with enhanced responses preceding suppressed responses by ~30 ms in all layers.

In the classic CCM model, ascending input excites both pyramidal cells and interneurons. Interneurons project to pyramidal cells leading to this characteristic pattern of excitation and suppression (Douglas and Martin, 1991; Douglas et al., 1995; see also Brunel and Wang, 2001; Chance et al., 2002)). Consistent with this model, we noted that putative pyramidal neurons (broad spiking units) and putative interneurons (narrow spiking units) were equally likely to display an initial enhancement in spiking following visual stimulation and that onset latencies did not differ between these populations.

Finally, intracellular recording studies highlight key differences in the time course of late suppression between superficial and deep pyramidal cells, and evidence suggests these differences are produced by $GABA_A$ and $GABA_B$ receptors (Douglas and Martin, 1991). The CCM model reflects these details by representing superficial and deep layers as two specialized nodes in the cortical microcircuit, and this laminar architecture forms the basis for several biologically constrained theories of cognitive

function (Douglas and Martin, 2004; Bastos et al., 2012). Consistent with these results, we also found differences in suppression between superficial and deep layers in SEF. Units recorded in superficial layers were more likely to respond with suppression, and, identical to classic findings in V1 (Douglas and Martin, 1991), we noted a longer time course for suppression in superficial layers compared to that recorded in deep layers. As expected, this effect was restricted to putative pyramidal cells suggesting laminar differences in $GABA_A$ versus $GABA_B$ expression in this cell type alone. Taken together, our CSD and unit data describe, in considerable detail, a functional CCM in SEF very similar to that observed in early sensory areas despite their gross anatomical differences.

4.4.2 Relation to previous anatomical studies

We observed short latency visual responses in SEF in layers III and V. Visual afferents to SEF include subcortical and cortical projections. Fast visual input may be received from the mediodorsal nucleus of the thalamus (Huerta and Kaas, 1990; Shook et al., 1990) that is innervated by the superior colliculus (Benevento and Fallon, 1975; Harting et al., 1980). Afferents from this nucleus terminate in lower layer III of SEF (Giguere and Goldman-Rakic, 1988). Visual afferents to SEF are also supplied by cortical areas, including the lateral intraparietal area, area 7a, the frontal eye field, the superior temporal polysensory area, visual area 6a (V6a), and the medial superior temporal area (MST) (Barbas and Pandya, 1987; Huerta and Kaas, 1990; Schall, 1991a; Shipp et al., 1998). Inputs from dorsal stream areas like MST and V6a can provide fast visual input to SEF. Consistent with our observations of initial sinks in layer III and V, orthograde tracer injections in MST (Maioli et al., 1998) and in V6a (Shipp et al., 1998) reveal terminals in layers III and V in SEF. Also, consistent with our observation that layer VI is the last layer to show visually related CSD, projections from dorsal stream

areas terminate only sparsely in layer VI of SEF (Maioli et al., 1998; Shipp et al., 1998). Thus, the laminar distribution of latencies is in good agreement with known anatomy.

4.4.3 Relation to cortical hierarchy

It is possible that this CCM will help reveal a cortical hierarchy in agranular cortex much as it has in granular cortex (Felleman and Van Essen, 1991). Our findings provide evidence supporting a model proposed by Shipp (2005) who extended principles of microcircuitry derived from early visual areas and conducted a meta-analysis to elucidate the hierarchical structure of agranular cortex. Across many tracer studies, Shipp noted that orthograde label appears in layers III and V of agranular cortex, and proposed that the ratio of layer III to layer V projections can be used to place agranular areas at their appropriate hierarchical level. The visually evoked CSD we report provides the first direct physiological support for this hypothesis by demonstrating driving input in layers III and V of agranular cortex. It remains to be seen, however, if the relative strength of these activations indicates the hierarchical location of a given agranular area. In our data, current sinks were observed in layers III and V with similar latency and magnitude after visual stimulation. This suggests both layers receive visual afferents. Future, laminar recordings from other areas of agranular cortex will provide data to test this agranular-hierarchy hypothesis.

4.5 Methods

4.5.1 Monkey care and surgical procedures

Data were collected from 1 male bonnet macaque (monkey E *Macaca radiata* 8.8 kg) and one female rhesus macaque (monkey X *Macaca mulatta* 6 kg). Animal care exceeded policies of the USDA and Public Health Service Policy on Humane Care and Use of Laboratory Animals. All procedures supervised and approved by the Vanderbilt

Institutional Animal Care and Use Committee. MRIs were acquired to aide in placement of recording chambers (Godlove et al., 2011b), with a Philips Intera Achieva 3 tesla scanner using SENSE Flex-S surface coils placed above and below the head. T1-weighted gradient-echo structural images were obtained with a 3D turbo field echo anatomical sequence (TR = 8.729 ms; 130 slices, 0.70 mm thickness). Cilux recording chambers (Crist Instruments, Hagerstown, MD) were implanted normal to the cortex (17° monkey E, 9° monkey X relative to stereotaxic vertical) centered on midline 30 mm (monkey E) and 28 mm (monkey X) anterior to the interaural line. Surgical placement of headposts has been described in detail (Godlove et al., 2011a).

4.5.2 Cortical mapping and electrode placement

Following recovery after surgery, chambers were mapped using tungsten microelectrodes (2-4 MΩ, FHC, Bowdoin, ME) to apply 200 ms trains of biphasic microstimulation (333 Hz, 200 μs pulse width) of up to 200 μA using a BAK (Sanford, FL) pulse generator and microstimulator in combination with an FHC (Bowdoin, ME) isolator in constant current mode to elicit limb, orofacial, and eye movements (Figure 4.3 A,B). SEF was identified as the area from which saccades could be elicited using < 50 μA of current (Schlag and Schlag-Rey, 1987; Schall, 1991a; Stuphorn and Schall, 2006).

We found lateral position granting access to SEF perpendicular to the cortical layers by consulting MRI scans. These positions were further refined through mapping the three dimensional orientation of gray matter within the chamber by listening to spontaneous neural activity as a function of depth, using a Grass Technologies (Warwick, RI) audio monitor. SEF is 1,992 μm (± 31 μm) thick in histological preparations (Matelli et al., 1991). Using Teflon coated tungsten microelectrodes, and driving at a speed of 25 μm per second, discriminated the gray-to-white matter transition (GWT) by the sudden paucity of units and the overall decrease in background "hash".

When entering cortex obliquely, the GWT was encountered >2 mm after contacting the pial surface. In the extreme, when the electrode was positioned within ~2 mm of the midline, electrode tracks traversed the medial wall so that GWT was never encountered. We found the position allowing a penetration perpendicular to the cortical surface by advancing electrodes at gradually more lateral positions until we discerned the GWT 2 mm after contacting the pial surface.

To confirm that these coordinates placed electrodes perpendicular to gray matter, we conducted CT scans with guide tubes in place and co-registered these data with structural MRIs using a point-based method implemented in OsiriX (Geneva Switzerland see section 4.7.2). CT scans were acquired using a Siemens microCAT II with an x-ray beam intensity of 180 mAs and an x-ray tube potential of 80 kVp. Images were reconstructed at 512 x 512 x 512 with a voxel size of 0.252 x 0.252 x 0.122 mm^3.

In monkey E, all recordings were obtained in a location 31 mm anterior to the interaural line, 5 mm lateral to the midline. In monkey X all recordings were obtained either 29 or 30 mm anterior and 5 mm lateral. These are the positions depicted in Figure 4.3 (30 mm anterior for monkey X). During mapping of the bank of the medial wall of cortex, we noted that both monkeys seemed to have chambers placed ~1 mm to the right with respect to midline of the brain. This was confirmed in the co-registered CT/MRI data. Thus, our stereotaxic estimates of 5 mm lateral may have actually been recorded ~4 mm lateral with respect to the cortical (as opposed to the skull-based stereotaxic) midline.

4.5.3 Estimation of electrode track angles

We segmented the pial surface and the GWT in coronal and sagittal slices directly beneath the guide tube for each monkey (cyan lines in Figure 4.3G-J) without reference to the co-registered CT images, and then transferred these boundaries to the

co-registered data. We then implemented a custom algorithm in MATLAB to estimate angles perpendicular to gray matter (thin yellow lines in Figure 4.3G-J). For every pixel representing the pial surface in the 2D image, the algorithm found and recorded the closest pixel in Euclidean space representing the GWT. This resulted in a network made up of triangular webs since a single GWT pixel was often found to be closest to several pial surface pixels. The algorithm then worked in reverse, matching every GWT pixel to its closest pial surface counterpart. Finally, the algorithm recorded the average angle of all connections between the pial surface and the GWT in a sliding window. We found that smoothing across 25 angles provided a balance between angle accuracy and spatial resolution. For display purposes we only plot every 10th angle calculated in this fashion in Figure 4.3. By comparing the estimated angles perpendicular to gray matter to the angle of the guide tubes (thick yellow lines in Figure 4.3G-J), one can clearly see that electrode tracks were made perpendicular to gray matter.

4.5.4 Data collection protocol

During recordings, monkeys sat in enclosed primate chairs with heads restrained 45 cm from CRT monitor (Dell, P1130 background luminance of 0.10 cd/m^2) running at 70 Hz subtending 46° x 36° of visual angle. The monitor was unplugged while saccades were recorded in darkness; the only source of illumination was a small bank of infrared light emitting diodes (5° x 7° of visual angle, 0.03 cd/m^2), which was necessary for video-based eye tracking. Flash presentation was contingent on eye position under computer control (TEMPO, Reflective Computing, Olympia, WA).

We carried out an identical daily recording protocol across monkeys and sessions. After advancing the electrode array to the desired depth, we waited 3-4 hours until recordings stabilized across contacts. This waiting period resulted in extremely stabile recordings since single units could almost always be held indefinitely. After

achieving recording stability, we recorded 1 hour of "resting state" activity in near-total darkness with the CRT monitor unplugged. These data will be the subject of a future report. We then presented wide-field flashes of light to the monkeys in blocks of 100-200 presentations. Whenever the monkey's gaze fell within 11° of the center of the CRT monitor, the central 40° x 36° of the CRT monitor flashed white (34.80 cd/m^2) for a single frame (14.3 ms at 70 Hz) every 500 ms for as long as the monkey maintained gaze. These blocks were interleaved with periods of near total darkness of ~5-10 minutes in length. Saccades made during these periods form the basis for the saccade-related CSD analysis. This blocked design prevented the monkeys from becoming fully dark adapted. We collected 500-1000 presentations of light flashes and ~30 minutes of saccades in darkness per day. After this, we allowed monkeys to complete ~2000-3000 trials of a saccade stop-signal task (Schall and Godlove, 2012); these data will be presented in a separate report. Daily recording sessions ran from around 8:00 AM to 5:00 PM. Data for this report was collected between 1:00 PM and 3:00 PM.

We acquired 12,342 trials (6,448 monkey E, 5,894 monkey X) across 17 sessions (7 monkey E, 10 monkey X). The number of sessions is similar to that used in previous studies (Maier et al., 2010; Maier et al., 2011; Spaak et al., 2012) although the number of trials per session is somewhat larger.

4.5.5 Data acquisition

Intracranial data were recorded using a 24-channel Plexon uprobe (Dallas, TX) with 150 μm inter-electrode spacing. The uprobes had 100 mm probe length with 30 mm reinforced tubing, 210 μm probe diameter, 30° tip angle, 500 μm to first contact. Contacts were referenced to the probe shaft, and grounded to the headpost. We penetrated uprobes into the cortex using custom built guide tubes consisting of 26 gauge polyether ether ketone (PEEK) tubing (Plastics One, Roanoke, VA) cut to length and

glued into 19 gauge stainless steel hypodermic tubing (Small Parts Inc., Logansport, IN) that had been cut to length, deburred, and polished. The stainless steel guide tube provided mechanical support, while the PEEK tubing electrically insulated the shaft of the uprobe, and provided an inert, low-friction interface that aided in loading and penetration. We used microdrive adapters that were fit to our recording chambers with < 400 μm of tolerance and locked in place at a single radial orientation (Crist Instruments, Hagerstown, MD). After setting up hydraulic microdrives (FHC, Bowdoin, ME) on these adapters, pivot points were locked in place by means of a custom mechanical clamp and neither guide tubes nor uprobes were removed from the microdrives once recording commenced within a single monkey. These methods ensured that we were able to sample neural activity from precisely the same location relative to the chamber on repeated sessions.

All data were streamed to a single data acquisition system (MAP box, Plexon, Dallas, TX). Time stamps of trial events were recorded at 500 Hz. Eye position data were streamed to the Plexon computer at 1 kHz using an EyeLink 1000 infrared eye-tracking system (SR Research, Kanata, Ontario, Canada). LFP and spiking data were processed with unity-gain high-input impedance head stages (HST/32o25-36P-TR, Plexon). LFP data were bandpass filtered at 0.2-300 Hz and amplified 1000 times with a Plexon preamplifier, and digitized at 1 kHz. Spiking data were bandpass filtered between 100 Hz and 8 kHz and amplified 1000 times with a Plexon preamplifier, filtered in software with a 250 Hz high-pass filter and amplified an additional 32,000 times. Waveforms were digitized 200 μS before and 1200 μS after threshold crossings at 40 kHz. Single units were sorted online using a software window discriminator and refined offline using principal components analysis implemented in Plexon offline sorter. Figure 4.8. shows 20 example channels (10 from each monkey) taken from various recording sessions in PCA space.

4.5.6 LFP and CSD analysis

Data analyses were carried out in MATLAB (Mathworks, Natick, MA). LFPs were time locked to stimulus onset or saccade initiation (defined as the instant that the eye exceeded 30°/s). Data were baseline corrected to the 200 ms interval preceding stimulus onset, or to the period -400 ms to -200 ms relative to saccade onset for our motor-related CSD analysis. To observe power in the γ range, LFP data were bandpass filtered 40-80 Hz using a zero phase shift digital filter with an order of 50 ms.

After constructing event-related LFPs, we estimated CSD by approximating the 2nd spatial derivative at each point in time using the equation:

$$CSD = S\frac{\Phi(x-h) - 2\Phi(x) + \Phi(x+h)}{h^2}$$

where Φ = the observed voltage, h = the inter-electrode spacing (150 in our case) and S = the average conductance of primate gray matter (0.4 S/m) (Logothetis et al., 2007). The CSD reveals local dendritic activity in gray matter where neural ensembles arborize together and depolarize in unison, allowing the summation of current flow to be observed at the mesoscopic scale (Freeman and Nicholson, 1975; Riera et al., 2012). We multiplied the results by 10^6, converting units from A/m^3 to the more tractable nA/mm^3. This allowed us to compare the magnitude of our CSD directly to published results (Maier et al., 2010; Maier et al., 2011). To approximate CSD continuously across space, we interpolated between electrode contacts using nearest neighbors to a density of 10 μm and convolved the result with a Gaussian filter (σ = 100 μm) (Pettersen et al., 2006). This was important since CSD data were averaged across recording sessions and successive CSD recordings could be offset by increments smaller than 150 μV (our inter-electrode spacing). Thus grand averaged CSD was sampled with higher resolution than our inter-electrode spacing, conceptually similar to the way in which the Hubble

Ultra Deep Field is increased in resolution by slight (half-pixel) perturbations in the position of the telescope across imaging sessions (Beckwith et al., 2006).

4.5.7 Automated depth alignment technique

Our recording depths were jittered from session to session, both intentionally by advancing the electrode array to different levels, and unintentionally by slight day-to-day deviations in cortical "dimpling" caused by viscoelasticity of the neural tissue. This made it necessary to develop methods to realign our CSD recordings in an unbiased fashion allowing comparison across sessions. We were unable to rely on microdrive depth measures, since these values do not take variable cortical dimpling into account. We adopted methods similar to those used by (Maier et al., 2010; see also Di et al., 1990; Riera et al., 2012), who aligned and averaged consecutive recording sessions relative to the peak of the initial visually evoked sink that is readily apparent in V1 following presentation of a flashed visual stimulus. Although we consistently observed a sink in consecutive recording sessions around 50 ms after presentation of a flashed stimulus, this sink was smaller in magnitude causing reductions in our overall signal-to-noise ratio (Figure 4.5). This lower signal-to-noise ratio may have biased our results if we had adopted a manual alignment procedure. Thus, we devised an automated depth alignment procedure to minimize differences between recording sessions using all available source and sink information in a given time window.

Specifically we treated the alignment across recording sessions as a model with N parameters (where N equals the number of recording sessions) specifying the optimal depth of each session. An error term was calculated for a given set of depth parameters by subtracting each CSD matrix from every other CSD matrix, squaring the results, and summing across space, time, and session number. This method was sensitive to the number of overlapping data points which differed as a function of the depth parameters

chosen. To address this issue, we divided the error term by the number of overlapping data points normalizing the sum of squared errors by the number of observations. We then implemented a genetic algorithm for parameter optimization to minimize our calculated error term. In practice, we fit the period of time 50-100 ms after stimulus onset, since we systematically observed large visually evoked activity during this time across monkeys and sessions. We also constrained the depth parameters to ensure at least 50% overlap between every recording session. Given our microdrive depth estimates, this was a conservative estimate.

4.5.8 Statistical Methods

We used 2 approaches to assess the statistical significance of the CSD. First we carried out a 4x2 ANOVA with factors of layer (I/II, III, V, versus VI) and time epoch (50-150 ms versus 151-250 ms after flash stimulus), to test for differences in the CSD across space and time. ANOVA assumes independence across samples, and this assumption was not strictly met by our CSD data. Additionally, of the sessions (N = 17), only a subset recorded activity from the deeper layers (N = 13). This difference in N was not accounted for in our across-sessions ANOVA. We therefore conducted a second test that compared CSD activity recorded at each channel location to CSD activity on the same channel recorded during the baseline period before stimulus presentation (reported in Figure 4.6). To do this, we adopted the same criteria applied to LFP data by Purcell et al., (2012a). We binned channels into 150 μm intervals (the inter-electrode spacing) and then compared CSD magnitude to that recorded during the 20 ms immediately before stimulus onset, or during the -220 to -200 period before saccade onset. To correct for multiple comparisons, channels were deemed to show saccade- or motor-related activity only if the CSD deviated significantly from baseline for 5 consecutive 10 ms time bins (Wilcoxon rank-sum test, $p < 0.05$) (Figure 4.6C,D).

Importantly, by carrying out statistics on individual recording depths differences in *N* caused by changes in electrode depth across days is accounted for and power is appropriately adjusted. Results of the ANOVAs and running Wilcoxon tests were in agreement, showing significant differences in CSD measured across depth and time.

We classified units as visually responsive or saccade related using the same running Wilcoxon method adopted by Purcell et al., (2012a) and described above. Rasters were convolved with a kernel resembling a postsynaptic potential (Thompson et al., 1996) to construct spike density functions for individual trials, and analyses were carried on these data.

CSD and single-unit onset latencies were measured using the same running Wilcoxon approach adopted by Purcell et al., (2012a). For CSD latency measures, data were collapsed across channels within layers and the Wilcoxon rank sum test was carried out on session means ($N = 17$). For single unit data, Wilcoxon rank sum tests were carried out within sessions on individual trials. Visual latency was defined as the first instant that the response deviated significantly from baseline ($p < 0.01$) given that this difference remained significant for at least 10 consecutive ms bins. The mean activation during this epoch was also used to classify units as either enhanced or suppressed. We classified units by depth simply by assigning them to the compartment belonging to the closest visually evoked sink. We carried out a 4x2 ANOVA with factors of layer (II, III, V, and VI) and response type (enhanced or suppressed) to test for differences in latencies between depths and unit groups.

Spike width was determined by interpolating mean spike waveforms to a resolution of 1 μs using a smoothing spline and then measuring the distance from peak to trough (Cohen et al., 2009). We excluded triphasic spikes [often recorded from axons (Lemon, 1984)] and abnormal monophasic spikes from our analysis by requiring that the peak exceed the maximum activity recorded before the trough by at least 1 SD. Across

our entire data set of 295 well-isolated units, this criterion eliminated 39 units (13%). This number is larger than the number of units excluded by visual inspection in a previous report (Mitchell et al., 2007). We speculate that this discrepancy may be explained by online selection bias in the recording methods. We did not select the units we recorded based on their waveforms or response characteristics, choosing instead to record from every neuron that we encountered near one of our electrode contacts.

4.6 Supplementary Results and Discussion

4.6.1 Single units recorded using the plexon uprobe

Few researchers have reported single unit data recorded with the newly developed electrode array used in the current study (Hansen and Dragoi, 2011; Hansen et al., 2012). Therefore in addition to spike width and spiking variability, we include samples of PCA space from representative recording sessions to demonstrate the signal-to-noise ratio of the units we recorded (Figure 4.8).

4.6.2 Gamma based alignment

Although the observed correspondence between visually evoked CSDs and physiological signals is close, it is not exact (Figure 4.5). In particular, our estimates of the average location of gray matter appear to be ~100-200 μm deep for several of monkey E's sessions, causing a few neurons to appear to have been recorded outside of the brain. Likewise, our average estimate of gray matter appears too superficial for a few of monkey X's sessions, since the pulse artifact (and presumably dura) is estimated to be within gray matter. Ideally, we could align our data on the locations of well-isolated single units since they must be recorded from cortex. But, there is considerable variability in the number and location of single units that we isolated from one day to another. However, we noted a clear relationship between the location of single unit

activity and elevated γ power on the majority of recording sessions, and elevated γ power was consistent in our recordings even when single units were few. Several recent studies have shown elevated γ power in superficial and middle layers (Maier et al., 2010; Xing et al., 2012; Smith and Sommer, 2013). We therefore attempted a second alignment using elevated γ power as a proxy of single unit activity to locate gray matter. Figure 4.6 shows the result of this alignment procedure. As expected, this alignment introduced more variability in the location of visually evoked sources and sinks recorded across sessions. This was guaranteed to be the case since our automated alignment routine explicitly searched for the solution that minimized differences between visually evoked sources and sinks. However, in a majority of sessions, we were still able to observe consistency in the location of visually evoked sources and sinks recorded across days. The γ-based alignment tended to place sessions recorded with monkey E somewhat deeper with respect to sessions recorded with monkey X.

The results (Figure 4.6B) are quite similar to those obtained using the automated alignment algorithm (Figure 4.7), showing 4 visually evoked sinks similar in timing and location to those we reported in the main text albeit with reduced magnitude. The deepest sink is somewhat less distinct when aligning to gamma onset. This may be because the γ alignment arranged the sessions so that deeper layers were sampled fewer times than they were with our automated alignment procedure. Since these results are qualitatively identical to those produced using our automated alignment technique, but the magnitude of the sources and sinks is reduced using the γ -based alignment, we conclude that visually evoked CSD is a more reliable depth measure than increased γ power alone. Aligning to LFP γ power simply produces a "blurred" (and therefore reduced magnitude) version of the same result.

4.6.3 Saccade-related neural responses

We recorded 27 single units (9%) with activity related to spontaneous saccades made in darkness (14 monkey E, 13 monkey X). Ten of these neurons (37%) also displayed visually evoked activity. We additionally recorded saccade-related multi-unit activity from 24 locations (12 monkey E, 12 monkey X). Seventeen of these multi-unit recordings (71%) also displayed visually evoked activity. Of these 51 saccade-related units, 23 (45%) showed pre-saccadic modulation and 28 (55%) showed post-saccadic responses. 26 units (51%) showed increased firing rates before and during saccades while the remaining 25 (49%) showed suppression. Neither depth (mean = 0.38 mm relative to current sink 1, sd = 0.67 mm, Wilcoxon rank sum W = 17323, p = 0.64), nor spike widths (mean = 350 μs, sd = 99 μs, Wilcoxon rank sum W = 5224, p = 0.44), nor the coefficients of variation in inter-spike intervals (mean CV = 1.42, sd CV = 0.49, Wilcoxon rank sum W = 6597, p = 0.39), differed significantly between visually related and saccade-related units. A 4x2 ANOVA showed that latencies did not differ across layers [F(3,43) = 1.12, p = 0.35], unlike visually responsive neurons, the latencies of enhanced and suppressed responses did not differ significantly [F(1,43) = 1.09, p = 0.30], and neither did the interaction between depth and response type reach significance [F(3,43) = 2.04, p = 0.12]. Table 4.1presents summary statistics for this neural population separated by layer. Other than demonstrating a relative lack of saccade related activity in SEF when saccades are initiated without visible goals, we do not consider these results to be definitive owing to the relatively small sample we recorded and the comparatively weak responses we observed.

4.6.4 Spike widths and variability

We classified neurons as either putative pyramidal cells or putative interneurons based on their respective spike widths (Constantinidis et al., 2002; Barthó et al., 2004;

Mitchell et al., 2007; Cohen et al., 2009; but see Vigneswaran et al., 2011). We did not include multi-unit activity in this analysis, focusing instead on well-isolated, biphasic single-units (Mitchell et al., 2007). The overall distribution of spike widths was similar to that reported for V4 (Mitchell et al., 2007) and FEF (Cohen et al., 2009) using similar criteria (Figure 4.9). We assessed variability in firing rates by calculating coefficients of variation measured on inter-spike intervals. Consistent with the hypothesized association between narrow spikes and interneurons, and in agreement with a previous report (Cohen et al., 2009), we found that narrow-spiking units displayed greater variability in spike timing than broad-spiking units (Wilcoxon rank sum $W = 23971$, $p < 0.001$). Across the pooled sample of single units, we found a small but significant correlation between spike width and recording depth [$r(254) = 0.15$ $p < 0.01$]. Separate regression analysis for narrow- and broad- spiking units revealed that broad-spiking units were the primary cause for this result. Broad-spiking units ($N = 203$) increased in width with recording depth [$r(201) = 0.42$ $p < 0.001$], while narrow-spiking units (N = 53) remained of the same width at successive depths [$r(51) = 0.07$ $p = 0.60$]. Testing for differences between spike widths of units with enhanced visual responses (340 μs mean ± 84 μs sd) and spike widths of units with suppressed responses (333 μs mean ± 89 μs sd) yielded no significant differences (Wilcoxon rank sum $W = 1979$, $p = 0.57$). These data provide additional information concerning the laminar microcircuitry of agranular frontal cortex. Broad-spiking units (putative pyramidal cells) and narrow-spiking units (putative interneurons) were observed in all layers and were equally likely to display enhanced or suppressed responses to flashed stimuli. This finding opens the interesting possibility that narrow-spiking units may reflect parvalbumin expressing interneurons since these are found throughout all layers in SEF (Figure 4.1C).

4.6.5 Relation to other physiological studies

Schroeder and colleagues recorded CSD and multi-unit activity from many areas of primate visual cortex using identical stimuli (Schroeder et al., 1989; Givre et al., 1994; Schultz, 1998). This enabled them to compare laminar activation profiles at successive stages of the visual hierarchy. Their findings generally matched feedforward and feedback patterns of activation consistent with anatomical descriptions of cortical microcircuitry (Hendrickson et al., 1978; Rockland and Pandya, 1979). Their work can be regarded as a standard description of laminar dendritic activation in the visual system of awake primates. We used the same stimulus paradigm, enabling us to compare the laminar activation profile of agranular frontal cortex with their findings in visual cortex.

The latency with which visually evoked CSD appeared in SEF was short (51 ms), but comparable to the latencies of visually evoked LFP onsets reported in SEF recently during a visual search task (Hendrickson et al., 1978; Rockland and Pandya, 1979; Purcell et al., 2012a). This latency also shows excellent agreement with the classic work of Schroeder and colleagues who reported latencies throughout the dorsal and ventral visual pathways and reported that the longest latencies were found in inferotemporal cortex at 49.2 ms (Schroeder et al., 1998). Moreover, the latencies of our single- and multi-unit responses are also in good agreement with previous reports (Purcell et al., 2012a) showing no signs of anticipatory responses. Thus, the visual latencies measured here correspond to previous values even though we used large, repetitive stimuli.

Overall, visual latencies did not differ statistically across depth, unlike observations in early visual areas (Bullier and Henry, 1980; Maunsell and Gibson, 1992; Raiguel et al., 1999). In combination with the CSD results, this suggests that our flashed stimuli excited neurons via distal dendritic arbors. As noted SEF lacks a granular layer where small spiny stellate cells arborize primarily in the layer containing the soma. Response suppression was a common feature of our unit recordings. Several

researchers have noted suppression of neural activity in response to visual stimuli in SEF, although the proportion of units displaying suppression varies across studies (Chen and Wise, 1995; Schall, 1991; Schlag and Schlag-Rey, 1987). This finding may depend crucially on stimulus parameters and task contingencies. Center/surround receptive field architecture has not been characterized in SEF, but a recent report documented such receptive fields in FEF (Cavanaugh et al., 2012). While the wide-field stroboscopic flash paradigm we employed is a necessary step for comparing CSD to published reports from early visual areas, it is difficult to compare our neural activity to that recorded previously in SEF using behaviorally relevant stimuli. Still, as noted above, our single- and multi-unit latency measures are in good agreement with previous results.

Our measurements of spike width and variability in SEF are also consistent with measures from other visual areas. Spike widths measured from trough to peak were very similar to those observed previously using similar metrics (Mitchell et al., 2007; Cohen et al., 2009). The proportion of narrow spiking to broad spiking units that we observed (79%) is similar to that reported in V4 (73%) (Mitchell et al., 2007). Additionally, narrow-spiking units in SEF displayed increased variability in spike timing, consistent with previous work in FEF (Cohen et al., 2009). In future work, it may be fruitful to apply this approach to individual recording sessions. By studying biophysical markers such as spike width and variability (Constantinidis et al., 2002; Barthó et al., 2004; Mitchell et al., 2007; Cohen et al., 2009) and combining these data with techniques such as Granger causality (Kaminski and Blinowska, 1991; Gregoriou et al., 2009; Hirabayashi et al., 2013) it may be possible to describe intact cortical microcircuits with unprecedented detail. In addition to studying microcircuitry in frontal cortex, these findings highlight a new and exciting development in the CSD technique as advances in electrode array technology now allow researchers to record well-isolated single units alongside CSD. Using sink/source patterns, one is now able to obtain an empirical

measure of the depth of each recorded neuron *in vivo*. This advance will undoubtedly prove crucial to future work describing neural interactions within intact, behaving monkeys.

4.7 Supplementary experimental procedures

4.7.1 MR/CT co-registration

We used 4 points on the skull that could be easily seen in both CT and MR images to carry out the co-registration; 1) the crest of the bone surface on the brow ridge midway between the supraorbital processes, 2) the point where the interior of the skull protrudes between the base of the occipital lobe and the cerebellum, and 3-4) the most lateral positions of the interior aspects of the left and right zygomatic arches. In both the MRI and the CT data, points 1 and 2 could be easily identified in a midline sagittal section. Points 3 and 4 could be identified in both imaging modalities by gradually advancing more lateral through sagittal slices and marking the location in the first slice where the anterior and posterior aspect of the zygomatic arch merged into one. These points were advantageous for several reasons. First, because each of these points represents an area of bone surrounded by soft tissue (as opposed to air filled sinuses) they were readily apparent in both imaging modalities. Second, these points are widely separated encompassing the majority of the skull in all 3 dimensions. Because these points bound the outer limits of the skull, and because our guide tube was positioned in between and close to the middle of all of these points, deviations in their placement resulted in comparatively small deviations in the guide tube position relative to cortex. By inspecting the data in all 3 dimensions we found that these points yielded excellent co-registrations.

4.7.2 Histology and cell counts

Histological material was gathered and processed as described previously (Schall et al., 1995; Pouget et al., 2009). Bright field images were photographed using a Nikon microscope through a 2x objective. A semi-automatic method for cell identification was implemented in the MATLAB program environment. The logic of this algorithm follows. A user first identified ~30 to 40 cells in each image manually. The algorithm recorded 8-bit RGB color data from each user-defined neuron and used these data to set threshold criteria for automated cell detection. Clusters of pixels that passed threshold criteria in each of the 3 color dimensions were isolated as candidate cells for further analysis. Clusters of pixels were discarded if they failed to pass any of the three following criteria: 1) the number of pixels within a given cluster was required to exceed a lower limit, 2) the number of pixels within a given cluster was required to fall below an upper limit, and 3) a given cluster was required to contain spatial frequencies (measured simply using the sum of gradients across all three 8-bit color dimensions, or $\sum\nabla$ RGB) higher than a lower limit. We found that neurons were satisfactorily identified within our images when color detection thresholds were set to 0.5 sd below the mean within each RGB dimension, when clusters were required to contain 30-400 pixels, and $\sum\nabla$ RGB values were required to exceed 30 8-bit color units.

CHAPTER 5

EVENT-RELATED POTENTIALS ELICITED BY ERRORS DURING THE STOP-SIGNAL TASK. I. MACAQUE MONKEYS

5.1 Abstract

The error-related negativity (ERN) and positivity (Pe) are components of event-related potential (ERP) waveforms recorded from humans that are thought to reflect performance-monitoring. Error-related signals have also been found in single-neuron responses and local-field potentials recorded in supplementary eye field and anterior cingulate cortex of macaque monkeys. However, the homology of these neural signals across species remains controversial. Here, we show that monkeys exhibit ERN and Pe components when they commit errors during a saccadic stop-signal task. The voltage distributions and current densities of these components were similar to those found in humans performing the same task. Subsequent analyses show that neither stimulus- nor response-related artifacts accounted for the error-ERPs. This demonstration of macaque homologues of the ERN and Pe forms a keystone in the bridge linking human and nonhuman primate studies on the neural basis of performance monitoring.[8]

5.2 Introduction

To thrive, organisms must detect when their responses fail to meet expectations through *performance monitoring*. Researchers investigating performance monitoring in humans have made inferences based on event-related potentials (ERPs) or neuroimaging methods, whereas investigators using monkeys have relied on intracranial

[8] This chapter was published as Godlove DC, Emeric EE, Segovis CM, Young MS, Schall JD, Woodman GF. Event-related potentials elicited by errors during the stop-signal task. I. macaque monkeys. Journal of Neuroscience 31: 15640-15649, 2011.

recordings (reviewed by Paus et al., 1993; Ridderinkhof et al., 2004; Schall and Boucher, 2007; Taylor et al., 2007; Hikosaka and Isoda, 2010; Passingham et al., 2010). The present work addresses this fundamental question: Is the monkey executive control system a valid model of human performance monitoring?

The first electrophysiological correlate of performance monitoring discovered in humans, the error-related negativity (ERN, also known as the Ne), was independently reported by Falkenstein et al. (1990) and Gehring et al. (1993). The ERN has a frontocentral scalp distribution and peaks ~50-100 ms following incorrect manual responses (reviewed by Gehring et al., 2011). Several groups have observed the ERN during the stop-signal task (also known as the countermanding task), which is used to investigate behavioral inhibition and executive control (Endrass et al., 2005; Liotti et al., 2005; van Boxtel et al., 2005; Kramer et al., 2007; Stahl and Gibbons, 2007; Vocat et al., 2008). Although the ERN is clearly associated with error commission, a variety of hypotheses concerning its relation to cognitive processes have been proposed (e.g. Gehring et al., 1993; Falkenstein et al., 2000; Holroyd and Coles, 2002; Luu et al., 2003; Yeung et al., 2004; Brown and Braver, 2005). A number of these theories make specific predictions concerning the anatomical, neurophysiological, and neurochemical mechanisms of the ERN. However, these theories have proven difficult to distinguish using behavioral and imaging data from humans. Animal models of error-ERPs can provide leverage to distinguish between alternative hypotheses of performance monitoring.

However, some have proposed that macaque monkeys do not have the neural substrates necessary to generate performance monitoring ERPs similar to those observed in humans (Cole, 2009; Cole, 2010; but see Schall and Emeric, 2010). The argument is based on cytoarchitectural differences in medial frontal cortex between species, as well as perceived differences in the signals observed in human and monkey

medial frontal cortex. The presence or absence of an ERN in monkeys would therefore shed light on an important, unresolved issue.

We recorded ERPs from monkeys while they performed the saccade stop-signal task. On trials without stop-signals (no-stop trials), monkeys made saccades to peripheral targets. These correct responses were rewarded. On trials containing stop-signals (stop trials), monkeys often made saccades to targets. These errant responses were not rewarded. Thus, saccades led to either correct responses or errors. By contrasting response aligned ERPs from these two trial types, we demonstrate the first evidence of error-ERPs in nonhuman primates.

5.3 Materials and Methods

5.3.1 Animal care

Data were collected from one male bonnet macaque (*Macaca radiata* ~8.5 kg) and one female rhesus macaque (*Macaca mulatta* ~7 kg). Both animals were cared for in accordance with policies set forth by the USDA and Public Health Service Policy on Humane Care and Use of Laboratory Animals and all procedures were carried out with supervision and approval from the Vanderbilt Institutional Animal Care and Use Committee.

Surgical details have been described (Godlove et al., 2011a). Most critically, solid gold surface electrodes, Teflon coated stainless steel wires, and plastic connectors were constructed and implanted following the method of Woodman et al. (2007). Implanted electrode locations are provided in Table 5.1.

	Monkey F		Monkey Y	
Electrode	AP	ML	AP	ML
Fpz	\	\	5.33	0
FpFz	\	\	4.3	0
Fp1	\	\	4.12	-1.75
Fp2	\	\	4.12	1.63
Fz	4.1	0	3.28	0
F1	2.7	-1.4	\	\
F2	2.7	1.4	\	\
F3	\	\	2.69	-1.59
F4	\	\	2.69	1.49
FCz	\	\	2.24	0
Cz	\	\	1.23	0
P3	\	\	-0.61	-2.19
P4	\	\	-0.61	2.19
Pz	\	\	-1.75	0
POz	\	\	-2.5	0
O1	-2.1	-1.4	-2.81	-1.64
O2	-2.1	1.4	-2.81	1.54
Oz	-2.5	0	-3.58	0

Table 5.1. Implanted electrode locations. Stereotaxic locations of imlanted electrodes in cm relative to interaural zero. Elecrode names refer to homologous human electrode locations from the international 10-20 electrode placement system. ML = medial to lateral, AP = anterior to posterior.

5.3.2 Stimuli and task

Stimulus presentation, task contingencies related to eye position, and delivery of liquid reinforcement were all under computer control in real time (TEMPO, Reflective Computing, Olympia, WA). Behavior and electrophysiological signals were recorded during the saccadic stop-signal (countermanding) task (Figure 5.1). Stimulus properties and task timing have been reported in detail (Godlove et al., 2011a). Additional details about the behavioral training regime and task have also been described (Hanes and Schall, 1995; Hanes et al., 1998).

Trials were initiated when monkeys fixated a centrally presented square. After a variable time, the central fixation point was extinguished and a target simultaneously appeared at 10° to the left or right of fixation. On no-stop trials (Figure 5.1 top), no further visual stimuli were presented. Monkeys were required to make saccades to targets and hold gaze for 600 ms to obtain reward. On stop trials (Figure 5.1 bottom), the fixation point was re-illuminated after a variable delay providing a *stop-signal*. To obtain reward on stop trials, monkeys withheld eye movements and maintained fixation for a minimum of 1800 ms. These trials were designated as *canceled*. If monkeys were unable to inhibit the movement, a 1500 ms timeout was added to the normal inter-trial interval of 200 ms, no rewards were given, and the trial was termed *noncanceled*. Thus, identical responses could be either correct or errant depending on trial context.

An initial set of stop-signal delays (SSDs) from 0 to 420 ms and separated by either 40 or 60 ms steps was selected for each recording session. We then manipulated SSD using an adaptive, stair-casing algorithm, which adjusted stopping difficulty based on performance. Stop trials made up 30 to 40% of all trials in a given session with a typical session consisting of several thousand trials. Saccade initiation and termination were detected offline using a custom algorithm which first detected instantaneous velocity elevated above 30°/s and then calculated the beginning and ending of the

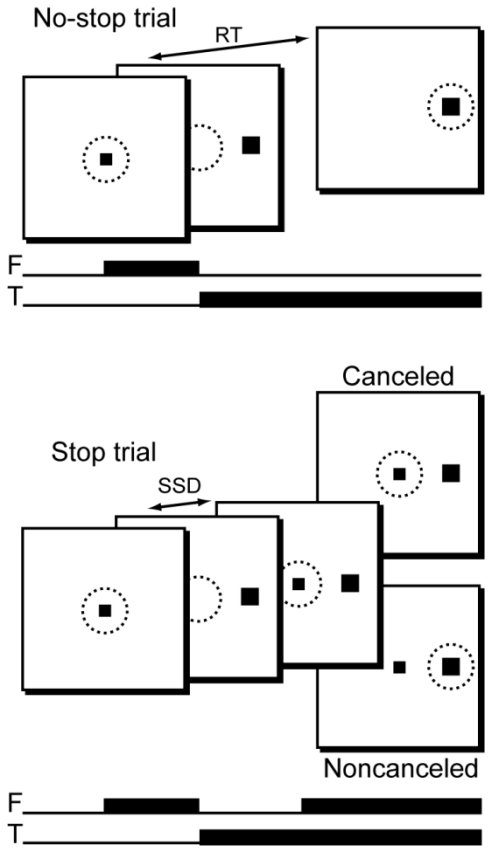

Figure 5.1. Schematic representation of the saccadic stop-signal (or countermanding) task. **No-stop trials** (top) were initiated when monkeys fixated a centrally presented fixation point. After a variable time, the fixation point was extinguished and simultaneously a peripheral target was presented at one of two possible locations. Monkeys were required to fixate targets with quick saccades for juice rewards. **Stop trials** (bottom) were initiated in the same way. After a variable time termed stop-signal delay (SSD), the fixation point was re-illuminated, instructing the monkeys to withhold movement. Successful inhibition of saccades resulted in rewarded **Canceled trials**, but errant saccades resulted in unrewarded **Noncanceled trials**. Black squares indicate stimulus locations. Dotted circles represent area of fixation. F = fixation point, T = target, RT = reaction time, SSD = stop-signal delay.

monotonic change in eye position. We adopted the procedures of Logan and Cowan (1984) implemented by Hanes et al. (1998) to estimate stop signal reaction time (SSRT). In brief, we estimated SSRT using one method which assumes that SSRT is a constant, and another method which assumes that SSRT is a random variable. Since there is no reason to assume an advantage of either of these methods, we averaged the two estimates together to obtain final SSRT measures.

5.3.3 Data acquisition

Eye position was monitored using an infrared eye-tracking system (ASL, Bedford, MA). Implanted EEG surface electrodes were referenced to linked ears using ear-clip electrodes (Electro-Cap International, Eaton, OH). All electrode impedances were less than 10 kΩ. The EEG from each electrode was amplified with a high-input impedance head stage (Plexon, Dallas, TX) and bandpass filtered between 0.7 and 170 Hz.

5.3.4 ERP analyses

ERPs were time-locked to saccade initiation or stop-signal onset. Waveforms were baseline corrected during the interval from 150 ms to 50 ms before these events. Stop trials on which subjects responded before stop-signal presentation (37% monkey F, 49% monkey Y) were not included in error-ERPs since subjects did not have the necessary information to deduce that an error had been committed at time of response. When constructing grand averages collapsed across left and right target locations, the number of trials presented at each location was matched in a given condition by excluding random trials from one target (26% monkey F, 18% monkey Y). Trials with voltage deflections greater than ±300 μV and trials with amplifier saturation were also excluded from analysis (3% monkey F, 1% monkey Y). Single trial EEG signals were

truncated 50 ms before the onset of the second, non-task-related saccade to eliminate artifacts arising from temporally smeared second-saccade activity (Godlove, 2010).

Significant ERP differences were assessed using the method of Emeric et al. (2008). This method tests for differences between error and correct ERPs using a thresholding approach similar to those often employed in single unit studies measuring activity onsets in spike-density functions. First, a difference wave was calculated by subtracting noncanceled error-ERPs from no-stop correct ERPs. Negative difference wave values indicated that error-ERPs were more negative than correct ERPs, while positive difference wave values indicated an opposite polarity effect. Difference wave values near zero indicated that error and correct ERPs did not differ. Thus, to test for significant differences between error and correct ERPs, we simply observed periods when the difference wave deviated from zero (i.e. baseline) by values larger than those expected by chance.

The intrinsic variability of the difference wave was assessed by calculating the standard deviation across time during the baseline period. This provided a measure of chance fluctuations between error and correct ERPs. Significant epochs were defined as periods when the difference wave deviated from baseline by >2 standard deviations for longer than 50 ms, provided it exceeded 3 standard deviations in that interval. For presentation, the grand average ERP collapsed across both monkeys was digitally filtered with a zero phase shift 35 Hz low-pass hamming window (*sd* = 6 ms). Unfiltered ERPs are presented individually for each monkey, and all statistical analyses were carried out on the unfiltered data.

5.3.5 Current density estimation

MRIs were acquired with a Philips Intera Achieva 3 Tesla scanner using SENSE Flex-S surface coils placed above and below the head. T1-weighted gradient-echo

structural images were obtained with a 3D turbo field echo anatomical sequence (TR = 8.729 ms; 130 slices, 0.70 mm thickness). Segmentations of skin, skull, and brain were carried out in CURRY 6 (Compumedics Neuroscan, Singen, Germany). The cranial surface electrode locations were co-registered to the head model guided by stereotaxic coordinates recorded during surgery. From this 3D head model, a three-compartment Boundary Element Method (BEM) volume conductor geometry was generated.

Source estimation used ERP difference waves (noncanceled error minus no-stop correct) at time windows of ±30 ms (ERN) and ±40 ms (Pe) centered on the peak amplitude of the difference wave from electrodes showing maximal ERN and Pe. Current density was estimated using the sLORETA-Weighted Accurate Minimum Norm method (SWARM) (Wagner et al., 2007). SWARM combines the methods of diagonally weighted Minimum Norm Least Squares (MNLS) (Dale and Sereno, 1993) and sLORETA (Pascual-Marqui, 2002) to compute a current density vector field with low localization error (see Wagner et al., 2007).

5.3.6 Tests for behavioral adjustments

For all analyses of behavioral adjustments related to error-ERPs, data were collected from electrodes that displayed maximum error-related amplitude differences, and data were drawn from the same windows used in current density analysis. We used two methods to test for relationships between error-ERPs and post-error RT adjustments. The first method relied on single trial amplitude measures. We identified errant noncanceled trials (trial n) which were followed by no-stop trials (trial n+1). We measured the maximum negative and positive deflections during ERN and Pe windows on trial n, and then determined post-error RT adjustments defined as ΔRT (RT on trial n+1 minus RT on trial n). We measured the correlation coefficient (ρ) values for maximum ERN/Pe amplitude versus ΔRT and subjected these distributions of ρ values

to 1 sample t-tests. This allowed us to determine if correlations tended to deviate from zero across the entire data set. For our second method, we first calculated median ΔRT separately for each monkey. We then constructed 2 ERPs aligned to the errant saccade on trial n based on a median split of ΔRT and tested for significant differences using 2 sample t-tests. To account for the effects of non-stationarity on RT estimates we repeated both of these analyses using the correction suggested by Nelson et al. (2010). For this correction, ΔRT was calculated as RT on trial n+1 minus RT on trial n-1. Since similar findings were obtained using both ΔRT measures, only data from the first ΔRT analyses are reported.

5.3.7 Tests for conflict

We also tested for relationships between the amplitude of the ERP negativity around SSRT and neural response conflict. We first normalized the raw EEG traces by z-scoring them to remove incidental inter-subject and inter-electrode amplitude differences. We then identified successfully canceled trials at each SSD. According to findings from Hanes et al. (1998) and Paré and Hanes (2003) canceled trials are those containing the largest magnitude of neural response conflict in the saccadic stop-signal task (see also Stuphorn et al., 2000). We identified no-stop trials from each session with RTs > SSD + SSRT. These latency-matched trials are those which were slow enough to have been successfully canceled had stop-signals been presented, providing an appropriate control for canceled trials (e.g. Hanes et al., 1998; Godlove et al., 2011a). We then constructed ERPs from canceled and no-stop trials at each SSD and measured mean amplitude on canceled trials and latency matched no-stop trials in the window -50 to +100 ms around SSRT. This window corresponds to the time of conflict-related neural modulation in the supplementary eye field (SEF)(Stuphorn et al., 2000; Emeric et al., 2010). By subtracting mean no-stop voltage from mean canceled voltage we

obtained measurements of the amplitude of the canceled-trial negativity. Finally, we tested to see if the amplitude of canceled-trial negativity was related to response conflict by assessing its correlation with SSD and the probability of committing an errant saccade.

5.4 Results

5.4.1 Behavior

Behavioral results are summarized for each monkey in Table 2. Both animals exhibited noncanceled trials with probability slightly > 50%. Because we used a stair-casing algorithm to adjust SSD, this departure suggests that both animals tended to speed up, causing a reduction in SSD. We have observed and reported this pattern of behavior before in animals performing the saccadic stop-signal task (Godlove et al., 2009; Godlove et al., 2011a). Other than a small tendency to speed responses, the data summarized in Table 2 suggest that the monkeys performed the task in a manner consistent with the race model of Logan and Cowan (1984).

5.4.2 Grand average error-ERPs

Figure 5.2 shows the saccade-aligned ERPs at electrode Fz collapsed across sessions and monkeys. In both instances, monkeys made saccades to target locations, but different contexts rendered no-stop trial responses correct and stop trial responses errant. In comparison to the correct no-stop ERPs, the errant noncanceled ERPs show a negativity beginning approximately 8 ms after the error and ending 73 ms later. This ERN reverses from 150-215 ms post response, becoming an error-related positivity (Pe). Taking into consideration known neural conduction velocity differences between human and macaque nervous systems (Woodman, 2011), the timing of these potentials show a

	no-stop RT	noncanceled RT	p(noncanceled)	SSRT
monkey F	285 ± 77	250 ± 75	0.54	94
monkey Y	252 ± 87	218 ± 92	0.53	71

Table 5.2. Summary statistics for stop-signal task performance. Reaction times (±1 SD), probability of committing errant noncanceled saccades, and SSRTs for each subject collapsed across sessions

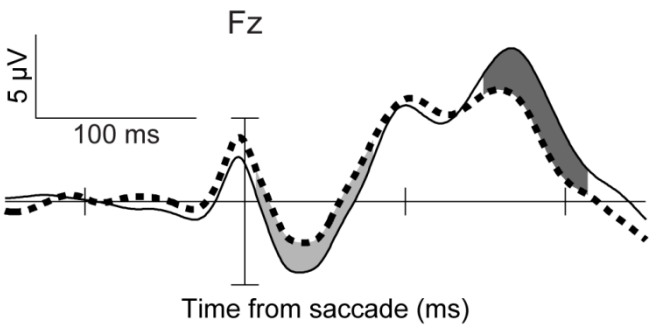

Figure 5.2. Monkey ERPs showing the ERN and Pe when errors are committed in the saccadic stop-signal task relative to correct trials with the same behavior. Response-aligned ERPs from correct no-stop trials (thin solid line) and errant noncanceled trials (thick broken line) are displayed. ERPs are collapsed across monkeys. On error trials, a significant negativity can be observed which begins 8 ms after the response and ends 81 ms after the response (light gray shading). A later positivity can also be observed 150 to 215 ms after the errant response (dark gray shading).

tight correspondence to the time courses of the ERN and Pe observed in humans (Reinhart et al., 2012).

5.4.3 Individual monkey error-ERPs

Figures 5.3 and 5.4 show that a similar pattern of ERN and Pe components was apparent in the frontal medial electrodes of each monkey. In monkey F, the observed ERN was maximal at electrode Fz, 97 ms after the response, and the Pe was maximal at electrodes F1 and F2 at 170 ms and 176 ms after the errant saccade, respectively. Monkey Y was implanted with a denser electrode array. This monkey showed a maximal ERN deflection at electrode FCz, 64 ms after the saccade, and a maximal Pe deflection at electrode Fz, 188 ms after the saccade.

5.4.4 Current density model

The dense electrode array of monkey Y, enabled us to investigate the spatial distribution of error-related components in more detail. We calculated current density distributions with the SWARM algorithm using the anatomical MRI from monkey Y. This method takes into account individual skull and brain morphology. Figure 5.5 shows the results. The current distribution contributing to the ERN explains 84% of the variance; while that contributing to the Pe explains 86% of the variance. The current density maps show that the ERN has a broad frontocentral distribution while the Pe has a more focal frontal distribution. The distribution of current sources extended onto medial frontal cortex for both the ERN and the Pe (Figure 5.6). These results are strikingly similar those obtained from humans performing the same task (Reinhart et al., 2012).

Because the stop-signal was only presented on trials in which errors were committed, our ERN and Pe results include a contribution from visually evoked ERPs elicited by the stop-signal. We addressed the contributions of this potential confound by

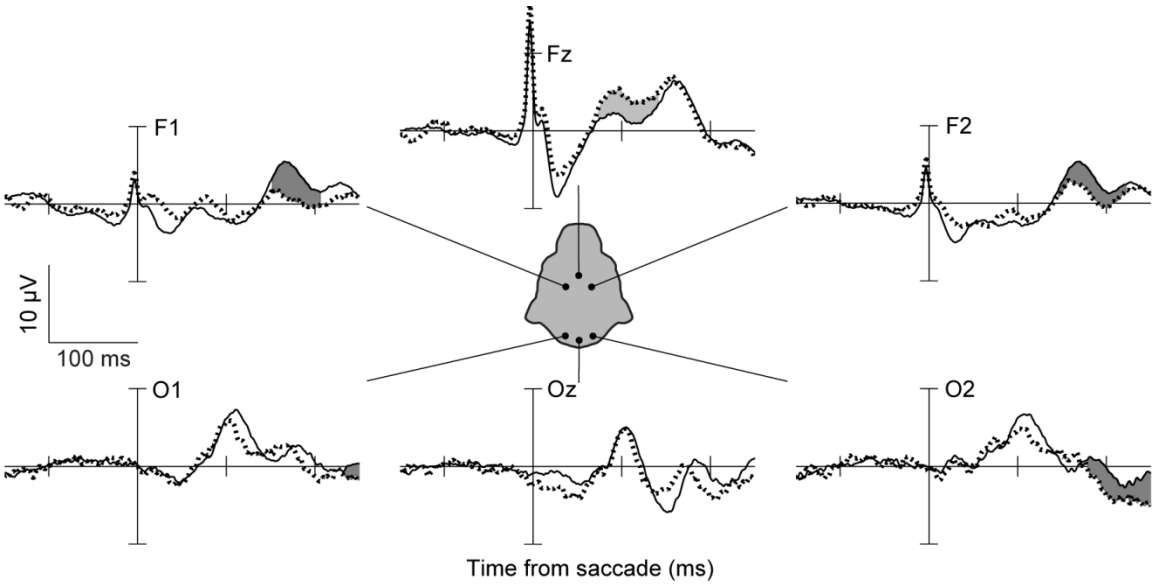

Figure 5.3. ERPs from monkey F showing the ERN and Pe when errors are committed in the saccadic stop-signal task. The figure uses the same conventions as in Figure 5.2. Response aligned ERPs from correct no-stop trials and errant noncanceled trials are displayed for multiple electrode locations. On error trials an early negativity can be observed on electrodes Fz, F1, and F2. This negativity was not of long enough duration to pass significance criteria. A later negativity can also be observed on electrode Fz which does pass significance criteria. Following this, a significant positivity is evident on electrodes F1 and F2. A later significant positivity is also evident on electrodes O1 and O2.

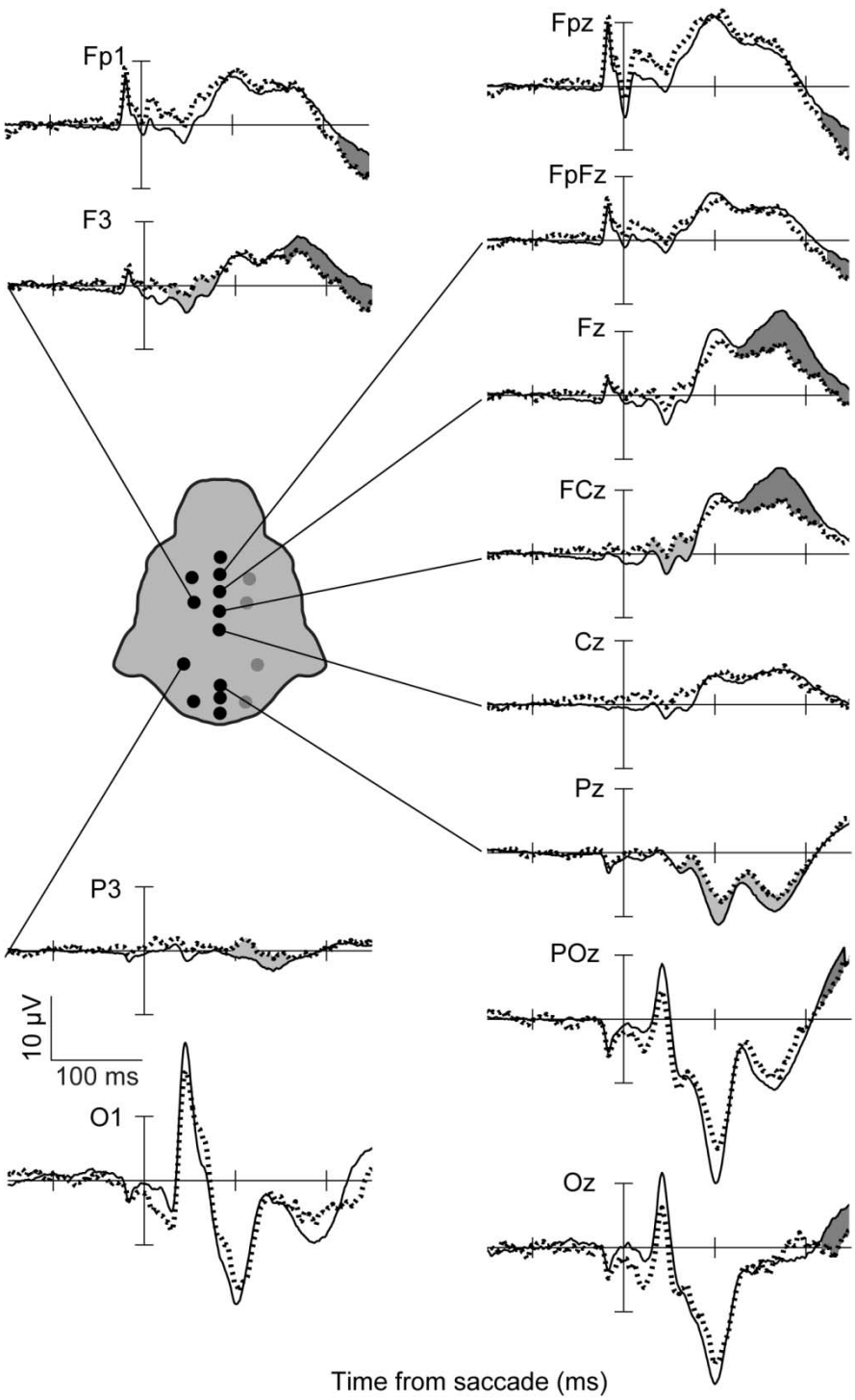

Figure 5.4. ERPs from monkey Y showing the ERN and Pe when errors are committed in the saccadic stop-signal task with the same conventions as in Figure 5.2. Response aligned ERPs from correct no-stop trials and errant noncanceled trials are displayed for multiple electrode locations. On error trials a significant negativity can be observed on electrodes FCz and F3, and a later negativity can also be observed on electrode Pz.

Following this, a significant positivity can be observed on the majority of electrodes. This positivity is earliest and highest in amplitude at frontal medial electrode sites.

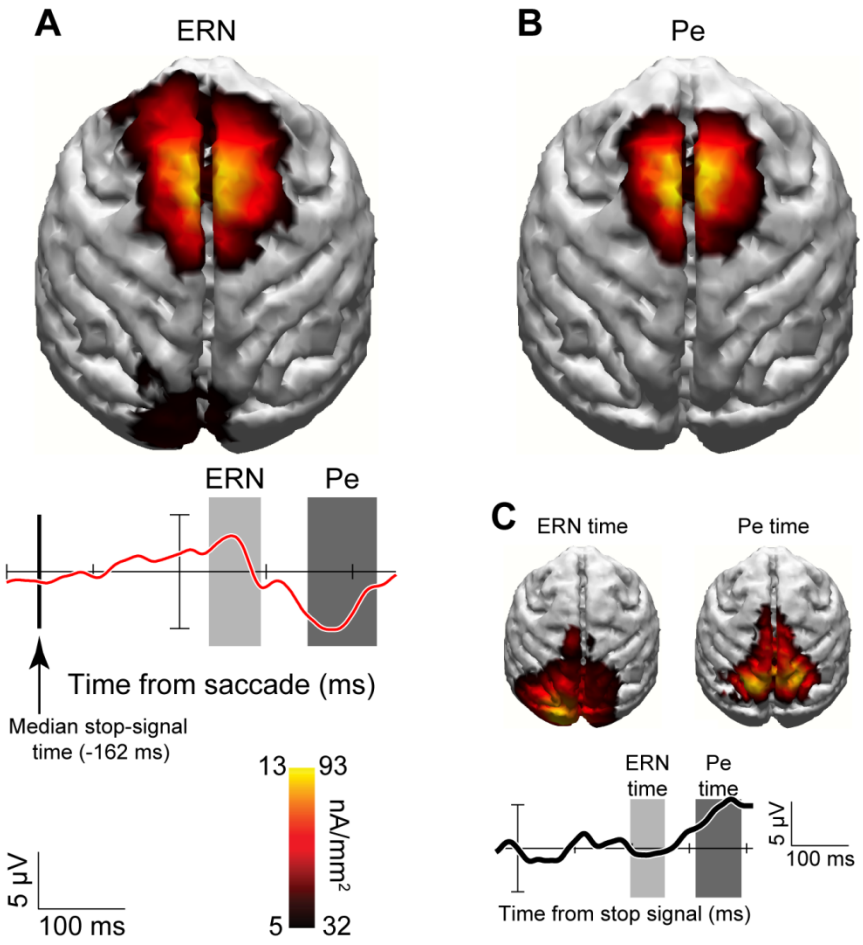

Figure 5.5. Current density distribution for ERN (**A**), Pe (**B**) and visual response to stop signal (**C**). Current density estimates are projected onto MRI reconstruction from the same monkey. Warmer colors indicate greater density of current flow according to scales for ERN (left) and Pe (right). Error minus correct difference wave (red) and response to stop signal on correct canceled trials (black) are shown with temporal windows measured for each component. Vertical line shows median stop signal presentation time relative to saccade initiation.

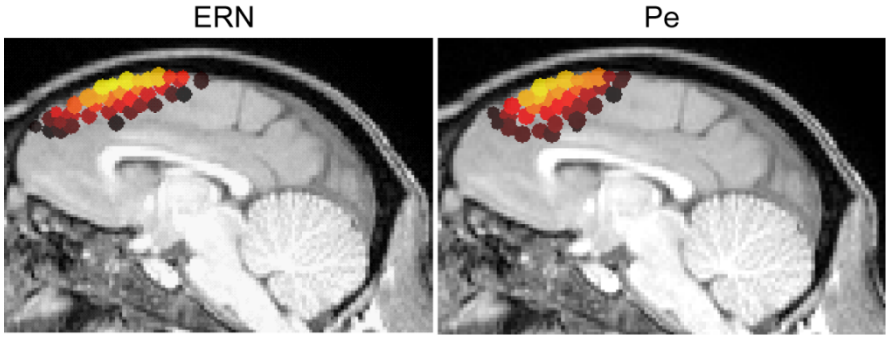

Figure 5.6. Saggital view of current density spatial distributions for ERN and Pe. Conventions are as in Figure 5.5.

comparing current density distributions of canceled and noncanceled trial ERPs during the same time periods relative to the stop-signal (Figure 5.5C). On these trials, the monkey held gaze at central fixation for at least 1800 ms following stop-signal presentation. Therefore, the current distribution on canceled trials reveals the contribution of stimulus-related ERPs to the error-related ERPs. No significant current densities were observed over medial frontal cortex during the ERN epoch when saccades were correctly canceled. Instead, significant effects were restricted to occipital and parietal regions. These results show that the ERN and Pe we observed are not sensory artifacts associated with stop-signal presentation.

5.4.5 Error-ERPs, RT adjustments, and response conflict

Some studies have suggested that error-ERP magnitudes are correlated with performance adjustments such as post-error slowing (Gehring et al., 1993; Nieuwenhuis et al., 2001; Rodriguez-Fornells et al., 2002; Kerns et al., 2004; Debener et al., 2005b; Holroyd et al., 2005; Klein et al., 2007; Ladouceur et al., 2007; West and Travers, 2008; Huster et al., 2011; but see Gehring and Fencsik, 2001; Hajcak et al., 2003; Nunez Castellar et al., 2010). To test for these effects and relate our ERP data to intracranial local-field potentials recorded in the SEF and anterior cingulate cortex (ACC) during this task (Emeric et al., 2008; 2010), we examined the relationship between error-related ERPs and post-error RT adjustments, as described above. Figure 5.7A illustrates this analysis for a sample session. Neither ERN amplitude nor Pe amplitude were significantly correlated with ΔRT in this session. Figure 5.7B and 5.7C display distributions of ρ values collapsed across all sessions. Neither of these distributions deviated significantly from zero (ERN $t_{(14)} = 0.68$, $p = 0.51$; Pe $t_{(14)} = -1.67$, $p = 0.12$).

Because raw EEG contains a great deal of variability, we also averaged the ERPs using a median split based on ΔRT and measured amplitudes during the windows

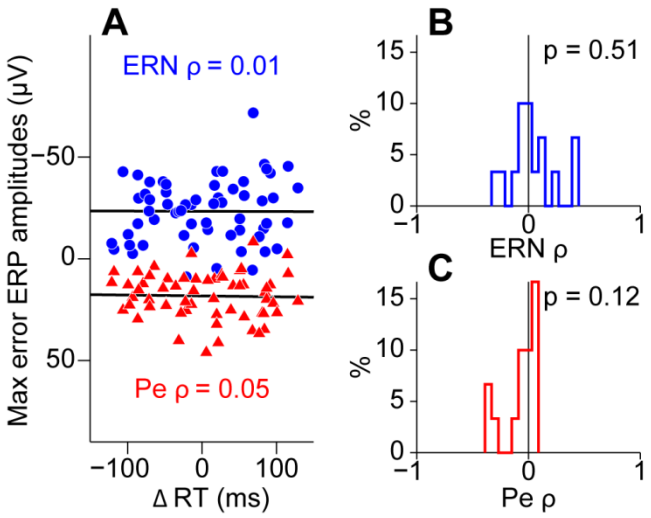

Figure 5.7. Single trial test for correlations between ERN/Pe amplitude and post-error RT adjustments. **A** Correlations between maximum ERN/Pe amplitude and ΔRT (RT on no-stop trial n+1 minus RT on noncanceled trial n) for a representative session. Neither the correlation between maximum ERN amplitude and ΔRT nor the correlation between maximum Pe amplitude and ΔRT reached significance. **B** Distribution of correlation coefficients (ρs) between maximum ERN amplitude and ΔRT across all sessions. **C** Distribution of ρs between maximum Pe amplitude and ΔRT across all sessions.

centered on the peak ERN and Pe. Figure 5.8A displays mean ERN amplitude for the fastest and slowest ΔRT trials separately for each monkey and averaged across both monkeys. Figure 5.8B displays the same relationship between Pe amplitude and ΔRT. Neither monkey showed significant differences in ERN amplitude (monkey F $t_{(18)}$ = -0.18, p = 0.86; monkey Y $t_{(8)}$ = -1.17, p = 0.28; grand $t_{(28)}$ = -0.71, p = 0.48) or in Pe amplitude as a function of ΔRT (monkey F $t_{(18)}$ = -0.06, p = 0.96; monkey Y $t_{(8)}$ = -1.47, p = 0.18; grand $t_{(28)}$ = -1.07, p = 0.29).

An influential theory posits that the ERN is produced by neural processing of response conflict (Botvinick et al., 2001; Yeung et al., 2004). The occurrence of response conflict is not restricted to error trials only, but is hypothesized to occur with varying timing and magnitude on all trial types (Yeung et al., 2004). In the stop-signal task, subjects must choose between committing responses and canceling them. Thus, in the saccadic stop-signal context, response conflict is engendered when subjects must choose between producing saccades and maintaining fixation. Distinct neural populations are active in the superior colliculus (SC) and frontal eye field (FEF) when saccades are produced or fixation is maintained. We and others have classified these neurons as *movement cells* and *fixation cells* (Bruce and Goldberg, 1985; Munoz and Wurtz, 1993a; Hanes et al., 1998), although alternate classifications have been proposed (Hafed et al., 2009). Movement and fixation cells in the SC (Paré and Hanes, 2003) and FEF (Hanes et al., 1998) are briefly coactive on canceled trials around the time that saccade cancelation occurs (SSRT). This coactivation is largest when saccades are successfully canceled under conditions in which they are likely to occur. Similar coactivation of movement and fixation cells has not been observed on errant noncanceled trials. In sum, the probability of successfully canceling action which varies as a function of SSD yields a reliable proxy measurement of neural response conflict on canceled trials in the saccadic stop-signal task. Using this metric, it has been shown

that response conflict may be reflected in single cell and LFP signals of SEF (Stuphorn et al., 2000; Emeric et al., 2010). But this conflict signal has not been observed in the single cell and LFP responses of ACC (Ito et al., 2003; Emeric et al., 2008).

We tested for conflict-related activity in ERPs aligned to SSRT on canceled trials using the method of Stuphorn et al. (2000). The mean voltage differences between canceled and no-stop trials in the -50 ms to +100 ms time window around SSRT at each SSD are plotted in Figure 5.9 as a function of both SSD and the probability of failing to cancel. These voltage differences did not show significant correlations with either SSD ($\rho_{(35)}$ = -0.08, p = 0.63) or the probability of committing errant noncanceled responses ($\rho_{(35)}$ = 0.27, p = 0.11).

5.4.6 Control for saccade related artifacts

To ensure that the observed error-ERPs were not due to response-related components, we quantified saccade dynamics on no-stop and noncanceled trials. Because we time-locked our ERPs to response onset, we could rule out the confounding effects of RT differences between trial types. However, if the task-related saccade amplitude or duration differed between correct and errant saccades it could lead to differences in the electromyogram or the corneoretinal potential between trial types (Luck, 2005; Godlove et al., 2011a) and these artifacts could be interpreted as performance monitoring ERPs (Godlove, 2010).

Figure 5.10 summarizes saccade amplitude and duration separated by monkey, target, and trial type. We carried out 3-way ANOVAs to test the hypotheses that saccade amplitude, velocity, or duration differed between monkey, target, or trial type. Saccade velocity and duration both differed significantly between monkeys. Monkey F made saccades with higher peak velocity ($F_{(1,52)}$ = 12.37, p < 0.001), and longer duration ($F_{(1,52)}$ = 5.22, p < 0.05) than monkey Y. This means that monkey F also tended to make

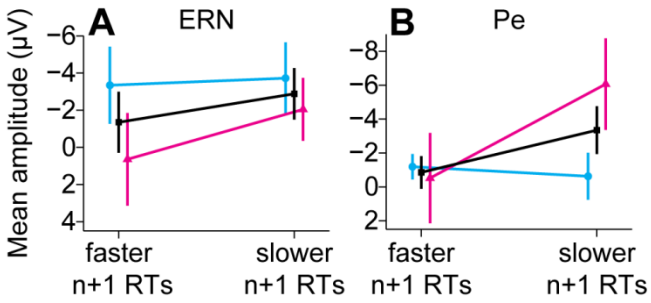

Figure 5.8. Median split ERP test for relationship between ERN/Pe amplitude and ΔRT. **A** Mean amplitude of the ERN followed by no-stop trials with faster RTs (left) or trials with slower RTs (right) for monkey F (cyan), monkey Y (magenta), and grand average (black). Error bars display standard error of the mean. **B** Mean Pe amplitude data presented in same format as in **A**. No comparisons reached statistical significance.

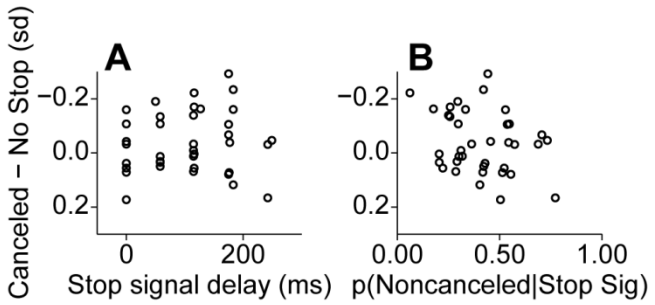

Figure 5.9. Test for conflict related activity in canceled ERP data. **A** Normalized mean voltage difference between canceled trials and latency matched no-stop trials in the -50 to 100 ms time window around SSRT plotted against SSD. **B** Same voltage data as in **A** plotted against the probability of committing an errant noncanceled saccade at each SSD. Significant correlations were not observed in either case (see Results).

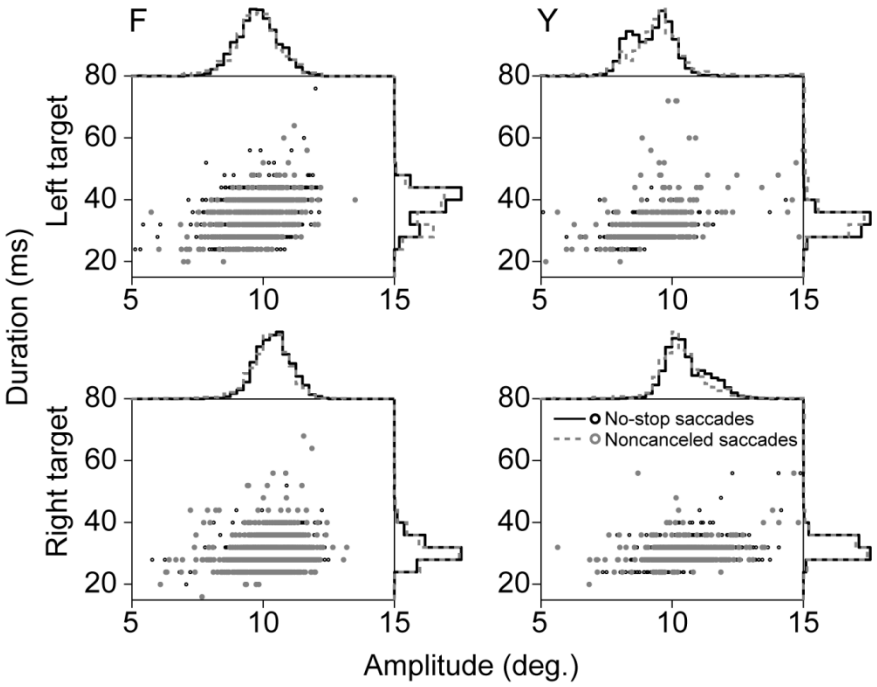

Figure 5.10. Saccade dynamics between conditions. Scatter plots display saccade amplitude versus duration across all sessions and both monkeys. Histograms display associated probability densities for each measurement. Bin widths are 4 ms for saccade duration distributions and 0.25 deg for amplitude distributions. Magenta dots and solid lines represent saccades on no-stop trials. Cyan dots and broken lines represent saccades on noncanceled trials. Rows separate data by target. Columns separate data by monkey. Although saccade dynamics were found to differ between monkeys and targets, neither saccade amplitude, nor saccade duration were found to differ significantly between trial types. These findings indicate that the observed monkey ERN and Pe are not caused by differences in saccade dynamics between conditions.

slightly larger amplitude saccades although this comparison did not reach statistical significance. Saccade dynamics differed modestly between targets for both monkeys. When monkeys made saccades to the rightward target, they tended to be of larger amplitude ($F_{(1,52)}$ = 27.36, p < 0.001), higher peak velocity ($F_{(1,52)}$ = 71.19, p < 0.001), and shorter duration ($F_{(1,52)}$ = 28.66, p < 0.001). This may be an artifact induced by the monocular eye tracking procedures we employed. Because we only tracked the right eye of each monkey, saccade traces to the right target reflected abduction of the tracked eye while saccade traces to the left target reflected adduction of the tracked eye. To ensure that target bias did not affect ERP component analysis, approximately equal numbers of trials were included in each ERP for each trial type (see Methods). A marginally significant effect was noted for saccade velocity between correct and errant trials. Both monkeys tended to make higher velocity saccades on error trials than correct trials ($F_{(1,52)}$ = 4.17, p = 0.05). However, velocity effects could not explain the different ERPs observed on error and correct trials unless saccadic endpoints also differed, shifting the corneoretinal potential to a greater degree on one type of trial relative to the other, or saccade duration differed smearing temporal saccade artifacts in one condition more than another. Critically, neither saccade amplitude ($F_{(1,52)}$ = 1.62, p = 0.2) nor saccade duration ($F_{(1,52)}$ = 1.17, p = 0.3) differed significantly between correct and errant trials. Therefore, no difference in correct and error saccade dynamics could explain the error-ERP effects.

5.5 Discussion

We have shown that during a saccadic stop-signal task macaques exhibit ERN and Pe components homologous to those recorded from humans. The precise timing and distributions of these error-related ERPs might initially appear to differ from those reported in humans using manual responses (reviewed by Gehring et al., 2011).

However, parallel experiments with humans show that the anterior distribution of monkey error-ERPs recorded during the saccadic stop-signal task is virtually identical to that found in humans (Reinhart et al., 2012).

In agreement with our parallel experiments with human subjects (Reinhart et al., 2012), we observed no single-trial correlations between ERN or Pe amplitude and post-error RT adjustments. Reported relationships between error-ERPs and post-error RT adjustments vary across the literature. Although some report such correlations (Gehring et al., 1993; Nieuwenhuis et al., 2001; Rodriguez-Fornells et al., 2002; Kerns et al., 2004; Debener et al., 2005; Holroyd et al., 2005; Klein et al., 2007; Ladouceur et al., 2007; West and Travers, 2008; Huster et al., 2011), others report no or contradictory evidence (Gehring and Fencsik, 2001; Hajcak et al., 2003; Nunez Castellar et al., 2010). Additionally, post-error slowing is not consistently observed in the stop-signal task (Emeric et al., 2007; Nelson et al., 2010; Bissett and Logan, 2011). Single-trial EEG has variability that is approximately an order of magnitude higher than ERPs (Luck, 2005), so we also analyzed the ERP data using a median split of post-error RT. Even with reduced variability due to averaging, we did not observe consistent error-ERP fluctuations predicting post-error RT adjustments. In addition, we did not observe conflict related modulation of ERPs. These findings agree with those from our parallel study with humans performing the same task, but challenge the view that error-ERPs reflect the activity of a general conflict monitoring system (Yeung et al. 2004).

We previously reported error-related LFPs recorded in ACC and SEF during the saccadic stop-signal task (Emeric et al., 2008; 2010). It is tempting to speculate that these LFPs give rise to the error-ERPs recorded at the surface, but several observations complicate this interpretation. First, error-related LFPs and ERPs differ in their relationships to behavior. Error-related LFP amplitude recorded from SEF is correlated with post error RT adjustments. And SEF LFPs also exhibit a negative potential during

periods of increased response conflict (Emeric et al., 2010). In contrast, LFPs recorded in ACC exhibit a positivity with increased response conflict (Emeric et al., 2008). We observed no such correlations in surface ERPs. These conflicting results from recording inside and outside the brain support the assumption that ERP signals arise from the summation of LFPs generated broadly throughout the brain (Luck, 2005; Nunez and Srinivasan, 2006). Thus, surface ERPs cannot be fully explained by LFPs in SEF or ACC. Second, timing differences between the ERPs and LFPs are obvious (Figure 5.11). The onset of the ERN and Pe on the surface precede intracranial LFP onsets. One possible explanation for these results is that subjects may show individual differences in timing of error-ERP onset, or that timing may change as subjects gain experience. Simultaneous ERP and LFP recordings must be carried out to test these explanations.

The observation of monkey error-ERPs will allow for their detailed neurophysiological characterization. Single units in ACC (Shima and Tanji, 1998; Ito et al., 2003; Amiez et al., 2005), and SEF (Stuphorn et al., 2000) are modulated when monkeys commit errors. Neurons in ACC modulate when monkeys switch responses after errors (Johnston et al., 2007; Quilodran et al., 2008). SEF neurons also show activity which may bias performance toward rewarding responses (Coe et al., 2002; Stuphorn et al., 2010), and stimulation of SEF improves saccadic stop-signal performance (Stuphorn and Schall, 2006). Despite these results, some have wondered whether intracranial recordings in monkeys are generated by the same error monitoring processes reflected in human ERPs (Cole et al., 2009; 2010; but see Schall and Emeric, 2010). The finding of monkey error-ERPs thus bridges a gap between human and monkey studies of executive control.

Several issues require clarification. First, the precise neuroanatomical loci of error-ERPs have not been described. Second, the neurophysiological events which give

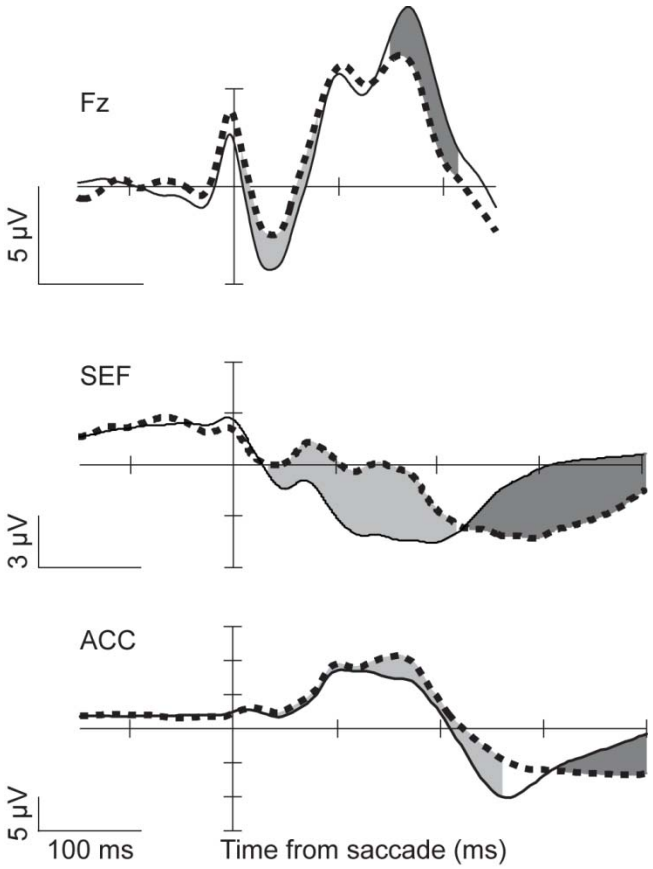

Figure 5.11. Comparison of error-ERPs to error-related LFPs. Error-ERPs from the current study (top) are plotted alongside error-related LFPs recorded in SEF (middle) (Emeric et al. 2010) and ACC (bottom) (Emeric et al. 2010) for amplitude and timing comparisons. Conventions are as in Figure 5.2.

rise to the ERN and Pe remain obscure. Third, several models have been proposed to explain the relationship of error-ERPs to performance monitoring generally, but the neural plausibility of these theories remains speculative. Neurophysiological recordings with nonhuman primates can shed much needed light on these questions. For the remainder of the Discussion, we will consider each of these issues in turn.

5.5.1 What are the anatomical sources of error-ERPs?

Dipole source modeling efforts and fMRI results suggest a central role for the dorsal ACC (e.g. Dehaene et al., 1994; Carter et al., 1998; Holroyd et al., 1998; reviewed by Taylor et al., 2007). However, it is well known that dipole source techniques rely on under-constrained solutions to the inverse problem of ERP localization (Helmholtz, 1853; Luck, 2005). Moreover, the link between electrophysiology and haemodynamic regulation is poorly understood (Logothetis and Wandell, 2004). Evidence indicates that other areas may play an important role in producing error-ERPs (reviewed by Gehring et al., 2011). In addition to the studies with monkeys described above, researchers have implicated the supplementary motor area, and rostral ACC as potential substrates for error-ERPs (Dehaene et al., 1994; Kiehl et al., 2000; Menon et al., 2001; Luu et al., 2003). And intracranial recordings in patients show error-related activity in multiple cortical areas beyond medial frontal cortex (Halgren et al., 2002; Brázdil et al., 2005). An animal model will be a great asset in the search for definitive neural generators.

5.5.2 What is the physiology underlying observed ERN and Pe?

The idea that mesocortical dopaminergic (DAergic) signaling produces the ERN has received substantial interest (Holroyd and Coles, 2002). However, relatively few researchers have experimentally manipulated DAergic signaling pathways (reviewed by

Jocham and Ullsperger, 2009). Because studies using the ERN have been carried out in humans, invasive neuroscientific techniques have been impractical. This is discouraging, since the DA hypothesis is rooted in classic neurophysiological studies using monkeys (Schultz et al., 1997; Schultz, 1998; see also Redgrave et al., 1999a, b). Although DA has received the most attention, several other neurotransmitters may also play a role in generating error-ERPs. These include norepinephrine (Riba et al., 2005b), serotonin (Fallgatter et al., 2004), and GABA (Johannes et al., 2001; de Bruijn et al., 2004; Riba et al., 2005a). The discovery of monkey error-ERPs will open new avenues for research on the neurochemical and neurophysiological events underlying these components. Now, tools such as selective agonist and antagonist micro-injections can be combined with surface electrode recordings to determine the contributions of various neurotransmitters and cell populations to error-ERPs.

5.5.3 What is the relationship between error-ERPs and performance monitoring?

The relationship between error-ERPs and performance monitoring is unclear. They were first thought to reflect neural processing of mismatch between committed and intended responses (Falkenstein et al., 1990; Gehring et al., 1993; Coles et al., 2001). This view has several drawbacks. For instance, if some area has access to a representation of the intended response, why was a different response executed (but see Murthy et al., 2007; Murthy et al., 2009)? Other theories allow performance monitoring to proceed without *a priori* knowledge of future outcomes. Several of these have been expressed as computational models that frame precise hypotheses (Botvinick et al., 2001; Holroyd and Coles, 2002; Yeung et al., 2004; Brown and Braver, 2005). The most influential computational models cannot be resolved using behavioral data alone. For instance, a major obstacle in testing the conflict monitoring theory arises from an inability to measure response conflict directly (Gehring et al., 2011). Similarly,

reinforcement-learning theories (e.g. Holroyd & Coles, 2002; Brown & Braver, 2005) have proven difficult to test using behavioral measures alone. However, specific assumptions of these models can be tested with neurophysiological measures in an animal model of error-ERP.

CHAPTER 6

THE CIRCUITRY UNDERLYING PERFORMANCE MONITORING IN MEDIAL FRONTAL CORTEX

6.1 Abstract

Error detection is an important aspect of human cognition, but its neural basis is poorly understood. Research has identified an electrophysiological correlate of error detection in humans and monkeys: the error-related negativity (ERN). By measuring local, intracranial current flow between electrodes combined with simultaneous EEG recordings in monkeys, we identify a cortical origin of the ERN in the supplementary eye field (SEF). Granger causality analysis showed that current flow in SEF was predictive of ERN voltage. A reward manipulation was used to parse the specific processes in SEF that contribute to the ERN. The ERN was sensitive to the magnitude of reward prediction errors (RPEs), but current flow in SEF was not. Populations of error- and RPE-related neurons showed little overlap and responded during separate trial epochs suggesting that these represent two independent processes. These results support a multi-process, multi-area view of error detection.

6.2 Introduction, Results, and Discussion

Humans make mistakes. Fortunately, we can reflect on our actions and detect our errors before experiencing the consequences. This faculty allows us to correct our errors and to avoid making similar mistakes in the future (Rabbit 1967; Laming 1979). Error detection is a hallmark of cognitive control, yet we know little about the neural basis of this ability.

Research has focused on an event-related potential (ERP) known as the error-related negativity (ERN) and its hemodynamic counterparts in medial frontal cortex (Falkenstein et al. 1990; Gehring et al. 1993; Kerns et al., 2004). These observations have led to several influential theories of performance monitoring. For example, the ERN may be produced by neural activity encoding mismatch between intended and actual responses (Gehring et al., 1993), monitoring response conflict (Botvinick et al., 2001), or detecting reward prediction errors (RPEs) (Holroyd & Coles 2002). Many researchers assume a single process model, viewing these theories as mutually exclusive, but each account may have merit. Behavioral studies have dissociated error awareness from the strategic adjustments that follow errors, suggesting that multiple processes are involved in error detection (Logan & Crump 2010). Neurophysiological studies have identified single units that encode error detection, response conflict, and reward-related variables (Stuphorn et al., 2000; Ito et al., 2003), suggesting that each process may contribute to the ERN. Anatomically, investigators have emphasized anterior cingulate cortex (ACC) as the origin of the ERN (Dehaene et al., 1994; Debener et al., 2005). But work carried out in non-human primates suggests that other areas may also play an important role. For instance, the supplementary eye field (SEF) contains neurons that encode errors and RPE (Stuphorn et al., 2000). Recently, we recorded ERNs from monkeys when they made errors during a saccade stop-signal task (Godlove et al., 2011b). Here, we asked if local current flow in SEF gives rise to the ERN, and if this activity can be explained as a RPE signal originating in SEF.

We recorded simultaneous ERPs, LFPs, and single unit responses while monkeys performed an asymmetrically rewarded saccade stop-signal task (Fig. 6.1A, behavior is presented in Fig. 6.4 and in section 6.7) (Kawagoe et al., 1998; Godlove et al., 2011a). Previous work identified error-related voltage deflections in SEF (Emeric et al., 2010), and suggested that this activity may underlie the ERN (Schall & Godlove

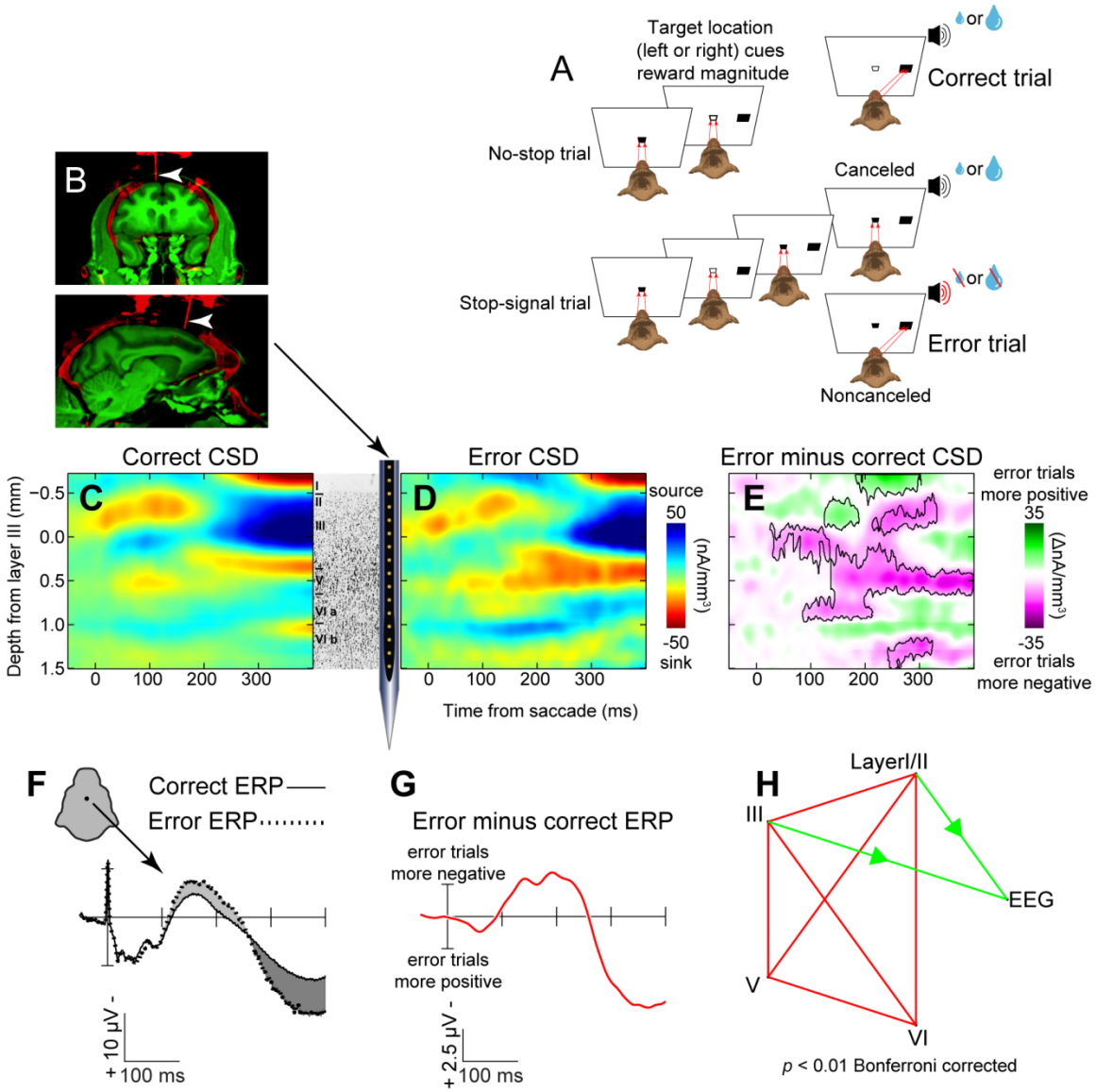

Figure 6.1 Error-related current flow in superficial layers of SEF Granger causes the ERN during the stop-signal task. A) Asymmetrically rewarded saccadic stop-signal task. Top, No-stop trials were initiated when monkeys fixated a central point. After a variable time, the center of the fixation point was extinguished leaving an outline. A peripheral target was presented simultaneously at one of two possible locations. The location of the target cued the monkey that either a large or small magnitude reward could be obtained on the current trial. These reward/location mappings reversed predictably in blocks. (Data in subsequent panels are collapsed across reward magnitude conditions.) Monkeys were required to fixate targets with quick saccades for juice rewards. Bottom, Stop trials were initiated in the same way using the same asymmetric reward manipulation. After a variable time (SSD), the center of the fixation point was re-illuminated, instructing the monkeys to withhold movement. Successful inhibition of saccades resulted in rewarded canceled trials, but errant saccades resulted in unrewarded noncanceled trials. B) MR (green) showing soft tissue with co-registered CT (red) showing bone and recording hardware. Guide tubes (highlighted with white arrows) indicate location and trajectory of recordings. C,D) Grand average laminar CSD

aligned on saccades recorded from SEF on correct (no-stop) and error (noncanceled) trials. Middle inset shows schematic representation of electrode array drawn to scale overlaid on Nissl section from SEF to indicate laminar architecture. (Adapted from Matelli et al., 1991 with permission.) E) CSD differences between correct and error trials. Outlined regions show layers and time periods at which CSD on error trials differs significantly from CSD on correct trials (FDR adjusted $p < 0.05$ in cluster sizes > 1,500 pixels). F) Response aligned ERPs recorded on correct and error trials. Upper left inset shows location of the surface electrode (approximating Fz). Light gray shading indicates interval when error-trial ERPs are significantly more negative than correct trial ERPs while dark shading indicates interval when error trial ERPs are significantly more positive. G) Difference wave subtracting correct trial from error trial ERPs. Monkey ERN begins ~95 ms after errant saccade and reverses to the error-related positivity at ~250 ms. H) Results of Granger causality analysis modeling interactions between current flow in SEF following errors and voltage recorded simultaneously at the surface. Red lines indicate significant bi-directional Granger causation, and green lines represent significant unidirectional Granger causation.

2012). However, this study did not rule out volume conduction from adjacent ACC. Therefore, we measured local current flow originating in SEF using a linear microelectrode array and deriving current source density (CSD) (Mitzdorf, 1985; Nicholson and Freeman, 1975; Schroeder et al., 1998; Chapter 4). We first asked if local current flow in SEF exhibits error-related activity. We contrasted CSD on correct and error trials and found activity in all layers that differed significantly between responses (Fig 6.1C-E). Thus error-related activity is reflected in local current flow originating in SEF. We also replicated our earlier finding of a monkey ERN during the stop-signal task in the simultaneously recorded EEG data (Fig 6.1F,G).

Next, we asked if error-related current flow in SEF contributes to this ERN. We used single-trial based Granger causality analysis applied to data realizations[9] 0-250 ms after the error response to test this hypothesis (Granger, 1969; Seth, 2010). Several potential problems with Granger causality as applied to fMRI data have recently been identified. But these problems are rooted in the variable timing of the hemodynamic response when used as a proxy for neural activity, and the fact that blood flow in one voxel cannot be logically claimed to cause blood flow in another voxel (David et al., 2008; Friston, 2009). In contrast, our recordings provide direct, temporally precise measures of neural activity, and according to Ohm's law intracranial current flow logically causes voltage fluctuations at the surface. Figure 6.1H plots the results of this analysis. As expected, all cortical layers showed significant bi-directional Granger causality with all other layers (Bonferroni corrected $p < 0.01$) indicating that current flow in each layer provides information useful for predicting subsequent current flow in all other layers. Thus, as in other areas of cortex, the layers of SEF are densy interconnected (Chapter 4). Activity in superficial layers I/II, and III also significantly Granger caused the EEG on

[9] Here, the phrase "data realizations" is used in place of "trial data" in keeping with the nomenclature of Seth 2010

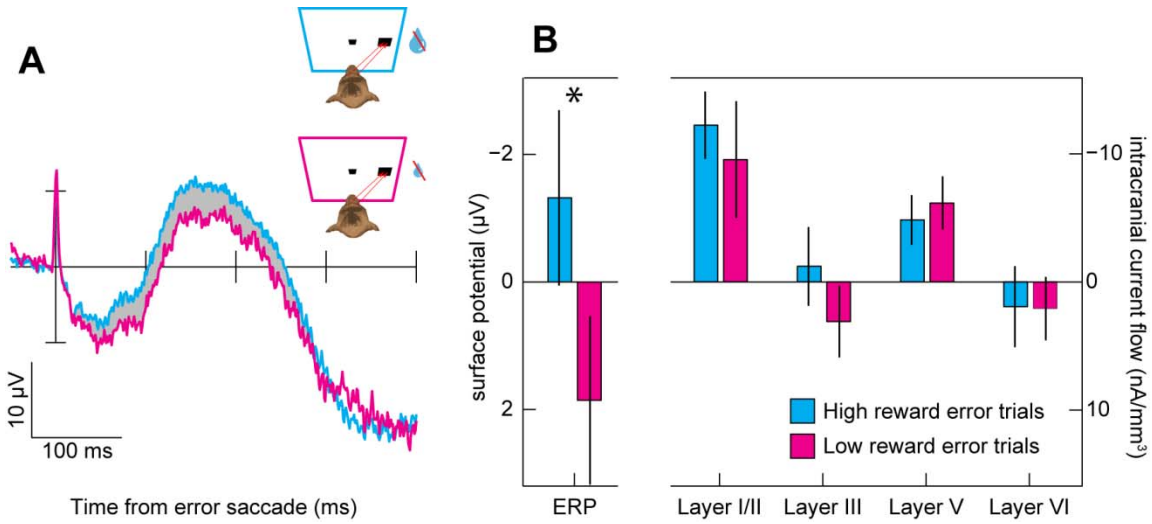

Figure 6.2 RPE modulation of ERN, but not SEF current flow. A) Response aligned ERP on error trials is more negative when the error prevents monkeys from obtaining large rewards (cyan) than when the error prevents monkeys from obtaining small rewards (magenta). Light gray shading highlights time of significant difference between waveforms. Upper right inset diagrams trial types under comparison. B) Average error-related voltage recorded at the cranial surface (left), and current flow recorded in SEF layers (right) during the interval highlighted in A (±SEM). Significant differences are only observed in surface potentials.

error trials indicating that current flow in these areas was predictive of subsequent EEG fluctuations. None of these interactions remained significant after randomly shuffling and reanalyzing the data. Moreover, current flow in SEF Granger caused EEG polarization on error trials with significantly greater magnitude than on correct trials (Wilcoxon rank sum $W = 2738$, $p < 0.001$). These results support the hypothesis that local current flow measured in SEF on error trials contributes to the ERN.

Dopaminergic projections conveying RPE signals to medial frontal cortex may underlie the ERN (Holroyd & Coles 2002), and RPE signals have been recorded in single unit responses of SEF (So & Stuphorn 2012). Therefore, we asked if the error related current flow in SEF and the ERN are both mediated by a RPE signal. We investigated this question using an asymmetrically rewarded variant of the stop-signal task. The initial target position cued the monkey that it would receive either a large or a small reward for completing the trial successfully. Mistakes resulted in negative RPEs because they suddenly reduced the probability of earning future rewards. When the target location signaled a small reward, we reasoned that the RPE would be reduced in magnitude, and that this effect would be evident as a reduced magnitude ERN. Fig. 6.2A demonstrates this effect. The ERN was reduced in magnitude when monkeys failed to earn small rewards compared to trials in which they failed to earn large rewards. Curiously, however, this RPE modulation was not present in the SEF current flow.

If we assume a single-process model of the ERN, this combination of results is confusing. On the one hand, Granger causality shows that error-related current flow in SEF is predictive of ERN amplitude. On the other hand, a RPE effect is evident in the ERN that is not mediated by SEF. To better understand these results, we recorded 538 single-units from SEF with task-related modulation. We capitalized on the fact that RPE signals are present during 2 trial epochs of the asymmetrically rewarded stop-signal task. As noted above, monkeys experienced large or small negative RPEs when they

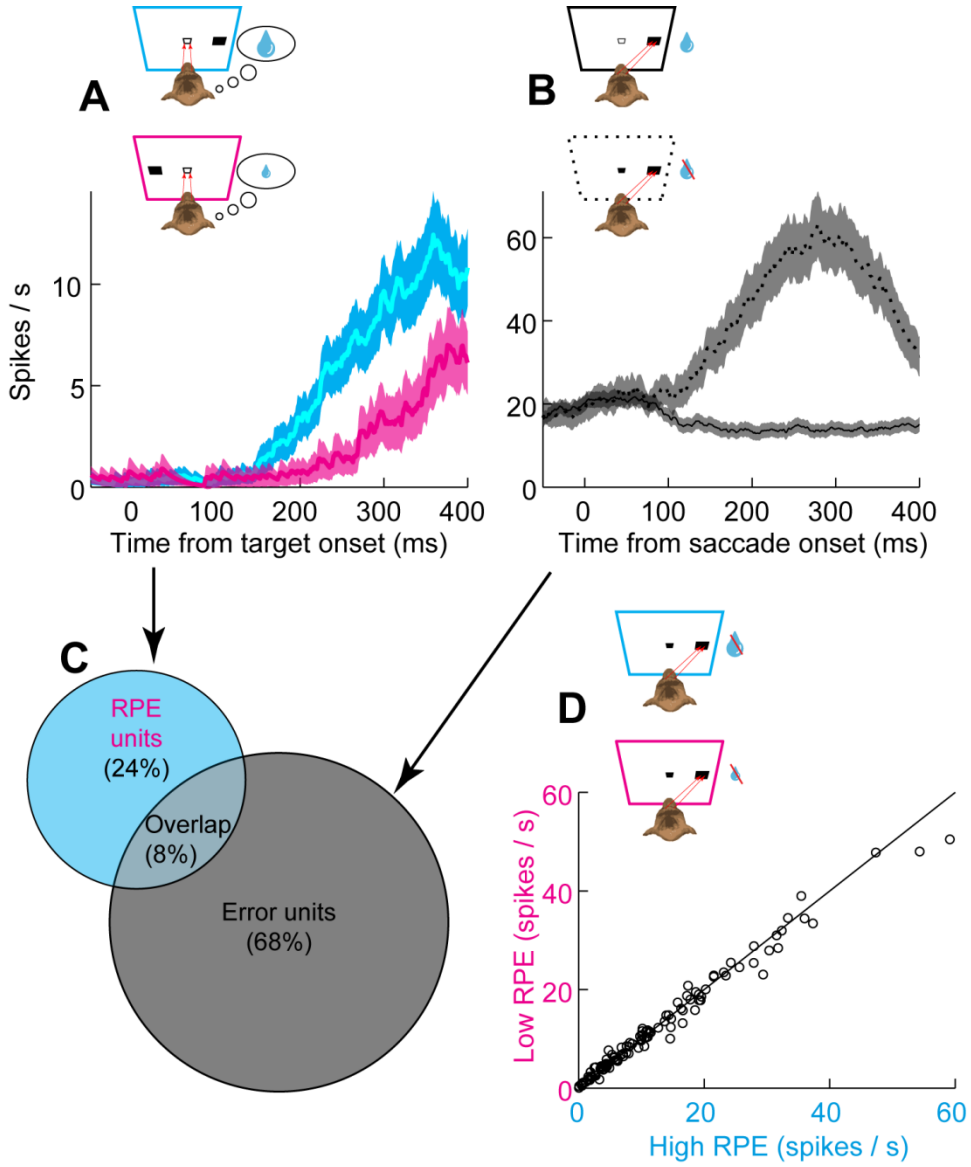

Figure 6.3 RPE and error-related activity signals are encoded by largely distinct neural populations in SEF. A) Target aligned spike density function (mean ± 1SD) for an example RPE unit contrasting target locations associated with large rewards (cyan) with target locations associated with small rewards (magenta). Inset in this and following panels provides schematic representation of trial types under comparison. B) Response aligned spike density function for an example error-related unit comparing correct trials (solid line) to error trials (broken line). This comparison is collapsed across high and low reward magnitude conditions. C) Proportional Venn diagram showing the number of units in each population and their relative overlap. 92% of the population falls in the XOR region. D) Average spiking rates (50-400 ms after response) for all error-related units in population contrasting errors on which monkeys failed to earn large rewards (cyan axis) with errors on which monkeys failed to earn small (magenta axis) rewards. No significant differences were noted across the population.

committed errors during the response epoch. But monkeys also experienced either positive or negative RPEs during the target-presentation epoch. A target that randomly appeared in one position cued the monkey that a large reward could be obtained at the end of the trial, eliciting a positive reward prediction error. Meanwhile, a target at the other location cued the monkey that a small reward would be delivered for a correct response, eliciting a negative reward prediciton error. Of the single units we recorded 46 (9%, 14 monkey E, 32 monkey X) encoded this stimulus-associated RPE. These results replicate an earlier report of stimulus-associated RPE activity in SEF during a gambling task (So & Stuphorn, 2012). We also recorded 110 single units (20%, 56 monkey E, 54 monkey X) that encoded error-related activity during the response epoch (Stuphorn et al., 2000). However, few neurons signaled both (8%, Figure 6.3C). And error-related units did not display RPE-related differences in firing rates during the response epoch (Figure 6.3D). Thus, stimulus-associated RPE and error detection are encoded separately in SEF.

Our results show that the amplitude of the ERN is partially determined by RPE signals, and partially determined by error-related current flow in SEF. The dissociation of these two determinants suggests that error detection is best explained by a combination of processes and is likely produced by several areas that monitor performance as a network. We suggest that the current focus on single process theories and on ACC as the locus of error detection is overly simplistic.

6.3 Methods

6.3.1 Animal care and surgical procedures

Data were collected from 1 male bonnet macaque (monkey E *Macaca radiata* 8.8 kg) and one female rhesus macaque (monkey X *Macaca mulatta* 6 kg). Animal care exceeded policies of the USDA and Public Health Service Policy on Humane Care and

Use of Laboratory Animals. All procedures were supervised and approved by the Vanderbilt Institutional Animal Care and Use Committee. MRIs were acquired to aide in placement of recording chambers as described before (Godlove et al., 2011b). Cilux recording chambers (Crist Instruments, Hagerstown, MD) were implanted normal to the cortex (17° monkey E, 9° monkey X relative to stereotaxic vertical) centered on midline 30 mm (monkey E) and 28 mm (monkey X) anterior to the interaural line. EEG electrodes used for these recordings were implanted centered on midline ~32 mm (monkey E) and ~30 mm (monkey X) anterior to the interaural line. Surgical placement of EEG electrodes and headposts has been described in detail (Woodman et al., ; Godlove et al., 2011a).

6.3.2 Data collection protocol

EEG and CSD data for this study were recorded in tandem during the same sessions as the data set reported in our previous CSD study (Chapter 4). Accordingly, cortical mapping using microstimulation, electrode placement using co-registered MR/CT imaging, estimation of electrode track angles, alignment of recordings across subsequent sessions, and estimation of the location of cortical layers were all carried out using methods identical to those reported previously. Single units were recorded simultaneously with this data set and during an additional 25 sessions. After advancing the electrode array to the desired depth, we waited 3-4 hours until recordings stabilized across contacts. This waiting period resulted in extremely stabile recordings since single units could almost always be held indefinitely. After achieving recording stability, we recorded 1 hour of "resting state" activity in near-total darkness with the CRT monitor unplugged. These data will be the subject of a future report. We then presented wide-field flashes of light to the monkeys in blocks of 100-200 presentations. As described previously, these data form the basis for our automated alignment algorithm that allowed

us to average data across recording sessions (Chapter 4). After this, we allowed monkeys to complete ~2000-3000 trials of the asymmetrically rewarded stop-signal task (Fig 6.1A; Schall and Godlove, 2012a; Kawagoe et al., 1998). These data form the basis for our current report.

The stop-signal task requires subjects to make quick responses to target stimuli. On some randomly interleaved trials, subjects are cued to withhold responses shortly after the target is presented. Additional details about the behavioral training regime and task have been described previously (Hanes and Schall 1995; Hanes, Patterson et al. 1998). In our implementation, trials were initiated when monkeys fixated a centrally presented square which subtended 0.34° of visual angle. After a foreperiod ranging from 600 ms to 1100 ms, the center of the fixation point was extinguished, leaving an open square outlined 1 pixel thick, and a target subtending 1° of visual angle simultaneously appeared centered at 10° to the left or right of fixation. The foreperiod was approximately non-aging, randomly sampled from a distribution described by the function:

$$p(t) = e^{-t/k}$$

where the probability of selecting a specific foreperiod $p(t)$ is an exponential function with time constant of k. We set k equal to 250 ms and shifted the distribution to fall between 600 and 1100 ms. On no-stop trials (Fig. 6.1A top), no further visual stimuli were presented. Monkeys were required to make a saccade to the target within 800 ms and hold fixation for 600 ms to obtain reward. Correct trials were rewarded with an audible tone followed 600 ms later by several drops of juice. On stop trials (Fig. 6.1A bottom), the center of the fixation point was re-illuminated either red or green (constant for each monkey) after a variable delay providing a “stop-signal” which instructed the monkeys to cancel their impending eye movements and maintain central fixation. In practice, two trial outcomes were then possible. If monkeys successfully withheld the

eye movement and maintained fixation for a minimum of 1600 ms, they obtained tone and juice reward. These trials were designated as "canceled". If monkeys were unable to inhibit the movement, an audible tone signaling timeout sounded and a variable timeout was added to the normal inter-trial interval. These trials were termed "noncanceled". As in our previous report (Godlove et al., 2011b) we studied error-related activity by comparing no-stop trials to noncanceled trials. An initial set of SSDs was selected for each recording session based on the monkey's previous behavior. We then manipulated SSD using an adaptive staircasing algorithm that adjusted stopping difficulty based on performance. When monkeys failed to inhibit responses, the SSD was decreased by a random step of 1, 2, or 3 increasing the likelihood of success on the next stop trial. Similarly, when monkeys successfully inhibited an eye movement, the next SSD was increased by a random step of 1, 2, or 3 decreasing the future probability of success. This procedure was used to ensure that subjects failed to inhibit action on ~50% of stop trials overall. Stop trials comprised 50% of all trials in a given session. All stimuli in the countermanding task had luminance values of 10 cd/m^2 on a 0.02 cd/m^2 background.

During the asymmetric reward manipulation, one stimulus location was associated with larger magnitudes of juice reward than the other stimulus location. The lower magnitude reward ranged from 0-50% of the higher magnitude reward and was adjusted by the experimenter to encourage the monkey to continue responding to both targets. The location of the high reward target changed predictably in blocks. Block lengths was determined by the number of correct trials performed, and ranged from 10-60. The experimenter adjusted block length to maintain the monkeys interest in both targets. In the vast majority of sessions block length was set at either 10 or 30 correct trials. As in previous implementations of asymmetrically rewarded tasks (Kawagoe et al., 1998), errors led to repetitions of target location, ensuring that monkeys did not

neglect low-reward targets in favor of high-reward targets. Figure 6.4 and Table 6.1 (Section 6.7) detail behavior during this task.

	no-stop RT		noncanceled RT		p(noncanceled)		SSRT	
	HR	LR	HR	LR	HR	LR	HR	LR
monkey E	300 ± 4	345 ± 8	291 ± 8	327 ± 7	53 ± 1	43 ± 2	135 ± 5	150 ± 5
monkey X	269 ± 11	302 ± 7	253 ± 6	282 ± 8	55 ± 1	48 ± 1	107 ± 5	111 ± 5

Table 6.1. Summary statistics for asymmetrically rewarded stop-signal task performance. Vaues are means ± SEM. Shown are reaction times (RTs), probabilities of committing errant noncanceled responses on stop trials (p(noncanceled)), and stop-signal reaction time (SSRTs) for each subject in each reward condition collapsed across sessions.

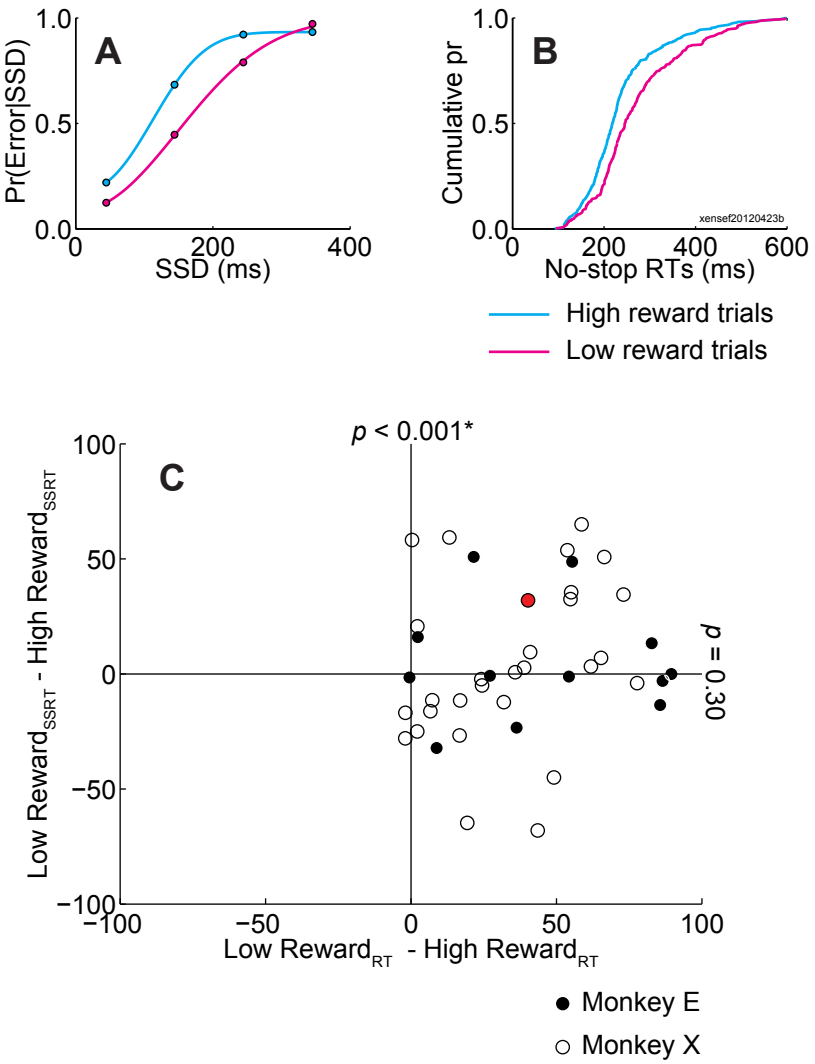

Figure 6.4 RT and SSRT during the asymmetrically rewarded stop-signal task. A) Inhibition function which plots the probability of committing a noncanceled error at each stop-signal delay (SSD) taken from an example session. Circles show data collected during the trials and curves plot fitted Weibull functions used to estimate SSRT. Data are plotted separately for high-reward (cyan) and low-reward (magenta) target locations. In this session, the monkey was significantly more likely to commit noncanceled errors in the high-reward condition. B) Cumulative RT distributions in separated by reward magnitude from the same session. In this session, the monkey was significantly faster when responding to high-reward targets. C) RT and SSRT differences between high and low reward conditions across the entire data set. Each circle represents data from a single session. The red circle shows data from the example session plotted in A and B. Its location in the upper right quadrant indicates that the monkeys RTs and SSRT were faster in the high reward condition than in the low reward condition. Across the data set, this RT effect was highly significant, but SSRTs were not significantly different between the two conditions.

6.3.3 Data acquisition

Implanted EEG surface electrodes were referenced to linked ears using ear-clip electrodes (Electro-Cap International). Data for this study were recorded from an EEG electrode approximating Fz in humans. All electrode impedances were < 10 kΩ. EEG and LFP data were amplified with high-input impedance head stages (Plexon), bandpass filtered between 0.7 and 170 Hz, and digitized at 1 kHz. LFP data acquisition has been described in detail (Chapter 4). Briefly, intracranial data were recorded using a 24-channel Plexon uprobe (Dallas, TX) with 150 μm inter-electrode spacing referenced to the probe shaft, and grounded to the headpost. All data were streamed to a single data acquisition system (MAP box, Plexon, Dallas, TX). Time stamps of trial events were recorded at 500 Hz. Eye position data were streamed to the Plexon computer at 1 kHz using an EyeLink 1000 infrared eye-tracking system (SR Research, Kanata, Ontario, Canada). LFP and spiking data were processed with unity-gain high-input impedance head stages (HST/32o25-36P-TR, Plexon). LFP data were bandpass filtered at 0.2-300 Hz and amplified 1000 times with a Plexon preamplifier, and digitized at 1 kHz. Spiking data were bandpass filtered between 100 Hz and 8 kHz and amplified 1000 times with a Plexon preamplifier, filtered in software with a 250 Hz high-pass filter and amplified an additional 32,000 times. Waveforms were digitized 200 μS before and 1200 μS after threshold crossings at 40 kHz. Single units were sorted online using a software window discriminator and refined offline using principal components analysis implemented in Plexon offline sorter.

6.3.4 LFP and CSD analysis

Data analyses were carried out in MATLAB (Mathworks, Natick, MA). LFPs were time locked to target onset or saccade initiation (defined as the instant that the eye exceeded 30°/s). Data were baseline corrected to the 200 ms interval preceding the

alignment event. After constructing event-related LFPs, we estimated CSD by approximating the 2nd spatial derivative at each point in time using the equation:

$$CSD = S\frac{\Phi(x-h) - 2\Phi(x) + \Phi(x+h)}{h^2}$$

where Φ = the observed voltage, h = the inter-electrode spacing (150 in our case) and S = the average conductance of primate gray matter (0.4 S/m) (Logothetis et al., 2007). The CSD reveals local dendritic activity in gray matter where neural ensembles arborize together and depolarize in unison, allowing the summation of current flow to be observed at the mesoscopic scale (Freeman and Nicholson, 1975; Riera et al., 2012). We multiplied the results by 10^6, converting units from A/m^3 to the more tractable nA/mm^3. This allowed us to compare the magnitude of our CSD directly to our previous results (Chapter 4) and other published results (Maier et al., 2011; Maier et al., 2010). To approximate CSD continuously across space, we interpolated between electrode contacts using nearest neighbors to a density of 10 μm and convolved the result with a Gaussian filter (σ = 100 μm) (Pettersen et al., 2006).

6.3.5 Statistical Methods

The nature of our recording and alignment procedure also meant that some deeper layers were not sampled on all recording sessions. Since our statistical tests were carried out on session means they automatically took these differences in *N* into account when calculating *p*-values.

Significant differences between CSD data in error and correct conditions were assessed in a continuous manner across space and time using the following methods. Matrices of *p*-values were calculated using point-by-point *t*-tests measured across a 5 ms window. The *p*-values were then corrected for multiple comparisons using a combined false-discovery rate (FDR) and cluster-based approach. The FDR correction

was applied first using the method of Benjamini & Hochberg (1995) as described by Ashby (2011). For this approach, *p*-values are rank-ordered. Each individual *p*-value (p_i) is then judged significant if it meets the criteria:

$$p_i < \frac{a \cdot i}{N}$$

We used $\alpha = 0.05$. To eliminate remaining false positives, we then applied a cluster-based criterion. FDR corrected *p*-values had to remain below α in a continuous cluster of no fewer than 1,500 pixels (the equivalent of activation across a single electrode location for 100 ms or some combination thereof) before being judged significant. ERPs were tested for significance using the same approach adopted by Emeric et al., (2008; 2010) to assess LFPs, and Godlove et al., (2011a) to assess ERPs. A difference wave was calculated by subtracting noncanceled error-ERPs from no-stop correct ERPs (Fig. 6.1G). The intrinsic variability of the difference wave was assessed by calculating the standard deviation across time during the baseline period. This provided a measure of chance fluctuations between error and correct ERPs. Significant epochs were defined as periods when the difference wave deviated from baseline by >2 standard deviations for longer than 50 ms, provided it exceeded 3 standard deviations in that interval.

Granger causality analysis was carried out in the time domain using the MATLAB toolbox developed by Seth (2010). Single trial data were isolated 0-250 ms after correct or error responses, and the multiple realization variants of each function were used. Data were first differenced, demeaned, and detrended. In all cases, this procedure produced covariance stationary time-series as assessed using the Augmented Dickey Fuller and KPSS tests. Appropriate model orders (i.e. the number of previous data points to fit in each autoregressive model) were determined using Bayesian information criteria scores. The model order was allowed to reach 100, but never saturated (mean 26.3, SEM 1.9). *F* statistics were determined using multivariate regression. Significance

thresholds were set at $\alpha = 0.01$ and were corrected for multiple comparisons using the Bonferroni method.

Neurons were classified as RPE- or error-related using a regression approach. The number of action potentials recorded from a given neuron on individual trials were binned in 2 windows of interest, and regressed against dummy variables representing trial type and against reaction times. To identify neurons with RPE activity after target onset, action potentials were binned during the 400 ms immediately following target onset and regressed against dummy variables representing either high value targets or low value targets. Spike rates were also regressed against the latency of the task-related saccade that was made during this epoch. Neurons that showed significant correlations between spike rate and trial type while not showing significant correlations between spike rate and RT were deemed RPE related. Error-related units were identified using a similar approach. Spike rates were binned during the 400 ms following correct or error response and regressed against dummy variables. Spike rates were also regressed against the RT of the second non-task related saccade that often occurred during this epoch on error trials. Neurons that showed significant correlations between spike rate and trial outcome while not showing significant correlations between spike rate and RT of the second task irrelevant saccade were deemed error-related. The number of trials per condition were matched for these analyses.

6.4 Supplementary Material

6.4.1 Behavior during the asymmetrically rewarded stop-signal task

Table 6.1 summarizes behavior during the asymmetrically rewarded saccade stop-signal task used in this study. Both monkeys performed the stop-signal task in a manner that conformed to the assumptions of Logan's race model. In particular, as the race model predicts, noncanceled RTs were faster than no-stop RTs. The probability of

committing a noncanceled error was near 50% in all conditions (though it as slightly higher in the high-reward condition and slightly lower in the low-reward condition). This shows that the tracking algorithm was successful in matching the monkeys' behavior. RTs and SSRTs were slightly higher than those reported previously for monkeys performing the saccade stop-signal task, but not unreasonable. The RT data also show that monkeys were appropriately sensitive to the asymmetric reward manipulation. As reported previously (Kawagoe et al., 1998) monkeys showed decreased RTs when responding to high-reward targets as compared to RTs toward low-reward targets.

Figure 6.4 summarizes the RT and SSRT findings across the data set. Although RTs were significantly faster when the monkeys responded to high-reward targets (Wilcoxon rank sum $W = 2117$, $p < 0.001$), SSRTs did not show significant differences in the two reward conditions (Wilcoxon rank sum $W = 1814$, $p = 0.30$).

CHAPTER 7

GENERAL DISCUSSION

7.1 Summary of results

Here I have presented studies of saccade execution and evaluation carried out using the saccade stop-signal paradigm. This task is ideally suited to studying saccade execution because it serves to poise the system on the knife's edge between executing and withholding a saccade. As we saw in Chapter 1, the tension between going and stopping is instantiated by separate neural populations at multiple levels within the oculomotor system. The task is also excellent for studying the evaluation of eye movements, because it elicits a large proportion of errors that are salient to the subject.

In the first group of studies, I sought to better characterize mechanisms of saccade execution by measuring muscle activity and small fixational eye movements when partially prepared saccades are canceled. Based on the known circuitry of the brainstem and on neural data recorded previously from SC and FEF during the stop-signal task, I reasoned that I would not observe increased muscle activation during periods when saccades were successfully canceled. This prediction was borne out by the data. Unexpectedly, however, I also observed a small but significant decrease in muscle activation during periods when saccades were canceled. This led me to hypothesize that microsaccades would show a similar decrease during the same period. I tested this hypothesis in the second study, and found that microsaccade frequency was reduced when monkeys canceled prepared saccades. Based on these studies, we can make several new conclusions concerning saccade execution. First of all, this work highlights a basic difference between the oculomotor system and skeletal motor system. Although exceptions to this general rule surely exist (McPeek and Keller, 2002; Murthy

et al., 2007), saccades are, in large part, ballistic movements (Becker, 1991). That is to say, once triggered, a saccade will proceed through to completion. As detailed in Chapter 3, based on previous data reporting the patterns of activity of neurons in rostral and caudal SC during the stop-signal task, my findings of decreased muscle activity and microsaccade production during periods when planned saccades are canceled also contradict predictions made by a new theory that suggests SC does not contain neurons related to fixation (Hafed et al., 2008; 2012). These data also have application outside of the immediate field of oculomotor control. They have implications for the premotor theory of attention which is intimately associated with the microsaccade theory of rostral SC function. This theory suggests that microsaccades should be directed toward areas that are attended covertly, and that this effect is mediated by attention-related subthreshold activation in SC (Hafed et al., 2009). Subthreshold activation is clearly present in caudal SC neurons during the time that saccades are canceled during the stop-signal task. But the microsaccade activity predicted by these theories were not observed in my data.

In the second series of studies, I investigated the evaluation of eye movements with particular focus on error-detection and the SEF. These studies also have implications that range far beyond the oculomotor system. First, I probed the functional microcircuitry of SEF using a newly developed microelectrode array to record single-unit responses and CSD. SEF is thought to play a critical role in evaluating eye movements and this area may participate in generating the ERN. I found many intriguing similarities between the laminar patterns of activation in SEF and those that have been described in early visual areas, suggesting that the same microcircuitry motifs are represented across all areas of cortex. These results suggest that microcircuitry models originally proposed to explain visual and somatosensory activation in primary sensory cortices may be usefully extended to performance monitoring signals in medial frontal cortex. This study

also deteails the development of several new techniques, making it possible to record and analyze CSD averaged across recording sessions, and to assign single- and multi-unit responses specific laminar origins based on the CSD recorded simultaneously. In my next study, I demonstrated that monkeys exhibit electrophysiological correlates of error-processing during eye-movement tasks homologous to those observed in humans (Godlove et al., 2011b; Reinhart et al., 2012). On the one hand, this finding creates a solid link between work that has been carried out in humans and non-human primates to investigate the bases of performance monitoring. On the other hand, this work establishes an animal model to investigate the neural origins of these error-related ERPs. Finally, in my last study, I combined recordings of the newly discovered monkey ERN with these newly developed recording techniques to better understand the neural basis of saccade evaluation. This work shows that local current flow in SEF contributes to the ERN recorded using surface EEG electrodes. Using an asymmetric reward manipulation, I also showed that the ERN is sensitive to the magnitude of reward prediction error (RPE) encountered by the monkeys. But I also demonstrated that SEF does not mediate this RPE effect. Taken together, these findings suggest that the ERN likely results from multiple overlapping components that arise from multiple cortical areas and reflects several neural processes. One of these processes must be a RPE signal, since the ERN is sensitive to the magnitude of RPE experienced by the subjects. But the contribution of SEF during the response epoch appears to be more closely related to detecting errors in and of themselves rather than evaluating errant saccades in light of the magnitude of RPEs that they produce. Together, this series of studies provides important new insight on the neural basis of saccade evaluation, and perhaps on performance monitoring more generally.

7.2 Potential limitations

The oculomotor system is, of course, an interesting topic and more than worthy of study in its own right. However, especially in reference to my second group of studies, it is also of interest to know to what extent these results generalize to other aspects of motor evaluation. Two important questions should be acknowledged. First, are the same neural processes of performance monitoring recruited in natural settings when subjects are not explicitly rewarded for appropriate saccadic responses? And second, are these same neural processes active when subjects make responses using other effector systems? I will address these two topics in turn.

In some respects, the saccade stop-signal task I have used to collect data for this work is specific to laboratory conditions. Under natural circumstances, targets rarely appear from thin air (discounting fireflies and lighting bugs). Also, under natural conditions activity in the oculomotor system does not lead to the immediate receipt of appetitive reward [discounting the "fly detectors" and "bug perceivers" of frog optic tectum (Lettvin et al., 1959)]. In any case, I can think of no examples from nature in which a primate redirects gaze to receive a squirt of juice. Animals look at things to attain information. Some researchers question the relevance of using the oculomotor system to study reward related activity (Goldberg personal communication). But, this criticism may not be as damaging as it appears. Recent work has shown that the same midbrain dopamine neurons that fire in response to unexpected rewards also fire in response to cues that instructs a subject that it will soon receive information pertaining to an upcoming reward outcome (Bromberg-Martin and Hikosaka, 2009). Importantly, in this study, the cue itself did not provide any information about whether or not a particular trial would be rewarded, and these results cannot therefore be explained as a simple RPE signal. Rather, these results show that the same circuitry which becomes active when appetitive rewards are unexpectedly delivered becomes active when information is

delivered even when that information is neutral with respect to reward outcomes. One way to interpret these results is that information is intrinsically rewarding, and making eye movements to attain information under natural circumstances may not be so different from making eye movements to receive squirts of juice in the laboratory.

However, other differences between effector systems persist. As discussed in Chapter 2, saccadic eye movements are somewhat ballistic processes, whereas manual responses can be canceled even during the response execution phase. There may also exist differences between the neural mechanisms that evaluate actions carried out using different effector systems. Several researchers have recorded error ERPs when subjects make errant saccades during oculomotor tasks (Nieuwenhuis et al., 2001; Endrass et al., 2005). But recent work suggests a more anterior distribution for these components (particularly the error-related positivity) than in tasks where subjects make manual responses (Reinhart et al., 2012). Further work is needed to identify similarities and differences, but for now, we must remain tentative in generalizing these results beyond the oculomotor system.

7.3 Future directions

7.3.1 Additional recordings in SC, FEF, and ACC

Many new and potentially fruitful avenues for future research are suggested by this work. The results from my first set of experiments of unexpected decreases in extraocular EMG and reduced incidence of microsaccades during the time of saccade cancelation point to the need for better understanding of the neural basis of saccade execution. The most widely accepted, current theory of the role of SC saccade execution and inhibition proposes that gaze is stabilized and saccades are withheld when neural activity is balanced across the vector map. It has been previously shown that neural activity is imbalanced across the vector map in SC when saccades are

canceled (Paré & Hanes 2003). Therefore, either an additional mechanism to prevent saccade execution must be proposed, or the current theory of SC function must be revised. Additionally, the late increase in microsaccades that were directed away from the target location remains unexplained by current theory. New data recorded from SC during the stop-signal task would shed light on these issues. In particular, duel, simultaneous recordings of neurons in the rostral and caudal SC, as well as duel recordings from ipsilateral and contralateral SC would be helpful for resolving these issues. It would also be helpful to record from omnipause neurons in the nRIP of the PPRF during the stop-signal task. Omnipause neurons cease tonic activity during microsaccades and normal saccades alike (Brien et al., 2009), so their behavior on canceled trials during the stop-signal task may prove to be enlightening.

The role of FEF during saccade cancelation should also be further explored. Previous work showed that movement and fixation cells in FEF are sufficient in their timing and response characteristics to control the execution of saccades during the stop-signal task (Hanes et al., 1998). But fixation neurons in FEF should be reevaluated in light of current theories of SC function. Just as in SC, further recordings should be carried out to collect data from fixation neurons in FEF during the stop-signal task using techniques that afford measurement of microsaccades.

Finally, the experiments that I detailed in Chapter 6 should be repeated in ACC. ACC has long been hypothesized to be an area important for detecting errors and generating the ERN. My results suggest the involvement of areas outside of SEF in generating the ERN. It may be found that the RPE effect that is evident in the ERN is mediated by activity in ACC.

7.3.2 Neural interactions

These experiments raise important questions about the nature of interactions between different populations of neurons. I recorded activity from many neurons, across all cortical laminae, representing several different functional groups. To advance our understanding of microcircuitry in agranular cortex, it would be useful to characterize interactions between neurons recorded simultaneously in different layers. It would also be useful to search for interactions between different classes of neurons both within and across layers. For instance, in Chapter 6 I recorded activity from neurons displaying both error-related and RPE-related activity. Although error-related neurons tended not to display RPE-related modulation and *vice versa*, it is possible that these two groups of neurons interact to perform a calculation related to performance monitoring. If so, perhaps one type of neuron tends to project to the other type of neuron. If this were found to be the case, it would aid in specifying a direction for information flow and help constrain the types of calculations that may be carried out by interacting populations of neurons in this area.

Several techniques have been used to test for interactions between neurons. One promising technique that has not yet been applied extensively to single cell recordings is Granger causality (but see (Kaminski and Blinowska, 1991; Gregoriou et al., 2009; Hirabayashi et al., 2013). As we have seen in Chapter 6, Granger causality can be a useful tool for assessing temporal correlations between continuous signals. This technique cannot be applied to point processes such as discrete action potential recordings, and it is sensitive to filtering which may preclude its use in analyzing spike density functions (Seth, 2010). However, Granger causality can be assessed in either the time or the frequency domain, and point processes such as sequences of action potentials can be converted to frequency spectra. Applying these techniques to search

for neural interactions could prove useful for studying the neural bases of saccade execution and evaluation.

7.3.3 Closing the loop: How does evaluation lead to better execution?

As stated in the introduction, a system for evaluating behavior is not much good unless this information helps to improve subsequent behavior. I did not observe any link between the amplitude of the ERN and subsequent changes in RT during my characterization of the monkey ERN in Chapter 5. However, the stop-signal task is unusual in that post-error slowing is often not observed (Emeric et al., 2007; Nelson et al., 2010; Bissett and Logan, 2011, 2012). Additionally, in the version of the stop-signal task that I employed, RT adjustments are actually not useful in optimizing performance. The SSD tracking procedure ensures that subjects commit errant noncanceled saccades on ~50% of stop trials regardless of the speed with which they respond. The monkeys I trained quickly learned that no advantage could be gained by slowing their responses. And in the version of the task that I designed and implemented, trial length was held constant such that the period of time from the start of one trial to the next does not change. Because of this contingency, monkeys are unable to increase the reward rate by responding faster. Faster response times simply lead to longer inter-trial intervals. Under these conditions, it is difficult to determine what a behavioral adjustment strategy would entail. The monkeys in these studies were (necessarily) highly trained. Exploratory behavior and learning-related adjustments were no longer produced by monkeys once neural recordings commenced.

On the other hand, my final study, detailed in Chapter 6, did elicit a form of speed accuracy tradeoff from monkey subjects. Although it was not the primary focus of the work presented here, monkeys sped up and showed decrements in their ability to cancel saccades when presented with targets indicating large rewards were possible.

Moreover, this reaction time effect unfolded gradually over the course of several trials after the target location signaling a large reward switched (Fig. 7.1). These behavioral adjustments are presumably driven by updating value representations of targets, and not evaluation of errant saccades. However, as we have seen in Chapter 6, error processing (as reflected electrophysiologically by the ERN) interacts with, and may be partially driven by reward-related activity. By testing if these electrophysiological and neurophysiological signals also evolve over time, and by testing for testing for potential correlations between the magnitude of these signals and the RT effects pictured in Fig. 7.1, we should gain additional insight into the potential link between saccade evaluation and subsequent execution.

7.3.4 Models linking action evaluation to execution

Many models deal primarily with the execution of actions. For instance, popular accumulator models assume that actions are executed when an accumulation process reaches a threshold (e.g. Nosofsky and Palmeri, 1997; Ratcliff and Rouder, 1998; Usher and McClelland, 2001; Bogacz et al., 2006). These models suggest mechanisms for instantiating performance adjustments. For example, it is often assumed that a speed-accuracy adjustment may be implemented by adjusting the model threshold (but see Pouget et al., 2011; Heitz and Schall, 2012). However, these models do not specify any details about the process that determines when behavioral adjustments are needed. Other models deal primarily with the process that signals the need for increased executive control (reviewed by Alexander and Brown, 2010). However, these models are typically vague as to the way in which executive control may be implemented. For example, Holroyd & Coles' (2002) much cited model linking the ERN to reinforcement learning simply suggests that multiple motor controllers vie to determine ultimate

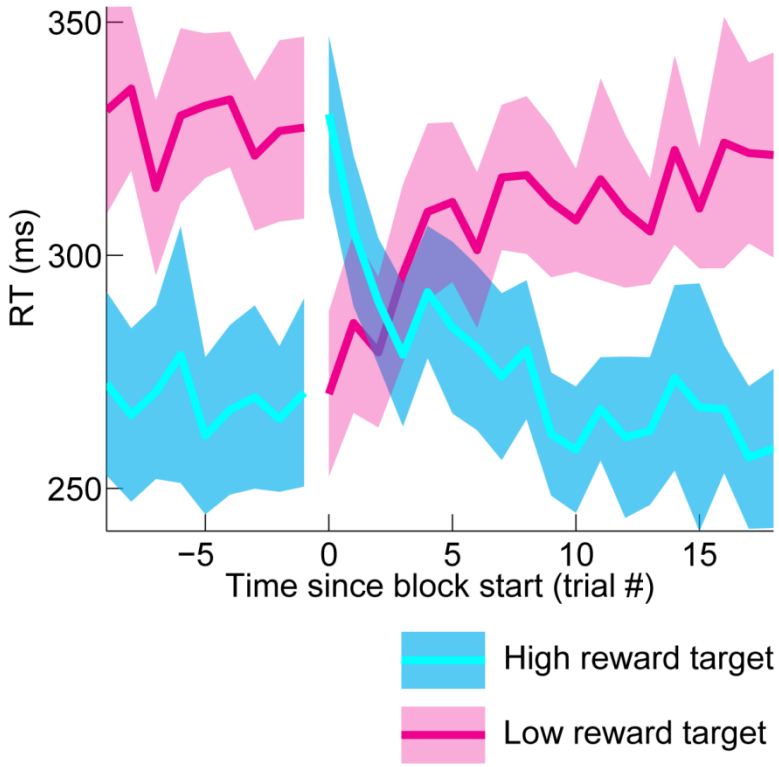

Figure 7.1. Grand average reaction times (±95% confidence intervals) for correct responses to stimuli that represent high reward vs. low reward.

behavioral outputs, and that executive control (implemented in ACC) selects from among these motor controllers to allow actions to occur. This is conceptually similar to the idea of competing schemas originally put forth by Norman and Shallice (1980). However, it is difficult to know what type of neural this type of cognitive control would reflect. The data presented in Chapter 6 may prove useful for developing links between these models, and for modeling performance monitoring at a lower, more biologically realistic level than has previously been possible. Not only do these data contain ERPs, CSD, and single-units recorded during a task that induces repeated speed accuracy trade-offs, but the intracranial data are also indexed by layer. This means that information about canonical cortical microcircuits may be brought to bear to help constrain new biophysically plausible models of performance monitoring. Ultimately, the tremendous gains made in describing the visual system during the 1970's and 1980's by describing and modeling the underlying microcircuitry may also prove useful in describing the neural bases of saccade execution and evaluation.

REFERENCES

Adamük E (1872) Über angeborene und erworbene Association von F. C. Donders. Albrecht o Gruefes Arch Ophrhal 18:153-164.

Agam Y, Hämäläinen MS, Lee AKC, Dyckman KA, Friedman JS, Isom M, Makris N, Manoach DS (2011) Multimodal neuroimaging dissociates hemodynamic and electrophysiological correlates of error processing. Proceedings of the National Academy of Sciences 108:17556-17561.

Akerfelt A, Colonius H, Diederich A (2006) Visual-tactile saccadic inhibition. Experimental Brain Research 169:554-563.

Alexander WH, Brown JW (2010) Computational models of performance monitoring and cognitive control. Topics in Cognitive Science 2:658-677.

Alexander WH, Brown JW (2011) Medial prefrontal cortex as an action-outcome predictor. Nature Neuroscience 14:1338-1344.

Allman JM, Hakeem A, Erwin JM, Nimchinsky E, Hof P (2001) The anterior cingulate cortex. Annals of the New York Academy of Sciences 935:107-117.

Amador N, Schlag-Rey M, Schlag J (2000) Reward-predicting and reward-detecting neuronal activity in the primate supplementary eye field. Journal of Neurophysiology 84:2166-2170.

Amador N, Schlag-Rey M, Schlag J (2004) Primate antisaccade. II. Supplementary eye field neuronal activity predicts correct performance. Journal of Neurophysiology 91:1672-1689.

Amiez C, Joseph JP, Procyk E (2005) Anterior cingulate error-related activity is modulated by predicted reward. European Journal of Neuroscience 21:3447-3452.

Anderson SR, Porrill J, Sklavos S, Gandhi NJ, Sparks DL, Dean P (2009) Dynamics of primate oculomotor plant revealed by effects of abducens microstimulation. Journal of Neurophysiology 101:2907-2923.

Armstrong IT, Munoz DP (2003) Inhibitory control of eye movements during oculomotor countermanding in adults with attention-deficit hyperactivity disorder. Experimental Brain Research 152:444-452.

Ashby FG (2011) Statistical analysis of fMRI data. Cambridge, MA: MIT Press.

Asrress KN, Carpenter RHS (2001) Saccadic countermanding: a comparison of central and peripheral stop signals. Vision Research 41:2645-2651.

Bahill AT, Clark MR, Stark L (1975) The main sequence, a tool for studying human eye movements. Mathematical Biosciences 24:191-204.

Bair W, O'Keefe LP (1998) The influence of fixational eye movements on the response of neurons in area MT of the macaque. Visual Neuroscience 15:779-786.

Balaban CD, Weinstein JM (1985) The human pre-saccadic spike potential - influences of a visual target, saccade direction, electrode laterality and instructions to perform saccades. Brain Research 347:49-57.

Band GPH, van der Molen MW, Logan GD (2003) Horse-race model simulations of the stop-signal procedure. Acta Psychologica 112:105-142.

Barbas H, Mesulam MM (1981) Organization of afferent input to subdivisions of area 8 in the rhesus monkey. Journal of Comparative Neurology 200:407-431.

Barbas H, Pandya DN (1987) Architecture and frontal cortical connections of the premotor cortex (area 6) in the rhesus monkey. Journal of Comparative Neurology 256:211-228.

Barlow HB (1952) Eye movements during fixation. The Journal of Physiology 116:290-306.

Barthó P, Hirase H, Monconduit L, Zugaro M, Harris KD, Buzsáki G (2004) Characterization of neocortical principal cells and interneurons by network interactions and extracellular features. Journal of Neurophysiology 92:600-608.

Bastos AM, Usrey WM, Adams RA, Mangun GR, Fries P, Friston KJ (2012) Canonical microcircuits for predictive coding. Neuron 76:695-711.

Bates JF, Goldman-Rakic PS (1993) Prefrontal connections of medial motor areas in the rhesus monkey. Journal of Comparative Neurology 336:211-228.

Becker W (1989) Metrics. In: The neurobiology of saccadic eye movements (Wurtz RH, Goldberg ME, eds), pp 13-61. Amsterdam: Elsevier.

Becker W (1991) Saccades. In: Vision and Visual Dysfunction. Eye Movements (Carpenter RHS, ed), pp 95-137. Boca Raton, FL: CRC Press.

Beckwith SVW, Stiavelli M, Koekemoer AM, Caldwell JAR, Ferguson HC, Hook R, Lucas RA, Bergeron LE, Corbin M, Jogee S (2006) The Hubble ultra deep field. The Astronomical Journal 132:1729.

Bellebaum C, Daum I (2008) Learning-related changes in reward expectancy are reflected in the feedbackâ€ related negativity. European Journal of Neuroscience 27:1823-1835.

Benevento LA, Fallon JH (1975) The ascending projections of the superior colliculus in the rhesus monkey (Macaca mulatta). Journal of Comparative Neurology 160:339-361.

Benjamini Y, Hochberg Y (1995) Controlling the false discovery rate: a practical and powerful approach to multiple testing. Journal of the Royal Statistical Society Series B (Methodological):289-300.

Berdyyeva TK, Olson CR (2009) Monkey supplementary eye field neurons signal the ordinal position of both actions and objects. The Journal of Neuroscience 29:591-599.

Berger B, Gaspar P, Verney C (1991) Dopaminergic innervation of the cerebral cortex: unexpected differences between rodents and primates. Trends in Neurosciences 14:21-27.

Bergeron A, Matsuo S, Guitton D (2003) Superior colliculus encodes distance to target, not saccade amplitude, in multi-step gaze shifts. Nature Neuroscience 6:404-413.

Bernstein P, Scheffers, MK, Coles, MGH. (1995) Where did I go wrong? A psychophysiological analysis of error detection. Journal of Experimental Psychology: Human Perception and Performance 21:1312–1322.

Berridge KC, Robinson TE (1998) What is the role of dopamine in reward: hedonic impact, reward learning, or incentive salience? Brain Research Reviews 28:309-369.

Biber MP, Kneisley LW, LaVail JH (1978) Cortical neurons projecting to the cervical and lumbar enlargements of the spinal cord in young and adult rhesus monkeys. Experimental neurology 59:492-508.

Bissett PG, Logan GD (2011) Post-stop-signal slowing: Strategies dominate reflexes and implicit learning. Journal of Experimental Psychology: Human Perception and Performance 38:746-757.

Bissett PG, Logan GD (2012) Post-stop-signal adjustments: Inhibition improves subsequent inhibition. Journal of Experimental Psychology: Learning, Memory & Cognition.

Bizzi E (1968) Discharge of frontal eye field neurons during saccadic and following eye movements in unanesthetized monkeys. Experimental Brain Research 6:69-80.

Blinn KA (1955) Focal anterior temporal spikes from external rectus muscles. Electroencephalography and Clinical Neurophysiology 7:299-302.

Bogacz R, Brown E, Moehlis J, Holmes P, Cohen JD (2006) The physics of optimal decision making: a formal analysis of models of performance in two-alternative forced-choice tasks. Psychological Review 113:700.

Bon L, Lucchetti C (1991) Behavioral and motor mechanisms of dorsomedial frontal cortex of macaca monkey. International Journal of Neuroscience 60:187-193.

Bon L, Lucchetti C (1992) The dorsomedial frontal cortex of the macaca monkey: fixation and saccade-related activity. Experimental Brain Research 89:571-580.

Boring EG (1950) A History of Experimental Psychology, 2nd Edition: New York: Appleton.

Botvinick M, Nystrom LE, Fissell K, Carter CS, Cohen JD (1999) Conflict monitoring versus selection-for-action in anterior cingulate cortex. Nature 402:179-181.

Botvinick MM, Braver TS, Barch DM, Carter CS, Cohen JD (2001) Conflict monitoring and cognitive control. Psychological Review 108:624-652.

Boucher L, Palmeri TJ, Logan GD, Schall JD (2007a) Inhibitory control in mind and brain: An interactive race model of countermanding Saccades. Psychological Review 114:376-397.

Boucher L, Stuphorn V, Logan GD, Schall JD, Palmeri TJ (2007b) Stopping eye and hand movements: Are the processes independent? Perception & Psychophysics 69:785-801.

Boynton GM (2011) Spikes, BOLD, Attention, and Awareness: A comparison of electrophysiological and fMRI signals in V1. Journal of Vision 11:1-16.

Braver TS, Barch DM, Gray JR, Molfese DL, Snyder A (2001) Anterior cingulate cortex and response conflict: effects of frequency, inhibition and errors. Cerebral Cortex 11:825-836.

Brázdil M, Dobšík M, Mikl M, Hlušík P, Daniel P, Pažourková M, Krupa P, Rektor I (2005) Combined event-related fMRI and intracerebral ERP study of an auditory oddball task. Neuroimage 26:285-293.

Brien DC, Corneil BD, Fecteau JH, Bell AH, Munoz DP (2009) The behavioural and neurophysiological modulation of microsaccades in monkeys. Journal of Eye Movement Research 3:1-12.

Broca P (1861) Perte de la parole, ramollissement chronique et destruction partielle du lobe antérieur gauche du cerveau. Bull Soc Anthropol 2:235-238.

Brockerhoff SE, Hurley JB, Janssen-Bienhold U, Neuhauss SC, Driever W, Dowling JE (1995) A behavioral screen for isolating zebrafish mutants with visual system defects. Proceedings of the National Academy of Sciences 92:10545-10549.

Brodmann K (1909) Vergleichende Lokalisationslehre der Grosshirnrinde in ihren Prinzipien dargestellt auf Grund des Zellenbaues. Leipzig: Barth.

Bromberg-Martin ES, Hikosaka O (2009) Midbrain dopamine neurons signal preference for advance information about upcoming rewards. Neuron 63:119-126.

Bromberg-Martin ES, Matsumoto M, Hikosaka O (2010) Dopamine in motivational control: rewarding, aversive, and alerting. Neuron 68:815-834.

Brooks VB (1986) How Does the Limbic System Assist Motor Learning? A Limbic Comparator Hypothesis (Part 1 of 2). Brain, Behavior and Evolution 29:29-41.

Brown JW, Braver TS (2005) Learned predictions of error likelihood in the anterior cingulate cortex. Science 307:1118-1121.

Brown JW, Hanes DP, Schall JD, Stuphorn V (2008) Relation of frontal eye field activity to saccade initiation during a countermanding task. Experimental Brain Research 190:135-151.

Bruce CJ, Goldberg ME (1985) Primate frontal eye fields. 1. Single neurons discharging before saccades. J Neurophysiol 53:603–635.

Bruce CJ, Goldberg ME, Bushnell MC, Stanton GB (1985) Primate frontal eye fields. 2. Physiological and anatomical correlates of electrically evoked eye movements. Journal of Neurophysiology 54:714-734.

Brunel N, Wang X-J (2001) Effects of neuromodulation in a cortical network model of object working memory dominated by recurrent inhibition. Journal of Computational Neuroscience 11:63-85.

Büttner-Ennever JA, Horn AKE, Henn V, Cohen B (1999) Projections from the superior colliculus motor map to omnipause neurons in monkey. Journal of Comparative Neurology 413:55-67.

Bullier J, Henry GH (1980) Ordinal position and afferent input of neurons in monkey striate cortex. Journal of Comparative Neurology 193:913-935.

Bullier J, Schall JD, Morel A (1996) Functional streams in occipito-frontal connections in the monkey. Behavioural Brain Research 76:89-97.

Bunney BS, Aghajanian GK (1976) Dopamine and norepinephrine innervated cells in the rat prefrontal cortex: pharmacological differentiation using microiontophoretic techniques. Life Sciences 19:1783-1792.

Burle B, Roger C, Allain S, Vidal F, Hasbroucq T (2008) Error negativity does not reflect conflict: A reappraisal of conflict monitoring and anterior cingulate cortex activity. Journal of Cognitive Neuroscience 20:1637-1655.

Bush RR, Mosteller F (1951a) A mathematical model for simple learning. Psychological Review 58:313-323.

Bush RR, Mosteller F (1951b) A model for stimulus generalization and discrimination. Psychological review 58:413.

Cabel DWJ, Armstrong IT, Reingold E, Munoz DP (2000) Control of saccade initiation in a countermanding task using visual and auditory stop signals. Experimental Brain Research 133:431-441.

Callaway EM (1998) Local circuits in primary visual cortex of the macaque monkey. Annual Review of Neuroscience 21:47-74.

Carbonnell L, Falkenstein M (2006) Does the error negativity reflect the degree of response conflict? Brain Research 1095:124-130.

Carpenter RHS (1981) Oculomotor procrastination. In: Eye movements: Cognition and visual perception (Fisher DF, Monty RA, Senders JW, eds), pp 237-246. Hillsdale, NJ: Lawrence Erlbaum Associates.

Carpenter RHS (1988) Movements of the eyes 2nd Edition. London: Pion Limited.

Carpenter RHS (1991) The visual origins of ocular motility. In: Vision and Visual Dysfunction. Eye Movements (Carpenter RHS, ed), pp 1-10. Boca Raton, FL: CRC Press.

Carter CS, Mintun M, Cohen JD (1995) Interference and facilitation effects during selective attention: an H215O PET study of Stroop task performance. Neuroimage 2:264-272.

Carter CS, Braver TS, Barch DM, Botvinick MM, Noll D, Cohen JD (1998) Anterior cingulate cortex, error detection, and the online monitoring of performance. Science 280:747-749.

Carter CS, Macdonald AM, Botvinick M, Ross LL, Stenger VA, Noll D, Cohen JD (2000) Parsing executive processes: Strategic vs. evaluative functions of the anterior cingulate cortex. Proceedings of the National Academy of Sciences 97:1944-1948.

Cavanaugh J, Joiner WM, Wurtz RH (2012) Suppressive surrounds of receptive fields in monkey frontal eye field. The Journal of Neuroscience 32:12284-12293.

Chance FS, Abbott LF, Reyes AD (2002) Gain modulation from background synaptic input. Neuron 35:773-782.

Chen LL, Wise SP (1995a) Supplementary eye field contrasted with the frontal eye field during acquisition of conditional oculomotor associations. Journal of Neurophysiology 73:1122-1134.

Chen LL, Wise SP (1995b) Neuronal activity in the supplementary eye field during acquisition of conditional oculomotor associations. Journal of Neurophysiology 73:1101-1121.

Chen LL, Wise SP (1996) Evolution of directional preferences in the supplementary eye field during acquisition of conditional oculomotor associations. The Journal of Neuroscience 16:3067-3081.

Clarke FJJ (1961) Visual recovery following local adaptation of the peripheral retina (Troxler's effect). Journal of Modern Optics 8:121-135.

Cohen JY, Pouget P, Heitz RP, Woodman GF, Schall JD (2009) Biophysical support for functionally distinct cell types in the frontal eye field. Journal of Neurophysiology 101:912-916.

Cohen RA, Kaplan RF, Moser DJ, Jenkins MA, Wilkinson H (1999) Impairments of attention after cingulotomy. Neurology 53:819-819.

Colby CL, Goldberg ME (1999) Space and attention in parietal cortex. Annual Review of Neuroscience 22:319-349.

Cole M, Yeung, N., Freiwald, WA., Botvinick, M. (2009) Cingulate cortex: diverging data from humans and monkeys. Trends in neurosciences 32:566-574.

Cole MW, Yeung, N., Freiwald, W., Botvinick, M. (2010) Conflict over cingulate cortex: Between-species differences in cingulate may support enhanced cognitive flexibility in humans. Brain, Behavior, and Evolution 75:239-240.

Coles MGH, Scheffers MK, Holroyd CB (2001) Why is there an ERN/Ne on correct trials? Response representations, stimulus-related components, and the theory of error-processing. Biological Psychology 56:173-189.

Collewijn H, Kowler E (2008) The significance of microsaccades for vision and oculomotor control. Journal of Vision 8:1-21.

Collewijn H, Erkelens CJ, Steinman RM (1988) Binocular co-ordination of human vertical saccadic eye movements. The Journal of Physiology 404:183-197.

Collins CE, Airey DC, Young NA, Leitch DB, Kaas JH (2010) Neuron densities vary across and within cortical areas in primates. Proceedings of the National Academy of Sciences 107:15927-15932.

Colonius H (1990) A note on the stop-signal paradigm, or how to observe the unobservable. Psychological Review 97:309-312.

Colonius H, Ozyurt J, Arndt PA (2001) Countermanding saccades with auditory stop signals: testing the race model. Vision Research 41:1951-1968.

Constantinidis C, Williams GV, Goldman-Rakic PS (2002) A role for inhibition in shaping the temporal flow of information in prefrontal cortex. Nature Neuroscience 5:175-180.

Corneil BD, Elsley JK (2005) Countermanding eye-head gaze shifts in humans: Marching orders are delivered to the head first. Journal of Neurophysiology 94:883-895.

Corneil BD, Olivier E, Munoz DP (2002) Neck muscle responses to stimulation of monkey superior colliculus. I. Topography and manipulation of stimulation parameters. Journal of Neurophysiology 88:1980-1999.

Cornsweet TN (1956) Determination of the stimuli for involuntary drifts and saccadic eye movements. Journal of the Optical Society of America 46:987-988.

Cowie RJ, Robinson DL (1994) Subcortical contributions to head movements in macaques. I. Contrasting effects of electrical stimulation of a medial pontomedullary region and the superior colliculus. Journal of Neurophysiology 72:2648-2664.

Creutzfeldt OD (1977) Generality of the functional structure of the neocortex. Naturwissenschaften 64:507-517.

Cui J, Wilke M, Logothetis NK, Leopold DA, Liang HL (2009) Visibility states modulate microsaccade rate and direction. Vision Research 49:228-236.

Curtis CE (2006) Prefrontal and parietal contributions to spatial working memory. Neuroscience 139:173-180.

Curtis CE, Cole MW, Rao VY, D'Esposito M (2005) Canceling planned action: An fMRI study of countermanding saccades. Cerebral Cortex 15:1281-1289.

d'Esposito M, Aguirre GK, Zarahn E, Ballard D, Shin RK, Lease J (1998) Functional MRI studies of spatial and nonspatial working memory. Cognitive Brain Research 7:1-13.

da Costa NM, Martin KAC (2010) Whose cortical column would that be? Frontiers in Neuroanatomy 4.

Dale AM, Sereno MI (1993) Improved localization of cortical activity by combining EEG and MEG with MRI cortical surface reconstruction - a linear-approach. Journal of Cognitive Neuroscience 5:162-176.

David O, Guillemain I, Saillet S, Reyt S, Deransart C, Segebarth C, Depaulis A (2008) Identifying neural drivers with functional MRI: an electrophysiological validation. PLoS biology 6:e315.

de Bruijn ERA, Hulstijn W, Verkes RJ, Ruigt GSF, Sabbe BGC (2004) Drug-induced stimulation and suppression of action monitoring in healthy volunteers. Psychopharmacology 177:151-160.

De Felipe J, Markram H, Rockland KS (2012) The neocortical column. Frontiers in Neuroanatomy 6.

de Garis H, Shuo C, Goertzel B, Ruiting L (2012) A world survey of artificial brain projects, Part I: Large-scale brain simulations. Neurocomputing 74:3-29.

De Jong R, Coles MGH, Logan GD (1995) Strategies and mechanisms in nonselective and selective inhibitory motor control. Journal of Experimental Psychology-Human Perception and Performance 21:498-511.

De Jong R, Coles MGH, Logan GD, Gratton G (1990) In search of the point of no return - the control of response processes. Journal of Experimental Psychology-Human Perception and Performance 16:164-182.

Dean P, Redgrave P, Sahibzada N, Tsuji K (1986) Head and body movements produced by electrical stimulation of superior colliculus in rats: effects of interruption of crossed tectoreticulospinal pathway. Neuroscience 19:367-380.

Debener S, Ullsperger M, Fiehler K, von Cramon DY, Engel AK (2005a) Monitoring error processing by means of simultaneous EEG/fMRI recordings II: Single-trial

independent component analysis of the error-related negativity (ERN). Journal of Psychophysiology 19:111-111.

Debener S, Ullsperger M, Siegel M, Fiehler K, von Cramon DY, Engel AK (2005b) Trial-by-trial coupling of concurrent electroencephalogram and functional magnetic imaging identifies the dynamics of performance monitoring. The Journal of Neuroscience 25:11730-11737.

DeHaan A, Halterman C, Langan J, Drew AS, Osternig LR, Chou LS, van Donkelaar P (2007) Cancelling planned actions following mild traumatic brain injury. Neuropsychologia 45:406-411.

Dehaene S, Posner MI, Tucker DM (1994) Localization of a neural system for error-detection and compensation. Psychological Science 5:303-305.

DesJardin JT, Holmes AL, Forcelli PA, Cole CE, Gale JT, Wellman LL, Gale K, Malkova L (2013) Defense-like behaviors evoked by pharmacological disinhibition of the superior colliculus in the primate. The Journal of Neuroscience 33:150-155.

Di S, Baumgartner C, Barth DS (1990) Laminar analysis of extracellular field potentials in rat vibrissa barrel cortex. Journal of Neurophysiology 63:832-840.

Ditchburn RW, Ginsborg BL (1952) Vision with a stabilized retinal image. Nature 170:36-37.

Ditchburn RW, Fender DH, Mayne S (1959) Vision with controlled movements of the retinal image. The Journal of Physiology 145:98-107.

Dodge R, Cline TS (1901) The angle velocity of eye movements. Psychological Review 8:145.

Donkers FCL, van Boxtel GJM (2005) Mediofrontal negativities to averted gains and losses in the slot-machine task. Journal of Psychophysiology 19:256-262.

Donkers FCL, Nieuwenhuis S, van Boxtel GJM (2005) Mediofrontal negativities in the absence of responding. Cognitive Brain Research 25:777-787.

Dorris MC, Taylor TL, Klein RM, Munoz DP (1999) Influence of previous visual stimulus or saccade on saccadic reaction times in monkey. Journal of Neurophysiology 81:2429-2436.

Douglas RJ, Martin KA (1991) A functional microcircuit for cat visual cortex. The Journal of Physiology 440:735-769.

Douglas RJ, Martin KAC (2004) Neuronal circuits of the neocortex. Annual Review of Neuroscience 27:419-451.

Douglas RJ, Koch C, Mahowald M, Martin KA, Suarez HH (1995) Recurrent excitation in neocortical circuits. Science 269:981-985.

Dreher J-C, Berman KF (2002) Fractionating the neural substrate of cognitive control processes. Proceedings of the National Academy of Sciences 99:14595-14600.

Dum RP, Strick PL (1991) The origin of corticospinal projections from the premotor areas in the frontal lobe. The Journal of Neuroscience 11:667-689.

Dum RP, Strick PL (1993) Cingulate motor areas. In: Neurobiology of cingulate cortex (Vogt BA, Gabriel M, eds), pp 415-441. Cambridge, MA: Birkhäuser.

Elsley JK, Nagy B, Cushing SL, Corneil BD (2007) Widespread presaccadic recruitment of neck muscles by stimulation of the primate frontal eye fields. Journal of Neurophysiology 98:1333-1354.

Elston GN (2000) Pyramidal cells of the frontal lobe: All the more spinous to think with. The Journal of Neuroscience 20:RC95.

Emeric EE, Leslie M, Pouget P, Schall JD (2010) Performance monitoring local field potentials in the medial frontal cortex of primates: Supplementary eye field. Journal of Neurophysiology 104:1523-1537.

Emeric EE, Brown JW, Leslie M, Pouget P, Stuphorn V, Schall JD (2008) Performance monitoring local field potentials in the medial frontal cortex of primates: Anterior cingulate cortex. Journal of Neurophysiology 99:759-772.

Emeric EE, Brown JW, Boucher L, Carpenter RHS, Hanes DP, Harris R, Logan GD, Mashru RN, Paré M, Pouget P, Stuphorn V, Taylor TL, Schall JD (2007) Influence of history on saccade countermanding performance in humans and macaque monkeys. Vision Research 47:35-49.

Endrass T, Cosima F, Norbert K (2005) Error awareness in a saccade countermanding task. Journal of Psychophysiology 19:275-280.

Engbert R (2012) Computational modeling of collicular integration of perceptual responses and attention in microsaccades. Journal of Neuroscience 32:8035-8039.

Engbert R, Kliegl R (2003) Microsaccades uncover the orientation of covert attention. Vision Research 43:1035-1045.

Eriksen BA, Eriksen CW (1974) Effects of noise letters upon the identification of a target letter in a nonsearch task. Perception & Psychophysics 16:143-149.

Evdokimidis I, Liakopoulos D, Papageorgiou C (1991) Cortical potentials preceding centrifugal and centripetal self-paced horizontal saccades. Electroencephalography and Clinical Neurophysiology 79:503-505.

Everling S, Krappmann P, Flohr H (1997) Cortical potentials preceding pro- and antisaccades in man. Electroencephalography and Clinical Neurophysiology 102:356-362.

Everling S, Paré M, Dorris MC, Munoz DP (1998) Comparison of the discharge characteristics of brain stem omnipause neurons and superior colliculus fixation neurons in monkey: Implications for control of fixation and saccade behavior. Journal of Neurophysiology 79:511-528.

Falkenstein M, Hohnsbein J, Blanke L (1990) Effects of errors in choice reaction tasks on the ERP under focused and divided attention. Psychophysiological Brain Research.

Falkenstein M, Hoormann J, Hohnsbein J (1996) Event-related potential components related to errors. Zeitschrift fur experimentelle Psychologie: Organ der Deutschen Gesellschaft fur Psychologie 44:117-138.

Falkenstein M, Hoormann J, Christ S, Hohnsbein J (2000) ERP components on reaction errors and their functional significance: a tutorial. Biological Psychology 51:87–107.

Falkenstein M, Hohnsbein, J., Hoormann, J., Blanke, L. (1991) Effects of crossmodal divided attention on late ERP components. 2. Error processing in choice reaction tasks. Electroencephalography and Clinical Neurophysiology 78:447–455.

Fallgatter AJ, Herrmann MJ, Roemmler J, Ehlis AC, Wagener A, Heidrich A, Ortega G, Zeng Y, Lesch KP (2004) Allelic variation of serotonin transporter function modulates the brain electrical response for error processing. Neuropsychopharmacology 29:1506-1511.

Felleman DJ, Van Essen DC (1991) Distributed hierarchical processing in the primate cerebral cortex. Cerebral Cortex 1:1-47.

Fellows LK, Farah MJ (2005) Different underlying impairments in decision-making following ventromedial and dorsolateral frontal lobe damage in humans. Cerebral cortex 15:58-63.

Ferrier D (1875) Experiments on the brain of monkeys. Philosophical Transactions of the Royal Society B: Biological Sciences 165:409-430.

Ferrier D, Turner WA (1901) Experimental lesion of the corpora quadrigemina in monkeys. Brain 24:27-46.

Fischer B, Ramsperger E (1984) Human express saccades: extremely short reaction times of goal directed eye movements. Experimental Brain Research 57:191-195.

Folstein JR, Van Petten C (2008) Influence of cognitive control and mismatch on the N2 component of the ERP: a review. Psychophysiology 45:152-170.

Freeman JA, Nicholson C (1975) Experimental optimization of current source-density technique for anuran cerebellum. Journal of Neurophysiology 38:369-382.

Fries W (1984) Cortical projections to the superior colliculus in the macaque monkey: a retrograde study using horseradish peroxidase. Journal of Comparative Neurology 230:55-76.

Friston K (2009) Causal modelling and brain connectivity in functional magnetic resonance imaging. PLoS biology 7:220-225.

Fuchs AF, Luschei ES (1970) Firing patterns of abducens neurons of alert monkeys in relationship to horizontal eye movement. Journal of Neurophysiology 33:382-392.

Fuchs AF, Kaneko CRS, Scudder CA (1985) Brain-stem control of saccadic eye-movements. Annual Review of Neuroscience 8:307-337.

Fujii N, Mushiake H, Tamai M, Tanji J (1995) Microstimulation of the supplementary eye field during saccade preparation. NeuroReport 6:2565-2568.

Gaarder K (1966) Transmission of edge information in the human visual system. Nature 212:321-323.

Gandhi NJ, Keller EL (1997) Spatial distribution and discharge characteristics of superior colliculus neurons antidromically activated from the omnipause region in monkey. Journal of Neurophysiology 78:2221-2225.

Gandhi NJ, Keller EL (1999a) Activity of the brain stem omnipause neurons during saccades perturbed by stimulation of the primate superior colliculus. Journal of Neurophysiology 82:3254-3267.

Gandhi NJ, Keller EL (1999b) Comparison of saccades perturbed by stimulation of the rostral superior colliculus, the caudal superior colliculus, and the omnipause neuron region. Journal of Neurophysiology 82:3236-3253.

Gandhi NJ, Katnani HA (2011) Motor functions of the superior colliculus. Annual Review of Neuroscience 34:205.

Garavan H, Ross TJ, Kaufman J, Stein EA (2003) A midline dissociation between error-processing and response-conflict monitoring. Neuroimage 20:1132-1139.

Gaspar P, Berger B, Febvret A, Vigny A, Henry JP (1989) Catecholamine innervation of the human cerebral cortex as revealed by comparative immunohistochemistry of tyrosine hydroxylase and dopamine-beta-hydroxylase. Journal of Comparative Neurology 279:249-271.

Gehring WJ, Knight RT (2000) Prefrontal-cingulate interactions in action monitoring. Nature Neuroscience 3:516-520.

Gehring WJ, Fencsik DE (2001) Functions of the medial frontal cortex in the processing of conflict and errors. Journal of Neuroscience 21:9430-9437.

Gehring WJ, Willoughby AR (2002) The medial frontal cortex and the rapid processing of monetary gains and losses. Science 295:2279-2282.

Gehring WJ, Liu Y, Orr JM, Carp J (2011) The error-related negativity (ERN/Ne). In: Oxford handbook of event-related potential components (Luck SJ, Kappenman E, eds). New York: Oxford University Press.

Gehring WJ, Goss B, Coles MGH, Meyer DE, Donchin E (1993) A neural system for error-detection and compensation. Psychological Science 4:385-390.

Gemba H, Sasaki K, Brooks VB (1986) Error potentials in limbic cortex (anterior cingulate area-24) of monkeys during motor learning. Neuroscience Letters 70:223-227.

Georgopoulos AP, Schwartz AB, Kettner RE (1986) Neuronal population coding of movement direction. Science 233:1416-1419.

Geyer S, Zilles K, Luppino G, Matelli M (2000) Neurofilament protein distribution in the macaque monkey dorsolateral premotor cortex. European Journal of Neuroscience 12:1554-1566.

Giguere M, Goldman-Rakic PS (1988) Mediodorsal nucleus: areal, laminar, and tangential distribution of afferents and efferents in the frontal lobe of rhesus monkeys. Journal of Comparative Neurology 277:195-213.

Gilbert CD (1983) Microcircuitry of the visual cortex. Annual Review of Neuroscience 6:217-247.

Giolli RA, Gregory KM, Suzuki DA, Blanks RH, Lui F, Betelak KF (2001) Cortical and subcortical afferents to the nucleus reticularis tegmenti pontis and basal pontine nuclei in the macaque monkey. Visual Neuroscience 18:725-740.

Givre SJ, Schroeder CE, Arezzo JC (1994) Contribution of extrastriate area V4 to the surface-recorded flash VEP in the awake macaque. Vision Research 34:415-428.

Glimcher PW (2011) Understanding dopamine and reinforcement learning: the dopamine reward prediction error hypothesis. Proceedings of the National Academy of Sciences 108:15647-15654.

Godlove DC (2010) Eye movement artifact may account for putative frontal feedback-related potentials in nonhuman primates. The Journal of Neuroscience 30:4187-4189.

Godlove DC, Emeric EE, Boucher L, Schall JD (2009) Express saccade production in a stop signal task. Society for Neuroscience Abstract.

Godlove DC, Garr AK, Woodman GF, Schall JD (2011a) Measurement of the extraocular spike potential during saccade countermanding. Journal of Neurophysiology 106:104-114.

Godlove DC, Emeric EE, Segovis CM, Young MS, Schall JD, Woodman GF (2011b) Event-related potentials elicited by errors during the stop-signal task. I. macaque monkeys. The Journal of Neuroscience 31:15640-15649.

Goffart L, Hafed ZM, Krauzlis RJ (2012) Visual fixation as equilibrium: evidence from superior colliculus inactivation. The Journal of Neuroscience 32:10627-10636.

Goldberg G (1985) Supplementary motor area structure and function: review and hypotheses. Behavioral and Brain Sciences 8:567-588.

Goldberg ME, Eggers HM, Gouras P (1991) The oculomotor system. In: Principles of neural science, 3rd Edition (Kandel ER, Schwartz JH, Jessell TM, eds), pp 660-676. New York, NY: Elsevier.

Goonetilleke SC, Doherty TJ, Corneil BD (2010) A within trial measure of the stop signal reaction time in a head-unrestrained oculomotor countermanding task. Journal of Neurophysiology 104:3677-3690.

Goyer JP, Woldorff MG, Huettel SA (2008) Rapid electrophysiological brain responses are influenced by both valence and magnitude of monetary rewards. Journal of Cognitive Neuroscience 20:2058-2069.

Granger CWJ (1969) Investigating causal relations by econometric models and cross-spectral methods. Econometrica: Journal of the Econometric Society:424-438.

Green DG (1970) Regional variations in the visual acuity for interference fringes on the retina. The Journal of Physiology 207:351.

Gregoriou GG, Gotts SJ, Zhou H, Desimone R (2009) High-frequency, long-range coupling between prefrontal and visual cortex during attention. Science 324:1207-1210.

Grinband J, Savitskaya J, Wager TD, Teichert T, Ferrera VP, Hirsch J (2011) The dorsal medial frontal cortex is sensitive to time on task, not response conflict or error likelihood. Neuroimage 57:303-311.

Grosbras MH, Lobel E, Van de Moortele PF, LeBihan D, Berthoz A (1999) An anatomical landmark for the supplementary eye fields in human revealed with functional magnetic resonance imaging. Cerebral Cortex 9:705-711.

Guitton D (1991) Control of saccadic eye and gaze movements by the superior colliculus and basal ganglia. In: Vision and Visual Dysfunction. Eye Movements (Carpenter RHS, ed), pp 244-276. Boca Raton, FL: CRC Press.

Hafed ZM, Clark JJ (2002) Microsaccades as an overt measure of covert attention shifts. Vision Research 42:2533-2545.

Hafed ZM, Krauzlis RJ (2012) Similarity of superior colliculus involvement in microsaccade and saccade generation. Journal of Neurophysiology 107:1904-1916.

Hafed ZM, Goffart L, Krauzlis RJ (2008) Superior colliculus inactivation causes stable offsets in eye position during tracking. The Journal of Neuroscience 28:8124-8137.

Hafed ZM, Goffart L, Krauzlis RJ (2009) A neural mechanism for microsaccade generation in the primate superior colliculus. Science 323:940-943.

Hafed ZM, Lovejoy LP, Krauzlis RJ (2011) Modulation of microsaccades in monkey during a covert visual attention task. Journal of Neuroscience 31:15219-15230.

Haider B, Duque A, Hasenstaub AR, McCormick DA (2006) Neocortical network activity in vivo is generated through a dynamic balance of excitation and inhibition. The Journal of Neuroscience 26:4535-4545.

Hajcak G, McDonald N, Simons RF (2003) To err is autonomic: Error-related brain potentials, ANS activity, and post-error compensatory behavior. Psychophysiology 40:895-903.

Hajcak G, Holroyd CB, Moser JS, Simons RF (2005) Brain potentials associated with expected and unexpected good and bad outcomes. Psychophysiology 42:161-170.

Hajcak G, Moser JS, Holroyd CB, Simons RF (2006) The feedback-related negativity reflects the binary evaluation of good versus bad outcomes. Biological psychology 71:148-154.

Hajcak G, Moser JS, Holroyd CB, Simons RF (2007) It's worse than you thought: The feedback negativity and violations of reward prediction in gambling tasks. Psychophysiology 44:905-912.

Halgren E, Boujon C, Clarke J, Wang C (2002) Rapid distributed fronto-parieto-occipital processing stages during working memory in humans. Cerebral Cortex 12:710-728.

Hanes DP, Schall JD (1995) Countermanding saccades in macaque. Visual Neuroscience 12:929-937.

Hanes DP, Schall JD (1996) Neural control of voluntary movement initiation. Science 274:427-430.

Hanes DP, Carpenter RHS (1999) Countermanding saccades in humans. Vision Research 39:2777-2791.

Hanes DP, Thompson KG, Schall JD (1995) Relationship of presaccadic activity in frontal eye field and supplementary eye field to saccade initiation in macaque: Poisson spike train analysis. Experimental Brain Research 103:85-96.

Hanes DP, Patterson WF, Schall JD (1998) Role of frontal eye fields in countermanding saccades: Visual, movement, and fixation activity. Journal of Neurophysiology 79:817-834.

Hanisch C, Radach R, Holtkamp K, Herpertz-Dahlmann B, Konrad K (2006) Oculomotor inhibition in children with and without attention-deficit hyperactivity disorder (ADHD). Journal of Neural Transmission 113:671-684.

Hansen BJ, Dragoi V (2011) Adaptation-induced synchronization in laminar cortical circuits. Proceedings of the National Academy of Sciences 108:10720-10725.

Hansen BJ, Chelaru MI, Dragoi V (2012) Correlated variability in laminar cortical circuits. Neuron 76:590-602.

Harting JK, Huerta MF, Frankfurter AJ, Strominger NL, Royce GJ (1980) Ascending pathways from the monkey superior colliculus: an autoradiographic analysis. Journal of Comparative Neurology 192:853-882.

Hatanaka N, Tokuno H, Hamada I, Inase M, Ito Y, Imanishi M, Hasegawa N, Akazawa T, Nambu A, Takada M (2003) Thalamocortical and intracortical connections of monkey cingulate motor areas. Journal of Comparative Neurology 462:121-138.

Heinen S, Yang S-n, Ford J (2011) Microstimulation supports a causal role for the supplementary eye field in an oculomotor decision. Journal of Vision 11:529-529.

Heinzle J, Hepp K, Martin KAC (2007) A microcircuit model of the frontal eye fields. The Journal of Neuroscience 27:9341-9353.

Heitz RP, Schall JD (2012) Neural mechanisms of speed-accuracy tradeoff. Neuron 76:616-628.

Helmholtz H (1853) Ueber einige gesetze der verteilung elektrischer ströme in körperlichen leitern mit anwendung auf die thierisch-elektrischen versuche. Psychophysiology 17:259-273.

Helmstaedter M, de Kock CPJ, Feldmeyer D, Bruno RM, Sakmann B (2007) Reconstruction of an average cortical column in silico. Brain Research Reviews 55:193-203.

Hemelt ME, Keller A (2008) Superior colliculus control of vibrissa movements. Journal of Neurophysiology 100:1245-1254.

Hendrickson AE, Wilson JR, Ogren MP (1978) The neuroanatomical organization of pathways between the dorsal lateral geniculate nucleus and visual cortex in Old World and New World primates. The Journal of comparative neurology 182:123.

Herrmann M, Rommler, J, Ehlis, AC, Heidrich, A, Fallgatter, AJ. (2004) Source localization (LORETA) of the error-related-negativity (ERN/Ne) and positivity (Pe). Brain Research Cognitive Brain Research 20:294-299.

Hess WR, Burgi S, V. B (1946) Motorische funktion des tektalund tegmentalgebietes. Psychiat Neurol 112:1-52.

Hikosaka O, Wurtz RH (1983a) Visual and oculomotor functions of monkey substantia nigra pars reticulata. 1. Relation of visual and auditory responses to saccades. Journal of Neurophysiology 49:1230-1253.

Hikosaka O, Wurtz RH (1983b) Visual and oculomotor functions of monkey substantia nigra pars reticulata .2. visual responses related to fixation of gaze. Journal of Neurophysiology 49:1254-1267.

Hikosaka O, Wurtz RH (1983c) Visual and oculomotor functions of monkey substantia nigra pars reticulata. 3. Memory-contingent visual and saccade responses. Journal of Neurophysiology 49:1268-1284.

Hikosaka O, Wurtz RH (1989) The basal ganglia. In: The neurobiology of saccadic eye movements (Wurtz RH, Goldberg ME, eds), pp 257-276. Amsterdam: Elsevier.

Hikosaka O, Isoda M (2010) Switching from automatic to controlled behavior: cortico-basal ganglia mechanisms. Trends in Cognitive Sciences 14:154-161.

Hikosaka O, Takikawa Y, Kawagoe R (2000) Role of the basal ganglia in the control of purposive saccadic eye movements. Physiological Reviews 80:953-978.

Hikosaka O, Igusa Y, Nakao S, Shimazu H (1978) Direct inhibitory synaptic linkage of pontomedullary reticular burst neurons with abducens motoneurons in cat. Experimental Brain Research 33:337-352.

Hikosaka OD, Wurtz RH (1985) Modification of saccadic eye movements by GABA-related substances. I. Effect of muscimol and bicuculline in monkey superior colliculus. Journal of Neurophysiology 53:266-291.

Hirabayashi T, Takeuchi D, Tamura K, Miyashita Y (2013) Functional Microcircuit Recruited during Retrieval of Object Association Memory in Monkey Perirhinal Cortex. Neuron 77:192-203.

Holroyd CB, Coles MGH (2002) The neural basis. of human error processing: Reinforcement learning, dopamine, and the error-related negativity. Psychological Review 109:679-709.

Holroyd CB, Coles MGH (2008) Dorsal anterior cingulate cortex integrates reinforcement history to guide voluntary behavior. Cortex 44:548-559.

Holroyd CB, Dien J, Coles MGH (1998) Error-related scalp potentials elicited by hand and foot movements: evidence for an output-independent error-processing system in humans. Neuroscience Letters 242:65-68.

Holroyd CB, Larsen JT, Cohen JD (2004a) Context dependence of the event-related brain potential associated with reward and punishment. Psychophysiology 41:245-253.

Holroyd CB, Nieuwenhuis S, Yeung N, Cohen JD (2003) Errors in reward prediction are reflected in the event-related brain potential. Neuroreport 14:2481-2484.

Holroyd CB, Yeung N, Coles MGH, Cohen JD (2005) A mechanism for error detection in speeded response time tasks. Journal of Experimental Psychology-General 134:163-191.

Holroyd CB, Nieuwenhuis S, Yeung N, Nystrom L, Mars RB, Coles MGH, Cohen JD (2004b) Dorsal anterior cingulate cortex shows fMRI response to internal and external error signals. Nature neuroscience 7:497-498.

Hong S, Hikosaka O (2008) The globus pallidus sends reward-related signals to the lateral habenula. Neuron 60:720-729.

Horowitz TS, Fine EM, Fencsik DE, Yurgenson S, Wolfe JM (2007) Fixational eye movements are not an index of covert attention. Psychological Science 18:356-363.

Horton JC, Adams DL (2005) The cortical column: a structure without a function. Philosophical Transactions of the Royal Society B: Biological Sciences 360:837-862.

Hubel DH, Wiesel TN (1962) Receptive fields, binocular interaction and functional architecture in the cat's visual cortex. The Journal of Physiology 160:106.

Hubel DH, Wiesel TN (1965) Receptive fields and functional architecture in two nonstriate visual areas (18 and 19) of the cat. Journal of Neurophysiology.

Hubel DH, Wiesel TN (1972) Laminar and columnar distribution of geniculo-cortical fibers in the macaque monkey. Journal of Comparative Neurology 146:421-450.

Hubel DH, Wiesel TN (1974) Sequence regularity and geometry of orientation columns in the monkey striate cortex. Journal of Comparative Neurology 158:267-293.

Huerta MF, Kaas JH (1990) Supplementary eye field as defined by intracortical microstimulation - connections in macaques. Journal of Comparative Neurology 293:299-330.

Huerta MF, Krubitzer LA, Kaas JH (1986) Frontal eye field as defined by intracortical microstimulation in squirrel-monkeys, owl monkeys, and macaque monkeys 1. Subcortical connections. Journal of Comparative Neurology 253:415-439.

Huerta MF, Krubitzer LA, Kaas JH (1987) Frontal eye field as defined by intracortical microstimulation in squirrel monkeys, owl monkeys, and macaque monkeys 2. Cortical connections. Journal of Comparative Neurology 265:332-361.

Huster RJ, Eichele T, Enriquez-Geppert S, Wollbrink A, Kugel H, Konrad C, Pantev C (2011) Multimodal imaging of functional networks and event-related potentials in performance monitoring. Neuroimage 56:1588-1597.

Isoda M, Tanji J (2002) Cellular activity in the supplementary eye field during sequential performance of multiple saccades. Journal of Neurophysiology 88:3541-3545.

Isoda M, Tanji J (2003) Contrasting neuronal activity in the supplementary and frontal eye fields during temporal organization of multiple saccades. Journal of Neurophysiology 90:3054-3065.

Isoda M, Hikosaka O (2007) Switching from automatic to controlled action by monkey medial frontal cortex. Nature Neuroscience 10:240-248.

Ito S, Stuphorn V, Brown JW, Schall JD (2003) Performance monitoring by the anterior cingulate cortex during saccade countermanding. Science 302:120-122.

Izawa Y, Suzuki H, Shinoda Y (2009) Response properties of fixation neurons and their location in the frontal eye field in the monkey. Journal of Neurophysiology 102:2410-2422.

Jacobson ZJ, Dodwell PC (1979) Saccadic eye movements during reading. Brain and Language 8:303-314.

Jocham G, Ullsperger M (2009) Neuropharmacology of performance monitoring. Neuroscience and Biobehavioral Reviews 33:48-60.

Johannes S, Wieringa BM, Nager W, Dengler R, Munte TF (2001) Oxazepam alters action monitoring. Psychopharmacology 155:100-106.

Johnston K, Levin HM, Koval MJ, Everling S (2007) Top-down control-signal dynamics in anterior cingulate and prefrontal cortex neurons following task switching. Neuron 53:453-462.

Joiner WM, Lee JE, Shelhamer M (2007) Behavioral analysis of predictive saccade tracking as studied by countermanding. Experimental Brain Research 181:307-320.

Jones EG (2000) Microcolumns in the cerebral cortex. Proceedings of the National Academy of Sciences 97:5019-5021.

Joti P, Kulashekhar S, Behari M, Murthy A (2007) Impaired inhibitory oculomotor control in patients with Parkinson's disease. Experimental Brain Research 177:447-457.

Juan C-H, Shorter-Jacobi SM, Schall JD (2004) Dissociation of spatial attention and saccade preparation. Proceedings of the National Academy of Sciences of the United States of America 101:15541-15544.

Jung HH, Kim CH, Chang JH, Park YG, Chung SS, Chang JW (2006) Bilateral anterior cingulotomy for refractory obsessive-compulsive disorder: long-term follow-up results. Stereotactic and functional neurosurgery 84:184-189.

Just MA, Carpenter PA (1980) A theory of reading: From eye fixations to comprehension. Psychological Review 87:329-354.

Kagan I, Gur M, Snodderly DM (2008) Saccades and drifts differentially modulate neuronal activity in V1: effects of retinal image motion, position, and extraretinal influences. Journal of Vision 8.

Kajikawa Y, Schroeder CE (2012) How Local Is the Local Field Potential? Neuron 72:847-858.

Kaminski MJ, Blinowska KJ (1991) A new method of the description of the information flow in the brain structures. Biological cybernetics 65:203-210.

Kaping D, Vinck M, Hutchison RM, Everling S, Womelsdorf T (2011) Specific contributions of ventromedial, anterior cingulate, and lateral prefrontal cortex for attentional selection and stimulus valuation. PLoS biology 9.

Kawagoe R, Takikawa Y, Hikosaka O (1998) Expectation of reward modulates cognitive signals in the basal ganglia. Nature Neuroscience 1:411-416.

Keizer K, Kuypers H (1989) Distribution of corticospinal neurons with collaterals to the lower brain stem reticular formation in monkey (Macaca fascicularis). Experimental Brain Research 74:311-318.

Keller EL (1989) The cerebellum. In: The neurobiology of saccadic eye movements (Wurtz RH, Goldberg ME, eds), pp 391-409. Amsterdam: Elsevier.

Kennerley SW, Wallis JD (2009a) Evaluating choices by single neurons in the frontal lobe: outcome value encoded across multiple decision variables. European Journal of Neuroscience 29:2061-2073.

Kennerley SW, Wallis JD (2009b) Encoding of reward and space during a working memory task in the orbitofrontal cortex and anterior cingulate sulcus. Journal of Neurophysiology 102:3352-3364.

Keren AS, Yuval-Greenberg S, Deouell LY (2010) Saccadic spike potentials in gamma-band EEG: Characterization, detection and suppression. Neuroimage 49:2248-2263.

Kerns JG, Cohen JD, MacDonald AW, Cho RY, Stenger VA, Carter CS (2004) Anterior cingulate conflict monitoring and adjustments in control. Science 303:1023-1026.

Khan O, Taylor SJ, Jones JG, Swart M, Hanes DP, Carpenter RHS (1999) Effects of low-dose isoflurane on saccadic eye movement generation. Anaesthesia 54:142-145.

Kiehl KA, Liddle PF, Hopfinger JB (2000) Error processing and the rostral anterior cingulate: An event-related fMRI study. Psychophysiology 37:216-223.

Kim Y-G, Badler JB, Heinen SJ (2005) Trajectory interpretation by supplementary eye field neurons during ocular baseball. Journal of Neurophysiology 94:1385-1391.

King AJ (2004) The superior colliculus. Current Biology 14:R335-R338.

Klein RM (2000) Inhibition of return. Trends in Cognitive Sciences 4:138-147.

Klein TA, Endrass T, Kathmann N, Neumann J, von Cramon DY, Ullsperger M (2007) Neural correlates of error awareness. Neuroimage 34:1774-1781.

Knight TA, Fuchs AF (2007) Contribution of the frontal eye field to gaze shifts in the head-unrestrained monkey: effects of microstimulation. Journal of Neurophysiology 97:618-634.

Ko H-k, Poletti M, Rucci M (2010) Microsaccades precisely relocate gaze in a high visual acuity task. Nature Neuroscience 13:1549-1553.

Ko YT, Miller J (2011) Nonselective motor-level changes associated with selective response inhibition: evidence from response force measurements. Psychonomic Bulletin & Review 18:813-819.

Kornylo K, Dill N, Saenz M, Krauzlis RJ (2003) Canceling of pursuit and saccadic eye movements in humans and monkeys. Journal of Neurophysiology 89:2984-2999.

Kramer UM, Cunillera T, Camara E, Marco-Pallares J, Cucurell D, Nager W, Bauer P, Schule R, Schols L, Rodriguez-Fornells A, Munte TF (2007) The impact of catechol-O-methyltransferase and dopamine D4 receptor genotypes on neurophysiological markers of performance monitoring. Journal of Neuroscience 27:14190-14198.

Krauzlis RJ (2004) Recasting the smooth pursuit eye movement system. Journal of Neurophysiology 91:591-603.

Krauzlis RJ (2008) Eye Movements. In: Fundamental Neuroscience, 3rd Edition (Squire LR, Berg D, Bloom FE, du Lac S, Ghosh A, Spitzer NC, eds), pp 775-792. Burlington, MA: Academic Press.

Krauzlis RJ, Basso MA, Wurtz RH (1997) Rostral superior colliculus influences pursuit eye movements in the primate as well as fixation and saccades. Investigative Ophthalmology & Visual Science 38:4343-4343.

Kurtzberg D, Vaughan HG (1982) Topographic analysis of human cortical potentials preceding self-initiated and visually triggered saccades. Brain Research 243:1-9.

Kustov AA, Robinson DL (1995) Modified saccades evoked by stimulation of the macaque superior colliculus account for properties of the resettable integrator. Journal of Neurophysiology 73:1724-1728.

Ladouceur CD, Dahl RE, Carter CS (2007) Development of action monitoring through adolescence into adulthood: ERP and source localization. Developmental Science 10:874-891.

Lakatos P, Chen CM, O'Connell MN, Mills A, Schroeder CE (2007) Neuronal oscillations and multisensory interaction in primary auditory cortex. Neuron 53:279-292.

Laming D (1979) Choice reaction performance following an error. Acta Psychologica 43:199-224.

Lappin JS, Eriksen CW (1966) Use of a delayed signal to stop a visual reaction-time response. Journal of Experimental Psychology 72:805-&.

Laubrock J, Engbert R, Kliegl R (2005) Microsaccade dynamics during covert attention. Vision Research 45:721-730.

Lee C, Rohrer WH, Sparks DL (1988) Population coding of saccadic eye movements by neurons in the superior colliculus. Nature 332:357-360.

Lee K, Tehovnik EJ (1995) Topographic Distribution of Fixation-related Units in the Dorsomedial Frontal Cortex of the Rhesus Monkey. European Journal of Neuroscience 7:1005-1011.

Lemon R (1984) Methods for neuronal recording in conscious animals. New York: Wiley.

Leopold DA, Logothetis NK (1998) Microsaccades differentially modulate neural activity in the striate and extrastriate visual cortex. Experimental Brain Research 123:341-345.

Leotti LA, Wager TD (2010) Motivational influences on response inhibition measures. Journal of Experimental Psychology-Human Perception and Performance 36:430-447.

Lettvin JY, Maturana HR, McCulloch WS, Pitts WH (1959) What the frog's eye tells the frog's brain. Proceedings of the IRE 47:1940-1951.

Levinsohn (1909) Uber die Beziehungen der Grosshimrinde beim Affen zu den Bewegungen des Auges. Graefe Arch Ophthalm 71:313-378.

Lins OG, Picton TW, Berg P, Scherg M (1993a) Ocular artifacts in EEG and event-related potentials I: Scalp topography. Brain Topography 6:51-63.

Lins OG, Picton TW, Berg P, Scherg M (1993b) Ocular artifacts in recording EEGs and event-related potentials II: Source dipoles and source components. Brain Topography 6:65-78.

Liotti M, Pliszka SR, Perez R, Kothmann D, Woldorff MG (2005) Abnormal brain activity related to performance monitoring and error detection in children with ADHD. Cortex 41:377-388.

Lipton ML, Liszewski MC, O'Connell MN, Mills A, Smiley JF, Branch CA, Isler JR, Schroeder CE (2010) Interactions within the Hand Representation in Primary Somatosensory Cortex of Primates. Journal of Neuroscience 30:15895-15903.

Lisberger SG, Morris EJ, Tychsen L (1987) Visual motion processing and sensory-motor integration for smooth pursuit eye movements. Annual Review of Neuroscience 10:97-129.

Lo CC, Boucher L, Paré M, Schall JD, Wang XJ (2009) Proactive inhibitory control and attractor dynamics in countermanding action: A spiking neural circuit model. Journal of Neuroscience 29:9059-9071.

Logan GD (1994) On the ability to inhibit thought and action: A users' guide to the stop signal paradigm. In: Inhibitory processes in attention, memory, and language (Dagenback D, Carr TH, eds), pp 189-239. San Diego: Academic Press.

Logan GD, Cowan WB (1984) On the ability to inhibit thought and action - a theory of an act of control. Psychological Review 91:295-327.

Logan GD, Irwin DE (2000) Don't look! Don't touch! Inhibitory control of eye and hand movements. Psychonomic Bulletin & Review 7:107-112.

Logan GD, Crump MJC (2010) Cognitive illusions of authorship reveal hierarchical error detection in skilled typists. Science 330:683-686.

Logothetis NK (2008) What we can do and what we cannot do with fMRI. Nature 453:869-878.

Logothetis NK, Wandell BA (2004) Interpreting the BOLD signal. Annual Review of Physiology 66:735-769.

Logothetis NK, Kayser C, Oeltermann A (2007) In vivo measurement of cortical impedance spectrum in monkeys: Implications for signal propagation. Neuron 55:809-823.

Lorente de Nó R (1949) Cerebral cortex: architecture, intracortical connections, motor projections. Physiology of the nervous system:288-330.

Lu X, Matsuzawa M, Hikosaka O (2002) A neural correlate of oculomotor sequences in supplementary eye field. Neuron 34:317-325.

Luck SJ (2005) An introduction to the event-related potential technique. Cambridge, MA: MIT Press.

Luppino G, Rozzi S, Calzavara R, Matelli M (2003) Prefrontal and agranular cingulate projections to the dorsal premotor areas F2 and F7 in the macaque monkey. European Journal of Neuroscience 17:559-578.

Luppino G, Matelli M, Camarda RM, Gallese V, Rizzolatti G (1991) Multiple representations of body movements in mesial area 6 and the adjacent cingulate cortex: an intracortical microstimulation study in the macaque monkey. Journal of Comparative Neurology 311:463-482.

Luu P, Pederson SM (2004) The anterior cingulate cortex: regulating actions in context. Cognitive neuroscience of attention:232-244.

Luu P, Collins P, Tucker DM (2000) Mood, personality, and self-monitoring: negative affect and emotionality in relation to frontal lobe mechanisms of error monitoring. Journal of Experimental Psychology: General 129:43.

Luu P, Tucker DM, Derryberry D, Reed M, Poulsen C (2003) Electrophysiological responses to errors and feedback in the process of action regulation. Psychological Science 14:47-53.

Maier A, Aura CJ, Leopold DA (2011) Infragranular sources of sustained local field potential responses in macaque primary visual cortex. The Journal of Neuroscience 31:1971-1980.

Maier AV, Adams GK, Aura C, Leopold DA (2010) Distinct superficial and deep laminar domains of activity in the visual cortex during rest and stimulation. Frontiers in Systems Neuroscience 4:1-11.

Maioli MG, Squatrito S, Samolsky-Dekel BG, Riva Sanseverino E (1998) Corticocortical connections between frontal periarcuate regions and visual areas of the superior temporal sulcus and the adjoining inferior parietal lobule in the macaque monkey. Brain Research 789:118-125.

Mann SE, Thau R, Schiller PH (1988) Conditional task-related responses in monkey dorsomedial frontal cortex. Experimental Brain Research 69:460-468.

Markov NT, Misery P, Falchier A, Lamy C, Vezoli J, Quilodran R, Gariel MA, Giroud P, Ercsey-Ravasz M, Pilaz LJ (2011) Weight consistency specifies regularities of macaque cortical networks. Cerebral Cortex 21:1254-1272.

Markram H (2006) The blue brain project. Nature Reviews Neuroscience 7:153-160.

Martinez-Conde S, Macknik SL, Hubel DH (2000) Microsaccadic eye movements and firing of single cells in the striate cortex of macaque monkeys. Nature Neuroscience 3:251-258.

Martinez-Conde S, Macknik SL, Hubel DH (2002) The function of bursts of spikes during visual fixation in the awake primate lateral geniculate nucleus and primary visual cortex. Proceedings of the National Academy of Sciences 99:13920-13925.

Martinez-Conde S, Macknik SL, Troncoso XG, Dyar TA (2006) Microsaccades counteract visual fading during fixation. Neuron 49:297-305.

Martinez-Conde S, Macknik SL, Troncoso XG, Hubel DH (2009) Microsaccades: a neurophysiological analysis. Trends in Neurosciences 32:463-475.

Martinez-Trujillo JC, Medendorp WP, Wang H, Crawford JD (2004) Frames of reference for eye-head gaze commands in primate supplementary eye fields. Neuron 44:1057-1066.

Masaki H, Falkenstein M, Stürmer B, Pinkpank T, Sommer W (2007) Does the error negativity reflect response conflict strength? Evidence from a Simon task. Psychophysiology 44:579-585.

Matelli M, Luppino G, Rizzolatti G (1991) Architecture of superior and mesial area-6 and the adjacent cingulate cortex in the macaque monkey. Journal of Comparative Neurology 311:445-462.

Mathalon DH, Whitfield SL, Ford JM (2003) Anatomy of an error: ERP and fMRI. Biological Psychology 64:119-141.

Mathewson KJ, Dywan J, Segalowitz SJ (2005) Brain bases of error-related ERPs as influenced by age and task. Biological Psychology 70:88-104.

Matsumoto M, Hikosaka O (2007) Lateral habenula as a source of negative reward signals in dopamine neurons. Nature 447:1111-1115.

Matsumoto M, Matsumoto K, Abe H, Tanaka K (2007) Medial prefrontal cell activity signaling prediction errors of action values. Nature Neuroscience 10:647-656.

Matzke D, Dolan CV, Logan GD, Brown SD, Wagenmakers EJ (2012) Bayesian Parametric Estimation of Stop-Signal Reaction Time Distributions. Journal of Experimental Psychology.

Maunsell JH, Gibson JR (1992) Visual response latencies in striate cortex of the macaque monkey. Journal of Neurophysiology 68:1332-1344.

May JG, Andersen RA (1986) Different patterns of corticopontine projections from separate cortical fields within the inferior parietal lobule and dorsal prelunate gyrus of the macaque. Experimental Brain Research 63:265-278.

McGarry T, Franks IM (1997) A horse race between independent processes: Evidence for a phantom point of no return in the preparation of a speeded motor response. Journal of Experimental Psychology-Human Perception and Performance 23:1533-1542.

McGarry T, Inglis JT, Franks IM (2000) Against a final ballistic process in the control of voluntary action: Evidence using the Hoffmann reflex. Motor Control 4:469-485.

McHaffie JG, Stein BE (1982) Eye movements evoked by electrical stimulation in the superior colliculus of rats and hamsters. Brain Research 247:243-253.

McPeek RM, Keller EL (2002) Superior colliculus activity related to concurrent processing of saccade goals in a visual search task. Journal of Neurophysiology 87:1805-1815.

McPeek RM, Keller EL (2004) Deficits in saccade target selection after inactivation of superior colliculus. Nature Neuroscience 7:757-763.

Menon V, Adleman NE, White CD, Glover GH, Reiss AL (2001) Error-related brain activation during a Go/NoGo response inhibition task. Human Brain Mapping 12:131-143.

Miltner WHR, Braun CH, Coles MGH (1997) Event-related brain potentials following incorrect feedback in a time-estimation task: Evidence for a "generic" neural system for error detection. Journal of Cognitive Neuroscience 9:788-798.

Mitchell JF, Sundberg KA, Reynolds JH (2007) Differential attention-dependent response modulation across cell classes in macaque visual area V4. Neuron 55:131-141.

Mitz AR, Wise SP (1987) The somatotopic organization of the supplementary motor area: intracortical microstimulation mapping. The Journal of Neuroscience 7:1010-1021.

Mitz AR, Godschalk M (1989) Eye-movement representation in the frontal lobe of rhesus monkeys. Neuroscience Letters 106:157-162.

Mitzdorf U (1985) Current source-density method and application in cat cerebral-cortex - Investigation of evoked-potentials and EEG phenomena. Physiological Reviews 65:37-100.

Mitzdorf U, Singer W (1979) Excitatory synaptic ensemble properties in the visual-cortex of the macaque monkey - Current source density analysis of electrically evoked-potentials. Journal of Comparative Neurology 187:71-83.

Mohler CW, Wurtz RH (1977) Role of striate cortex and superior colliculus in visual guidance of saccadic eye movements in monkeys. Journal of Neurophysiology 40:74-94.

Moorman DE, Olson CR (2007) Combination of neuronal signals representing object-centered location and saccade direction in macaque supplementary eye field. Journal of Neurophysiology 97:3554-3566.

Morein-Zamir S, Kingstone A (2006) Fixation offset and stop signal intensity effects on saccadic countermanding: a crossmodal investigation. Experimental Brain Research 175:453-462.

Moschovakis AK, Scudder CA, Highstein SM (1996) The microscopic anatomy and physiology of the mammalian saccadic system. Progress in Neurobiology 50:133-254.

Moster ML, Goldberg G (1990) Topography of scalp potentials preceding self-initiated saccades. Neurology 40:644-648.

Mott FW, Schaefer EA (1890) On associated eye-movements produced by cortical faradization of the monkey’s brain. Brain 13:165-173.

Mountcastle VB (1957) Modality and topographic properties of single neurons of cat's somatic sensory cortex. J neurophysiol 20:408-434.

Mountcastle VB (1997) The columnar organization of the neocortex. Brain 120:701-722.

Munoz DP, Guitton D (1991) Control of orienting gaze shifts by the tectoreticulospinal system in the head-free cat. II. Sustained discharges during motor preparation and fixation. J Neurophysiol 66:1624-1641.

Munoz DP, Wurtz RH (1993a) Fixation cells in monkey superior colliculus. I. Characteristics of cell discharge. Journal of Neurophysiology 70:559–575.

Munoz DP, Wurtz RH (1993b) Fixation cells in monkey superior colliculus .2. reversible activation and deactivation. Journal of Neurophysiology 70:576-589.

Munoz DP, Wurtz RH (1995) Saccade-related activity in monkey superior colliculus. I. Characteristics of burst and buildup cells. Journal of Neurophysiology 73:2313-2333.

Munoz DP, Schall JD (2004) Concurrent, distributed control of saccade initiation in the frontal eye field and superior colliculus. In: The Superior Colliculus: New Approaches For Studying Sensorimotor Integration (Hall WC, Moschovakis AK, eds), pp 55-82. Boca Raton, FL: CRC Press.

Munoz DP, Everling S (2004) Look away: the anti-saccade task and the voluntary control of eye movement. Nature Reviews Neuroscience 5:218-228.

Munoz DP, Waitzman DM, Wurtz RH (1996) Activity of neurons in monkey superior colliculus during interrupted saccades. Journal of Neurophysiology 75:2562-2580.

Munoz DP, Dorris MC, Pare M, Everling S (2000) On your mark, get set: Brainstem circuitry underlying saccadic initiation. Canadian Journal of Physiology and Pharmacology 78:934-944.

Murthy A, Ray S, Shorter SM, Schall JD, Thompson KG (2009) Neural control of visual search by frontal eye field: effects of unexpected target displacement on visual selection and saccade preparation. Journal of Neurophysiology 101:2485-2506.

Murthy A, Ray S, Shorter SM, Priddy EG, Schall JD, Thompson KG (2007) Frontal eye field contributions to rapid corrective Saccades. Journal of Neurophysiology 97:1457-1469.

Nakamura K, Roesch MR, Olson C R (2005) Neuronal activity in macaque SEF and ACC during performance of tasks involving conflict. Journal of Neurophysiology 93:884–908. .

Neggers SFW, Huijbers W, Vrijlandt CM, Vlaskamp BNS, Schutter DJLG, Kenemans JL (2007) TMS pulses on the frontal eye fields break coupling between visuospatial attention and eye movements. Journal of Neurophysiology 98:2765-2778.

Neggers SFW, van Diepen RM, Zandbelt BB, Vink M, Mandl RCW, Gutteling TP (2012) A functional and structural investigation of the human fronto-basal volitional saccade network. Plos One 7.

Nelson MJ, Boucher L, Logan GD, Palmeri TJ, Schall JD (2010) Nonindependent and nonstationary response times in stopping and stepping saccade tasks. Attention, Perception & Psychophysics 72:1913-1929.

Nicholson C, Freeman JA (1975) Theory of current source-density analysis and determination of conductivity tensor for anuran cerebellum. Journal of Neurophysiology 38:356-368.

Nieuwenhuis S, Holroyd CB, Mol N, Coles MGH (2004) Reinforcement-related brain potentials from medial frontal cortex: origins and functional significance. Neuroscience and Biobehavioral Reviews 28:441-448.

Nieuwenhuis S, Ridderinkhof KR, Blow J, Band GPH, Kok A (2001) Error-related brain potentials are differentially related to awareness of response errors: Evidence from an antisaccade task. Psychophysiology 38:752-760.

Nieuwenhuis S, Ridderinkhof KR, Talsma D, Coles MGH, Holroyd CB, Kok A, Van der Molen MW (2002) A computational account of altered error processing in older age: dopamine and the error-related negativity. Cognitive, Affective, & Behavioral Neuroscience 2:19-36.

Niki H, Watanabe M (1979) Prefrontal and cingulate unit-activity during timing behavior in the monkey. Brain Research 171:213-224.

Norman DA, Shallice T (1980) Attention to action: Willed and automatic control of behavior. In: DTIC Document.

Nosofsky RM, Palmeri TJ (1997) An exemplar-based random walk model of speeded classification. Psychological Review; Psychological Review 104:266.

Nouraei SAR, de Pennington N, Jones JG, Carpenter RHS (2003) Dose-related effect of sevoflurane sedation on higher control of eye movements and decision making. British Journal of Anaesthesia 91:175-183.

Nunez Castellar E, Kuhn S, Fias W, Notebaert W (2010) Outcome expectancy and not accuracy determines posterror slowing: ERP support. Cognitive Affective & Behavioral Neuroscience 10:270-278.

Nunez PL, Srinivasan R (2006) Electric fields of the brain: the neurophysics of EEG: Oxford University Press.

Ohmae S, Lu X, Takahashi T, Uchida Y, Kitazawa S (2008) Neuronal activity related to anticipated and elapsed time in macaque supplementary eye field. Experimental Brain Research 184:593-598.

Oliveira FTP, McDonald JJ, Goodman D (2007) Performance monitoring in the anterior cingulate is not all error related: expectancy deviation and the representation of action-outcome associations. Journal of Cognitive Neuroscience 19:1994-2004.

Olsen SR, Bortone DS, Adesnik H, Scanziani M (2012) Gain control by layer six in cortical circuits of vision. Nature 483:47-52.

Olson CR, Gettner SN (1995) Object-centered direction selectivity in the macaque supplementary eye field. Science 269:985-988.

Olson CR, Gettner SN (1999) Macaque SEF neurons encode object-centered directions of eye movements regardless of the visual attributes of instructional cues. Journal of Neurophysiology 81:2340-2346.

Olson CR, Gettner SN (2002) Neuronal activity related to rule and conflict in macaque supplementary eye field. Physiology & behavior 77:663-670.

Olvet DM, Hajcak G (2009) The stability of error-related brain activity with increasing trials. Psychophysiology 46:957-961.

Optican LM, Robinson DA (1980) Cerebellar-dependent adaptive control of primate saccadic system. Journal of Neurophysiology 44:1058-1076.

Ottes FP, Van Gisbergen JAM, Eggermont JJ (1986) Visuomotor fields of the superior colliculus: a quantitative model. Vision Research 26:857-873.

Overbeek TrsJM, Nieuwenhuis S, Ridderinkhof KR (2005) Dissociable components of error processing: On the functional significance of the Pe vis-à-vis the ERN/Ne. Journal of Psychophysiology 19:319.

Ozyurt J, Colonius H, Arndt PA (2003) Countermanding saccades: Evidence against independent processing of go and stop signals. Perception & Psychophysics 65:420-428.

Papez JW (1937) A proposed mechanism of emotion. Archives of Neurology and Psychiatry 38:725.

Pardo JV, Pardo PJ, Janer KW, Raichle ME (1990) The anterior cingulate cortex mediates processing selection in the Stroop attentional conflict paradigm. Proceedings of the National Academy of Sciences 87:256-259.

Paré M, Guitton D (1994) The fixation area of the cat superior colliculus - effects of electrical-stimulation and direct connection with brain-stem omnipause neuron. Experimental Brain Research 101:109-122.

Paré M, Hanes DP (2003) Controlled movement processing: Superior colliculus activity associated with countermanded saccades. Journal of Neuroscience 23:6480-6489.

Pascual-Marqui RD (2002) Standardized low-resolution brain electromagnetic tomography (sLORETA): Technical details. Methods and Findings in Experimental and Clinical Pharmacology 24:5-12.

Passingham RE, Bengtsson SL, Lau HC (2010) Medial frontal cortex: from self-generated action to reflection on one's own performance. Trends in Cognitive Sciences 14:16-21.

Paus T (1996) Location and function of the human frontal eye-field: a selective review. Neuropsychologia 34:475-483.

Paus T, Petrides M, Evans AC, Meyer E (1993) Role of the human anterior cingulate cortex in the control of oculomotor, manual, and speech responses: a positron emission tomography study. Journal of Neurophysiology 70:453–469.

Paxinos G, Huang X-F, Toga AW (2000) The rhesus monkey brain in stereotaxic coordinates. San Diego, CA: Academic Press

Pennartz C (1995) The ascending neuromodulatory systems in learning by reinforcement: Comparing computational conjectures with experimental findings. Brain Research Reviews 21:219-245.

Petersen CCH, Crochet S (2013) Synaptic computation and sensory processing in neocortical layer 2/3. Neuron 78:28-48.

Pettersen KH, Devor A, Ulbert I, Dale AM, Einevoll GT (2006) Current-source density estimation based on inversion of electrostatic forward solution: effects of finite extent of neuronal activity and conductivity discontinuities. Journal of Neuroscience Methods 154:116-133.

Phillips JM, Johnston K, Everling S (2010) Effects of anterior cingulate microstimulation on pro-and antisaccades in nonhuman primates. Journal of Cognitive Neuroscience 23:481-490.

Picton TW, van Roon P, Armilio ML, Berg P, Ille N, Scherg M (2000) Blinks, saccades, extraocular muscles and visual evoked potentials (reply to Verleger). Journal of Psychophysiology 14:210-217.

Platt JR (1964) Strong inference. Science 146:347-353.

Platt ML, Glimcher PW (1999) Neural correlates of decision variables in parietal cortex. Nature 400:233-238.

Pochon J-B, Riis J, Sanfey AG, Nystrom LE, Cohen JD (2008) Functional imaging of decision conflict. The Journal of Neuroscience 28:3468-3473.

Porter JD, Andrade FH, Baker RS (2003) The extraocular muscles. In: Adler's physiology of the eye, 10 Edition (Kaufman PL, Alm A, eds), pp 787-817. St. Louis: Mosby.

Posner MI (1980) Orienting of attention. Quarterly Journal of Experimental Psychology 32:3-25.

Posner MI, Cohen Y (1984) Components of visual orienting. In: Attention and performance (Bouma H, Bouwhuis D, eds), pp 531-556: Erlbaum.

Posner MI, Petersen SE, Fox PT, Raichle ME (1988) Localization of cognitive operations in the human brain. Science 240:1627-1631.

Potts GF, Martin LE, Burton P, Montague PR (2006) When things are better or worse than expected: the medial frontal cortex and the allocation of processing resources. Journal of Cognitive Neuroscience 18:1112-1119.

Pouget P, Emeric EE, Stuphorn V, Reis K, Schall JD (2005) Chronometry of visual responses in frontal eye field, supplementary eye field, and anterior cingulate cortex. Journal of Neurophysiology 94:2086-2092.

Pouget P, Logan GD, Palmeri TJ, Boucher L, Paré M, Schall JD (2011) Neural basis of adaptive response time adjustment during saccade countermanding. Journal of Neuroscience 31:12604-12612.

Pouget P, Stepniewska I, Crowder EA, Leslie MW, Emeric EE, Nelson MJ, Schall JD (2009) Visual and motor connectivity and the distribution of calcium-binding proteins in macaque frontal eye field: implications for saccade target selection. Frontiers in Neuroanatomy 3.

Powell TP, Mountcastle VB (1959) Some aspects of the functional organization of the cortex of the postcentral gyrus of the monkey: a correlation of findings obtained in a single unit analysis with cytoarchitecture. Bulletin of the Johns Hopkins Hospital 105:133.

Purcell BA, Weigand PK, Schall JD (2012a) Supplementary eye field during visual search: salience, cognitive control, and performance monitoring. The Journal of Neuroscience 32:10273-10285.

Purcell BA, Schall JD, Logan GD, Palmeri TJ (2012b) From salience to saccades: multiple-alternative gated stochastic accumulator model of visual search. The Journal of Neuroscience 32:3433-3446.

Purcell BA, Heitz RP, Cohen JY, Schall JD, Logan GD, Palmeri TJ (2010) Neurally constrained modeling of perceptual decision making. Psychological Review 117:1113.

Quaia C, Optican LM (2003) Three-dimensional rotations of the eye. In: Adler's physiology of the eye (Kaufman PL, Alm A, eds), pp 818-829. St. Louis: Mosby.

Quaia C, Ying HS, Optican LM (2009) The viscoelastic properties of passive eye muscle in primates. III: force elicited by natural elongations. PLoS One 5:A236-A254.

Quilodran R, Rothe M, Procyk E (2008) Behavioral shifts and action valuation in the anterior cingulate cortex. Neuron 57:314-325.

Rabbitt P, Rodgers B (1977) What does a man do after he makes an error? An analysis of response programming. The Quarterly Journal of Experimental Psychology 29:727-743.

Rabbitt PM (1966) Errors and error correction in choice-response tasks. Journal of Experimental Psychology 71:264.

Rafal RD, Calabresi PA, Cameron CW, Sciolto TK (1989) Saccade preparation inhibits reorienting to recently attended locations. Journal of Experimental Psychology: Human Perception and Performance 15:673-685.

Raiguel SE, Xiao DK, Marcar VL, Orban GA (1999) Response latency of macaque area MT/V5 neurons and its relationship to stimulus parameters. Journal of Neurophysiology 82:1944-1956.

Ratcliff R, Rouder JN (1998) Modeling response times for two-choice decisions. Psychological Science 9:347-356.

Ray S, Pouget P, Schall JD (2009) Functional distinction between visuomovement and movement neurons in macaque frontal eye field during saccade countermanding. Journal of Neurophysiology 102:3091-3100.

Rayner K (1998) Eye movements in reading and information processing: 20 years of research. Psychological bulletin 124:372.

Rayner K, Pollatsek AW (1989) The psychology of reading. Englewood Cliffs, NJ: Prentice Hall.

Reader T, Ferron A, Descarries L, Jasper HH (1979) Modulatory role for biogenic amines in the cerebral cortex. Microiontophoretic studies. Brain Research 160:217-229.

Redgrave P, Prescott TJ, Gurney K (1999a) The basal ganglia: A vertebrate solution to the selection problem? Neuroscience 89:1009-1023.

Redgrave P, Prescott TJ, Gurney K (1999b) Is the short-latency dopamine response too short to signal reward error? Trends in Neurosciences 22:146-151.

Reinhart RMG, Carlisle NB, Kang MS, Woodman GF (2012) Event-related potentials elicited by errors during the stop-signal task. II: Human effector specific error responses. J Neurophysiol.

Rescorla RA, Wagner AR (1972) A theory of Pavlovian conditioning: Variations in the effectiveness of reinforcement and nonreinforcement. Classical conditioning II: Current research and theory:64-99.

Riba J, Rodriguez-Fornells A, Munte TF, Barbanoj MJ (2005a) A neurophysiological study of the detrimental effects of alprazolam on human action monitoring. Cognitive Brain Research 25:554-565.

Riba J, Rodriguez-Fornells A, Morte A, Munte TF, Barbanoj MJ (2005b) Noradrenergic stimulation enhances human action monitoring. Journal of Neuroscience 25:4370-4374.

Richardson NR, Gratton A (1998) Changes in medial prefrontal cortical dopamine levels associated with response-contingent food reward: an electrochemical study in rat. The Journal of Neuroscience 18:9130-9138.

Ridderinkhof KR, Ullsperger M, Crone EA, Nieuwenhuiss S (2004) The role of the medial frontal cortex in cognitive control. Science 306:443-447.

Ridderinkhof KR, de Vlugt Y, Bramlage A, Spaan M, Elton M, Snel J, Band GPH (2002) Alcohol consumption impairs detection of performance errors in mediofrontal cortex. Science 298:2209-2211.

Riemslag FCC, Vanderheijde GL, Vandongen MMMM, Ottenhoff F (1988) On the origin of the presaccadic spike potential. Electroencephalography and Clinical Neurophysiology 70:281-287.

Riera JJ, Ogawa T, Goto T, Sumiyoshi A, Nonaka H, Evans A, Miyakawa H, Kawashima R (2012) Pitfalls in the dipolar model for the neocortical EEG sources. Journal of Neurophysiology 108:956-975.

Riggs LA, Armington JC, Ratliff F (1954) Motions of the retinal image during fixation. Journal of the Optical Society of America 44:315-321.

Robinson DA (1964) The mechanics of human saccadic eye movement. Journal of Physiology 174:245-264.

Robinson DA (1970) Oculomotor unit behavior in monkey. Journal of Neurophysiology 33:393-&.

Robinson DA (1972) Eye-movements evoked by collicular stimulation in alert monkey. Vision Research 12:1795-1808.

Robinson DA, Fuchs AF (1969) Eye movements evoked by stimulation of frontal eye fields. Journal of Neurophysiology.

Robinson DL, McClurkin JW (1989) The visual superior colliculus and pulvinar. In: The neurobiology of saccadic eye movements (Wurtz RH, Goldberg ME, eds), pp 337-356. Amsterdam: Elsevier.

Rockel AJ, Hiorns RW, Powell TPS (1980) The basic uniformity in structure of the neocortex. Brain 103:221-244.

Rockland KS (2009) Five points on columns. Frontiers in Neuroanatomy 4.

Rockland KS, Pandya DN (1979) Laminar origins and terminations of cortical connections of the occipital lobe in the rhesus monkey. Brain Research 179:3-20.

Rockland KS, Ichinohe N (2004) Some thoughts on cortical minicolumns. Experimental Brain Research 158:265-277.

Rodriguez-Fornells A, Kurzbuch AR, Munte TF (2002) Time course of error detection and correction in humans: Neurophysiological evidence. Journal of Neuroscience 22:9990-9996.

Roesch MR, Olson CR (2003) Impact of expected reward on neuronal activity in prefrontal cortex, frontal and supplementary eye fields and premotor cortex. Journal of Neurophysiology 90:1766-1789.

Rolfs M, Kliegl R, Engbert R (2008) Toward a model of microsaccade generation: The case of microsaccadic inhibition. Journal of Vision 8:1-23.

Rushworth MFS, Hadland KA, Gaffan D, Passingham RE (2003) The effect of cingulate cortex lesions on task switching and working memory. Journal of Cognitive Neuroscience 15:338-353.

Rushworth MFS, Walton ME, Kennerley SW, Bannerman DM (2004) Action sets and decisions in the medial frontal cortex. Trends in Cognitive Sciences 8:410-417.

Russo GS, Bruce CJ (1993) Effect of eye position within the orbit on electrically elicited saccadic eye movements: a comparison of the macaque monkey's frontal and supplementary eye fields. Journal of Neurophysiology 69:800-818.

Russo GS, Bruce CJ (1996) Neurons in the supplementary eye field of rhesus monkeys code visual targets and saccadic eye movements in an oculocentric coordinate system. Journal of Neurophysiology 76:825-848.

Russo GS, Bruce CJ (2000) Supplementary eye field: representation of saccades and relationship between neural response fields and elicited eye movements. Journal of Neurophysiology 84:2605-2621.

Sander V, Soper B, Everling S (2010) Nonhuman primate event-related potentials associated with pro- and anti-saccades. Neuroimage 49:1650-1658.

Saslow MG (1967) Effects of components of displacement-step stimuli upon latency for saccadic eye movement. Journal of the Optical Society of America 57:1024-1029.

Sato T, Murthy A, Thompson KG, Schall JD (2001) Search efficiency but not response interference affects visual selection in frontal eye field. Neuron 30:583-591.

Scangos KW, Stuphorn V (2010) Medial frontal cortex motivates but does not control movement initiation in the countermanding task. Journal of Neuroscience 30:1968-1982.

Schaefer KP (1970) Unit analysis and electrical stimulation in the optic tectum of rabbits and cats. Brain, Behavior and Evolution 3:222-240.

Schafer RJ, Moore T (2011) Selective attention from voluntary control of neurons in prefrontal cortex. Science 332:1568-1571.

Schall JD (1991a) Neuronal activity related to visually guided saccadic eye movements in the supplementary motor area of rhesus monkeys. Journal of Neurophysiology 66:530-558.

Schall JD (1991b) Neuronal-activity related to visually guided saccades in the frontal eye fields of rhesus-monkeys - comparison with supplementary eye fields. Journal of Neurophysiology 66:559-579.

Schall JD (1995) Neural basis of saccade target selection. Reviews in the Neurosciences 6:63-85.

Schall JD (2004) On the role of frontal eye field in guiding attention and saccades. Vision Research 44:1453-1467.

Schall JD, Hanes DP (1993) Neural basis of saccade target selection in frontal eye field during visual search. Nature 366:467-469.

Schall JD, Boucher L (2007) Executive control of gaze by the frontal lobes. Cognitive Affective & Behavioral Neuroscience 7:396-412.

Schall JD, Emeric EE (2010) Conflict in cingulate cortex function between humans and macaque monkeys: more apparent than real. Comment on "Cingulate cortex: diverging data from humans and monkeys. Brain, Behavior and Evolution 75:237–238.

Schall JD, Godlove DC (2012) Current advances and pressing problems in studies of stopping. Current Opinion in Neurobiology.

Schall JD, Morel A, Kaas JH (1993) Topography of supplementary eye field afferents to frontal eye field in macaque: implications for mapping between saccade coordinate systems. Visual Neuroscience 10:385-393.

Schall JD, Stuphorn V, Brown JW (2002) Monitoring and control of action by the frontal lobes. Neuron 36:309-322.

Schall JD, Morel A, King DJ, Bullier J (1995) Topography of visual cortex connections with frontal eye field in macaque: convergence and segregation of processing streams. The Journal of Neuroscience 15:4464-4487.

Schall JD, Purcell BA, Heitz RP, Logan GD, Palmeri TJ (2012) Neural mechanisms of saccade target selection: gated accumulator model of the visualâ€“motor cascade. European Journal of Neuroscience 33:1991-2002.

Schiller PH, True SD, Conway JL (1979) Effects of frontal eye field and superior colliculus ablations on eye movements. Science 206:590-592.

Schiller PH, True SD, Conway JL (1980) Deficits in eye movements following frontal eye-field and superior colliculus ablations. Journal of Neurophysiology 44:1175-1189.

Schlag-Rey M, Amador N, Sanchez H, Schlag J (1997) Antisaccade performance predicted by neuronal activity in the supplementary eye field. Nature 390:398-401.

Schlag J, Schlag-Rey M (1987) Evidence for a Supplementary Eye Field. Journal of Neurophysiology 57:179-200.

Schlag J, Schlag-Rey M, Pigarev I (1992) Supplementary eye field: influence of eye position on neural signals of fixation. Experimental Brain Research 90:302-306.

Schmahmann JD, Pandya DN (1989) Anatomical investigation of projections to the basis pontis from posterior parietal association cortices in rhesus-monkey. Journal of Comparative Neurology 289:53-73.

Schnyder H, Reisine H, Hepp K, Henn V (1985) Frontal eye field projection to the paramedian pontine reticular formation traced with wheat germ agglutinin in the monkey. Brain Research 329:151-160.

Schroeder CE, Mehta AD, Givre SJ (1998) A spatiotemporal profile of visual system activation revealed by current source density analysis in the awake macaque. Cerebral Cortex 8:575-592.

Schroeder CE, Tenke CE, Arezzo JC, Vaughan Jr HG (1989) Timing and distribution of flash-evoked activity in the lateral geniculate nucleus of the alert monkey. Brain Research 477:183-195.

Schultz W (1998) Predictive reward signal of dopamine neurons. Journal of Neurophysiology 80:1-27.

Schultz W (2013) Updating dopamine reward signals. Current Opinion in Neurobiology 23:229-238.

Schultz W, Apicella P, Ljungberg T (1993) Responses of monkey dopamine neurons to reward and conditioned stimuli during successive steps of learning a delayed response task. The Journal of Neuroscience 13:900-913.

Schultz W, Dayan P, Montague PR (1997) A neural substrate of prediction and reward. Science 275:1593-1599.

Scudder CA, Kaneko CRS, Fuchs AF (2002) The brainstem burst generator for saccadic eye movements - A modern synthesis. Experimental Brain Research 142:439-462.

Seamans JK, Yang CR (2004) The principal features and mechanisms of dopamine modulation in the prefrontal cortex. Progress in neurobiology 74:1-58.

Segraves MA (1992) Activity of monkey frontal eye field neurons projecting to oculomotor regions of the pons. Journal of Neurophysiology 68:1967-1985.

Segraves MA, Goldberg ME (1987) Functional-properties of corticotectal neurons in the monkeys frontal eye field. Journal of Neurophysiology 58:1387-1419.

Seo H, Lee D (2007) Temporal filtering of reward signals in the dorsal anterior cingulate cortex during a mixed-strategy game. The Journal of Neuroscience 27:8366-8377.

Seo H, Lee D (2009) Behavioral and neural changes after gains and losses of conditioned reinforcers. The Journal of Neuroscience 29:3627-3641.

Seth AK (2010) A MATLAB toolbox for Granger causal connectivity analysis. Journal of Neuroscience Methods 186:262-273.

Sharp DJ, Bonnelle V, De Boissezon X, Beckmann CF, James SG, Patel MC, Mehta MA (2010) Distinct frontal systems for response inhibition, attentional capture, and error processing. Proceedings of the National Academy of Sciences of the United States of America 107:6106-6111.

Shima K, Tanji J (1998) Role for cingulate motor area cells in voluntary movement selection based on reward. Science 282:1335-1338.

Shinoda Y, Sugiuchi Y, Takahashi M, Izawa Y (2011) Neural substrate for suppression of omnipause neurons at the onset of saccades. Annals of the New York Academy of Sciences 1233:100-106.

Shipp S (2005) The importance of being agranular: a comparative account of visual and motor cortex. Philosophical Transactions of the Royal Society B: Biological Sciences 360:797-814.

Shipp S, Blanton M, Zeki S (1998) A visuo-somatomotor pathway through superior parietal cortex in the macaque monkey: cortical connections of areas V6 and V6A. European Journal of Neuroscience 10:3171-3193.

Shook BL, Schlag-Rey M, Schlag J (1988) Direct projection from the supplementary eye field to the nucleus raphe interpositus. Experimental Brain Research 73:215-218.

Shook BL, Schlagrey M, Schlag J (1990) Primate supplementary eye field .1. comparative aspects of mesencephalic and pontine connections. Journal of Comparative Neurology 301:618-642.

Silberberg G, Gupta A, Markram H (2002) Stereotypy in neocortical microcircuits. Trends in Neurosciences 25:227-230.

Sklavos S, Porrill J, Kaneko CRS, Dean P (2005) Evidence for wide range of time scales in oculomotor plant dynamics: Implications for models of eye-movement control. Vision Research 45:1525-1542.

Smith MA, Sommer MA (2013) Spatial and Temporal Scales of Neuronal Correlation in Visual Area V4. The Journal of Neuroscience 33:5422-5432.

Snodderly D, Kagan I, Gur M (2001) Selective activation of visual cortex neurons by fixational eye movements: Implications for neural coding. Visual Neuroscience 18:259-277.

So NY, Stuphorn V (2010) Supplementary eye field encodes option and action value for saccades with variable reward. Journal of Neurophysiology 104:2634-2653.

Sommer MA, Wurtz RH (2002) A pathway in primate brain for internal monitoring of movements. Science 296:1480-1482.

Sommer MA, Wurtz RH (2008) Brain circuits for the internal monitoring of movements. Annual review of neuroscience 31:317.

Spaak E, Bonnefond M, Maier A, Leopold DA, Jensen O (2012) Layer-specific entrainment of gamma-band neural activity by the alpha rhythm in monkey visual cortex. Current Biology.

Sparks DL (2002) The brainstem control of saccadic eye movements. Nature Reviews Neuroscience 3:952-964.

Sparks DL, Hartwich-Young R (1989) The deep layers of the superior colliculus. In: The neurobiology of saccadic eye movements (Wurtz RH, Goldberg ME, eds), pp 213-245. Amsterdam: Elsevier.

Stahl J, Gibbons H (2007) Dynamics of response-conflict monitoring and individual differences in response control and behavioral control: an electrophysiological investigation using a stop-signal task. Clinical Neurophysiology 118:581-596.

Stanton GB, Goldberg ME, Bruce CJ (1988) Frontal eye field efferents in the macaque monkey .2. topography of terminal fields in midbrain and pons. Journal of Comparative Neurology 271:493-506.

Stanton GB, Bruce CJ, Goldberg ME (1993) Topography of projections to the frontal lobe from the macaque frontal eye fields. Journal of Comparative Neurology 330:286-301.

Stanton GB, Bruce CJ, Goldberg ME (1995) Topography of projections to posterior cortical areas from the macaque frontal eye fields. Journal of Comparative Neurology 353:291-305.

Stanton GB, Deng SY, Goldberg EM, McMullen NT (1989) Cytoarchitectural characteristic of the frontal eye fields in macaque monkeys. Journal of Comparative Neurology 282:415-427.

Stein BE, Meredith MA (1993) The merging of the senses. Cambridge, MA: MIT Press.

Stein BE, Stanford TR (2008) Multisensory integration: current issues from the perspective of the single neuron. Nature Reviews Neuroscience 9:255-266.

Steinman RM, Haddad GM, Skavenski AA, Wyman D (1973) Miniature eye movement. Science 181:810-819.

Stemmer B, Segalowitz SJ, Witzke W, Schönle PW (2004) Error detection in patients with lesions to the medial prefrontal cortex: an ERP study. Neuropsychologia 42:118-130.

Stemmers B, Segalowitz, S.J., Witzke, W., Lacher, S., Schönle, P.W., (2000) Do patients with damage to the anterior cingulate and adjacent regions produce an error-related negativity (ERN)? Psychophysiology 37:S95.

Stevenson SA, Elsley JK, Corneil BD (2009) A "gap effect" on stop signal reaction times in a human saccadic countermanding task. Journal of Neurophysiology 101:580-590.

Stroop JR (1935) Studies of interference in serial verbal reactions. Journal of experimental psychology 18:643.

Stuphorn V, Schall JD (2006) Executive control of countermanding saccades by the supplementary eye field. Nature Neuroscience 9:925-931.

Stuphorn V, Emeric EE (2012) Proactive and reactive control by the medial frontal cortex. Frontiers in Neuroengineering 5.

Stuphorn V, Taylor TL, Schall JD (2000) Performance monitoring by the supplementary eye field. Nature 408:857-860.

Stuphorn V, Brown JW, Schall JD (2010) Role of supplementary eye field in saccade initiation: executive, not direct, control. Journal of Neurophysiology 103:801-816.

Sugiuchi Y, Izawa Y, Takahashi M, Na J, Shinoda Y (2007) Controversy on "fixation zone" of the superior colliculus. Neuro-Ophthalmology 31:147-155.

Sutton RS, Barto AG (1998) Reinforcement learning: An introduction: Cambridge Univ Press.

Swick D, Turken U (2002) Dissociation between conflict detection and error monitoring in the human anterior cingulate cortex. Proceedings of the National Academy of Sciences 99:16354-16359.

Syka J, Radil-Weiss T (1971) Electrical stimulation of the tectum in freely moving cats. Brain Research 28:567-572.

Sylvestre PA, Choi JTL, Cullen KE (2003) Discharge dynamics of oculomotor neural integrator neurons during conjugate and disjunctive saccades and fixation. Journal of Neurophysiology 90:739-754.

Szentagothai J (1978) The Ferrier lecture, 1977: the neuron network of the cerebral cortex: a functional interpretation. Proceedings of the Royal Society of London Series B, Biological Sciences:219-248.

Takagi M, Zee DS, Tamargo RJ (1998) Effects of lesions of the oculomotor vermis on eye movements in primate: saccades. Journal of Neurophysiology 80:1911-1931.

Taylor SF, Stern ER, Gehring WJ (2007) Neural systems for error monitoring: Recent findings and theoretical perspectives. Neuroscientist 13:160-172.

Tehovnik EJ, Yeomans JS (1986) Two converging brainstem pathways mediating circling behavior. Brain Research 385:329-342.

Tehovnik EJ, Lee K (1993) The dorsomedial frontal cortex of the rhesus monkey: topographic representation of saccades evoked by electrical stimulation. Experimental Brain Research 96:430-442.

Tehovnik EJ, Lee K, Schiller PH (1994) Stimulation-evoked saccades from the dorsomedial frontal cortex of the rhesus monkey following lesions of the frontal eye fields and superior colliculus. Experimental Brain Research 98:179-190.

Tehovnik EJ, Slocum WM, Schiller PH (1999) Behavioural conditions affecting saccadic eye movements elicited electrically from the frontal lobes of primates. European Journal of Neuroscience 11:2431-2443.

Tehovnik EJ, Slocum WM, Tolias AS, Schiller PH (1998) Saccades induced electrically from the dorsomedial frontal cortex: evidence for a head-centered representation. Brain Research 795:287-291.

Thickbroom GW, Mastaglia FL (1985) Presaccadic spike potential - investigation of topography and source. Brain Research 339:271-280.

Thompson KG, Hanes DP, Bichot NP, Schall JD (1996) Perceptual and motor processing stages identified in the activity of macaque frontal eye field neurons during visual search. Journal of Neurophysiology 76:4040-4055.

Thomson AM, West DC, Wang Y, Bannister AP (2002) Synaptic connections and small circuits involving excitatory and inhibitory neurons in layers 2-5 of adult rat and cat neocortex: triple intracellular recordings and biocytin labelling in vitro. Cerebral Cortex 12:936-953.

Thorndike EL (1898) Animal intelligence: An experimental study of the associative processes in animals. Psychological Monographs: General and Applied 2:i-109.

Thorndike EL (1927) The law of effect. The American Journal of Psychology 39:212-222.

Tieges Z, Richard Ridderinkhof K, Snel J, Kok A (2004) Caffeine strengthens action monitoring: evidence from the error-related negativity. Cognitive brain research 21:87-93.

Tremblay Lo, Gettner SN, Olson CR (2002) Neurons with object-centered spatial selectivity in macaque SEF: Do they represent locations or rules? Journal of Neurophysiology 87:333-350.

Troxler D (1804) Ophthalmologische Bibliothek. Jena: Springer.

Tse PU, Sheinberg DS, Logothetis NK (2004) The, distribution of microsaccade directions need not reveal the location of attention - Reply to Rolfs, Engbert, and Kliegl. Psychological Science 15:708-710.

Tu TA, Keating EG (2000) Electrical stimulation of the frontal eye field in a monkey produces combined eye and head movements. Journal of Neurophysiology 84:1103-1106.

Tzschentke TM (2001) Pharmacology and behavioral pharmacology of the mesocortical dopamine system. Progress in Neurobiology 63:241-320.

Ullsperger M (2006) Performance monitoring in neurological and psychiatric patients. International Journal of Psychophysiology 59:59-69.

Ullsperger M, von Cramon DY (2001) Subprocesses of performance monitoring: a dissociation of error processing and response competition revealed by event-related fMRI and ERPs. Neuroimage 14:1387-1401.

Ullsperger M, von Cramon DY (2006) The role of intact frontostriatal circuits in error processing. Journal of Cognitive Neuroscience 18:651-664.

Ullsperger M, von Cramon DY, Müller NG (2002) Interactions of focal cortical lesions with error processing: evidence from event-related brain potentials. Neuropsychology 16:548.

Usher M, McClelland JL (2001) The time course of perceptual choice: the leaky, competing accumulator model. Psychological Review 108:550.

Valentine DE, Sinha SR, Moss CF (2002) Orienting responses and vocalizations produced by microstimulation in the superior colliculus of the echolocating bat, Eptesicus fuscus. Journal of Comparative Physiology A 188:89-108.

Valsecchi M, Turatto M (2007) Microsaccadic response to visual events that are invisible to the superior colliculus. Behavioral Neuroscience 121:786-793.

van Boxtel GJM, Van Der Molen MW, Jennings JR (2005) Differential involvement of the anterior cingulate cortex in performance monitoring during a stop-signal task. Journal of Psychophysiology 19:1–10.

van Boxtel GJM, van der Molen MW, Jennings JR, Brunia CHM (2001) A psychophysiological analysis of inhibitory motor control in the stop-signal paradigm. Biological Psychology 58:229-262.

van Veen V, Carter CS (2002) The timing of action-monitoring processes in the anterior cingulate cortex. Journal of Cognitive Neuroscience 14:593-602.

Verbruggen F, Logan GD (2008) Response inhibition in the stop-signal paradigm. Trends in Cognitive Sciences 12:418-424.

Vigneswaran G, Kraskov A, Lemon RN (2011) Large identified pyramidal cells in macaque motor and premotor cortex exhibit "thin spikes" : implications for cell type classification. The Journal of Neuroscience 31:14235-14242.

Vocat R, Pourtois G, Vuilleumier P (2008) Unavoidable errors: A spatio-temporal analysis of time-course and neural sources of evoked potentials associated with error processing in a speeded task. Neuropsychologia 46:2545-2555.

Vogt BA (1993) Structural organization of cingulate cortex: areas, neurons, and somatodendritic transmitter receptors. Neurobiology of cingulate cortex and limbic thalamus: A comprehensive handbook:19-70.

Vogt BA, Pandya DN (1987) Cingulate cortex of the rhesus monkey: II. Cortical afferents. Journal of Comparative Neurology 262:271-289.

Vogt BA, Nimchinsky EA, Vogt LJ, Hof PR (1995) Human cingulate cortex: surface features, flat maps, and cytoarchitecture. Journal of Comparative Neurology 359:490-506.

Vogt BA, Vogt L, Farber NB, Bush G (2005) Architecture and neurocytology of monkey cingulate gyrus. Journal of Comparative Neurology 485:218-239.

von Economo CF, Parker S (1929) The cytoarchitectonics of the human cerebral cortex: Humphrey Milford.

Voogd J, Barmack NH (2006) Oculomotor cerebellum. Progress in brain research 151:231-268.

Wagner M, Fuchs M, Kastner J (2007) SWARM: sLORETA-weighted accurate minimum norm inverse solutions. International Congress Series 1300:185-188.

Walker AE (1940) A cytoarchitectural study of the prefrontal area of the macaque monkey. Journal of Comparative Neurology 73:59-86.

Walls GL (1942) The vertebrate eye and its adaptive radiation. Bloomfield Hills, Mich: Cranbrook Institute of Science.

Walton MMG, Gandhi NJ (2006) Behavioral evaluation of movement cancellation. Journal of Neurophysiology 96:2011-2024.

Walton MMG, Sparks DL, Gandhi NJ (2005) Simulations of saccade curvature by models that place superior colliculus upstream from the local feedback loop. Journal of Neurophysiology 93:2354-2358.

West R, Travers S (2008) Tracking the temporal dynamics of updating cognitive control: An examination of error processing. Cerebral Cortex 18:1112-1124.

Westheimer G (1954) Eye movement responses to a horizontally moving visual stimulus. Archives of Ophthalmology 52:932.

Williams SM, Goldman-Rakic PS (1993) Characterization of the dopaminergic innervation of the primate frontal cortex using a dopamine-specific antibody. Cerebral Cortex 3:199-222.

Winterson BJ, Collewun H (1976) Microsaccades during finely guided visuomotor tasks. Vision Research 16:1387-1390.

Womelsdorf T, Johnston K, Vinck M, Everling S (2010) Theta-activity in anterior cingulate cortex predicts task rules and their adjustments following errors. Proceedings of the National Academy of Sciences 107:5248-5253.

Wong-Lin K, Eckhoff P, Holmes P, Cohen JD (2010) Optimal performance in a countermanding saccade task. Brain Research 1318:178-187.

Woodman GF (2010) Masked targets trigger event-related potentials indexing shifts of attention but not error detection. Psychophysiology 47:410-414.

Woodman GF (2011) Homologues of human event-related potential components in nonhuman primates. In: Oxford handbook of event-related potential components (Luck SJ, Kappenman E, eds). New York: Oxford University Press.

Woodman GF, Kang MS, Rossi AF, Schall JD (2007) Nonhuman primate event-related potentials indexing covert shifts of attention. Proc Natl Acad Sci U S A 104:15111-15116.

Wurtz RH, Goldberg ME (1972) Acitvity of superior colliculus in behaving monkey .3. cells discharging before eye-movements. Journal of Neurophysiology 35:575-586.

Xing D, Yeh C-I, Burns S, Shapley RM (2012) Laminar analysis of visually evoked activity in the primary visual cortex. Proceedings of the National Academy of Sciences 109:13871-13876.

Yang S-n, Hwang H, Ford J, Heinen S (2010) Supplementary eye field activity reflects a decision rule governing smooth pursuit but not the decision. Journal of Neurophysiology 103:2458-2469.

Yarbus AL (1956) The motion of the eye in the process of changing points of fixation. Biofizika 1:76-78.

Yeung N, Sanfey AG (2004) Independent coding of reward magnitude and valence in the human brain. The Journal of Neuroscience 24:6258-6264.

Yeung N, Nieuwenhuis S (2009) Dissociating response conflict and error likelihood in anterior cingulate cortex. The Journal of Neuroscience 29:14506-14510.

Yeung N, Botvinick MM, Cohen JD (2004) The neural basis of error detection: Conflict monitoring and the error-related negativity. Psychological Review 111:931-959.

Yeung N, Cohen JD, Botvinick MM (2011) Errors of interpretation and modeling: A reply to Grinband et al. Neuroimage 57:316-319.

Yeung N, Bogacz R, Holroyd CB, Nieuwenhuis S, Cohen JD (2007) Theta phase resetting and the error-related negativity. Psychophysiology 44:39-49.

Yuval-Greenberg S, Tomer O, Keren AS, Nelken I, Deouell LY (2008) Transient induced gamma-band response in EEG as a manifestation of miniature saccades. Neuron 58:429-441.

Zhou W, King WM (1998) Premotor commands encode monocular eye movements. Nature 393:692-695.

Zuber BL, Stark L (1965) Microsaccades and velocity-amplitude relationship for saccadic eye movements. Science 150:1459-1460.